AFRL-RX-WP-TM-2008-4056

MATERIALS PROCESSING TECHNOLOGY INITIATIVES

Delivery Order 0019-08: Material Behavior Modeling for Optimization of Thermomechanical Processes

S. Tamirisakandala

Technical Management Concepts, Inc.

NOVEMBER 2000
Final Report

AIR FORCE RESEARCH LABORATORY
MATERIALS AND MANUFACTURING DIRECTORATE
WRIGHT-PATTERSON AIR FORCE BASE, OH 45433-7750
AIR FORCE MATERIEL COMMAND
UNITED STATES AIR FORCE

NOTICE AND SIGNATURE PAGE

AFRL-RX-WP-TM-2008-4056 HAS BEEN REVIEWED AND IS APPROVED FOR PUBLICATION IN ACCORDANCE WITH ASSIGNED DISTRIBUTION STATEMENT.

*//Signature//	//Signature//
SCOTT M. PEARL Integration & Technology Branch Manufacturing Technology Division	WILLIAM E. RUSSELL, JR. Manufacturing Technology Division Materials and Manufacturing Directorate

*Disseminated copies will show "//Signature//" stamped or typed above the signature blocks.

REPORT DOCUMENTATION PAGE

Form Approved
OMB No. 0704-0188

1. REPORT DATE *(DD-MM-YY)*	2. REPORT TYPE	3. DATES COVERED *(From - To)*
November 2000	Final	01 September 1998 – 01 September 2000

4. TITLE AND SUBTITLE
MATERIALS PROCESSING TECHNOLOGY INITIATIVES
Delivery Order 0019-08: Material Behavior Modeling for Optimization of Thermomechanical Processes

5a. CONTRACT NUMBER
F33615-96-D-5835-0019

5b. GRANT NUMBER

5c. PROGRAM ELEMENT NUMBER
62102F

6. AUTHOR(S)
S. Tamirisakandala (Ohio University)

5d. PROJECT NUMBER
4347

5e. TASK NUMBER
91

5f. WORK UNIT NUMBER
43479101

7. PERFORMING ORGANIZATION NAME(S) AND ADDRESS(ES)

By	For
Ohio University Research & Sponsored Programs Research & Technology Center 105 Athens, OH 45701-2979	Technical Management Concepts, Inc. P.O. Box 340345 Beavercreek, OH 45434-0345

8. PERFORMING ORGANIZATION REPORT NUMBER

9. SPONSORING/MONITORING AGENCY NAME(S) AND ADDRESS(ES)
Air Force Research Laboratory
Materials and Manufacturing Directorate
Wright-Patterson Air Force Base, OH 45433-7750
Air Force Materiel Command
United States Air Force

10. SPONSORING/MONITORING AGENCY ACRONYM(S)
AFRL/RXMT

11. SPONSORING/MONITORING AGENCY REPORT NUMBER(S)
AFRL-RX-WP-TM-2008-4056

12. DISTRIBUTION/AVAILABILITY STATEMENT
Approved for public release; distribution unlimited.

13. SUPPLEMENTARY NOTES
This is the best quality available for this report. No Public Affairs Office public release clearance data for this document was available at publication.

14. ABSTRACT
This report describes the important results obtained on the material modeling behavior of the most important titanium alloy, Ti-6Al-4V. Detailed experiments were conducted to characterize the deformation behavior, and the influence of process parameters on the thermomechanical processing was studied. Microstructural mechanisms over wide temperature and strain rate ranges have been identified, and optimum conditions for safe processing were established. The results are reported in the form of publications which were published in international journals.

15. SUBJECT TERMS

16. SECURITY CLASSIFICATION OF:			17. LIMITATION OF ABSTRACT:	18. NUMBER OF PAGES	19a. NAME OF RESPONSIBLE PERSON (Monitor)
a. REPORT	b. ABSTRACT	c. THIS PAGE			Scott M. Pearl
Unclassified	Unclassified	Unclassified	SAR	102	19b. TELEPHONE NUMBER *(Include Area Code)* N/A

Standard Form 298 (Rev. 8-98)
Prescribed by ANSI Std. Z39-18

SUMMARY: Material Behavior Modeling for Optimization of Thermomechanical Processes

Thermomechanical processing is an important step in the manufacture of engineering components to obtain desired shapes with specific mechanical properties. In the case of advanced materials, complex multi-stage metal forming operations are often required in order to produce products with specific microstructures. In view of the high sensitivity of microstructural evolution to the process parameters like temperature, strain, and strain rate, understanding of material behavior is essential for the control of microstructure. In recent years, materials modeling behavior modeling has been proven effective in achieving this goal which helps to developing optimization methodologies.

In this research project, the deformation behavior of a titanium alloy, Ti-6Al-4V, which is the most widely used and accounts for more than 50% among all titanium alloys, has been studied over wide temperature and strain rate ranges relevant to bulk metalworking processes like forging, extrusion and rolling. The processing-microstructure relationship is found to be very sensitive to the oxygen content and starting microstructure. The influence of these variables on the hot deformation behavior has been investigated with the help of laboratory experiments. Detailed material modeling has been conducted to characterize the microstructural and damage mechanisms. Optimum conditions for safe processing without defect generation have been identified. The major results from these studies are reported in the form of publications which are compiled in this report.

PUBLICATIONS

1. Hot Deformation Mechanisms in ELI Grade Ti-6Al-4V
   T. Seshacharyulu, S.C. Medeiros, J.T. Morgan. J.C. Malas, W.G. Frazier, and Y.V.R.K. Prasad
   Scripta Materialia, Vol. 41, No. 3 (1999) pp. 283-288.

2. Hot Deformation and Microstructural Damage Mechanisms in Extra-Low Interstitial (ELI) Grade Ti-6Al-4V
   T. Seshacharyulu, S.C. Medeiros, J.T. Morgan, J.C. Malas, W.G. Frazier, and Y.V.R.K. Prasad
   Materials Science and Engineering A, Vol. A279 (2000) pp. 289-299.

3. Effect of Prior β Grain Size on the Hot Deformation Behavior of Ti-6Al-4V: Coarse vs. Coarser
   Y.V.R.K. Prasad, T. Seshacharyulu, S.C. Medeiros, and W.G. Frazier
   Journal Materials Engineering and Performance, Vol. 9, No. 2 (2000) pp. 153-160.

4. Effect of Preform Microstructure on the Hot Working Mechanisms in ELI Grade Ti-6Al-4V: Transformed β vs. Equiaxed (α+β)
   Y.V.R.K. Prasad, T. Seshacharyulu, S.C. Medeiros, and W.G. Frazier
   Materials Science and Technology, Vol. 16, No. 5 (2000) pp. 511-516.

5. Hot Working of Commercial Ti-6Al-4V with an Equiaxed α-β Microstructure: Materials Modeling Considerations
   T. Seshacharyulu, S.C. Medeiros, W.G. Frazier, and Y.V.R.K. Prasad
   Materials Science and Engineering A, Vol. 284 (2000) pp. 184-194.

6. Titanium Alloy Processing
   Y.V.R.K. Prasad, T. Seshacharyulu, S.C. Medeiros, W.G. Frazier, J.T. Morgan, and J.C. Malas
   Advanced Materials and Processes, June (2000) pp. 85-89.

7. Microstructural Modeling and Process Control During Hot Working of Commercial Ti-6Al-4V: Response of Lamellar and Equiaxed Starting Microstructures
Y.V.R.K. Prasad, T. Seshacharyulu, S.C. Medeiros, and W.G. Frazier
Materials and Manufacturing Processes, Vol. 15, No. 4 (2000) pp. 581-604.

8. Hot Deformation Mechanisms in Ti-6Al-4V with a Transformed β Starting Microstructure: Commercial vs. Extra-Low Interstitial Grade
Y.V.R.K. Prasad, T. Seshacharyulu, S.C. Medeiros, W.G. Frazier and J.C. Malas III
Materials Science and Technology, Vol. 16, No. 9 (2000) pp. 1029-1036.

9. Mechanisms of Hot Working in Extra-Low Interstitial Grade Ti-6Al-4V with Equiaxed (α+β) Microstructure
T. Seshacharyulu, S.C. Medeiros, W.G. Frazier, and Y.V.R.K. Prasad
Zeitschrift für Metallkunde, in print

10. Influence of Oxygen Content on the Forging Response of Equiaxed α+β Preform of Ti-6Al-4V: Commercial vs. ELI Grade
Y.V.R.K. Prasad, T. Seshacharyulu, S.C. Medeiros, and W.G. Frazier
Journal of Materials Processing Technology, in print.

Pergamon

Scripta Materialia, Vol. 41, No. 3, pp. 283–288, 1999
Elsevier Science Ltd

1359-6462/99/$–see front matter

PII S1359-6462(99)00163-3

HOT DEFORMATION MECHANISMS IN ELI GRADE Ti-6A1-4V

T. Seshacharyulu, S.C. Medeiros, J.T. Morgan, J.C. Malas, W.G. Frazier, and Y.V.R.K. Prasad

Materials Process Design Branch, Materials and Manufacturing Directorate, Air Force Research Laboratory, Wright-Patterson Air Force Base, OH 45433-7995, USA

(Received April 21, 1999)
(Accepted April 30, 1999)

Keywords: Ti-6A1-4V; Hot working; Microstructure; Mechanisms

Introduction

Ti-6A1-4V (Ti-6-4) is an $\alpha+\beta$ titanium alloy widely used in aerospace applications. A variety of microstructures with different α morphologies can be obtained by thermomechanical processing of this alloy and these range from lamellar to equiaxed. Lamellar structures are preferred in rupture critical applications while equiaxed structures offer excellent low-cycle fatigue properties. Though extensive studies are reported (1) on the hot deformation mechanisms in Ti-6-4 with equiaxed starting structure, similar data on lamellar starting microstructure are not available. These will be of particular interest for designing industrial processes. Hot working above the β transus (β phase field) is an important step for homogenization of the cast structure while deformation below the transus (α-β phase field) converts the transformed β structure to equiaxed $\alpha+\beta$ structure. An understanding of the fundamental mechanisms during these stages will be highly beneficial to achieve microstructural control in deformation processing. The aim of this investigation is to characterize the hot deformation behavior of extra-low interstitial (ELI) grade Ti-6-4 with a transformed β starting microstructure over wide ranges of temperature and strain rate. The ELI grade is preferred for aerospace applications where the fracture toughness property is to be maximized. In this investigation, a processing map has been developed, and kinetic analysis is carried out to determine the rate-controlling step in the process.

Experimental

Ti-6-4 used in this study had the following composition: 6.02A1, 3.91V, 0.13O, 0.08Fe, 0.008N, balance Ti. The β transus reported for this grade is about 975°C. The starting Widmanstätten-type microstructure consisted of acicular α (transformed β) colonies in large prior β grains of about 2–3 mm and a primary α layer of about 5 μm thick at the prior β grain boundaries. Isothermal, constant true strain rate compression tests were conducted over the temperature range 750–1100°C at 50°C intervals and strain rate range 0.001–100 s^{-1} at order magnitude intervals using a servohydraulic testing machine. Specimens of 15 mm height and 10 mm diameter were used for testing in the α-β range while larger specimens of 22.5 mm height and 15 mm diameter were used to obtain accurate flow stress

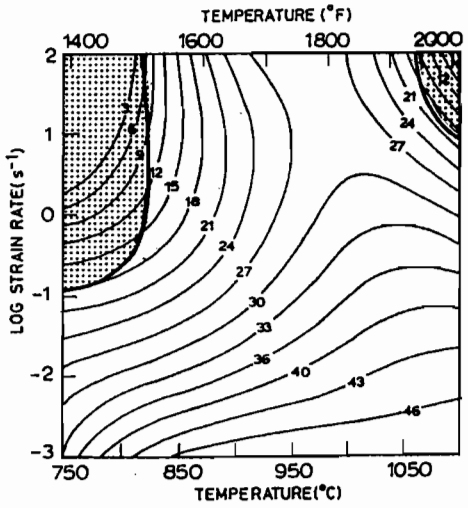

Figure 1. Processing map at a strain of 0.5. Numbers represent percent efficiency of power dissipation.

measurements in the β range. The specimens were coated with a borosilicate glass paste for lubrication and environmental protection. They were deformed to half the height in each case to impose a true strain of 0.7 and were air-cooled to room temperature after deformation. The resulting load-stroke data were processed to obtain true stress-true plastic strain using the standard method. The flow stress data at different temperatures and strain rates were used to compute the power dissipation efficiency parameter (η) given by $2m/(m + 1)$ where m is the strain rate sensitivity of flow stress. A power dissipation map was developed by plotting the variation of efficiency with temperature and strain rate. Regimes of flow instability were delineated using a continuum criterion based on the rate of change in m with strain rate as explained earlier (2). Details of development, interpretation, and application of processing maps to hot working processes can be found in reference (3). In brief, the map depicts domains of local efficiency maxima representing specific microstructural mechanisms and regimes of flow instability which may be validated by microstructural examination of the deformed specimens.

Results and Discussion

The processing map showing iso-efficiency contours in a temperature-strain rate frame at a strain of 0.5 is given in Fig. 1. The map exhibits a single domain extending over the entire test temperature range and strain rates below about 0.1 s^{-1} with a peak efficiency of 46%. However, since this range of temperature has different phases covering the β transus at $\approx$975°C, it is logical to interpret the domain to consist of different mechanisms with similar power dissipation characteristics. Furthermore, at high strain rates and lower temperatures, a regime of flow instability occurring by adiabatic shear band formation is identified (marked as shaded area in Fig. 1). Another flow localization regime occurs in the β range at temperatures higher than 1050°C and strain rates higher than 10 s^{-1}.

A. Domain in the α-β Phase Field

The microstructures obtained on specimens deformed in the α-β phase field domain indicate significant morphological change of α phase from acicular to equiaxed which occurs by the process of globularization of the colony structure (Fig. 2). Furthermore, the shapes of stress-strain curves in this domain exhibited continuous flow softening and tended to reach a steady-state at larger strains.

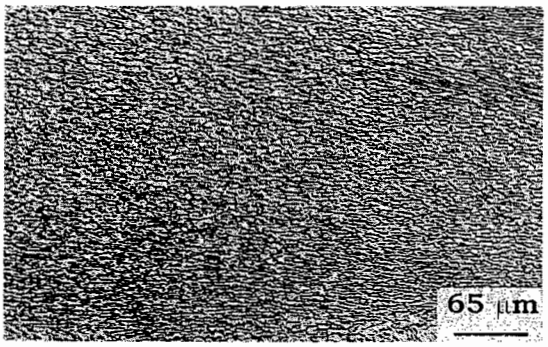

Figure 2. Microstructure obtained on a specimen deformed at 950°C/0.001 s^{-1}.

In order to understand the rate-controlling step during globularization, the flow stress data are analyzed using the kinetic rate equation given by:

$$\dot{\varepsilon} = A(\sigma/E)^n exp(-Q/RT) \tag{1}$$

where $\dot{\varepsilon}$: strain rate, σ : flow stress, A: frequency factor, E: Young's modulus, Q: apparent activation energy, R: gas constant, T: temperature in Kelvin, and n: stress exponent. A plot of ln $\dot{\varepsilon}$ vs. $\ln(\sigma/E)$ corresponding to the globularization domain is given in Fig. 3(a), while the variation of $\ln(\sigma/E)$ vs. $1/T$ is given in Fig. 3(b). From these plots, stress exponent and apparent activation energy have been estimated to be 4.6 and 453 kJ/mole, respectively. In α-titanium, the activation energy estimated (4) for lattice diffusion is 150 kJ/mole while an apparent activation energy of 242 kJ/mole was reported (5) for power-law creep. The presently estimated apparent activation energy in the globularization domain (453 kJ/mole) is much higher than these two values, ruling out dislocation climb as a possible mechanism. In view of this conclusion, it is necessary to analyze the data further using other models for thermally activated flows. This analysis is carried out below using the models proposed by Schöck (6) and Kocks *et al.* (7).

The equation for thermally activated cross-slip proposed by Schöck (6) is given by:

$$\dot{\varepsilon} = \dot{\varepsilon}_0 exp[-U(\sigma)/kT] \tag{2}$$

$$U(\sigma) = -A' ln(\sigma/\sigma_0) \tag{3}$$

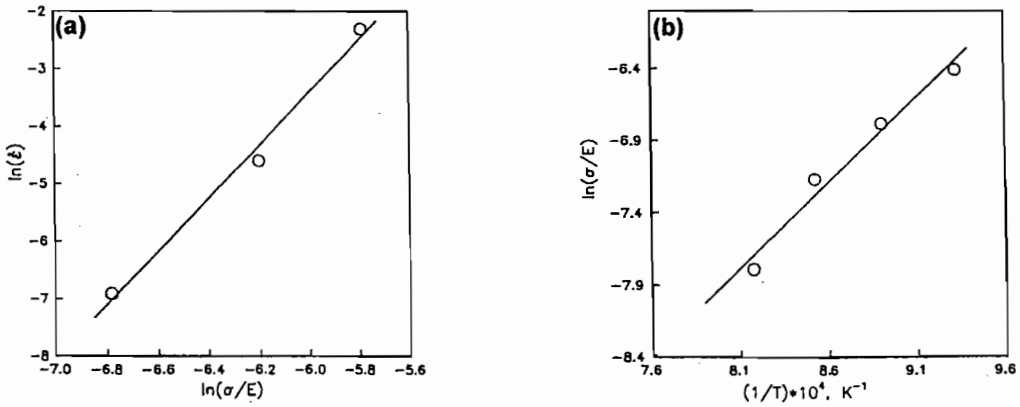

Figure 3. Plot of (a) ln $\dot{\varepsilon}$ vs. ln(σ/E) and (b) 1/T vs. ln(σ/E) in the globularization domain.

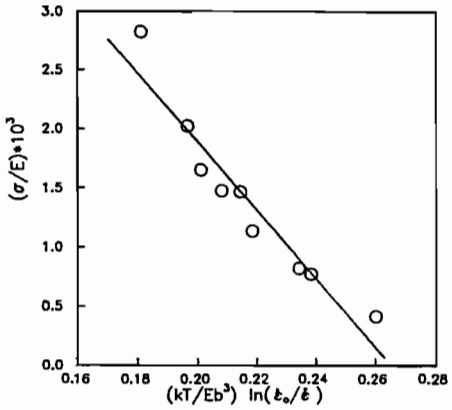

Figure 4. Plot of $(kT/Eb^3)\ \ln(\dot{\varepsilon}_0/\dot{\varepsilon})$ vs. σ/E in the globularization domain.

where $\dot{\varepsilon}_0$: a constant (assumed to be $10^7\ s^{-1}$ in the present analysis), $U(\sigma)$: stress-dependent activation energy, k: Boltzman's constant, A': temperature- and stress-independent constant, and σ_0: stress required to overcome the activation barrier in the absence of any thermal activation. Using the plots in Fig. 3, the threshold stress σ_0 in Eq. (3) is evaluated and the corresponding activation energy values are estimated to be 165 to 240 kJ/mole. These values agree well with that for lattice diffusion and power law creep. With a view to understand the recovery mechanism, the activation volume is evaluated further. The thermal activation model proposed by Kocks *et al.* (7) in a simplified form is given by:

$$\frac{\sigma}{E} = \frac{\sigma_{ath}}{E} + \frac{\sigma_0}{E}\left(1 - \frac{kT}{g_0 Eb^3} ln\frac{\dot{\varepsilon}_0}{\dot{\varepsilon}}\right) \tag{4}$$

In this expression, g_0 is the normalized total activation free enthalpy, b the Burgers vector, σ/E the normalized flow stress, σ_{ath}/E the athermal component of the flow stress due to long-range obstacles, and σ_0 and $\dot{\varepsilon}_0$ have the same meaning as in Eqs. (2) and (3). Since the activation energies are being evaluated at high temperature, σ_{ath} will be very small and it can be neglected. A plot of (σ/E) vs. $(kT/Eb^3)\ \ln(\dot{\varepsilon}_0/\dot{\varepsilon})$ is shown in Fig. 4. The σ_0/E value is evaluated by extrapolation, from which the apparent activation energy is determined. These values are in the range 170 to 225 kJ/mole which are very near to that for self diffusion in α-titanium (150 kJ/mole). The variation of activation energy with stress using Schöck and Kocks models are shown in Fig. 5 and the activation volume is evaluated from

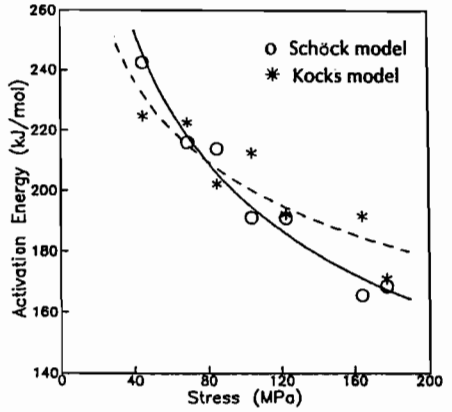

Figure 5. Variation of apparent activation energy with stress in the globularization domain.

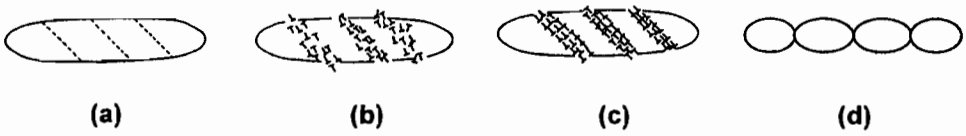

Figure 6. Schematic illustrating steps of globularization process.

the slopes of these curves. The normalized activation volumes (V/b^3) in the globularization domain are 18 to 78 and 13 to 85, as determined from Schöck and Kocks models, respectively. The apparent activation energy values and activation volume estimates suggest that cross-slip is the rate-controlling mechanism.

The process of globularization may be visualized in simple terms to consist of the following steps which are schematically shown in Fig. 6.

a) Shearing of laths due to imposed shear strain: This process is strain dependent and may reach completion at larger strains. Initially, a few colonies that are favorably oriented with respect to the applied stress will participate in the shearing process, which will rotate the neighboring colonies to favorable orientations facilitating further shear.
b) Generation of dislocations of both signs along the line of shear.
c) Simultaneous recovery by cross-slip leading to annihilation of opposite sign dislocations on intersecting slip planes and leaving behind groups of dislocations with same sign to nucleate an interface along the line of shear.
d) Migration of interfaces by diffusion to minimize the surface energy forming the globules.

Thus, the globularization process may also be regarded as a type of dynamic recrystallization since it also involves two competitive processes viz., rate of nucleation and rate of migration.

B. Domain in the β Phase Field

The β phase exhibits low flow stress and steady-state flow curves in the temperature range 980–1100°C and strain rate range 0.001–0.1 s^{-1}. The strain rate sensitivity of flow stress in this regime is $\approx$0.33 and the tensile ductility measured at 1050°C and a nominal strain rate of 0.01 s^{-1} is close to 100%. In view of these observations, it may be inferred that β is deforming by the mechanism of large-grained superplasticity (LGSP) which is generally referred to as 'Class I superplasticity in coarse-grained materials' (8). A number of materials like β brasses, β titanium alloys, and aluminides are found to exhibit LGSP. It is generally explained in terms of the sliding of boundaries generated within the large prior β grain, due to the high rate of dynamic recovery in the bcc structure with a concurrent diffusion accommodated flow. In the present case it is likely that the stable prior colony boundary structure with the boundaries preferentially oriented at 45 degrees to the compression axis will participate in the sliding process and contribute to the larger strains for causing LGSP. Activation analysis is carried out using the kinetic rate equation (Eq. 1) to evaluate the rate-controlling step in LGSP. A plot of $\ln\dot{\varepsilon}$ vs. $\ln(\sigma/E)$ is given in Fig. 7(a), while the variation of $\ln(\sigma/E)$ vs. $1/T$ is given in Fig. 7(b). Stress exponent and apparent activation energy evaluated from these plots yielded values of 3.9 and 184 kJ/mole, respectively. In β titanium, the activation energy for self diffusion is reported (9) to be 153 kJ/mole and the presently estimated value is in close agreement with this indicating that the β large-grained superplasticity process is diffusion-controlled.

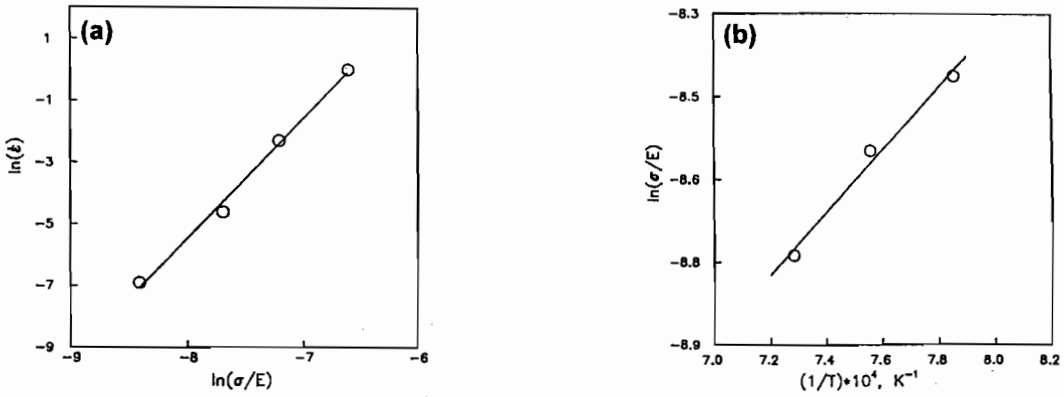

Figure 7. Plot of (a) ln ε vs. ln(σ/E) and (b) 1/T vs. ln(σ/E) in the large-grained superplasticity domain

Conclusions

The processing map developed on Ti-6-4 with Widmanstätten starting microstructure revealed the material exhibits globularization in the α-β phase field while the β phase deforms by the mechanism of large-grained superplasticity. The apparent activation energy for hot deformation in the α-β range using kinetic analysis yielded a value of 453 kJ/mole, while a value of 165–240 kJ/mole is obtained using Schöck and Kocks models. The latter value of activation energy together with an estimated activation volume of 13–85 b^3 suggests that cross-slip is the rate controlling mechanism for globularization. The apparent activation energy for β large-grained superplasticity (184 kJ/mole) matches well with that of self-diffusion in β.

Acknowledgements

One of the authors (YVRKP) is thankful to the National Research Council, USA, for awarding him an associateship and to the Director of the Indian Institute of Science, Bangalore, for granting him a sabbatical leave. The assistance rendered by Mr. S. Sasidhara and Mr. R. Ravi of Department of Metallurgy, Indian Institute of Science is gratefully acknowledged.

References

1. M.W. Mahoney, in Materials Properties Handbook: Titanium Alloys, ed. R. Boyer, G. Welsch, and E.W. Collings, p. 1101, ASM International, Materials Park, OH (1994).
2. Y.V.R.K. Prasad, Ind. J. Tech. 28, 435 (1990).
3. Y.V.R.K. Prasad and S. Sasidhara, ed., Hot Working Guide: A Compendium of Processing Maps, ASM International, Materials Park, OH (1997).
4. F. Dyment and C.M. Libanati, J. Mater. Sci. 3, 349 (1968).
5. M. Doner and H. Conrad, Metall. Trans. 4, 2809 (1973).
6. G. Schöck, in ed. F.R.N. Nabarro, Dislocations in Solids, vol. 3, p. 63, North-Holland, Amsterdam (1980).
7. U.F. Kocks, A.S. Argon, and M.F. Ashby, Prog. Mater. Sci. 21, 110 (1975).
8. T.G. Nieh, J. Wadsworth, and O.D. Sherby, Superplasticity in Metals and Ceramics, Cambridge University Press, Cambridge, UK (1997).
9. H.J. Frost and M.F. Ashby, Deformation Mechanism Maps, p. 44, Pergamon Press, London (1982).

ELSEVIER

Materials Science and Engineering A279 (2000) 289–299

MATERIALS SCIENCE & ENGINEERING A

www.elsevier.com/locate/msea

Hot deformation and microstructural damage mechanisms in extra-low interstitial (ELI) grade Ti–6Al–4V

T. Seshacharyulu *, S.C. Medeiros, J.T. Morgan, J.C. Malas, W.G. Frazier, Y.V.R.K. Prasad

Materials Process Design Branch, Materials and Manufacturing Directorate, Air Force Research Laboratory, Wright-Patterson Air Force Base, OH 45433-7746, USA

Received 22 February 1999; received in revised form 5 April 1999

Abstract

The hot deformation behavior of extra-low interstitial (ELI) grade Ti–6Al–4V alloy with Widmanstätten preform microstructure over wide temperature (750–1100°C) and strain rate ranges (0.001–100 s^{-1}) has been studied with the help of processing maps. In the lower temperature and strain rate regime (850–950°C and 0.001–0.1 s^{-1}), globularization of the lamellar structure occurs while at higher temperatures (980–1100°C) the β phase exhibits large-grained superplasticity. The tensile ductility reaches peak values under conditions corresponding to these two processes. A dip in ductility occurs at the β transus and is attributed to a possible nucleation of voids within prior β grains. At lower temperatures and strain rates below about 0.1 s^{-1}, cracking at the prior β grain boundaries occurs under mixed mode conditions. At strain rates higher than 1 s^{-1} and temperatures lower than about 950°C, the material exhibits a wide regime of flow instabilities. On the basis of these results, a temperature–strain rate window for hot working this material without microstructural defects is identified. Published by Elsevier Science S.A.

Keywords: Hot deformation behaviour; Strain rate regime; α and β Deformation

1. Introduction

Ti–6Al–4V (Ti-6-4) is an α + β titanium alloy extensively used in aerospace applications. This alloy can acquire a large variety of microstructures with different α morphologies depending on thermomechanical treatments. Its mechanical properties are strongly influenced by oxygen content and preform microstructure. The extra-low interstitial (ELI) grade contains a maximum oxygen content of 1300 ppm as against 1500–2000 ppm in commercial grade, and is preferred in applications where fracture toughness is to be maximized [1]. The reported β transus for ELI grade Ti-6-4 is about 975°C which increases to more than 995°C for commercial grades since oxygen stabilizes the α phase.

The processing–microstructure relationship in titanium alloys is sensitive [2] to the preform microstructure which ranges from equiaxed α to lamellar α (transformed β). Extensive hot deformation studies have been carried out on Ti-6-4 with equiaxed preform structure and the occurrence of fine-grained superplasticity in the α + β range has been well documented [3–5]. However in Ti-6-4 with transformed β microstructure, strain induced porosity occurs during processing under certain conditions of temperature and strain rate [6]. To explain its hot tensile and non-isothermal forging behavior, ductile fracture models have been developed for the cavity nucleation and coalescence involving tensile work and hydrostatic stress respectively [7,8]. While these models have provided important insights to fracture phenomenon, the state-of-stress in any metalworking process is more complex than that considered in these studies. As regards the mechanism of hot deformation in the β phase field, much attention has not been given since working in this regime does not pose any problem. The objective of this study is to characterize the hot deformation behavior of ELI grade Ti-6-4 with a transformed β (Widmanstätten) preform microstructure over wide

* Corresponding author.

0921-5093/00/$ - see front matter Published by Elsevier Science S.A.
PII: S0921-5093(99)00173-2

temperature and strain rate ranges with a view to model the microstructural mechanisms of hot deformation in both the $\alpha+\beta$ and β phase fields. This study will be highly beneficial for designing hot working schedules to optimize intrinsic workability, control microstructural evolution, and avoid defect formation in products.

In this paper, the approach of processing maps has been adopted to represent and analyze the constitutive behavior of ELI grade Ti-6-4. The basis and principles of this approach are described in detail by Prasad [9,10] and recently reviewed by Prasad and Seshacharyulu [11]. Its application to hot working of a wide range of materials is compiled by Prasad and Sasidhara [12]. Depicted in a frame of temperature and strain rate, power dissipation maps represent the pattern in which power is dissipated by the material through microstructural changes. The rate of this change is given by the dimensionless parameter called the efficiency of power dissipation:

$$\eta = \frac{2m}{m+1} \tag{1}$$

where m is strain rate sensitivity of flow stress. Over this frame is superimposed a continuum instability criterion for identifying regimes of flow instabilities, developed on the basis of extremum principles of irreversible thermodynamics as applied to large plastic flow [13] and given by another dimensionless parameter:

$$\xi(\dot{\varepsilon}) = \frac{\partial \ln(m/m+1)}{\partial \ln \dot{\varepsilon}} + m < 0 \tag{2}$$

where $\dot{\varepsilon}$ is the applied strain rate. These two maps together constitute a processing map which exhibits domains with local efficiency maxima representing certain specific microstructural mechanisms and also regimes of flow instabilities due to flow localization.

2. Experimental

ELI grade Ti-6-4 supplied by RMI Titanium Company, OH, USA having the following composition (weight percent) was used in this study: 6.02Al, 3.91V, 0.13O, 0.08Fe, 0.008N, balance Ti. The starting microstructure is shown in Fig. 1. It is a typical Widmanstätten structure consisting of lamellar α (transformed β) colonies in large prior β grains of about 1000 μm, primary α layer of 5 μm thick at the prior β grain boundaries and a very thin β layer in-between the colony boundaries and primary α.

Compression specimens of 15 mm height and 10 mm diameter were machined for testing in the $\alpha+\beta$ range, while larger specimens of 22.5 mm height and 15 mm diameter were used to obtain an accurate measurement of the flow stress in the β range. Concentric grooves of 0.5 mm depth were made on the top and bottom faces of the specimens to trap lubricant and assist in reducing friction. A 1 mm 45° chamfer was provided on the specimen edges to avoid fold-over of the material during the initial stages of compression. A small hole of 0.8 mm diameter and 5 mm depth was drilled at mid height of the specimen for inserting a thermocouple which is used to measure the actual temperature of the specimen as well as adiabatic temperature rise if any during testing. Isothermal hot compression tests were conducted using a servohydraulic testing machine. A resistance heating split furnace with SiC elements was used to surround the platens and specimen. The specimens were coated with a borosilicate glass paste for lubrication and environmental protection. Compression testing was carried out in the temperature range 750–1100°C at an interval of 50°C and strain rate range 0.001–100 s^{-1} at an interval of an order magnitude. The temperature of the specimen was monitored using a chromel-alumel thermocouple inserted in the specimen and isothermal condition was maintained within ± 2°C fluctuation. Adiabatic temperature rise (significant at higher strain rates) was recorded using a transient oscilloscope. The specimens were deformed to half the height in each case to impose a true strain of 0.7 and were air-cooled to room temperature after deformation. Deformed specimens were sectioned parallel to the compression axis and the cut surface was prepared for metallographic examination using standard techniques. The specimens were etched with Kroll's reagent and polarized light micrographs were recorded.

The load-stroke data obtained in compression were processed to obtain true stress–true plastic strain using standard method. The flow stress data obtained at different temperatures, strain rates and strains were corrected for adiabatic temperature rise, if any, by

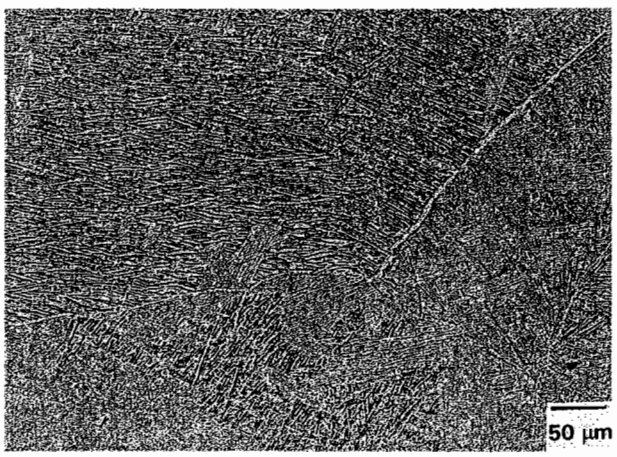

Fig. 1. Microstructure of ELI grade Ti-6-4 used in this investigation.

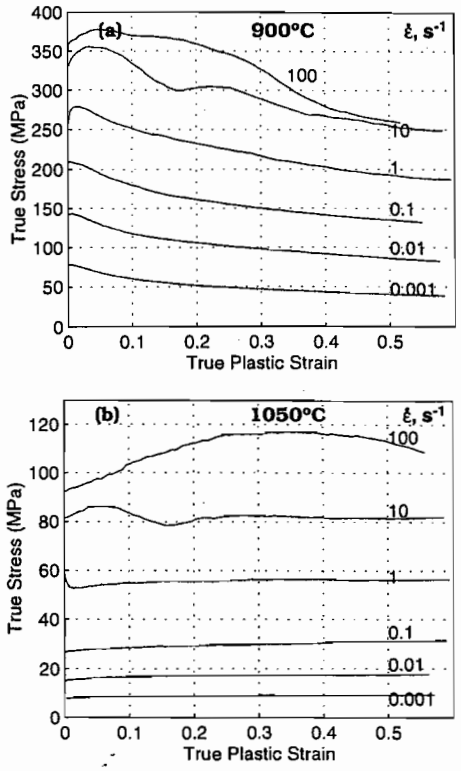

Fig. 2. True stress–true plastic strain curves obtained on ELI Ti-6-4 deformed in compression at (a) 900 and (b) 1050°C and at different strain rates.

linear interpolation between $\log \sigma$ and $1/T$ where σ is the flow stress and T is the temperature in Kelvin. Cubic spline fit between $\log \sigma$ and $\log \dot{\varepsilon}$ was used to obtain the strain rate sensitivity (m) as a function of strain rate. This was repeated at different temperatures. The efficiency of power dissipation (η) through microstructural changes was then calculated as a function of temperature and strain rate using Eq. (1) and plotted as iso-efficiency contour map. The data were also used to evaluate the flow instability parameter $\xi(\dot{\varepsilon})$ using Eq. (2) as a function of temperature and strain rate to obtain instability map.

Hot tensile tests were also conducted in the temperature range 800–1100°C at a nominal strain rate of 0.01 s^{-1} (constant actuator speed of 0.25 mm s^{-1}). Cylindrical specimens of 25 mm gauge length and 4 mm gauge diameter were used for this purpose. The specimens were pulled to fracture and total elongation as a function of temperature was recorded.

3. Results and discussion

3.1. Stress–strain behavior

True stress–true plastic strain curves obtained at 900°C and different strain rates are shown in Fig. 2(a). The curves exhibit continuous flow softening behavior at lower strain rates while oscillations were observed at higher strain rates (≥ 10 s^{-1}) and this is representative of the material response in the α–β phase field. The stress-strain curves in the β phase field revealed that the material exhibits steady-state flow at strain rates of 0.1 s^{-1} and slower, representative curves of which are shown in Fig. 2(b) for a deformation temperature of 1050°C. The flow stress data as a function of temperature, strain rate and strain are given in Table 1.

3.2. Power dissipation map

The power dissipation map showing isoefficiency contours in a temperature-strain rate frame at a strain of 0.5 is shown in Fig. 3. The maps at lower strains have similar features. The map exhibits a single domain extending over the entire test temperature range and at strain rates below about 0.1 s^{-1} with a peak efficiency of 49%. However, since this range of temperature has different phases and covers the β transus at ≈ 975°C, it is logical to interpret the domain to consist of different mechanisms with closely equal power dissipation characteristics. In such a case, detailed metallographic examination and hot ductility variation are required to interpret, validate and confirm the mechanisms. These are further discussed below:

3.2.1. Lower temperature regime: α–β deformation

Detailed microstructural examination of specimens deformed at lower temperatures (< 850°C) and lower strain rates (< 0.1 s^{-1}) revealed extensive cracking at the prior β grain boundaries. Microstructures of specimens deformed at 750°C/0.01 s^{-1} and 800°C/0.01 s^{-1} are shown in Fig. 4(a) and (b) respectively. The compression axis is vertical in these microstructures. A statistical measure of the orientation of the cracked boundaries with respect to the compression axis is shown in Fig. 5 which covers data on at least 50 boundaries. The distribution clearly shows that majority of the population are oriented between 40 and 60° with respect to the compression axis. Further, their presence is predominant around the bulge region of the specimens where a secondary (circumferential) tensile stress develops. Suzuki et al., [14] also reported such intergranular cracking resulting in a severe drop in ductility. The morphology and characteristics of these cracks indicate that these are associated with the occurrence of sliding at the prior β grain boundaries. The mechanism of cracking is explained with the following simple microstructural model:

The β transformed Widmanstätten structure consists of three micro constituents: lamellar α colonies,

Table 1
Corrected flow stress values (in MPa) of ELI grade Ti-6-4 at different temperatures, strain rates and strains.

Strain	Strain rate ($s^{(1)}$)	Temperature (°C)							
		750	800	850	900	950	1000	1050	1100
0.1	0.001	218.5	145.5	94.8	60.4	22.8	12.0	8.4	6.4
	0.010	326.1	238.5	184.6	118.4	63.3	23.2	16.6	14.3
	0.100	422.7	375.8	262.8	180.2	99.2	44.1	28.3	28.4
	1.000	541.9	419.1	367.8	251.6	164.0	74.5	54.9	43.7
	10.00	548.3	542.8	424.0	342.4	214.3	122.2	84.0	71.4
	100.0	677.2	573.2	489.2	385.8	259.9	154.8	103.1	87.1
0.2	0.001	193.1	130.9	85.8	51.6	19.3	11.9	8.8	6.6
	0.010	301.4	217.4	163.9	106.0	56.2	22.1	17.2	14.9
	0.100	386.9	337.1	229.4	161.0	91.2	43.0	29.2	29.6
	1.000	503.5	395.1	336.4	233.0	150.2	70.9	55.5	44.4
	10.00	530.1	509.6	392.8	309.0	188.8	117.6	80.2	71.6
	100.0	684.6	577.2	489.1	375.7	257.5	159.8	112.0	93.8
0.3	0.001	178.6	122.4	79.5	46.8	17.8	11.7	9.0	6.8
	0.010	284.7	205.0	153.4	98.1	52.3	21.8	17.5	15.2
	0.100	361.9	308.1	209.5	149.8	85.7	41.4	29.5	30.1
	1.000	457.4	362.0	306.4	217.2	141.8	69.4	56.3	45.4
	10.00	473.4	470.2	373.1	296.3	184.9	113.7	82.3	75.0
	100.0	637.5	534.6	448.5	342.4	246.0	159.8	116.2	99.0
0.4	0.001	168.9	112.6	73.2	43.4	17.1	11.8	9.1	7.0
	0.010	270.8	194.7	141.5	91.8	49.5	22.6	17.4	15.4
	0.100	345.9	291.5	195.7	141.5	80.5	41.0	30.4	30.2
	1.000	415.5	332.1	279.1	202.7	133.7	67.6	56.5	46.0
	10.00	430.7	408.0	342.7	272.6	170.0	110.3	81.8	73.3
	100.0	649.6	490.9	383.4	294.1	231.8	154.8	116.1	100.5
0.5	0.001	161.0	104.3	69.0	40.4	17.0	12.2	9.1	7.2
	0.010	261.9	187.5	133.7	86.2	47.4	22.9	17.4	15.5
	0.100	341.1	280.0	187.0	135.3	77.7	40.9	31.1	30.8
	1.000	415.3	320.4	260.5	192.7	126.7	66.2	56.0	46.1
	10.00	435.0	399.3	328.8	260.8	164.1	107.2	81.4	74.3
	100.0	777.7	444.6	287.4	268.7	216.9	147.0	113.5	98.3

primary α at the prior β grain boundaries and a thin layer of β in-between the colony boundary and the primary α layer. Out of these three, the colonies have the highest strength due to the specific crystallographic orientation relationship while the β layer is inherently the softest phase at the deformation temperature in view of its bcc structure. During deformation by uniaxial compression, sliding of the prior β boundary with a near 45° orientation occurs across the soft β layer and produces stress concentration at the primary α/thin β interface. If the stress concentration is not relieved by the deformation of adjacent primary α phase, cracks are expected to form along the interface under mixed mode stress conditions (shear + tensile). As deformation of α phase is thermally activated, it is likely to undergo dynamic recovery at lower temperatures and higher strain rates. The rate of softening due to dynamic recovery may not be sufficient to avoid cracking and therefore the cracks have sharp tips (Fig. 4(a)). As the temperature is increased, the microstructure exhibits fine equiaxed α grains ahead of crack tip which can be interpreted to be the result of dynamic recovery followed by static recrystallization thereby blunting the crack tip (Fig. 4(b)). At much higher temperatures and lower strain rates, the α phase is likely to undergo dynamic recrystallization (DRX) [2] which softens the boundary layer at the rates required to prevent cracking totally. Thus, the limiting temperature and strain rate conditions for cracking are decided by those that can initiate DRX of primary α at the grain boundary. Since the resolved shear stress is responsible for the sliding at the prior β boundaries and the occurrence of cracks is not specific only to triple junctions, it seems appropriate to describe them as 'shear' cracks so as to distinguish from the commonly known 'wedge' cracks.

3.2.2. Intermediate temperature regime: α–β deformation

In the domain occurring over the temperature range 850–950°C and strain rate range 0.001–0.01 s^{-1} with a peak power dissipation efficiency of 49%, the microstructures obtained on deformed specimens indicate significant morphological change of α phase from lamellar to equiaxed. Typical microstructures obtained at 850, 900 and 950°C on specimens deformed at 0.001 s^{-1} are shown in Fig. 6(a–c), all of which exhibit globularization of the colony structure. The shapes of stress-strain curves in this domain Fig. 2(a) have exhibited continuous flow softening. Gegel et al. [15] have shown that the flow curves of transformed β preforms become asymptotic to those of equiaxed α-β preforms at sufficiently large strains (~ 0.6) since the process of globularization converts metastable Widmanstätten structure to a more stable equiaxed configuration.

The process of globularization may be visualized in simple terms to consist of the following steps which are schematically shown in Fig. 7.

1. Shearing of laths due to imposed shear strain: This process is strain dependent and may reach completion at larger strains. At a time, a few colonies which are favorably oriented with respect to the applied stress will participate in the shearing process and will rotate the neighboring unfavorable orientations, facilitating further shear.
2. Generation of dislocations of both signs along the line of shear.
3. Simultaneous recovery by cross-slip leading to annihilation of opposite sign dislocations on intersecting slip planes and leaving behind groups of dislocations with same sign to nucleate an interface along the line of shear.

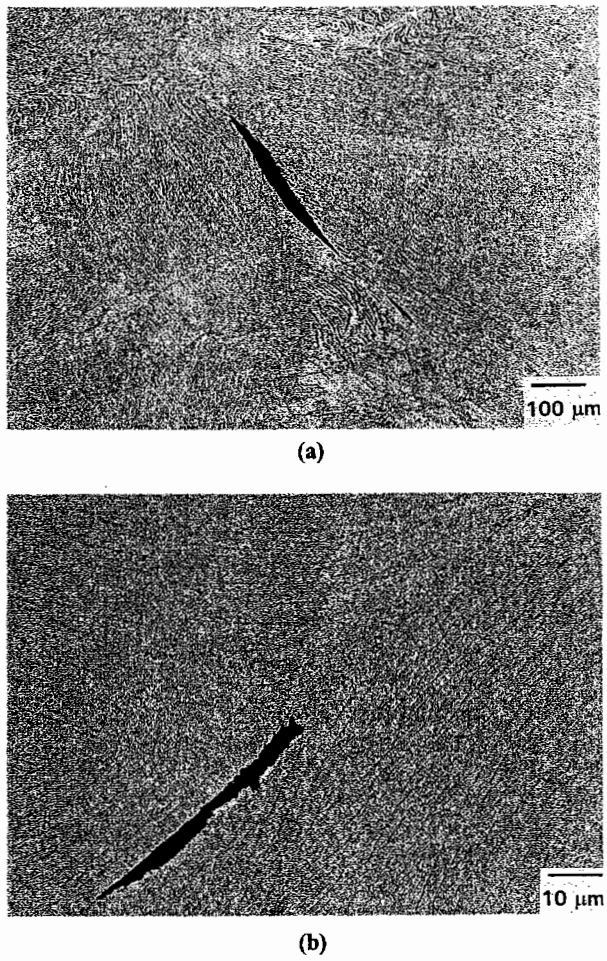

Fig. 4. Microstructures obtained on ELI Ti-6-4 deformed at (a) 750°C/0.01 s^{-1}; and (b) 800°C/0.01 s^{-1}. The compression axis is vertical.

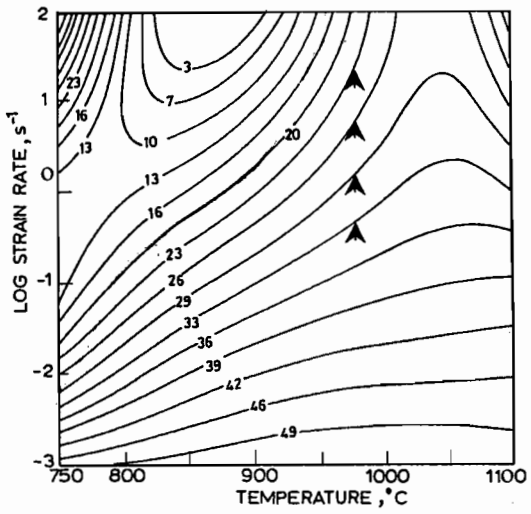

Fig. 3. Power dissipation map obtained on ELI Ti-6-4 at a strain of 0.5. Contour numbers represent percent efficiency of power dissipation.

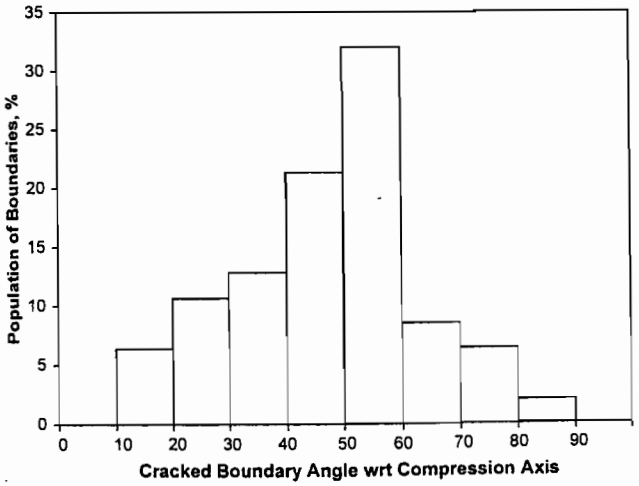

Fig. 5. Statistical distribution of the angle between cracked prior β grain boundary and compression axis.

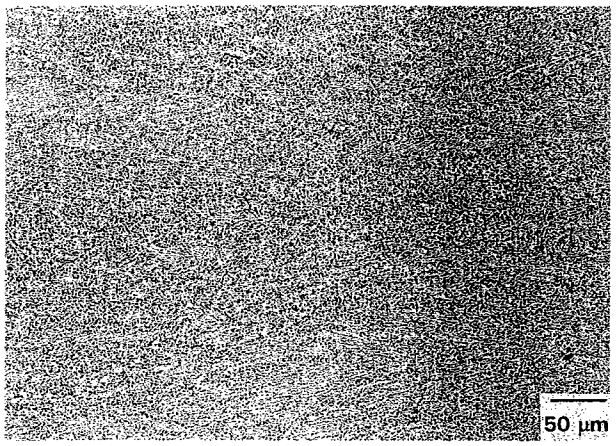

(a)

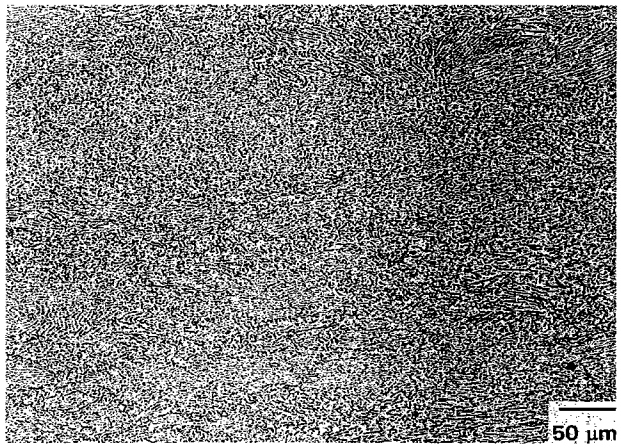

(b)

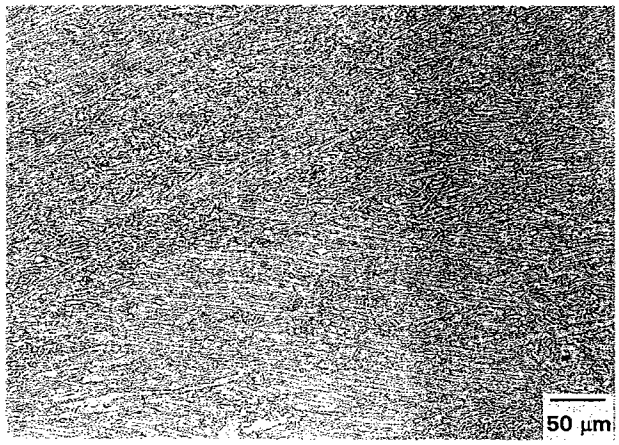

(c)

Fig. 6. Microstructures of specimens deformed at (a) 850°C/0.001 s^{-1}; (b) 900°C/0.001 s^{-1}; and (c) 950°C/0.001 s^{-1}. The compression axis is vertical.

4. Migration of interfaces by diffusion to minimize the surface energy forming the globules

Thus, the globularization process may also be regarded as a type of dynamic recrystallization since it also involves two competitive processes viz., rate of nucleation and rate of migration. Globularization assumes considerable importance in the conversion step of ingot to semi-product (billet) using cogging or extrusion since this step produces the desired fine grained equiaxed α–β microstructures for further processing into finished shapes.

3.2.3. Deformation in the β transus region

The power dissipation map exhibited points of inflexion in the iso-efficiency contours at ≈975°C when the strain rate is higher than about 0.1 s^{-1} and these are indicated by arrows in Fig. 3. A change in slope of the contours occurred at these points.[1] It may be noted that the β transus for ELI Ti-6-4 was reported to be about 975°C [1] and thus the indications of the β transus from the map matches well with that reported in the literature. Such inflexions in contours indicate that phase changes are occurring in the system since the efficiency of power dissipation actually represents the relative rate of entropy production [9–11]. However, any significant inflexions in the contours did not appear at strain rates lower than 0.1 s^{-1} indicating that the deformation

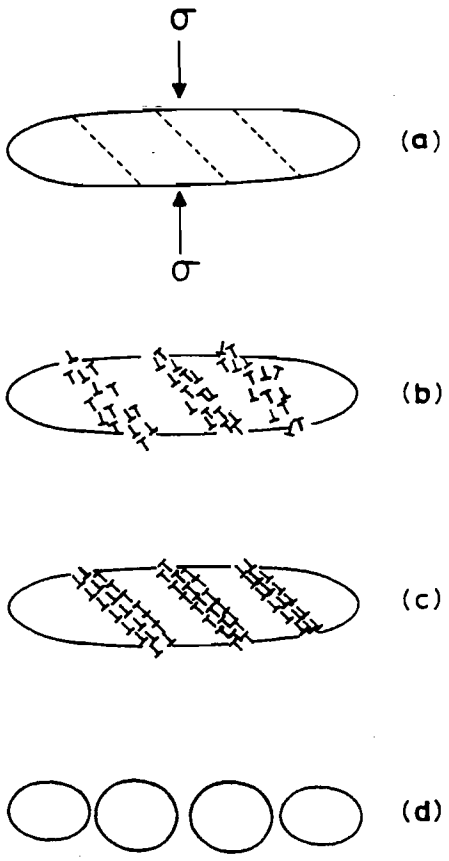

Fig. 7. Schematic illustrating the steps of globularization process.

[1] Although the inflexions associated with phase transformation in this material are not so clearly evident, striking changes have been observed in a large number of other systems [12].

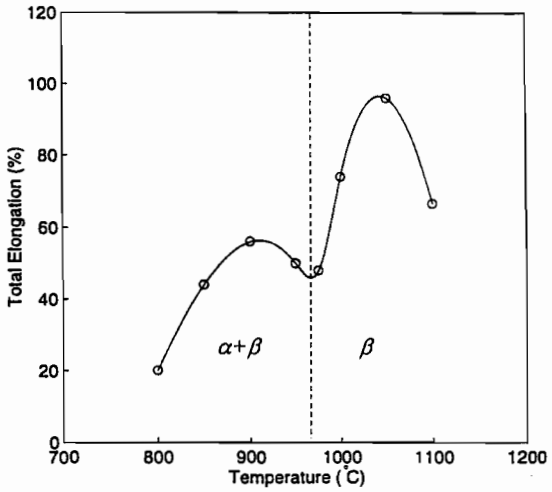

Fig. 8. Variation of total tensile elongation with temperature at a nominal strain rate of 0.01 s^{-1}.

mechanism occurring at transus and lower strain rates has an efficiency of power dissipation similar to the mechanisms occurring on either side of the transus. Also, deformation at transus may involve nucleation of microstructural damage which has a higher power dissipation efficiency. This is further discussed in the light of tensile ductility results.

3.2.4. Tensile ductility

The variation of total elongation to failure with temperature at a nominal strain rate of 0.01 s^{-1} for ELI grade Ti-6-4 is shown in Fig. 8 which exhibits the following features:

1. Low ductilities ($\sim$20%) are recorded at temperatures less than 850°C and these are attributed to the shear cracking occurring under these conditions as discussed in Section 3.2.1.
2. The ductility attains a peak in the $\alpha-\beta$ range around 920°C which corresponds to near equal volume fractions of the two phases. The drop in ductility beyond 920°C may be attributed to a rapid increase in the β volume fraction with increase in temperature [4].
3. In the β range, the ductility peak occurs at 1050°C and the ductility values are high ($\sim$100%) even at a strain rate of 0.01 s^{-1}.
4. At the transus ($\approx$975°C) a local minimum in the ductility has occurred indicating that microstructural damage may have been nucleated at these strain rates. The microstructure of the specimen deformed in tension at 975°C and 0.01 s^{-1} did not reveal any indication of microstructural damage like voids or wedge cracks. However, this does not rule out the nucleation of defects which are not easily observable under optical microscope as discussed by Ridley [16]. The mechanisms of β deformation and void nucleation at transus are discussed in the next section.

3.2.5. Deformation in the β range

The β phase exhibits low flow stress and steady-state flow curves (Fig. 2(b)) in the temperature range 980–1100°C and strain rate range 0.001–0.1 s^{-1}. The strain rate sensitivity of flow stress in this regime is $\approx$0.33 and the tensile ductility measured at 1050°C and a nominal strain rate of 0.01 s^{-1} is close to 100%. In view of these observations, it may be inferred that β is deforming by the mechanism of large-grained superplasticity (LGSP) which is generally referred to as 'Class I superplasticity in coarse-grained materials' [17]. A number of materials like β brasses [18], β titanium alloys [19], and aluminides [20–22] are found to exhibit LGSP. It is generally explained in terms of the sliding of boundaries generated within the large prior β grain, due to the high rate of dynamic recovery in the bcc structure with a concurrent diffusion accommodated flow. These boundaries are often seen in the 'frozen' specimens as a network of finer grains in a large prior β grain boundary. Further, in microstructures with Widmanstätten colonies within prior β grains, as the β volume fraction increases with temperature the colony structure will dissolve leaving behind the colony boundaries. These may be called 'prior colony boundaries' (PCBs) which have angular misorientations ($\sim$8–10°) smaller than large angle grain boundaries but higher than the conventional subboundaries. The orientation of the PCBs with respect to the compression axis has been measured on a specimen deformed at 960°C/0.05 s^{-1} and is shown in Fig. 9. There is a large population of these boundaries with orientation at 30–60° which allows them to slide under slow strain rate deformation

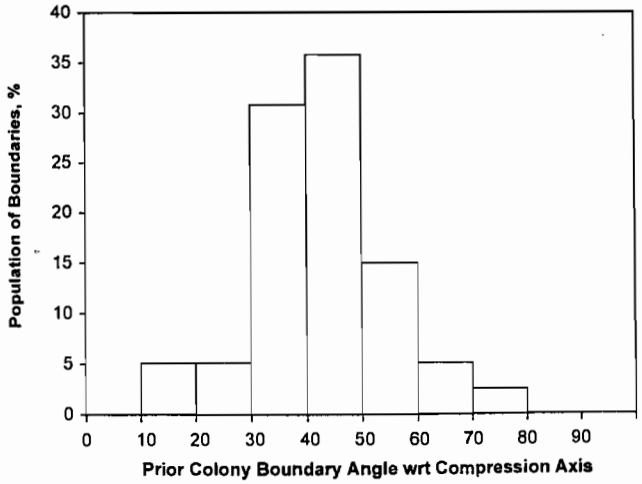

Fig. 9. Statistical distribution of the prior colony boundary orientation with respect to the compression axis in a sample deformed at 950°C and 0.05 s^{-1}.

conditions. The PCB structure will be stable up to a certain temperature and the sliding of these boundaries results in LGSP when the strain at their triple junctions is accommodated by self diffusion of β-phase atoms. In view of the smaller degrees of misorientation of the PCBs, the strain rate sensitivity of flow stress associated with their sliding is likely to be moderate and may not result in very large elongations as in conventional fine-grained superplasticity. Also, as observed in the conventional superplastic materials, there is always a possibility for nucleation of cavities at the prior colony triple junctions due to a mismatch between sliding rate and accommodation rate as may be the case just at the transus, leading to a ductility dip. At very high (>1050°C) temperatures, however, the prior colony substructure will be unstable and prevents the occurrence of LGSP.

3.2.6. Contiguity of mechanisms over the temperature range 750–1100°C

As discussed earlier, the power dissipation map exhibits a single domain over the entire range of test temperature when the strain rate is below 0.1 s^{-1}. The domain consists of different processes including shear cracking, globularization, void nucleation and LGSP. The similarity in the efficiency of power dissipation requires that there should be a contiguity between the mechanisms as the temperature is increased and that they should occur under similar conditions of strain rate and state-of-stress. At lower temperatures, shear cracking occurs at the prior β boundaries due to a stress concentration caused by sliding of soft β layer. As the temperature is increased, the stress concentration is relieved by the occurrence of DRX of primary α at the boundary. Simultaneously, the shearing of platelets in the Widmanstätten colony will also take place leading to globularization. Further increase in temperature causes an increase in the β volume fraction and when it is beyond 50–60%, the increase is very steep until the transus (β approach curve) [4]. Thus, around the transus region, β deformation mechanism decides the flow behavior which consists of sliding of prior colony boundaries. Whether void nucleation occurs or not depends on the rate of diffusional flow and the stability of the prior colony boundaries. The rate of diffusion in β phase at the transus may not be sufficient to accommodate the stress concentration at the triple junctions and due to this a distinct possibility for void nucleation exists. At temperatures well within the β phase field, the rate of diffusion increases and mitigates void nucleation giving rise to LGSP. However, beyond a critical temperature, the prior colony structure itself will not be sufficiently stable to contribute to strain and results in a drop in the ductility. It may be noted that the presence of shear stress and lower strain rates are essential requirements for the occurrence of all the above mechanisms responsible for the contiguity.

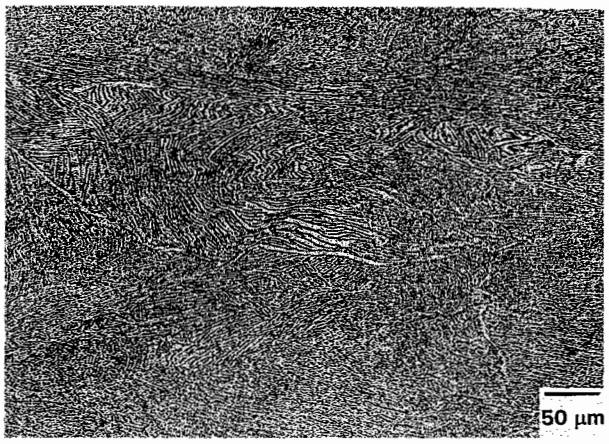

Fig. 10. Microstructure of specimen deformed at 950°C and 10 s^{-1}. The compression axis is vertical.

Deformation mechanisms in ELI Ti-6-4 are also temperature dependent when the strain rate is above 0.1 s^{-1}. In the lower $\alpha+\beta$ temperature range, the material exhibits flow localization and cracking as the strain rate is increased. This is discussed further in the next section. In the intermediate $\alpha+\beta$ temperature range, the microstructure of the deformed specimens exhibit kinking of lamellae in the colony structure which is not very sensitive to increase in strain rate. Typical microstructure of specimen deformed at 950°C and 10 s^{-1} is shown in Fig. 10. In the higher temperature range, it is likely that β undergoes dynamic recovery at higher strain rates since the occurrence of LGSP will be restricted by the absence of PCB sliding.

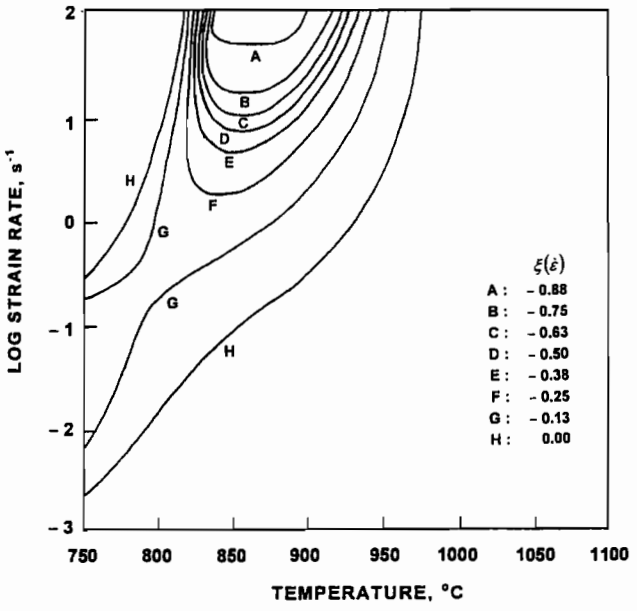

Fig. 11. Instability map obtained on ELI Ti-6-4 at a strain of 0.5.

3.3. Flow instabilities

The instability map developed using the criterion given by Eq. (2) is shown in Fig. 11. The map shows that a large regime of flow instability occurs at temperatures lower than 950°C and strain rates higher than 0.01 s^{-1} in the α–β range. The instability regime is validated with the help of microstructural observations on deformed specimens under various conditions (Fig. 12(a–i)). These microstructures exhibit flow localization bands which become diffused with increasing temperatures and decreasing strain rates and confirm the predictions of the instability criterion Eq. (2). The formation of these bands may be attributed to the adiabatic conditions created during deformation and low thermal conductivity of Ti-6-4. During deformation at higher strain rates, the heat generated due to plastic deformation is not conducted away since the time available is too short. As the flow stress is lower at higher temperatures, further deformation is preferred in this band thereby causing localization. The localized flow causes a microstructural change in the band region which reveals very fine grains (Fig. 12) presumably formed due to recrystallization after dynamic recovery.

At low temperatures (< 800°C) and very high strain rates (> 1 s^{-1}), the microstructures showed that the flow localization is very intense and causes cracking along the adiabatic shear band (Fig. 12(a) and (b)). As expected, the continuum criterion for flow instability breaks down when such cracking occurs. Instead, the power dissipation map (Fig. 3) exhibits a steep efficiency hill corresponding to this regime with a peak efficiency of 39% at 750°C/100 s^{-1}.

4. Conclusions

From the processing maps generated in the temperature range 750–1100°C and strain rate range 0.001–

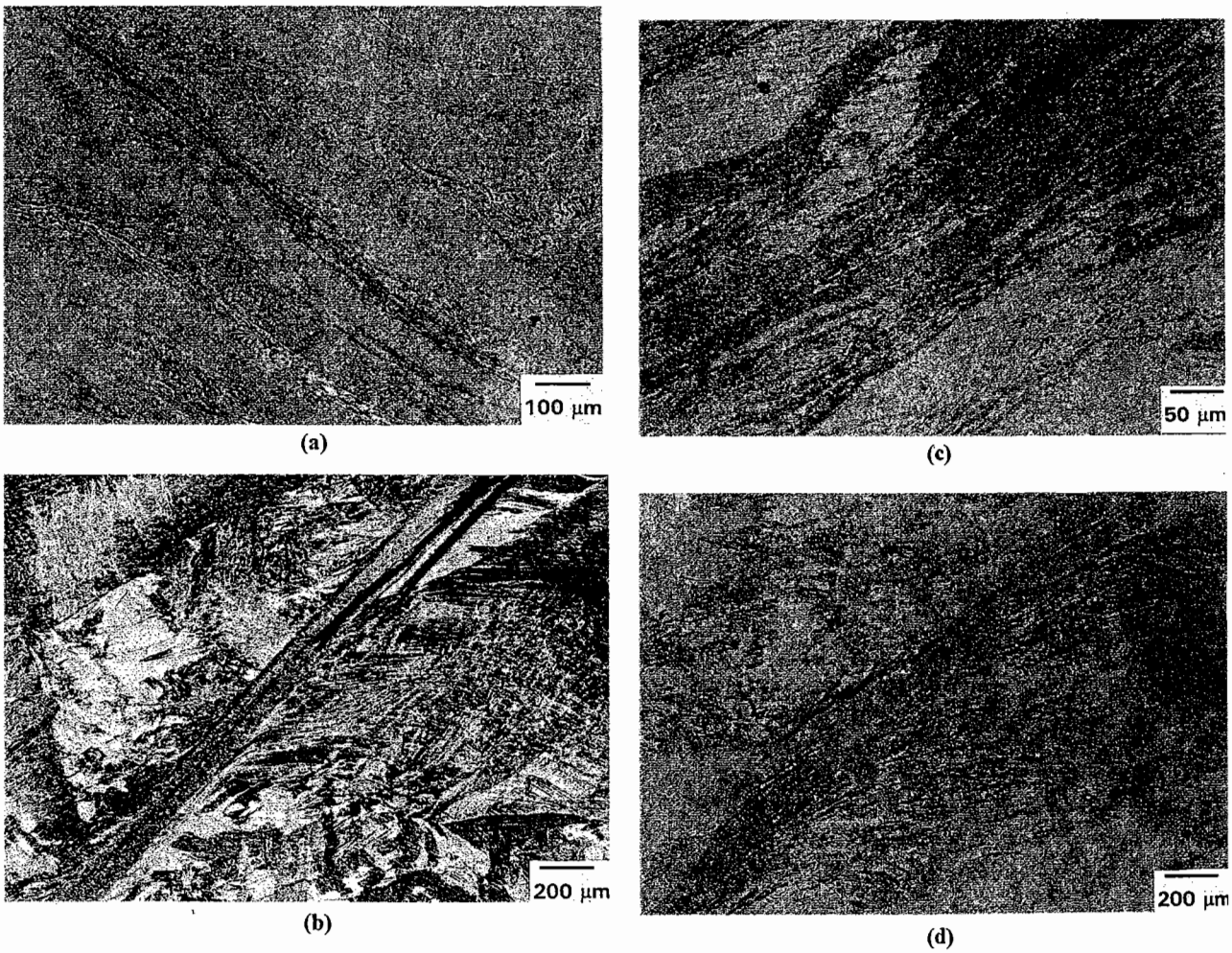

Fig. 12. Microstructures of ELI Ti-6-4 specimens exhibiting flow instabilities: (a) deformed at 750°C/10 s^{-1}; (b) 750°C/100 s^{-1}; (c) 800°C/1 s^{-1}; (d) 800°C/10 s^{-1}; (e) 800°C/100 s^{-1}; (f) 850°C/1 s^{-1}; (g) 850°C/10 s^{-1}; (h) 850°C/100 s^{-1}; (i) 900°C/100 s^{-1}; and (j) 950°C/100 s^{-1}. The compression axis is vertical.

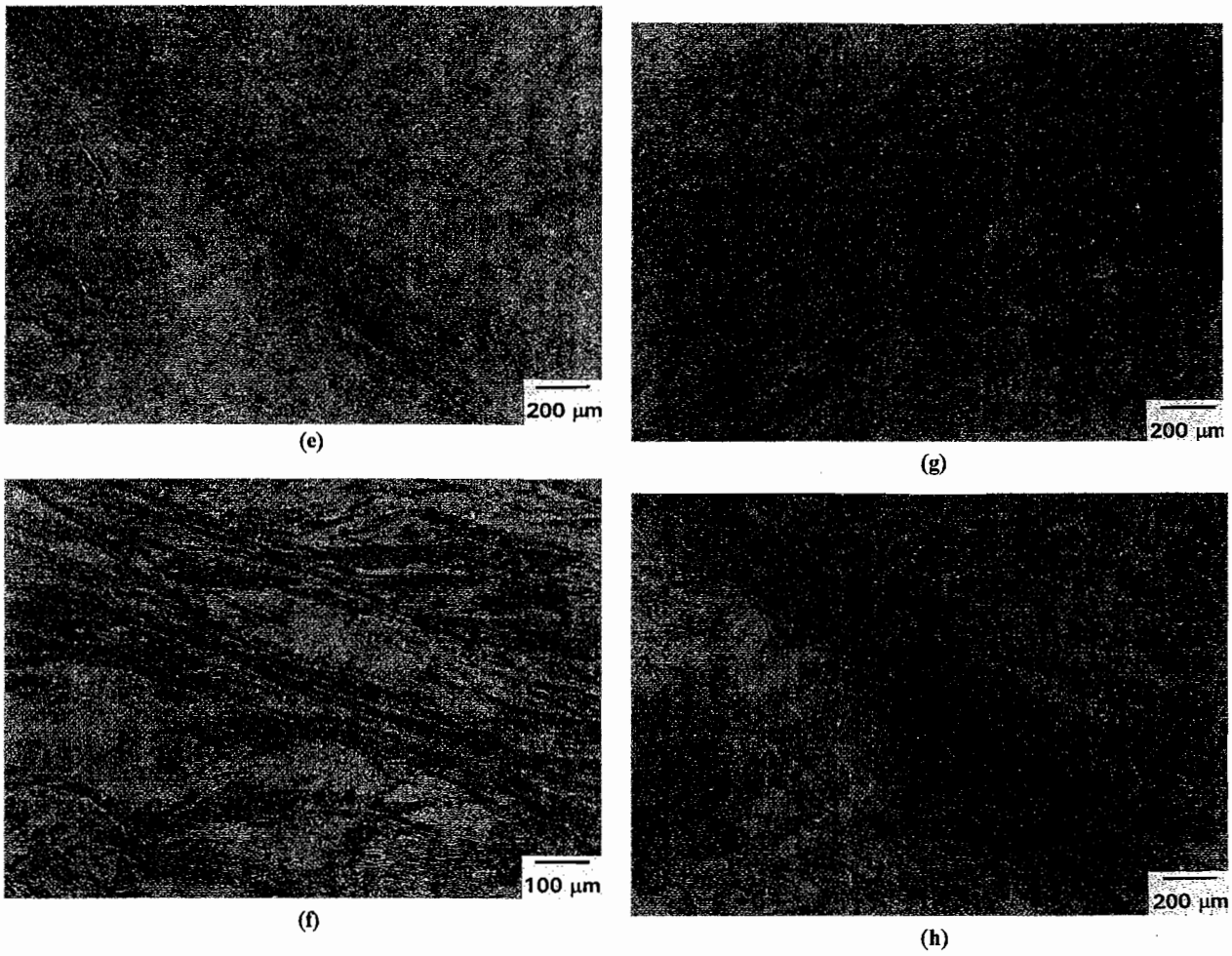

Fig. 12. (*Continued*)

100 s^{-1} on ELI grade Ti-6-4 with Widmanstätten preform microstructure, the following conclusions are drawn:

(1) The material exhibits cracking at prior β grain boundaries when deformed at lower temperatures (< 800°C) and slower strain rates (< 0.1 s^{-1}).

(2) Strain dependent globularization occurs in the temperature range 850–950°C and at strain rates below 0.1 s^{-1}. This mechanism assumes considerable importance during ingot conversion stage.

(3) The β phase exhibits large-grained superplasticity which occurs by the sliding of prior colony boundaries with simultaneous diffusion accommodated flow.

(4) At the transus and lower strain rates, a dip in tensile ductility occurs indicating that voids may be nucleating during deformation.

(5) The material exhibits flow instabilities at lower temperatures (< 950°C) and higher strain rates (> 0.1 s^{-1}) in the α–β range which manifest in the form of adiabatic shear bands. At very high strain rates cracking occurs along the bands.

Acknowledgements

One of the authors (Y.V.R.K. Prasad) is thankful to the National Research Council, USA, for awarding him an associateship and to the Director of the Indian Institute of Science, Bangalore, for granting him a sabbatical leave. The assistance rendered by S. Sasidhara and R. Ravi of Department of Metallurgy, Indian Institute of Science is gratefully acknowledged.

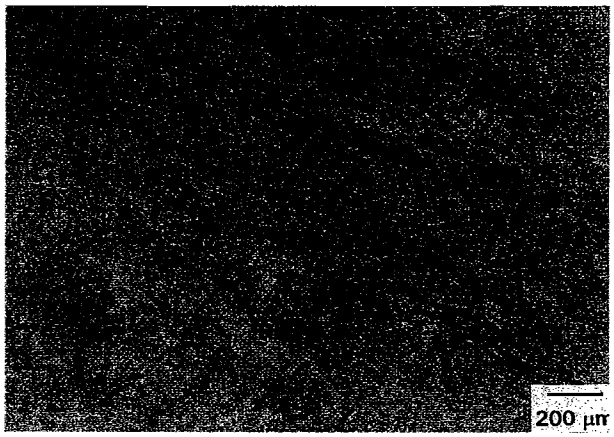

(i)

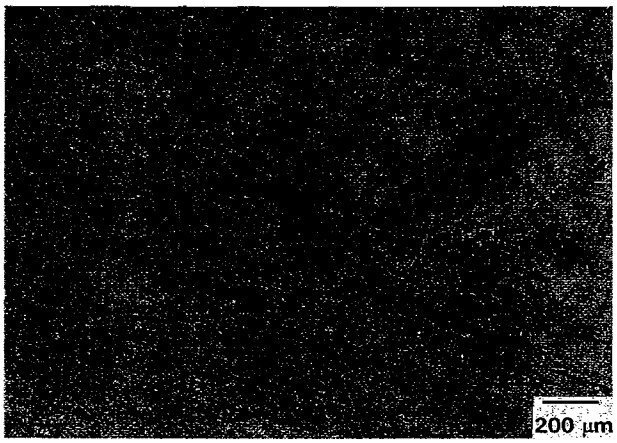

(j)

Fig. 12. (*Continued*)

References

[1] R. Boyer, G. Welsch, E.W. Collings (Eds.), Materials Properties Handbook: Titanium Alloys, ASM International, Materials Park, OH, 1994, 488 pp.

[2] Y.V.R.K. Prasad, T. Seshacharyulu, Mater. Sci. Eng. A243 (1998) 82.

[3] D. Lee, W.A. Backofen, Trans. AIME 239 (1967) 1034.

[4] M.T. Cope, N. Ridley, Mater. Sci. Technol. 2 (1986) 140.

[5] M.W. Mohoney, in: R. Boyer, G. Welsch, E.W. Collings (Eds.) Materials Properties Handbook: Titanium Alloys, ASM International, Materials Park, OH, 1994, 1101 pp.

[6] S.L. Semiatin, V. Seetharaman, I. Weiss, Mater. Sci. Eng. A243 (1998) 1.

[7] S.L. Semiatin, V. Seetharaman, A.K. Ghosh, E.B. Shell, M.P. Simon, P. Fagin, Mater. Sci. Eng. A256 (1998) 92.

[8] S.L. Semiatin, R.L. Goetz, E. B. Shell, V. Seetharaman, A.K. Ghosh, Metall. Mater. Trans. 30A (1999) 1411.

[9] Y.V.R.K. Prasad, Ind. J. Technol. 28 (1990) 435.

[10] Y.V.R.K. Prasad, Metall. Mater. Trans. 27A (1996) 235.

[11] Y.V.R.K. Prasad, T. Seshacharyulu, Intl. Mater. Rev. 43 (1998) 243.

[12] Y.V.R.K. Prasad, S. Sasidhara (Eds.), Hot Working Guide: A Compendium of Processing Maps, ASM International, Materials Park, OH, 1997.

[13] H. Ziegler, in: I.N. Sneddon, R. Hill (Eds.) Progress in Solid Mechanics, vol. 4, North-Holland, Amsterdam, 1963, 93 pp.

[14] H.G. Suzuki, H. Fujii, N. Takano, K. Kaku, in: P. Lacombe, R. Tricot, G. Béranger (Eds.), Sixth World Conference on Titanium, Societé Francaise de Metallurgie, Les Ulie Cedex, France, 1988, 1427 pp.

[15] H.L. Gegel, J.C. Malas, S.M. Doraivelu, V.A. Shende, in: Metals Handbook, vol. 14, ASM International, Materials Park, OH, 1101 pp.

[16] N. Ridley, AGARD Lecture Series No. 168, chapter 4, France, 1989.

[17] T.G. Nieh, J. Wadsworth, O.D. Sherby, Superplasticity in Metals and Ceramics, 1997, Cambridge University Press.

[18] D. Padmavardhani, Y.V.R.K. Prasad, Mater. Sci. Technol. 7 (1991) 947.

[19] P. Griffiths, C. Hammond, Acta Metall. 20 (1972) 935.

[20] P.K. Sagar, D. Banerjee, K. Muraleedharan, Y.V.R.K. Prasad, Metall Trans. 27A (1996) 2593.

[21] T.G. Nieh, W.C. Oliver, Scr. Metall. 23 (1989) 851.

[22] D. Lin, A. Shan, Y. Liu, D. Lin, Scr. Metall Mater. 33 (1995) 681.

JMEPEG (2000) 9:153-160

Effect of Prior β-Grain Size on the Hot Deformation Behavior of Ti-6Al-4V: Coarse vs Coarser

Y.V.R.K. Prasad, T. Seshacharyulu, S.C. Medeiros, and W.G. Frazier

(Submitted 18 August 1999; in revised form 14 September 1999)

The hot deformation behavior of extra low interstitial (ELI) grade Ti-6Al-4V with a transformed β-preform microstructure was studied in coarse (0.5 to 1 mm) and coarser (2 to 3 mm) (prior β) grained materials using hot compression testing in the temperature range of 750 to 1100 °C and a strain rate range of 0.001 to 100 s^{-1}. Processing maps were developed on the basis of the flow stress data as a function of temperature and strain rate. The maps revealed that the domain of globularization of the lamellar structure and region of large grained superplasticity of β were not influenced by the prior β-grain size. However, the regimes of cracking at the prior β-grain boundaries occurring at lower temperatures and strain rates and the flow instability occurring at lower temperatures and higher strain rates were both wider for the coarse grained material than the coarser grained material. The β- instability regime, however, was more pronounced in the coarser grained material. From the hot workability viewpoint, the present results show that there is no remarkable benefit in refining the prior β-grain size. On the contrary, it will somewhat restrict the workability domain by widening the adjacent regimes, causing microstructural damage.

Keywords grain size, hot processing, titanium, Ti-6Al-4V alloy

1. Introduction

The Ti-6Al-4V is a two-phase titanium alloy with a β transus ($\alpha + \beta \rightarrow \beta$) in the temperature range of 970 to 1020 °C depending on the interstitial impurity (primarily oxygen) content. The alloy is extensively used in the aerospace industry, and the extra low interstitial (ELI) grade is preferred for applications where high fracture toughness is an important requirement.[1] The primary processing of Ti-6Al-4V ingots generally involves hot working in the β range, air cooling to obtain a transformed β microstructure, and mechanical working in the α-β range to obtain fine grained equiaxed ($\alpha + \beta$) structure. Such a microstructure results in good fracture toughness and low cycle fatigue properties. Conversely, the transformed β microstructure consists of acicular or lamellar morphology depending on the rate of cooling from the β-solutionizing temperature, and this type of microstructure results in good creep resistance and high temperature strength. Air cooling, for example, produces Widmanstätten colonies of ($\alpha + \beta$) lamellae within large prior β grains with their boundaries containing a thin primary α layer. The prior β-grain size has an influence on the mechanical properties, and sizes below about 200 μm are considered desirable.[2] In view of faster diffusion rates, hot working in the β range produces very coarse prior β grains, and refinement by β recrystallization often requires interspacing the β forging with a few steps of α-β forging. While a finer prior β-grain size is beneficial for the mechanical properties in the heat-treated component, its influence on the hot workability in the α-β regime is not clearly understood. Semiatin *et al.*[3] reported that the reduction in hot ductility with a decrease in temperature is greater for larger prior β-grain sizes, and the ductility trough is deeper. Suzuki *et al.*[4] explained such an effect in terms of void formation and growth occurring during sliding at the thin β layer in between the primary alpha and the Widmanstätten sideplates. While the prior β-grain size is expected to have an effect on the fracture processes occurring at the prior β-grain boundaries, it is important to understand its influence on all the mechanisms that influence hot workability. The goal of this study was to examine the effect of prior β-grain size on the overall hot working behavior of Ti-6Al-4V with a transformed β-starting (Widmanstätten) microstructure. For this purpose, studies were conducted on coarse vs coarser prior β structures of an ELI grade Ti-6Al-4V.

In this study, the approach of processing maps was adopted to represent and analyze the constitutive behavior of Ti-6Al-4V during hot deformation. The basis and principles of this approach have been described elsewhere,[5,6] and its application to the hot working of a wide range of materials has been compiled recently.[7] In brief, depicted in a frame of temperature and strain rate, power dissipation maps represent the pattern in which power is dissipated by the material through microstructural changes. The rate of this change is given by a dimensionless parameter called the efficiency of power dissipation:

$$\eta = \frac{2m}{m+1} \qquad \text{(Eq 1)}$$

where m is the strain rate sensitivity of flow stress. Over this frame is superimposed a continuum instability criterion for identifying the regimes of flow instabilities, developed on the basis of extremum principles of irreversible thermodynamics as applied to large plastic flow[8] and given by another dimensionless parameter:

$$\xi(\dot{\varepsilon}) = \frac{\partial \ln(m/m+1)}{\partial \ln \dot{\varepsilon}} + m \qquad \text{(Eq 2)}$$

where $\dot{\varepsilon}$ is the applied strain rate. Flow instabilities are predicted to occur when $\xi(\dot{\varepsilon})$ is negative. These two maps together consti-

Y.V.R.K. Prasad, T. Seshacharyulu, S.C. Medeiros, and **W.G. Frazier** Materials Process Design Branch, Materials and Manufacturing Directorate, Air Force Research Laboratory, Wright-Patterson Air Force Base, OH 45433.

tute a processing map that exhibits domains with local efficiency maxima representing certain specific microstructural mechanisms together with regimes of flow instabilities.

2. Experimental Procedures

2.1 Materials

The Ti-6Al-4V alloy used in this investigation was of an ELI grade and had the following composition (wt.%): 6.04-Al, 3.91-V, 0.13-O, 0.08-Fe, 0.008-N, with titanium balance. The β transus for this material was about 970 °C. The alloy was upset forged in the β range at 1180 °C, α-β cogged at 960 °C, and β cogged at 1080 °C, followed by water quench. Due to differential deformation history from the surface to the center, different prior β-grain sizes were produced in the cogged billet. The center region of the billet had a prior β-grain size in the range 2 to 3 mm (called "coarser" hereafter), while the surface region had a range of about 0.5 to 1.0 mm (called "coarse" hereafter). Figures 1(a) and (b) show the initial microstructures of these two grain sizes. It can be noted that minor variations in the thickness of the primary α layer at the prior β boundary and in the size of the Widmanstätten colonies also existed in these microstructures.

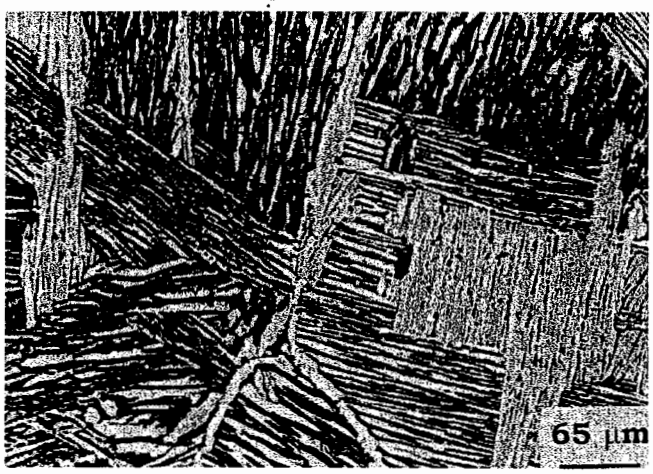

(a)

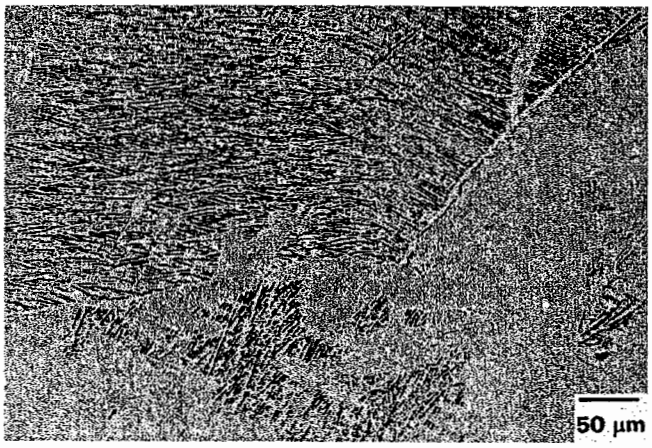

(b)

Fig. 1 Initial microstructures of Ti-6Al-4V used for testing: (**a**) coarser (2 to 3 mm) and (**b**) coarse (0.5 to 1 mm) prior β-grain sized material

2.2 Hot Compression Testing

Isothermal, constant true strain rate compression tests were conducted using a servohydraulic testing machine over the temperature range of 750 to 1100 °C at 50 °C intervals and at constant true strain rates 0.001, 0.01, 0.1, 1, 10, and 100 s^{-1}. Specimens of 15 mm height and 10 mm diameter were used for testing in the α-β range, while larger specimens of 22.5 mm height and 15 mm diameter were used to obtain accurate flow stress measurements in the β range. The specimens were coated with a borosilicate glass paste for lubrication and environmental protection. They were deformed to half the height in each case to impose a true strain of about 0.7 and were air cooled to room temperature after deformation. The deformed specimens were sectioned parallel to the compression axis and prepared for microstructural examination using standard techniques. The specimens were etched with Kroll's reagent, and polarized light micrographs were recorded.

2.3 Flow Stress Data Analysis

The load-stroke data obtained from the compression tests were processed to obtain true stress-true plastic strain curves using the standard method. The data were corrected for adiabatic temperature rise (significant at higher strain rates) using a linear interpolation between ln (σ) and ($1/T$), where σ is flow stress and T is temperature in Kelvin. The strain rate sensitivity, m, was computed using a spline interpolation between ln (σ) and ln ($\dot{\varepsilon}$), and this procedure was repeated at different temperatures. The power dissipation efficiency parameter and instability parameter were calculated as a function of temperature and strain rate at different strains as per Eq 1 and 2, respectively, and were plotted in the temperature-strain rate plane to obtain power dissipation and instability maps.

3. Results and Discussion

3.1 Stress-Strain Behavior

Figures 2 and 3 show the true stress-true plastic strain curves obtained on the coarse and coarser grained Ti-6Al-4V at 800 °C (α-β range) and 1100 °C (β range), respectively. In the α-β range (Fig. 2a and b), the curves exhibited continuous flow softening, which is typically observed in transformed β microstructures.[9] It can be noted that at lower strain rates (<0.1 s^{-1}), the extent of flow softening is not dependent on the prior β-grain size, while at higher strain rates, the flow softening is more prominent in the coarse grained material (Fig. 2b) than in the coarser material. Differences with grain size are also observed in the β-deformation range (Fig. 3a and b). In the coarse grained material (Fig. 3b), steady-state, stress-strain curves were obtained at strain rates below about 1 s^{-1} with similar behavior observed in the coarser material at strain rates below about 0.1 s^{-1}. A significant difference is observed at higher strain rates where the curves exhibited broad oscillations that are more striking and have extended to lower strain rates in the coarser material (Fig. 3a).

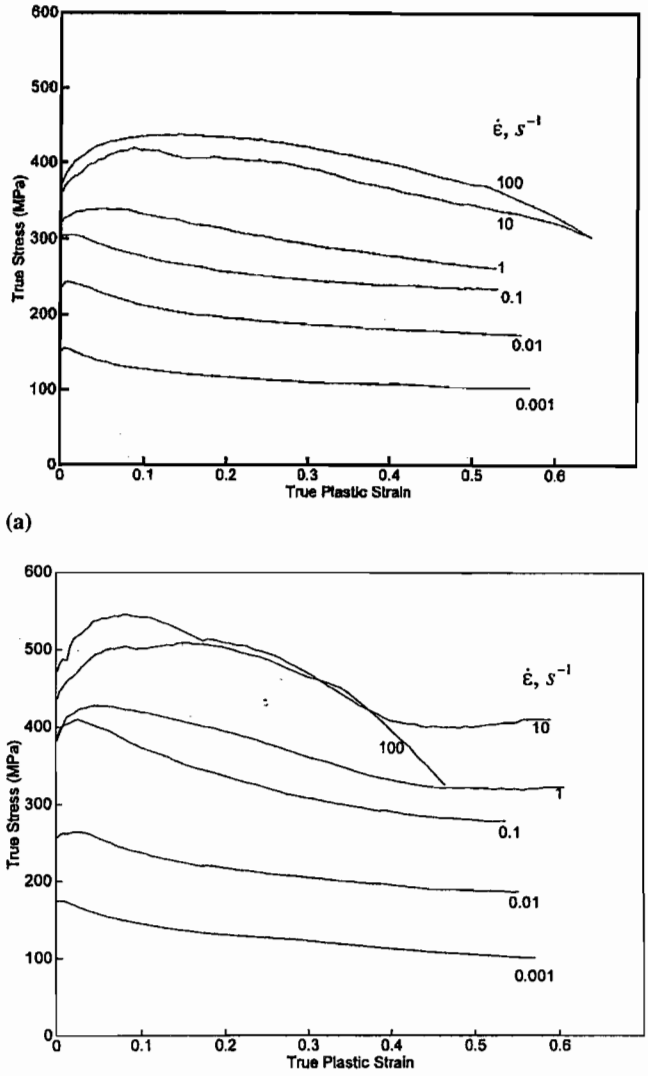

Fig. 2 Flow curves obtained on Ti-6A1-4V in the α-β regime (800 °C) and different strain rates: (**a**) coarser grained material and (**b**) coarse grained material

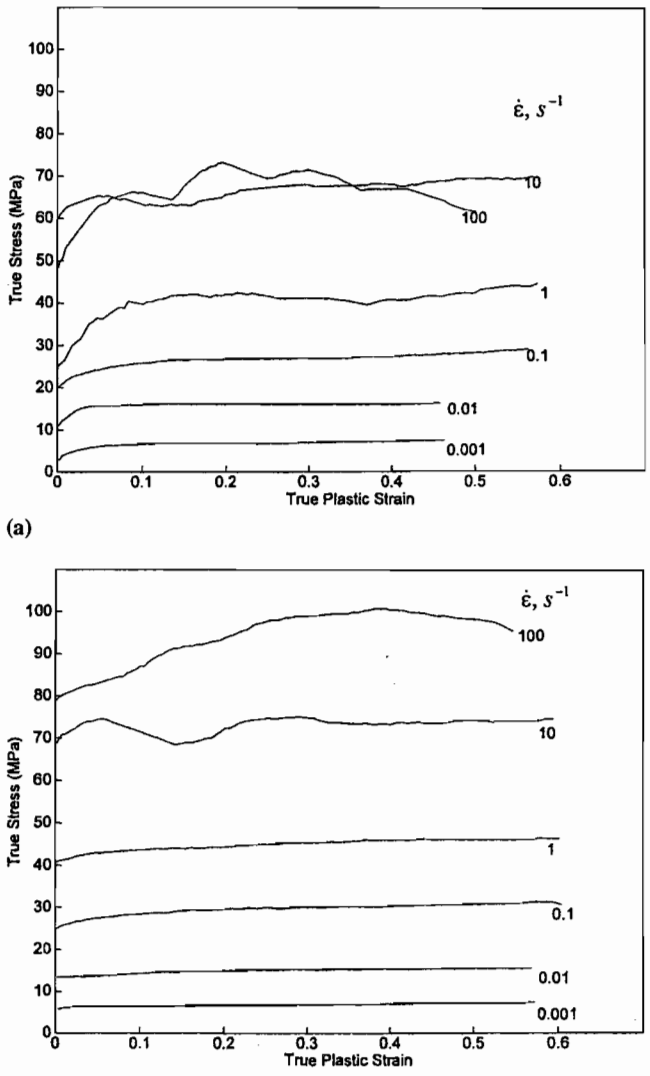

Fig. 3 Flow curves obtained on Ti-6A1-4V in the β regime (1100 °C) and different strain rates: (**a**) coarser grained material and (**b**) coarse

3.2 Processing Maps

The processing maps obtained on the two grain sizes corresponding to a true plastic strain of 0.5 are shown in Fig. 4(a) and (b). The contour numbers in the map represent the percent of efficiency of power dissipation (Eq 1), and the shaded area represents the regime where flow instability is predicted (Eq 2). The maps obtained at lower strains are not significantly different from those presented in Fig. 4, suggesting that strain within this range does not have a major influence.

The map for the coarser grained material (Fig. 4a) exhibits a single domain at strain rates lower than about 1.0 s^{-1} and over a wide temperature range with a local efficiency maximum of about 46%. The map also reveals two regimes of flow instability—one at temperatures below about 825 °C (α-β range) and strain rates above 0.1 s^{-1} and the other at temperatures higher than about 1050 °C (β range) and strain rates above 10 s^{-1}.

The single domain occurring at lower strain rates covers both the α-β and the β ranges, and therefore, must represent the mechanisms of hot deformation of (α+ β) and β-phase microstructures. In general, the map delineates the temperature of phase transformation by exhibiting points of inflexion (change in the curvature) in the contours around this temperature.[7] In the present case, such inflexions are not clearly evident, and this result is interpreted in terms of merging of domains with similar efficiencies of power dissipation across the transus. At the transus, such a merging has been attributed[10] to the sliding of intercolony boundaries that may cause void nucleation at their triple junctions. Such a process will have an efficiency of power dissipation similar to the adjacent processes and will result in a sharp drop in the tensile ductility.

3.3 Globularization Domain

In the α-β regime, the microstructures recorded on the deformed specimens exhibited globularization of the lamellar microstruc-

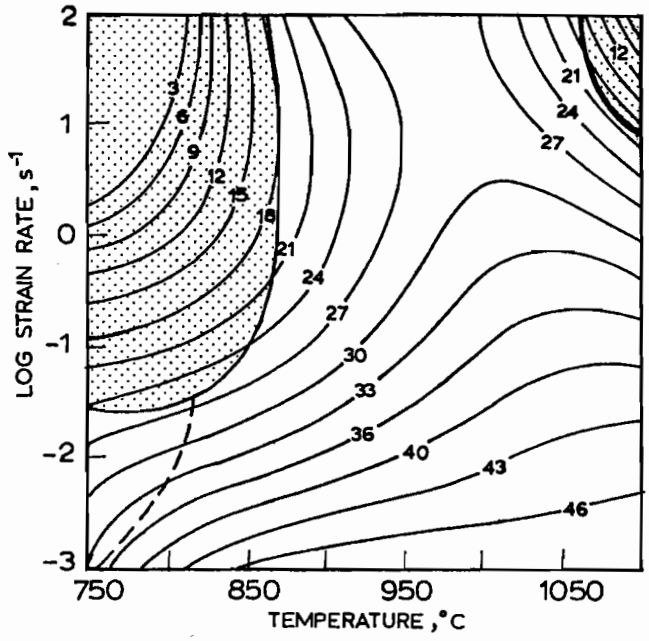

(a)

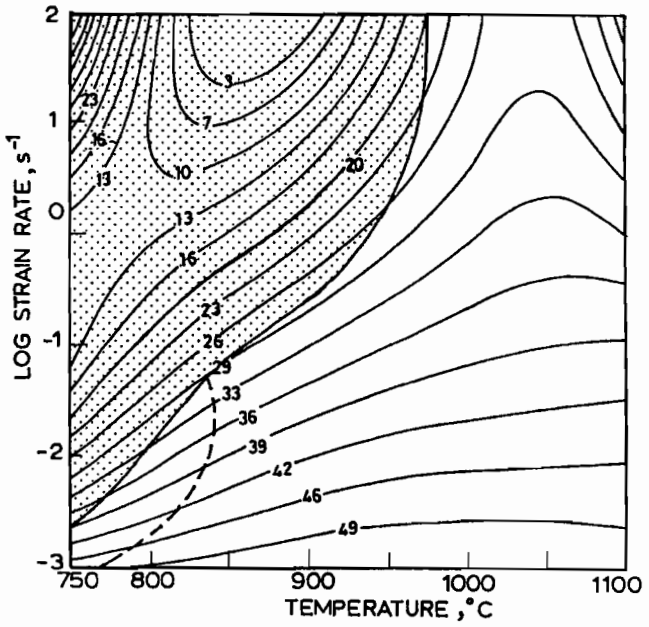

(b)

Fig. 4 Processing maps obtained on Ti-6A1-4V at a true plastic strain of 0.5: **(a)** coarser grained material and **(b)** coarse grained material. Contour numbers represent percent efficiency of power dissipation. Shaded region corresponds to flow instability. Dotted boundary represents the upper limits of prior β-boundary cracking

ture. Figure 5(a) shows a typical specimen, which corresponds to a coarser grained specimen deformed to a true strain of about 0.7 at 900 °C and 0.001 s^{-1}. In this domain, the extents of globularization and the globular size are less at lower temperatures and higher strain rates. The mechanism of globularization has been discussed elsewhere.[10] Briefly, the process consists of shearing of the lamellae, which are favorably oriented to the stress axis; simultaneous occurrence of dynamic recovery by cross-slip to

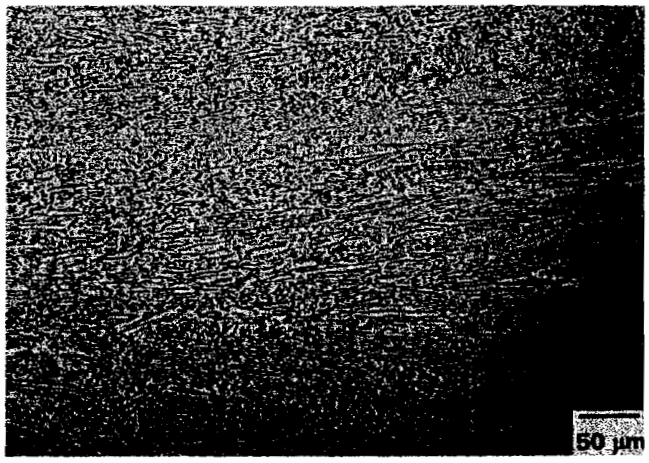

(a)

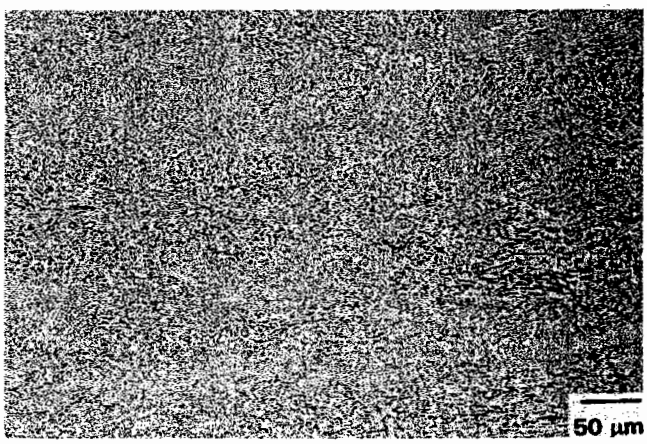

(b)

Fig. 5 Microstructures obtained on Ti-6A1-4V specimens deformed at 900 °C and 0.001 s^{-1} exhibiting globularization of lamellar structure: **(a)** coarser grained material and **(b)** coarse grained material

nucleate an interface; and migration of the interfaces to form globules for reducing the total interface energy. The rate controlling step, however, was evaluated to be the occurrence of the cross-slip.[11] On the basis of the temperature dependence of flow stress, which follows the kinetic rate equation given by

$$\dot{\varepsilon} = A\sigma^n \exp(-Q/RT) \qquad \text{(Eq 3)}$$

where $\dot{\varepsilon}$ is the strain rate, A is a constant, σ is the flow stress, n is the stress exponent, Q is the activation energy, R is the gas constant, and T is the temperature, the apparent activation energy for the globularization process has been calculated. Figure 6 shows the Arrhenius plot, demonstrating the variation of flow stress with temperature at a strain rate of 0.001 s^{-1}, which confirms the validity of Eq 3 and shows that the apparent activation energy is approximately 394 kJ/mole for this process.

Figure 4(b) shows the processing map for the coarse grained material, which exhibits two domains. The first domain is at lower strain rates (<0.1 s^{-1}) covering a wide temperature range with a local maximum of efficiency of power dissipation of about 49%. This domain is very similar to the domain described previously for

the coarser grained material (Fig. 4a). The second domain occurs at temperatures lower than 800 °C and at strain rates higher than about 1 s^{-1}, which is actually in the regime of flow instability as predicted by the criterion given by Eq 2. The mechanism occurring in the second domain is discussed in a following section along with the manifestations of flow instabilities. Regarding the instability regime, the coarse grained material exhibited a much wider area of flow instability in the α-β range than did the coarser grained material, but in the β range, the deformation was free from flow instabilities in the coarse grained material unlike in the coarser grained material.

The interpretation of the lower strain rate domain in the processing map for the coarse grained material (Fig. 4b) is similar to that described above and consists of two deformation mechanisms in the α-β and β regimes merging at the transus. The microstructural features of a coarse grained specimen deformed in the α-β range (900 °C and 0.001 s^{-1}) are shown in Fig. 5(b), which exhibits globularization very similar to that observed in the coarser grained material (Fig. 5a). The Arrhenius plot for the coarse grained material is shown in Fig. 6, which yields apparent activation energy values similar to those obtained on the coarser grained material. Thus, the domain of globularization and its characteristics are not significantly affected by changing the grain size from coarser to coarse as can be expected from the intragranular nature of the mechanism.

3.4 Prior β-Cracking Regime

Additional microstructural investigations have revealed that at temperatures below about 800 °C and strain rates lower than about 0.1 s^{-1}, cracking at the prior β boundaries has occurred and a majority of cracks are found at the bulge regions of the compression specimen. Figure 4(a) schematically shows the crocking regime as dotted lines on the processing map, and a typical microstructure is shown in Fig. 7(a), which corresponds to a coarser grained specimen deformed at 750 °C and 0.01 s^{-1}. These cracks occurred preferentially on boundaries which were near 45° orientation with respect to the compression axis and may be termed "shear" cracks. The mechanism of cracking was discussed in detail in an earlier publication.[10] The cracks nucleate at the soft β layer existing at the interface between the primary α layer and the colony sideplates of the prior β boundary and grow under a combined state of stress existing at the bulge region of the compression specimen. The limiting condition for mitigating the formation of cracks is the occurrence of dynamic recrystallization of the primary α at the prior β boundary, which is ensured at higher temperatures and lower strain rates.

The regime of prior β cracking for the coarse grained material is shown schematically in Fig. 4(b), and this regime is wider than that in the coarser grained material (Fig. 4a). Figure 7(b) shows typical microstructure of a coarse grained specimen deformed at 750 °C and 0.01 s^{-1}, and the features of cracking such as its origin and orientation with respect to the compression axis are similar to those of the coarser material. The wider regime in the map for the coarse grained material can be attributed to the increased probability of the prior β boundaries with the near 45° orientation,

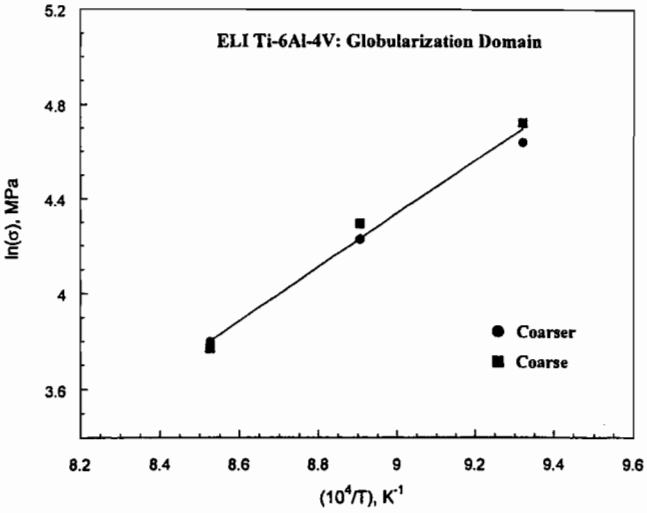

Fig. 6 Arrhenius plot showing the variation of the flow stress with the inverse of temperature in the globularization domain of Ti-6Al-4V

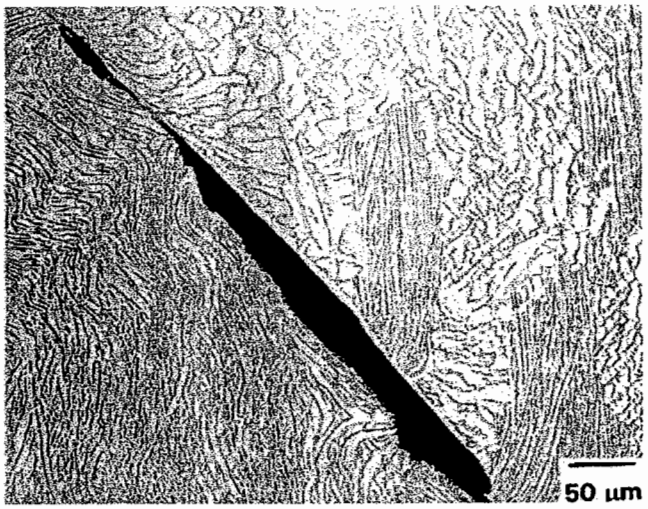

(a)

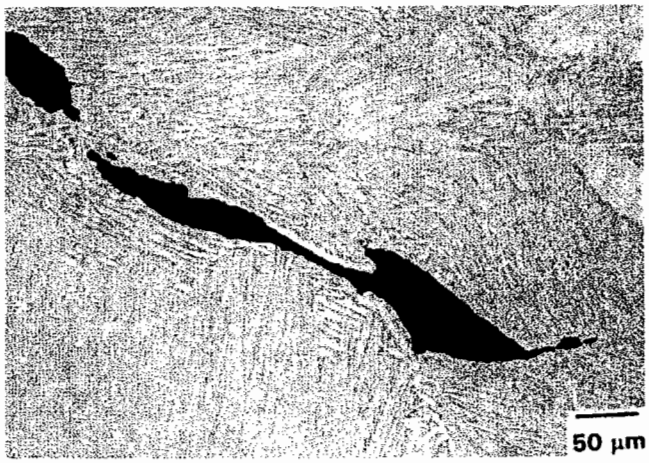

(b)

Fig. 7 Microstructures of Ti-6Al-4V specimens deformed at 800 °C and 0.01 s^{-1} exhibiting cracking at the prior β boundaries: **(a)** coarser grained material and **(b)** coarse grained material. The compression axis is vertical

which can help in enhancing the nucleation process. Thus, the results indicate that reducing the grain size from coarser to coarse grains is not beneficial from the point of view of prior β cracking because it restricts the globularization domain on the lower temperature side.

3.5 Mechanism of β-Deformation

The processing maps do not exhibit any specific domains in the β-deformation range because the power dissipation efficiencies are similar to those for the globularization domains. However, tensile ductility measurements in the β range have shown high elongations (≈100%) at a strain rate even as fast as 0.01 s^{-1}.[10] This suggests that mechanisms similar to those causing large grained superplasticity (LGSP) are responsible for the β deformation. The apparent activation energy for the process has been estimated using the kinetic rate equation.[3]

Figure 8 shows the Arrhenius plots using the data on the coarser and coarse grained materials in the β-temperature range. The plot yielded a value of about 256 kJ/mole, which is near that for self-diffusion in β titanium (153 kJ/mole),[12] suggesting that the process is controlled by diffusion. The prior β-grain size does not have much influence on the apparent activation energy. On the basis of high elongations, moderate strain rate sensitivity (≈0.3), the apparent activation energy values, and the steady-state stress-strain curves (Fig. 3), it can be concluded that LGSP is the most likely mechanism of β deformation. It is likely that the prior Widmanstätten colony boundaries within large β grains are stable during deformation and tend to slide under shear stress when their orientation is near 45° with respect to the compression axis. The sliding process contributes significantly to the total strain if the stress at their triple junctions is accommodated by diffusional flow, which is possible at higher temperatures (*e.g.*, 1050 °C). The characteristics of LGSP domain are not affected by the prior β-grain size as expected from the intragranular (within the β grains) nature of the mechanism as explained previously.

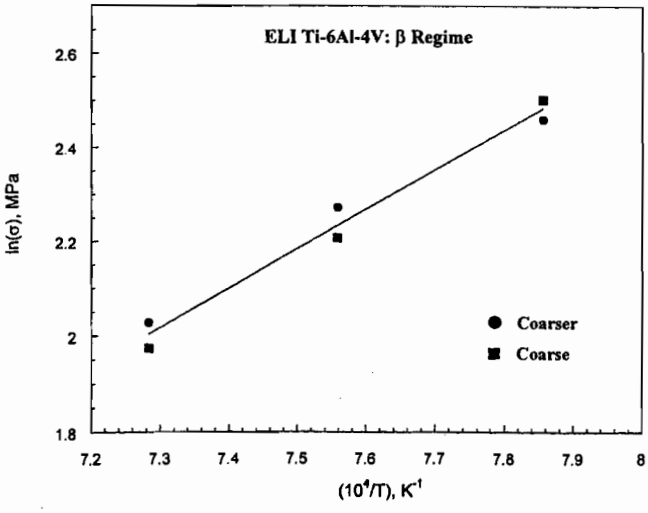

Fig. 8 Arrhenius plot showing the variation of the flow stress with the inverse of temperature in the β regime of Ti-6-4

3.6 Flow Instabilities

A comparison of the flow instability regimes in the processing maps for the coarse and coarser grained materials (Fig. 4a and b) reveals that the instability regime in the α-β range is wider in the coarse material than the coarser material, while that in the β regime occurs only in the coarser material. While the manifestation of the β instability is difficult to capture metallographically due to the phase transformation occurring during cooling of the specimen, the nature of the flow instabilities in the α-β regime can be studied in detail using microstructural observations.

Typical microstructures obtained on specimens deformed in the instability regime at 750 °C/100 s^{-1} and 850 °C/100 s^{-1} are shown in Fig. 9 and 10, respectively. In each of the figures, the micrographs for the coarser and coarse grained materials are compared. At 750 °C, intense adiabatic shear banding has occurred in both the materials, although the adiabatic shear bands resulted in cracking of the specimens in the coarse material (Fig. 9b), thereby showing a domain of high efficiency (Fig. 4b). The flow localization bands became increasingly diffused with increasing temperature (Fig. 9 vs Fig. 10). Figure 11 shows the microstructures recorded on specimens deformed at 850 °C/10 s^{-1}, and

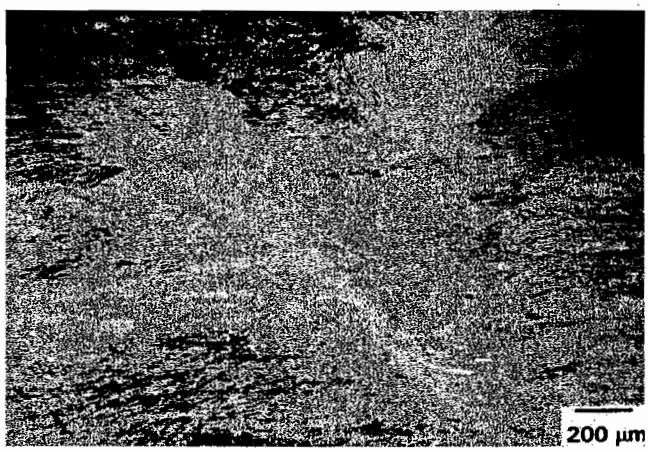

(a)

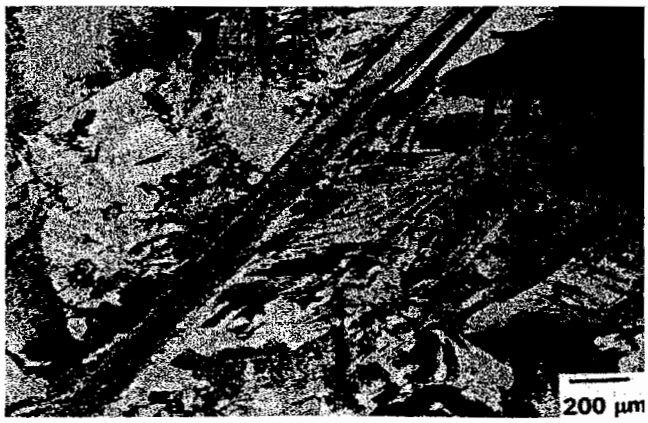

(b)

Fig. 9 Microstructures obtained on Ti-6A1-4V specimens deformed at 750 °C and 100 s^{-1}: **(a)** coarser grained material and **(b)** coarse grained material. The compression axis is vertical

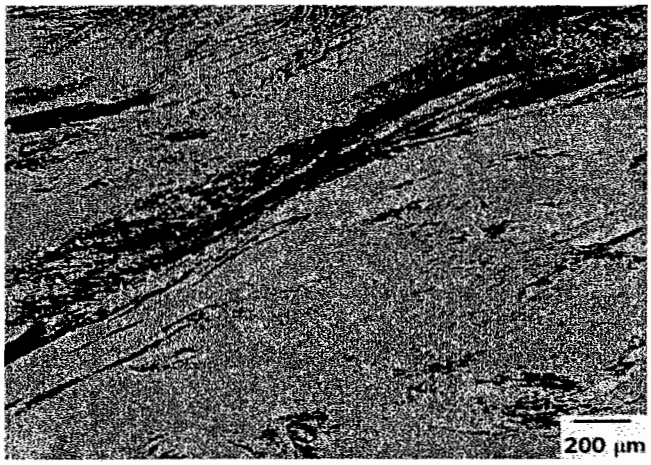

(a)

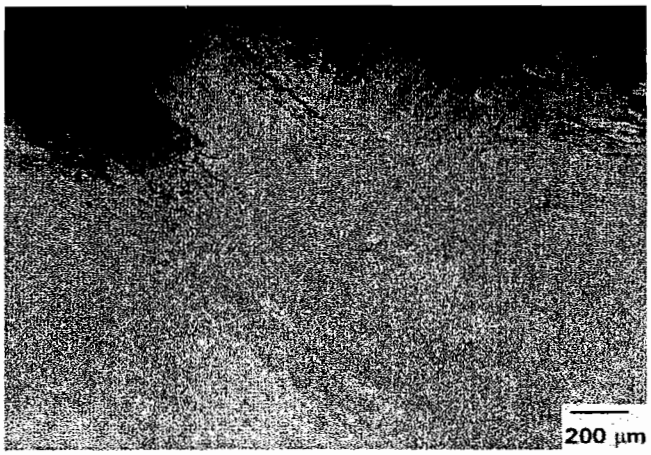

(b)

Fig. 10 Microstructures obtained on Ti-6A1-4V specimens deformed at 850 °C and 100 s^{-1}: **(a)** coarser grained material and **(b)** coarse grained material. The compression axis is vertical

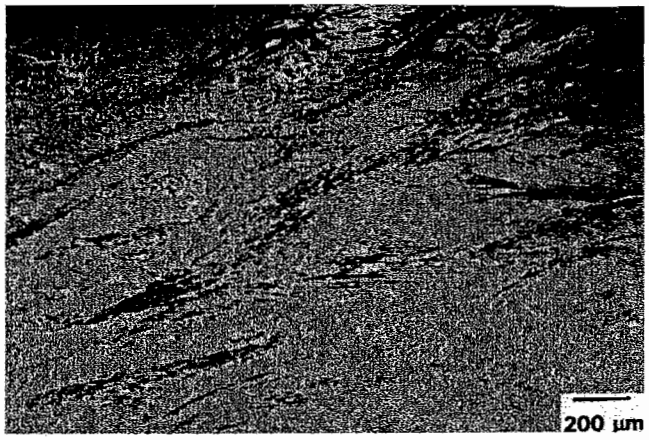

(a)

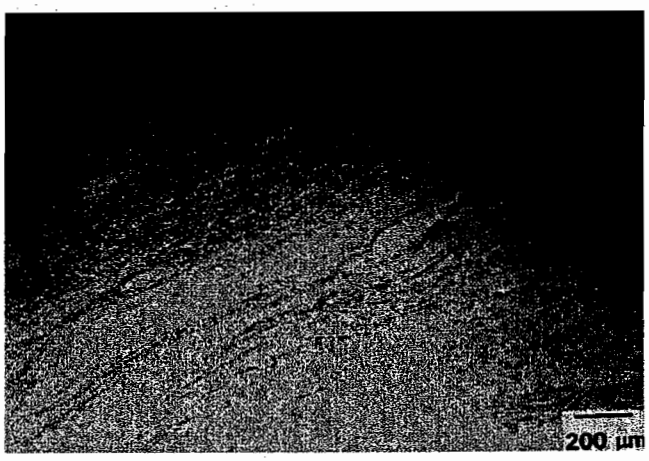

(b)

Fig. 11 Microstructures obtained on Ti-6A1-4V specimens deformed at 850 °C and 10 s^{-1}: **(a)** coarser grained material and **(b)** coarse grained material. The compression axis is vertical

a comparison with Fig. 10 reveals that the intensity of flow localization reduces with a decrease in strain rate.

The formation of the flow localization bands can be attributed to the adiabatic conditions created during deformation and the low thermal conductivity of Ti-6A1-4V. The heat generated at higher strain rates was not conducted away due to insufficient time, which reduces the flow stress locally leading to flow localization. In the case of coarser material, the higher temperature limit for flow instability is less by about 50 °C than that of the coarse material, and this difference can be attributed to the extent of flow softening observed in these two grain sizes (Fig. 2a and b). At strain rates higher than 1 s^{-1}, the coarse grained material has a much higher degree of flow softening than the coarser material.

Unlike the coarse grained material, the coarser material does not exhibit flow localization at temperatures higher than about 900 °C. A comparison of the microstructures of specimens deformed at 900 °C/100 s^{-1} is given in Fig. 12, which confirms the previous conclusion. Thus, the results on the instability analysis and microstructural validation show that the coarser grained material exhibits narrower regimes of flow instability in the α-β regime than does the coarse grained material. However, in the β-deformation range of coarser material, flow instabilities occur at strain rates higher than 10 s^{-1}.

4. Conclusions

The hot deformation behavior of ELI grade Ti-6A1-4V has been studied in coarse and coarser (prior β) grained specimens using processing maps in the temperature range 750 to 1100 °C and a strain rate range of 0.001 to 100 s^{-1}. The interpretations are validated by microstructural examination. The following conclusions can be drawn from this investigation on the influence of prior β-grain size.

- The process of globularization of the ($\alpha + \beta$) lamellae and the process of large grained superplasticity of the β phase are not significantly influenced by the prior β-grain size, because both the mechanisms are essentially intragranular in nature.
- The region of prior β-boundary cracking occurring at lower temperatures and strain rates is wider in the coarse grained material than the coarser material.

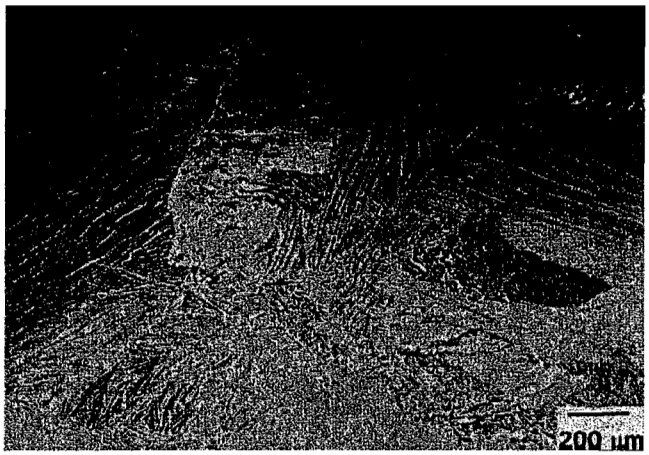

(a)

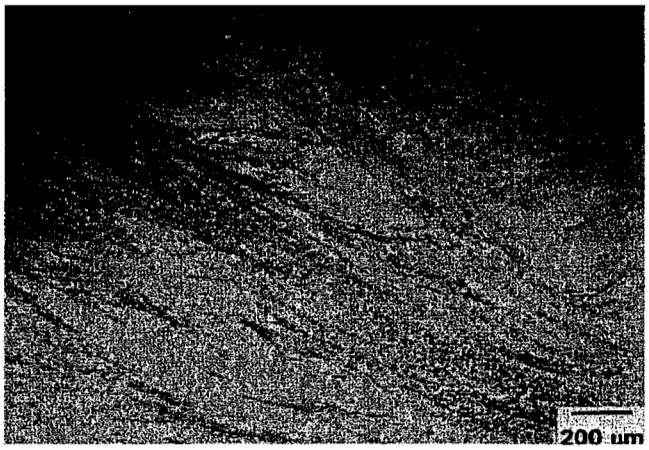

(b)

Fig. 12 Microstructures obtained on Ti-6A1-4V specimens deformed at 900 °C and 100 s^{-1}: (**a**) coarser grained material and (**b**) coarse grained material. The compression axis is vertical

- The flow instability regime in the α-β range, which manifests as adiabatic shear band formation and flow localization, is wider in the coarse grained material than in the coarser material. However, the flow instability of the β deformation is prominent in the coarser grained material.
- From the hot workability viewpoint, the present results show that there is no remarkable benefit in refining the prior β-grain size. Conversely, it will somewhat restrict the workability domain by widening the damage regimes.

Acknowledgments

One of the authors, Y.V.R.K. Prasad, is thankful to the National Research Council, United States, for awarding him an associateship and to the Director of the Indian Institute of Science, Bangalore, for granting him a sabbatical leave. The assistance rendered by Messrs. S. Sasidhara and R. Ravi of the Department of Metallurgy, Indian Institute of Science, is also gratefully acknowledged.

References

1. *Materials Properties Handbook: Titanium Alloys,* R. Boyer, G. Welsch, and E.W. Collings, eds., ASM International, Materials Park, OH, 1994, pp. 594-617.
2. M. Brun, N. Anoshkin, and G. Shakhanova: *Mater. Sci. Eng. A,* 1998, vol. 243, pp. 77-81.
3. S.L. Semiatin, V. Seetharaman, A.K. Ghosh, E.B. Shell, M.P. Simon, and P. Fagin: *Mater. Sci. Eng. A,* 1998, vol. 256, pp. 92-110.
4. H.G. Suzuki, H. Fujii, N. Takano, and K. Kaku: *6th World Conf. on Titanium,* P. Lacombe, R. Tricot, and G. Béranger, eds., Societé Francaise de Metallurgie, Les Ulie Cedex, France, 1988, pp. 1427-32.
5. Y.V.R.K. Prasad: *Ind. J. Technol.,* 1990, vol. 28, pp. 435-51.
6. Y.V.R.K. Prasad and T. Seshacharyulu: *Int. Mater. Rev.,* 1998, vol. 43 (1), pp. 243-58.
7. Y.V.R.K. Prasad and S. Sasidhara: *Hot Working Guide: A Compendium of Processing Maps,* ASM International, Materials Park, OH, 1997.
8. H. Ziegler: *in Progress in Solid Mechanics,* I.N. Sneddon and R. Hill, eds., North-Holland, Amsterdam, 1963, vol. 4., pp. 93-193.
9. H.L. Gegel, J.C. Malas, S.M. Doraivelu, and V.M. Shende: *Metals Handbook,* vol. 14, *Forging and Forming,* ASM International, Metals Park, OH, 1988, pp. 418.
10. T. Seshacharyulu, S.C. Medeiros, J.T. Morgan, J.C. Malas, W.G. Frazier, and Y.V.R.K. Prasad: *Mater. Sci. Eng. A,* 2000, vol. 279, pp. 289-99.
11. T. Seshacharyulu, S.C. Medeiros, J.T. Morgan, J.C. Malas, W.G. Frazier, and Y.V.R.K. Prasad: *Scripta Mater.,* 1999, vol. 41 (3), pp. 283-88.
12. N.E.W. de Reca and C.M. Libanati: *Acta Metall.,* 1968, vol. 16, pp. 1297-1305.

Effect of preform microstructure on the hot working mechanisms in ELI grade Ti–6Al–4V: transformed β *v.* equiaxed ($\alpha + \beta$)

Y. V. R. K. Prasad, T. Seshacharyulu, S. C. Medeiros, and W. G. Frazier

Processing of Ti–6Al–4V includes hot working above and below the β transus and the various stages of manufacture involve preforms with either transformed β (Widmanstätten colony type) or equiaxed ($\alpha + \beta$) microstructure. For achieving defect free products during manufacture, it is important to understand the response of these two preform microstructures to the imposed hot working conditions. In this paper, the influence of the preform microstructure on the hot working mechanisms of extra low interstitial (ELI) grade Ti–6Al–4V has been studied with the help of hot compression experiments conducted in the temperature range 750–1100°C and strain rate range 0·001–100 s^{-1}. The data have been analysed using the standard kinetic approach as well as the more recent approach of processing maps. In the α–β range, the stress–strain behaviour of transformed β preform is marked by a higher flow stress and a continuous flow softening while the equiaxed ($\alpha + \beta$) preform exhibits steady state flow at lower strain rates. By deforming in the α–β range, the transformed β microstructure is converted into an equiaxed one by a process of globularisation. On the other hand, the equiaxed ($\alpha + \beta$) preform deforms superplastically with an associated minor change in its microstructure. In the β range, the transformed β deforms by a process of large grained superplasticity involving the sliding of prior colony (Widmanstätten) boundaries with an associated diffusion accommodated flow. However, dynamic recrystallisation of β occurs in the equiaxed preform. Deformation near the transus for both the preforms is associated with local minima in the tensile ductility indicating the possibility of void nucleation. At strain rates higher than about 0·1 s^{-1}, both the preforms exhibit flow instabilities manifested in the form of flow localisation due to adiabatic shear band formation which is severe in the case of transformed β preform.

MST/4494

The authors are in the Materials Process Design Branch, Air Force Research Laboratory (AFRL/MLMR), Wright Patterson Air Force Base, OH,. 45433 USA. *Manuscript received 10 November 1999; accepted 6 January 2000.*

Introduction

The alloy Ti–6Al–4V (Ti-6-4) is extensively used in aerospace applications and the extra low interstitial (ELI) grade contains oxygen in the range 0·1–0·13 wt-%. The ELI grade is preferred for applications where high fracture toughness is a critical requirement since it has a 30% higher fracture toughness than the commercial grade.[1] In general, Ti-6-4 ingots are processed by forging/cogging initially in the β range (supra-transus) followed by deformation in the α–β range (sub-transus) to manufacture semiproducts like bars, plates, sheets, and other merchant shapes.[2] Component manufacture is done either by β processing followed by a suitable heat treatment or by α–β forging followed by homogenisation/stress relief anneal, depending upon the required mechanical properties. Thus, in the primary, secondary, or component manufacturing stages, the material being processed will have basically two different preform microstructures: one is the transformed β (referred to hereafter as β_t) with Widmanstätten (lamellar) colony structure and the other is an equiaxed ($\alpha + \beta$) (referred to below as $(\alpha + \beta)_e$) structure. The former one is present in the as cast ingot as well as in the material heat treated above the transus and air/fan cooled, while the latter one is produced by extensive mechanical working of the lamellar structure in the α–β range. As these two preforms respond differently to mechanical processing, it is necessary to characterise their behaviours so that the processing parameters are suitably chosen and controlled in the relevant stages of manufacture. The objective of the present investigation is to distinguish between their responses in terms of identifying the 'safe' processing windows so that defect free products are manufactured.

There are few studies on the fundamental mechanisms of hot deformation of the ELI grade Ti-6-4 in the literature. The early studies of Grant *et al.*[3] and Wu and Lowrie[4] have shown that the $(\alpha + \beta)_e$ preform exhibits abnormal elongation in the α–β range. Arieli and Rosen,[5] and Paton and Hamilton[6] have studied several aspects of superplastic deformation of ELI grade Ti-6-4 and correlated the behaviour with several microstructural parameters. Cope and coworkers[7,8] have identified optimum temperature and strain rate for obtaining highest superplastic elongation and also observed that this process is associated with cavitation at large strains. As regards the hot deformation behaviour of β_t preform, Semiatin *et al.*[9] established the conditions under which cavitation and failure occurs during hot forging in the α–β range, and proposed a fracture criterion to explain such damage. Seshacharyulu *et al.*[10] have used processing maps to identify the 'safe' processing windows wherein microstructural damage including prior β boundary cracking, void nucleation, lamellae kinking, and adiabatic shear band formation are avoided. In the α–β range, a process of globularisation of the lamellar structure was identified as the safe hot deformation mechanism.

In comparing the microstructural responses of the two preforms of Ti-6-4, the results on the stress–strain behaviour, the kinetic analysis, and the processing maps have been considered along with their impact on industrial processing. Details about these approaches of analysing hot deformation mechanisms in materials have been discussed in a recent review.[11] In particular, a processing maps approach has been found[12] to be beneficial in arriving at optimum processing parameters and in avoiding microstructural defects including flow instabilities.

The conventional approach[13] to analysing the hot deformation behaviour has been kinetic analysis. It is

shown that the steady state flow stress σ is related to the applied strain rate $\dot{\varepsilon}$ and temperature T through an Arrhenius type rate equation

$$\dot{\varepsilon} = A\sigma^n \exp(-Q/RT) \quad \ldots \quad (1)$$

where A is a constant, n is known as the stress exponent, Q is the activation energy, and R is the gas constant. On the basis of the stress exponent and activation energy values, the atomistic mechanisms are identified. In recent years, the processing maps approach has been applied to characterising and optimising the hot deformation behaviour of materials. The principles and basis for this approach have been described previously[11] and its application to a wide range of materials has been discussed in a recent compilation.[12] Briefly, this approach considers the workpiece as a dissipator of power that is converted into thermal (temperature rise) and microstructural forms. The factor that partitions power into these two forms is the strain rate sensitivity m of flow stress. By comparing the dissipation characteristics of the workpiece, which is a non-linear dissipator, with that of an ideal linear dissipator ($m = 1$), a dimensionless parameter called efficiency of power dissipation has been defined as[11]

$$\eta = \frac{2m}{m+1} \quad \ldots \quad (2)$$

The three-dimensional variation of η with temperature and strain rate at a constant strain, constitutes a power dissipation map. This map depicts the manner in which power is dissipated through microstructural changes that occur during deformation and hence reveals domains in which a specific mechanism may become an attractor for minimising the energy of the dissipated state. By utilising the principle of maximum rate of entropy production,[14] a continuum criterion for the occurrence of flow instabilities is defined in terms of another dimensionless parameter

$$\xi(\dot{\varepsilon}) = \frac{\partial \ln[m/(m+1)]}{\partial \ln \dot{\varepsilon}} + m \leqslant 0 \quad \ldots \quad (3)$$

The variation of $\xi(\dot{\varepsilon})$ with temperature and strain rate constitutes an instability map in which regimes of negative $\xi(\dot{\varepsilon})$ values represent flow instabilities. A superposition of the power dissipation map and the instability map gives a processing map which may be used to characterise different domains where different microstructural mechanisms occur as well as the regimes that exhibit flow instabilities.

Experimental

The chemical composition of the ELI grade of Ti-6-4 used in the present investigation was: Ti–(5·9–6·2)Al–(3·8–4·1)V–(0·1–0·13)O–(0·02–0·08)Fe–(0·001–0·005)C (wt-%). Cylindrical specimens of 10 mm dia. and 15 mm height were machined from bar stock keeping the compression axis along the rolling direction. Constant true strain rate compression tests were carried out in the temperature range 750–1100°C at intervals of 50°C and in the true strain rate range 0·001–100 s^{-1} at intervals of one order of magnitude. Details of the tests have been described elsewhere.[12] All the specimens were deformed to a true strain of about 0·5 and air-cooled from the test temperature. The load–stroke data obtained from the experiments were converted into true stress–true plastic strain using standard equations. For the analysis of the hot deformation behaviour, the input data consisted of flow stress values (corrected for adiabatic temperature rise) as a function of temperature, strain rate, and strain. The deformed specimens were sectioned parallel to the compression axis and prepared for metallographic examination using standard polishing and etching techniques.

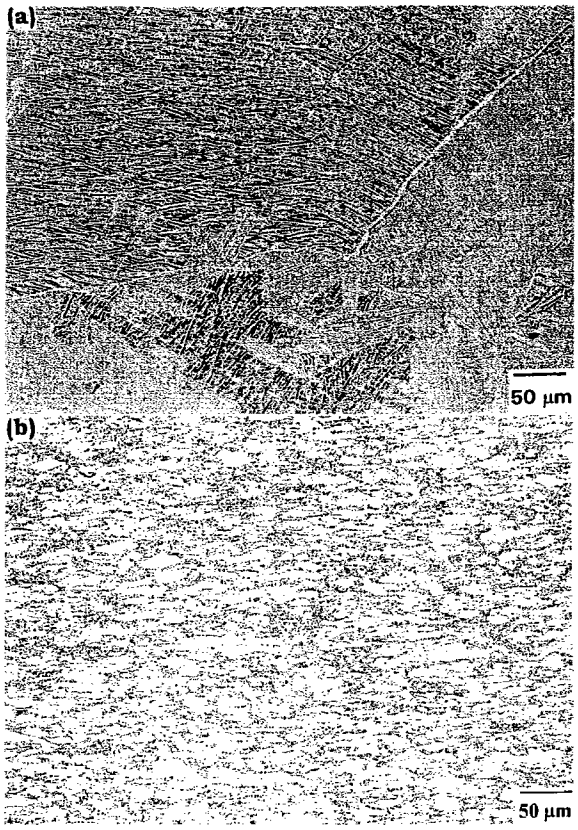

a transformed β preform; *b* equiaxed ($\alpha + \beta$) preform

1 Starting microstructures of experimental Ti–6Al–4V alloy

Results and discussion

The initial microstructures of the β_t and $(\alpha + \beta)_e$ preforms are shown in Fig. 1*a* and *b* respectively. The β_t microstructure has a prior β grain size of about 0·5–1·0 mm with a primary α layer of about 5 μm thick at the prior β boundary. The Widmanstätten colonies have lamellae oriented in different directions. The $(\alpha + \beta)_e$ preform has a very fine two phase structure with an average α grain size of about 10 μm with a small amount (~10%) of intergranular β. The $(\alpha + \beta) \rightarrow \beta$ transformation temperature (β transus) is about 975°C for this ELI grade.

STRESS–STRAIN BEHAVIOUR

The true stress–true plastic strain curves of the two preforms obtained at different strain rates are shown in Fig. 2*a* and *b*, which correspond to deformation temperatures of 850°C (representative of the α–β range) and 1100°C (representative of the β range), respectively. In the α–β range, it is observed that the stress–strain curves for the β_t preform exhibit continuous flow softening unlike that of the $(\alpha + \beta)_e$ preform which show near steady state behaviour. At a given strain rate and temperature, the β_t preform has a higher flow stress than the $(\alpha + \beta)_e$ preform. Also the curves at high strain rates (>1 s^{-1}) contain oscillations in both cases. In the β range, the β_t preform is stronger than the $(\alpha + \beta)_e$ preform and the shapes of stress–strain curves are similar for both the preforms. At strain rates lower than 1 s^{-1}, the flow curves are of steady state type while at higher strain rates oscillations are observed.

The continuous flow softening in the β_t preform is attributed[15] to the conversion of the lamellar microstructure to an equiaxed one by a process of globularisation which

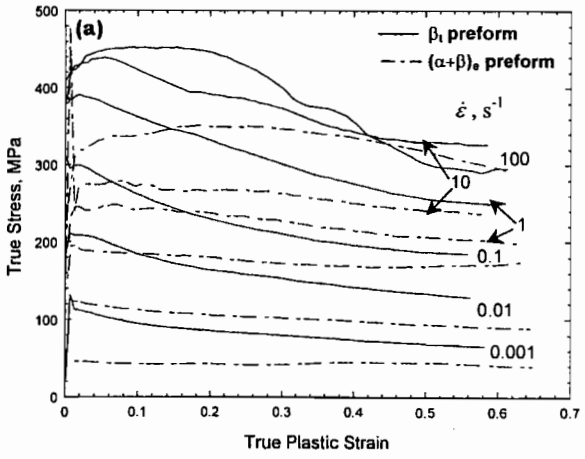

a 850°C; *b* 1100°C

2 True stress–strain plastic strain curves obtained on Ti–6Al–4V for different strain rates at given temperatures

is caused by shearing of the lamellae followed by interface migration. This process reaches completion at large strains when all the colonies participate in the shearing process and the flow curves become asymptotic to those of equiaxed microstructure. The steady state behaviour in a two phase material can be representative of superplastic deformation while in a single phase material (high temperature β phase here), such a behaviour is indicative of dynamic recrystallisation (DRX) or large grained superplasticity (LGSP). Likewise, oscillations in the stress–strain curves may be indicative of either DRX or flow instabilities. In order to evaluate the actual mechanism, therefore, further analysis of the temperature and strain rate dependence of flow stress will be required and therefore other modelling methods will have to be applied.

KINETIC ANALYSIS

The variation of $\log \sigma$ with $\log \dot{\varepsilon}$ is not linear over the entire range of strain rate in the two phase region, suggesting that the kinetic rate equation given by equation (1) is not valid. However, over a limited strain rate range (0·001–0·1 s^{-1}) and temperature range (750–950°C in the α–β range and 1000–1100°C in the β range), validity of equation (1) has been established. The Arrhenius plots obtained on the two preforms at a strain rate of 0·001 s^{-1} are shown in Fig. 3 in the α–β and β ranges of deformation temperature. The estimated values of the stress exponent and the apparent activation energy are given in Table 1 for the two preforms of Ti-6-4. In the α–β range, the apparent activation energy values are much higher than that for self-

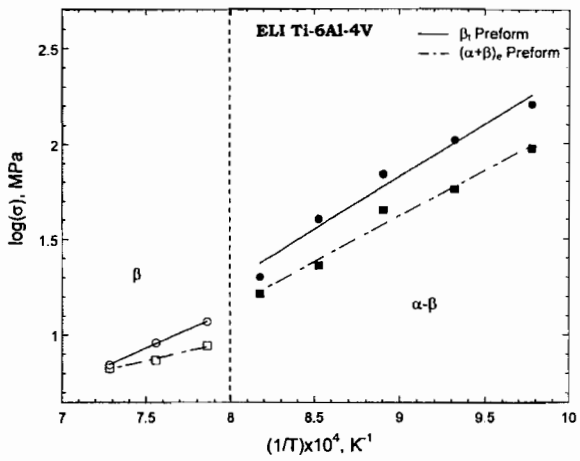

3 Arrhenius plot showing the variation of flow stress with inverse of temperature in the α–β and β ranges of experimental Ti–6Al–4V material

diffusion in α-Ti (150 kJ mol^{-1}) (Ref. 16), the difference being more in the case of the β_t preform. In this range, the process of globularisation occurs and a typical microstructure of a β_t specimen deformed at 900°C and 0·001 s^{-1} is shown in Fig. 4*a*. Alternate thermally activated analyses of the globularisation process in the β_t preform using Shöcks and Kocks models have shown that cross-slip of screw dislocations is the rate controlling step.[17] In the $(\alpha+\beta)_e$ preform, however, the mechanism of deformation has been established to be superplastic deformation since the material, which has such a fine grained two phase structure, exhibits abnormal elongations (>1000%).[7] Typical microstructure of $(\alpha+\beta)_e$ specimen deformed at 800°C and 0·001 s^{-1} is shown in Fig. 4*b*. While sliding of α/α interfaces essentially contributes to the superplasticity, the critical step in this process is the accommodation of the stress concentration at the grain boundary triple junctions. Since the β phase is present at the triple junctions, the rate controlling step is shown[18] to be the dynamic recovery of the β phase and this explains why the apparent activation energy for superplasticity does not match with that for self-diffusion in either of the phases of pure titanium.

A plot of the variation of flow stress with the temperature compensated strain rate parameter (Zener–Hollomon) Z given by

$$Z = \dot{\varepsilon} \exp(Q/RT) \quad \ldots\ldots\ldots\ldots\ldots\ldots (4)$$

is shown in Fig. 5 which confirms the validity of the kinetic rate equation (equation (1)) for both the preforms of Ti-6-4. It may be noted that a small change in the slope reflects the difference in the value of the stress exponent (Table 1). The variation of the globule size in the β_t preform and α grain size in the $(\alpha+\beta)_e$ preform, with the Z parameter are shown in Fig. 6. Such a plot will be useful in controlling these microstructural parameters during processing.

The kinetic analysis was also carried out in the β range of testing and the corresponding values of the stress

Table 1 Kinetic parameters and microstructural mechanisms in hot deformation of ELI Ti–6Al–4V

	α–β range			β range		
Preform	n	Q_{app}, kJ mol^{-1}	Mechanism	n	Q_{app}, kJ mol^{-1}	Mechanism*
β_t	3·7	370	Globularisation	3·7	287	LGSP
$(\alpha+\beta)_e$	3·2	240	Superplasticity	3·8	151	DRX

*LGSP large grained superplasticity, DRX dynamic recrystallisation.

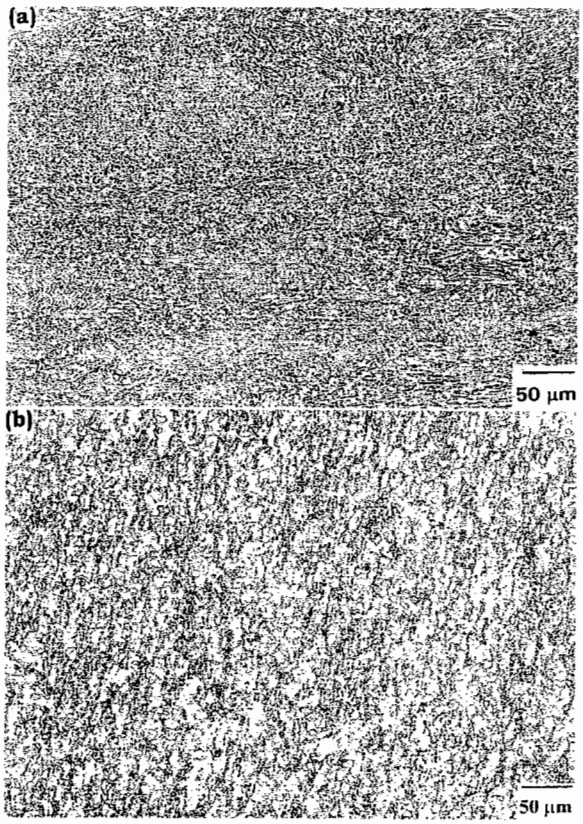

4 Microstructures obtained from *a* transformed β preform specimen deformed at 900°C and 0·001 s^{-1} and *b* equiaxed $(\alpha+\beta)$ preform specimen deformed at 800°C and 0·001 s^{-1}

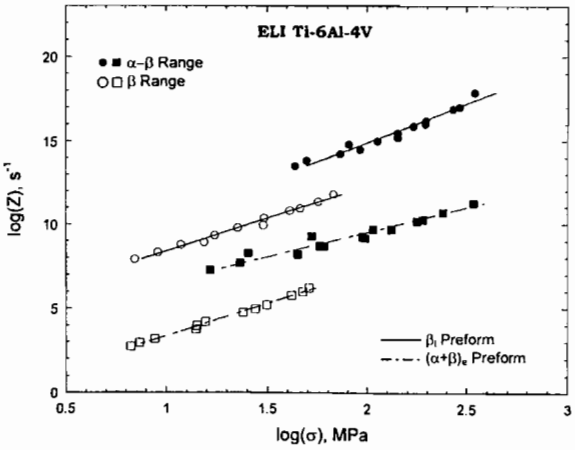

5 Variation of flow stress σ with Zener–Hollomon parameter Z in α–β and β ranges of experimental Ti–6Al–4V alloy

exponent and the apparent activation energy (Fig. 3) are also included in Table 1 for the two preforms. The stress exponent is nearly independent of the preform microstructure while the apparent activation energy in the β_t preform is higher than that in the $(\alpha+\beta)_e$ preform and that for self-diffusion in β-Ti (153 kJ mol^{-1}, Ref. 19). It is interesting to note that the latter two values matched very well. Detailed microstructural investigations and ductility measurements in the β range have shown that the mechanism of deformation in the β_t preform is LGSP (Ref. 10) and that in the $(\alpha+\beta)_e$ preform is DRX.[18] It may

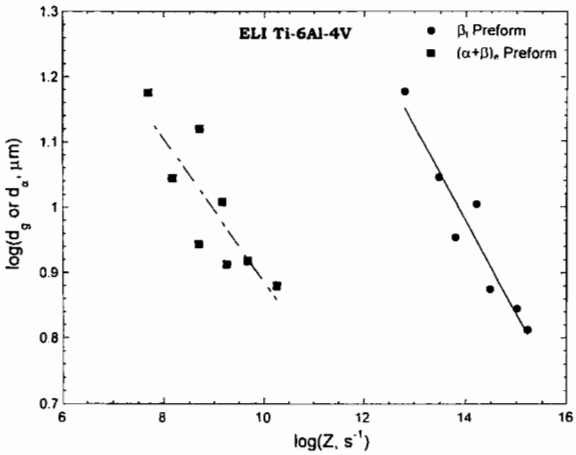

6 Variation of globule size d_g and α grain size d_α with Zener–Hollomon parameter Z in α–β range of Ti–6Al–4V

be noted that LGSP occurs by the sliding of prior (Widmanstätten) colony boundaries and DRX is controlled by the rate of migration of grain boundaries. It is obvious that LGSP cannot occur in the equiaxed preform since there is no Widmanstätten colony structure. The variation of flow stress with Z parameter for the β range is shown in Fig. 5. Again, the influence of preform structure on the slopes of the lines is not significant (similar stress exponents).

PROCESSING MAPS

The processing maps for the β_t and $(\alpha+\beta)_e$ preforms are shown in Fig. 7*a* and *b*, respectively. The contour numbers represent the percentage efficiency of power dissipation projected on a temperature–strain rate plane. Referring to Fig. 7*a*, an efficiency peak of 49% occurs over a wide temperature regime at a strain rate of 0·001 s^{-1}. In materials where a phase transformation occurs, it is expected that the contours show change in their curvatures[12] at the transformation temperature. However, in the map for the β_t preform the contours do not show any discontinuity across the transus (~975°C) which may be interpreted in terms of merging of two domains with similar power dissipation efficiency values on either side of the transus. At the transus, it is argued that the Widmanstätten colony boundaries within the large β grains slide at slow strain rates and the stress concentration at their triple junctions is responsible for the nucleation of voids. Tensile ductility variation with temperature in this preform has shown[10] that a local ductility minimum occurs at the transus, further corroborating such a possibility. These void nuclei may grow during soaking at temperatures close to the transus under conditions of large tensile residual stresses. In the α–β range, the process of globularisation occurs in the temperature range 850–950°C and strain rate range 0·001–0·01 s^{-1} with its optimum at 925°C and 0·001 s^{-1} and under these conditions, the tensile ductility exhibits a peak. The lower temperature limit for the use of globularisation for defect free processing is set by the occurrence of shear cracking at the prior β boundaries or wedge cracking at their triple junctions[10] while the higher temperature limit is set by the void nucleation process. In the β regime, the material exhibits LGSP resulting in an optimum workability at 1050°C. The mechanism for this process is the same as that causing void nucleation at the transus but in LGSP, the void nucleation is mitigated by diffusion accommodated flow at higher temperatures. The map also exhibits another domain with a peak efficiency of 39% at 750°C and 100 s^{-1} which represents the process of cracking along the adiabatic shear bands as discussed below.

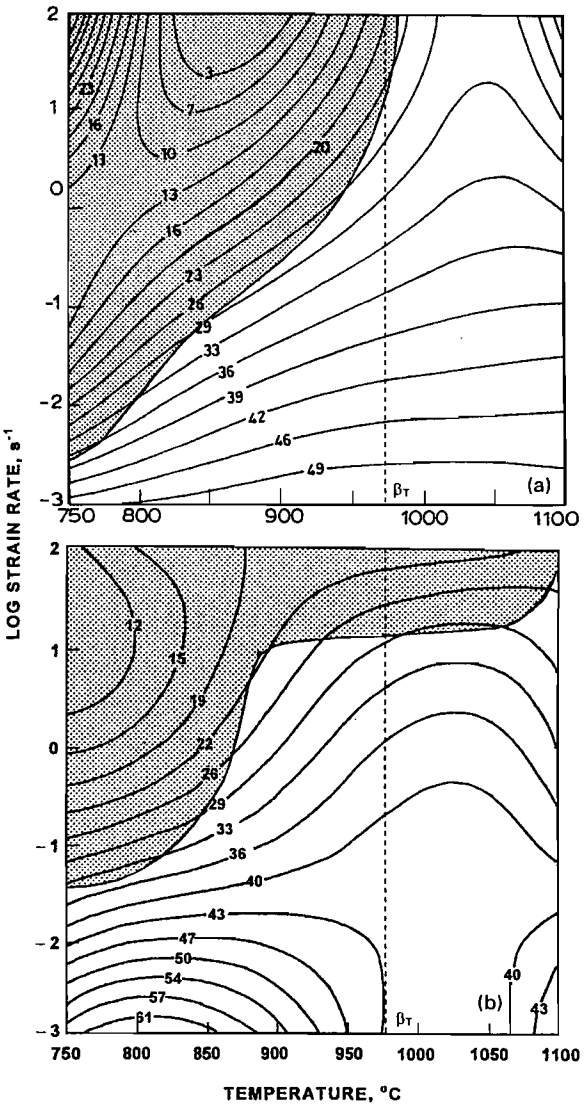

a transformed β preform; *b* equiaxed $(\alpha+\beta)$ preform

7 Processing maps obtained on two types of preform at a strain of 0·4: contour numbers represent percentage efficiency of power dissipation; shaded region corresponds to flow instability as predicted by the criterion given by equation (3)

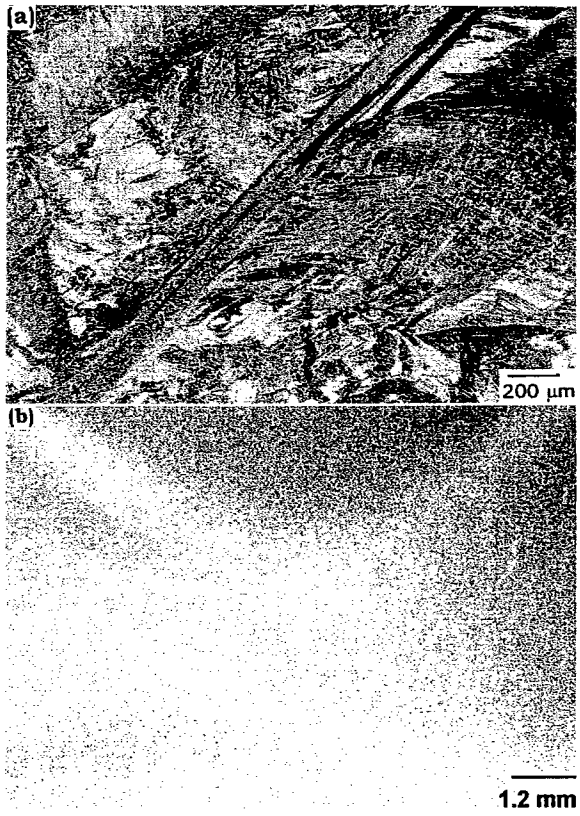

a transformed β preform; *b* equiaxed $(\alpha+\beta)$ preform (macrograph)

8 Microstructures obtained for specimens deformed in flow instability region at 750°C and 100 s^{-1}

The processing map for the $(\alpha+\beta)_e$ preform also exhibits two domains: one in the α–β range and the other in the β range. The α–β domain has a peak efficiency of 61% at 825°C and 0·001 s^{-1} while the β domain has a peak efficiency of 43% at 1100°C and 0·001 s^{-1}. On the basis of ductility measurements[7] and grain size variations (Fig. 6), these domains are interpreted to represent fine grained superplasticity and β DRX respectively. It may be noted that superplastic deformation may result in cavitation damage particularly at lower temperatures of the domain and at very large strains. The higher temperature limit for superplasticity is set by the temperature at which the β volume fraction exceeds 50%. Higher β volume fraction creates a larger number of α–β boundaries which do not favour superplasticity. Also, the ductility measurements in this domain have shown[7] that the peak ductility occurs over a very narrow range of temperature (about 50 K) and hence stringent controls would be required for superplastic forming of this grade of Ti-6-4. These mechanisms are summarised in Table 1 for the two preforms and the two ranges of deformation temperature. It is interesting to note that the ductility data of Wu and Lowrie[4] revealed that a local minimum in ductility occurs at the transus in the $(\alpha+\beta)_e$ preform similar to that seen in the β_t preform,[10] indicating the possibility of a microstructural damage mechanism around the transus.

In both the preforms of ELI grade, a wide regime of flow instability (shown as shaded area in Fig. 7*a* and *b*) is present in the α–β regime at strain rates higher than about 0·1 s^{-1}. These are manifested as flow localisation due to adiabatic shear band formation which is more intense in the β_t preform resulting in cracking along the adiabatic shear bands. Typical microstructures obtained on specimens deformed at 750°C and 100 s^{-1} are shown in Fig. 8 which exhibit shear bands formed at an angle of $\sim$45° with respect to the compression axis. Further, in the instability regime, the stress–strain curves exhibit continuous flow softening (Fig. 2*a*) and/or oscillations (Fig. 2*b*).

Conclusions

On the basis of the characterisation of deformation behaviour of the transformed β and equiaxed $(\alpha+\beta)$ preforms of ELI grade Ti-6-4 in the ranges 750–1100°C and 0·001–100 s^{-1} using kinetic analysis and processing maps, the following conclusions are drawn on the influence of preform microstructure on processing of this material.

1. The stress–strain behaviour of transformed β_t preform is marked by a higher flow stress and a continuous flow softening while the equiaxed $(\alpha+\beta)$ preform exhibits steady state flow at lower strain rates.

2. By deforming in the α–β range, the transformed β microstructure is converted into an equiaxed one by a

process of globularisation. On the other hand, the equiaxed $(\alpha + \beta)$ preform deforms superplastically associated with no significant change in its microstructural features.

3. In the β range, the transformed β preform deforms by a process of large grained superplasticity involving the sliding of prior colony (Widmanstätten) boundaries with an associated diffusion accommodated flow, while dynamic recrystallisation of β phase occurs in the equiaxed preform.

4. Deformation at the transus for both the preforms is associated with a local minima in the tensile ductility indicating the possibility of void nucleation.

5. At strain rates higher than about $0{\cdot}1\ s^{-1}$ and in the α–β range, both the preforms exhibit flow instabilities manifested in the form of flow localisation due to adiabatic shear band formation which is severe in the case of transformed β preform.

Acknowledgements

The authors would like to acknowledge Dr J. C. Malas for many stimulating discussions. One of the authors (YVRKP) is thankful to the National Research Council, USA, for awarding him an associateship and to the Director of the Indian Institute of Science, Bangalore, for granting him a sabbatical leave. The assistance rendered by S. Sasidhara and R. Ravi of Department of Metallurgy, Indian Institute of Science, Bangalore is gratefully acknowledged.

References

1. R. W. HERTZBERG: 'Deformation and fracture mechanics of engineering materials', 3rd edn, 366; 1987, New York, J. Wiley.
2. R. BOYER, G. WELSCH, and E. W. COLLINGS (eds.): 'Materials properties handbook: titanium alloys', 596; 1994, Materials Park, OH, ASM International.
3. N. J. GRANT, W. IOUP, and R. H. KANE: in 'The science, technology and application of titanium', (ed. R. I. Jaffe and N. E. Promisel), 607–613; 1990, London, Pergamon.
4. K. C. WU and R. E. LOWRIE: *Met. Eng. Q.*, Aug. 1972, 25–29.
5. A. ARIELI and A. ROSEN: *Metall. Trans. A*, 1977, **8A**, 1591.
6. N. E. PATON and C. H. HAMILTON: *Metall. Trans. A*, 1979, **10A**, 241–250.
7. M. T. COPE and N. RIDLEY: *Mater. Sci. Technol.*, 1986, **2**, 140.
8. M. T. COPE, D. R. EVETTS, and N. RIDLEY: *J. Mater. Sci.*, 1986, **21**, 4003.
9. S. L. SEMIATIN, R. L. GOETZ, E. B. SHELL, V. SEETHARAMAN, and A. K. GHOSH: *Metall. Mater. Trans. A*, 1999, **30A**, 1411.
10. T. SESHACHARYULU, S. C. MEDEIROS, J. T. MORGAN, J. C. MALAS, W. G. FRAZIER, and Y. V. R. K. PRASAD: *Mater. Sci. Eng. A*, 2000, **A279**, 289–299.
11. Y. V. R. K. PRASAD and T. SESHACHARYULU: *Int. Mater. Rev.*, 1998, **43**, 243.
12. Y. V. R. K. PRASAD and S. SASIDHARA (eds.): 'Hot working guide: a compendium of processing maps'; 1997, Materials Park, OH, ASM International.
13. J. J. JONAS, C. M. SELLARS, and W. J. MCG. TEGART: *Metall. Rev.*, 1969, **14**, 1.
14. H. ZIEGLER: in 'Progress in solid mechanics', (ed. I. N. Sneddon and R. Hill), Vol. 4, 93–193; 1963, Amsterdam, North-Holland.
15. H. L. GEGEL, J. C. MALAS, S. M. DORAIVELU, and V. A. SHENDE: in 'Metals handbook', 9th edn, Vol. 14, 417–438; 1988, Materials Park, OH, ASM International.
16. F. DYMENT and C. M. LIBANATI: *J. Mater. Sci.*, 1968, **3**, 349.
17. T. SESHACHARYULU, S. C. MEDEIROS, J. T. MORGAN, J. C. MALAS, W. G. FRAZIER, and Y. V. R. K. PRASAD: *Scr. Mater.*, 1999, **41**, 283–288.
18. T. SESHACHARYULU, S. C. MEDEIROS, W. G. FRAZIER, and Y. V. R. K. PRASAD: Unpublished work, Wright-Patterson Air Force Base.
19. N. E. W. DE RECA and C. M. LIBANATI: *Acta Metall.*, 1968, **16**, 1297.

ELSEVIER

Materials Science and Engineering A284 (2000) 184–194

MATERIALS SCIENCE & ENGINEERING A

www.elsevier.com/locate/msea

Hot working of commercial Ti–6Al–4V with an equiaxed α–β microstructure: materials modeling considerations

T. Seshacharyulu, S.C. Medeiros, W.G. Frazier *, Y.V.R.K. Prasad

Materials Process Design Branch (AFRL/MLMR), Materials and Manufacturing Directorate, Air Force Research Laboratory, Wright-Patterson Air Force Base, OH 45433-7746, USA

Received 14 October 1999; received in revised form 11 January 2000

Abstract

The hot deformation behavior of Ti–6Al–4V with an equiaxed α–β preform microstructure is modeled in the temperature range 750–1100°C and strain rate range 0.0003–100 s^{-1}, for obtaining processing windows and achieving microstructural control during hot working. For this purpose, a processing map has been developed on the basis of flow stress data as a function of temperature, strain rate and strain. The map exhibited two domains: (i) the domain in the α–β phase field is identified to represent fine-grained superplasticity and the peak efficiency of power dissipation occurred at about 825°C/0.0003 s^{-1}. At this temperature, the hot ductility exhibited a sharp peak indicating that the superplasticity process is very sensitive to temperature. The α grain size increased exponentially with increase in temperature in this domain and the variation is similar to the increase in the β volume fraction in this alloy. At the temperature of peak ductility, the volume fraction of β is about 20%, suggesting that sliding of α–α interfaces is primarily responsible for superplasticity while the β phase present at the grain boundary triple junctions restricts grain growth. The apparent activation energy estimated in the α–β superplasticity domain is about 330 kJ mol^{-1}, which is much higher than that for self diffusion in α-titanium. (ii) In the β phase field, the alloy exhibits dynamic recrystallization and the variation of grain size with temperature and strain rate could be correlated with the Zener–Hollomon parameter. The apparent activation energy in this domain is estimated to be 210 kJ mol^{-1}, which is close to that for self diffusion in β. At temperatures around the transus, a ductility peak with unusually high ductility has been observed, which has been attributed to the occurrence of transient superplasticity of β in view of its fine grain size. The material exhibited flow instabilities at strain rates higher than about 1 s^{-1} and these are manifested as adiabatic shear bands in the α–β regime. Published by Elsevier Science S.A.

Keywords: Hot deformation behavior; Ti–6Al–4V; Equiaxed α–β microstructure

1. Introduction

Ti–6Al–4V (Ti–6–4) alloy is a two-phase alloy, which has low density and attractive mechanical and corrosion resistant properties that make it an ideal choice for many aerospace applications [1]. It is commercially available in two grades — low oxygen (ELI) grade and high oxygen (commercial) grade. It is the high oxygen grade that is widely used in gas turbine engine parts, chemical reactors and bioengineering applications. The alloy may be heat treated [2] to obtain a variety of microstructures ranging from β-transformed (martensitic/lamellar) to equiaxed α–β. Bulk mechanical processing of this material to manufacture semi-products includes ingot breakdown at temperatures above the β transus and 'conversion' of transformed β lamellar structure into equiaxed α–β by subtransus deformation [3–5]. The finishing operations for component manufacture are generally conducted [6] on the equiaxed structure in the α–β phase field during which only minor changes in the microstructure take place. One of the very common industrial processes used for this purpose is superplastic forming, which requires very fine grain sizes and slow speeds of deformation [7,8]. The characteristics of superplastic deformation in Ti–6–4 have been studied extensively in the literature [9–14]. Although superplastic elongations have been recorded by several investigators, there are reports of cavity formation at higher strains and lower tempera-

* Corresponding author. Tel.: +1-937-90444325; fax: +1-937-6567995.

E-mail address: william.frazier@afrl.af.mil (W.G. Frazier)

0921-5093/00/$ - see front matter Published by Elsevier Science S.A.
PII: S0921-5093(00)00741-3

tures (< 850°C) [12,15]. The constitutive behavior of commercial grade Ti–6–4 during hot deformation in the α–β range has been characterized by Sheppard and Norley in torsion [16] and Seetharaman et al. in compression [17] and microstructural mechanisms have been identified to be dynamic recrystallization (DRX) and spheroidization respectively.

The objective of this study is to model the microstructural mechanisms of hot deformation of commercial Ti–6–4 with an equiaxed α–β microstructure over a wide range of temperature and strain rate such that windows for industrial processing may be identified for optimizing workability and controlling microstructure. To reach this objective, the characteristics of the alloy have been studied in the temperature ranges covering not only α–β and β phase fields but also the transus. Likewise, a wide strain rate range that encompasses the speeds of commonly used machines in the industry like hydraulic presses (slow), mechanical/friction screw presses and hammers (medium), continuous rolling and ring rolling (fast) mills, is investigated.

Several approaches of materials modeling are in vogue and these include analysis of shapes of stress–strain curves [5], kinetic analysis [18], and processing maps [19] and these have been reviewed recently [20]. Although all the approaches have been followed in this paper, the emphasis has been on processing maps since this approach has been found to be consistent in predicting the behavior of a wide range of materials [21]. In brief, the processing maps consist of a superimposition of power dissipation maps and instability maps developed in a frame of temperature and strain rate. The power dissipation maps represent the pattern in which the power is dissipated by the material through microstructural changes. The rate of this change is given by a dimensionless parameter called the efficiency of power dissipation:

$$\eta = \frac{2m}{m+1} \quad (1)$$

where m is strain rate sensitivity of flow stress. Over this frame is superimposed a continuum instability criterion for identifying the regimes of flow instabilities, developed on the basis of extremum principles of irreversible thermodynamics as applied to large plastic flow [13] and given by:

$$\xi(\dot{\varepsilon}) = \frac{\partial \ln(m/m+1)}{\partial \ln \dot{\varepsilon}} + m < 0 \quad (2)$$

where $\xi(\dot{\varepsilon})$ is a dimensionless instability parameter and $\dot{\varepsilon}$ is the applied strain rate. Flow instabilities are predicted to occur when $\xi(\dot{\varepsilon})$ becomes negative. The processing maps exhibit domains in which specific microstructural mechanisms operate as well as regimes where there will be flow instabilities like adiabatic shear bands or flow localization.

2. Materials and procedures

2.1. Material

Commercial grade Ti–6–4 having the following composition (wt.%) was used in this study: 6.28 Al, 3.97 V, 0.18 O, 0.052 Fe, 0.0062 N, 0.008 C, 0.0049 H, and balance Ti. The β transus for this material is about 1010°C. As received bar stocks of 20 mm diameter in the mill annealed condition were used for testing and the starting microstructure is shown in Fig. 1. It consisted of equiaxed α grains of about 8 μm average diameter with a small amount of intergranular β.

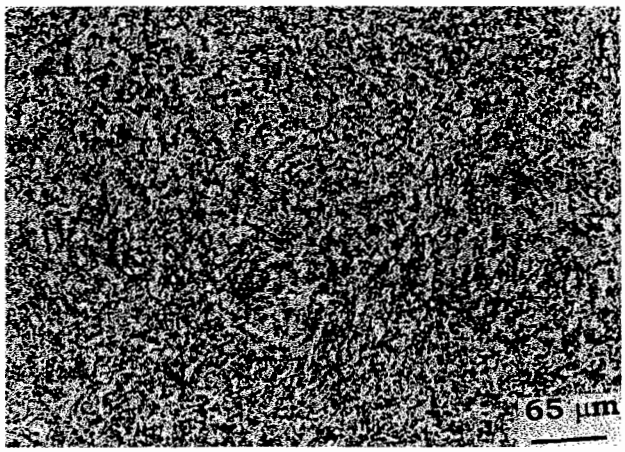

Fig. 1. Starting microstructure of Ti–6Al–4V used in this study.

2.2. Hot compression testing

Compression specimens of 15 mm height and 10 mm diameter were machined for testing in the α + β range, while larger specimens of 22.5 mm height and 15 mm diameter were used to obtain an accurate measurement of the flow stress in the β range. Concentric grooves of 0.5 mm depth were made on the top and bottom faces of the specimens to trap lubricant and assist in reducing friction. A 1-mm 45° chamfer was provided on the specimen edges to avoid fold-over of the material during the initial stages of compression. A small hole of 0.8 mm diameter and 5 mm depth was drilled at mid height of the specimen for inserting a thermocouple which is used to measure the actual temperature of the specimen as well as adiabatic temperature rise, if any, during testing. Isothermal hot compression tests were conducted using a servohydraulic testing machine. A resistance heating split furnace with SiC elements was used to surround the platens and specimen. The specimens were coated with a borosilicate glass paste for lubrication and environmental protection.

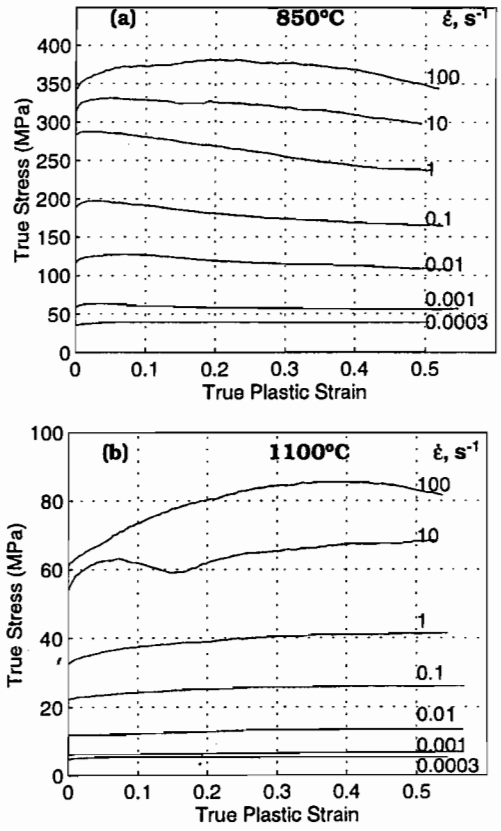

Fig. 2. Flow curves obtained on Ti–6Al–4V deformed in compression at (a) 850°C and (b) 1100°C and at different strain rates.

The test matrix consisted of temperature range 750–1100°C at an interval of 50°C and constant true strain rates of 0.0003, 0.001, 0.01, 0.1, 1, 10 and 100 s^{-1}. The temperature of the specimen was monitored using a chromel–alumel thermocouple inserted in the specimen and isothermal condition was maintained within ± 2°C fluctuation. Adiabatic temperature rise (significant at higher strain rates) was recorded using a transient oscilloscope. The specimens were deformed to half the height in each case to impose a true strain of 0.7 and were air-cooled to room temperature after deformation. Deformed specimens were sectioned parallel to the compression axis and the cut surface was prepared for metallographic examination using standard techniques. The specimens were etched with Kroll's reagent and polarized light micrographs were recorded.

2.3. Flow stress data analysis

The load-stroke data obtained in compression were processed to obtain true stress-true plastic strain curves using the standard method. The flow stress data obtained at different temperatures, strain rates and strains were corrected for adiabatic temperature rise, if any, by linear interpolation between $\log \sigma$ and $1/T$ where σ is the flow stress and T is the temperature in Kelvin. A cubic spline fit between $\log \sigma$ and $\log \dot{\varepsilon}$ was used to obtain the strain rate sensitivity (m) as a function of strain rate. This was repeated at different temperatures. The efficiency of power dissipation (η) through microstructural changes was then calculated as a function of temperature and strain rate using Eq. (1) and plotted as an iso-efficiency contour map. The data were also used to evaluate the flow instability parameter $\xi(\dot{\varepsilon})$ using Eq. (2) as a function of temperature and strain rate to develop an instability map.

2.4. Hot tensile testing

Hot tensile tests were conducted in the temperature range 800–1100°C at a nominal strain rate of 0.01 s^{-1} (constant actuator speed of 0.25 mm s^{-1}). Cylindrical specimens of 25 mm gauge length and 4 mm diameter were used for this purpose. The specimens were pulled to fracture and total elongation as a function of temperature was recorded.

3. Results and discussion

3.1. Stress–strain behavior

The shapes of stress–strain curves indicate some features that help in identifying the mechanisms of hot deformation, although not in a conclusive fashion. Commercial Ti–6–4 with equiaxed $\alpha+\beta$ microstructure exhibited three different generic shapes of stress–strain curves in the ranges of temperature and strain rate covered in this investigation. Curves representing these features are given Fig. 2a and b, which reveal the following features:

1. At strain rates slower than 0.1 s^{-1} and at all temperatures including two phase $\alpha+\beta$ as well as single phase β phase fields, the curves were of steady-state type. Such curves indicate that the mechanisms of softening are sufficiently fast to balance the rate of work hardening and are suggestive of mechanisms like dynamic recrystallization, superplasticity or dynamic recovery occurring at very high rates. Further analysis of the flow stress data as a function of temperature and strain rate, is required for arriving at the exact mechanism(s).
2. At higher strain rates (>0.1 s^{-1}) in the α–β range (<1000°C) (Fig. 2a), the material exhibited a continuous flow softening behavior. Such a feature is observed for globularization process of lamellar structures, flow instability due to flow localization, or micro-cracking during deformation. Since the starting microstructure in the present case is not a lamellar structure, the first possibility may be ruled out. However detailed microstructural examination is required to decide between the other two. This aspect is discussed in detail subsequently.

3. In the β range at high strain rates (>1 s^{-1}), oscillatory flow curves were observed (Fig. 2b) particularly at a strain rate of 10 s^{-1}. Oscillations in the stress–strain curves are indications of DRX under certain conditions of strain rate and temperature, unstable deformation, or cracking. In this case also, further analysis is required to arrive at the actual mechanism that causes these stress–strain features.

The flow stress data obtained at different temperatures, strain rates and strains are given in Table 1.

3.2. Kinetic analysis

The temperature and strain rate dependence of flow stress in hot deformation is generally expressed in terms of a kinetic rate equation [18] given by:

$$\dot{\varepsilon} = A\sigma^n \exp(-Q/RT) \quad (3)$$

where $\dot{\varepsilon}$, strain rate; σ, flow stress; A, frequency factor; Q, apparent activation energy, R, gas constant, T, temperature in Kelvin, and n, stress exponent. In order to identify the mechanism(s) of hot deformation, the kinetic parameters, n and Q in Eq. (3) are to be evaluated. The variation of flow stress with strain rate is shown in Fig. 3 on a log–log scale. The inverse of the slope of this curve represents the stress exponent, n. From Fig. 3, it is seen that n is strain rate dependent when considered over the entire range of strain rate employed in this study. However, over a limited strain rate range of 0.0003–0.01 s^{-1} the kinetic rate equation is obeyed and a linear fit is obtained at all the temperatures. The $(\alpha+\beta)\rightarrow\beta$ transus for this grade of Ti–6–4 is about 1010°C and so the kinetic parameters may be evaluated separately in the two phase region (750–

Table 1
Corrected flow stress values (in MPa) of CP Ti–6–4 with equiaxed α–β preform microstructure as a function of temperature, strain rate and strain

Strain	Strain rate (s^{-1})	Temperature (°C)							
		750	800	850	900	950	1000	1050	1100
0.1	0.0003	109.0	60.9	39.5	20.1	14.1	7.3	6.2	5.4
	0.001	166.3	93.4	60.7	31.1	19.8	10.5	7.5	6.1
	0.010	273.5	182.5	125.9	75.1	36.0	21.0	15.2	12.2
	0.100	354.2	264.5	191.4	145.8	72.6	33.3	27.4	24.1
	1.000	446.9	353.4	280.6	196.1	106.1	47.6	46.3	37.3
	10.00	502.0	436.9	329.0	258.9	145.2	73.8	74.8	62.0
	100.0	523.0	455.4	372.7	298.4	188.6	106.7	81.1	73.3
0.2	0.0003	98.3	58.5	39.7	20.4	14.7	7.2	6.2	5.4
	0.001	153.4	87.6	58.2	29.9	18.9	10.1	7.7	6.4
	0.010	261.0	173.0	119.1	71.2	34.9	20.8	15.8	12.9
	0.100	342.3	249.1	180.9	137.2	70.1	33.3	28.4	25.2
	1.000	434.2	340.0	269.2	190.1	103.7	50.2	48.8	39.0
	10.00	497.1	431.1	325.8	257.2	142.1	74.9	72.9	61.6
	100.0	547.0	469.1	380.8	307.5	196.9	116.5	89.8	79.9
0.3	0.0003	91.9	57.0	38.6	20.5	14.4	7.4	6.4	5.3
	0.001	144.3	84.3	57.1	30.1	18.9	10.1	7.9	6.5
	0.010	252.1	167.1	115.3	68.9	34.3	20.6	16.1	13.3
	0.100	330.2	236.6	173.8	130.0	67.8	33.5	29.3	25.8
	1.000	416.2	323.4	255.8	182.6	101.6	52.2	50.5	40.5
	10.00	465.9	416.7	318.7	253.0	143.8	79.0	77.7	65.3
	100.0	533.2	463.9	376.9	305.3	200.3	121.8	93.2	84.2
0.4	0.0003	87.1	54.5	38.4	20.5	14.2	7.6	6.4	5.3
	0.001	134.8	81.6	55.9	30.6	18.9	9.8	8.1	6.7
	0.010	242.1	161.3	112.1	67.1	33.5	20.2	16.3	13.4
	0.100	321.9	227.6	168.3	125.1	65.7	32.9	29.3	26.0
	1.000	398.2	310.1	243.4	175.5	98.7	53.7	51.1	40.9
	10.00	454.7	403.8	309.5	244.9	139.0	81.1	78.0	67.3
	100.0	522.1	451.6	367.8	295.9	195.1	121.2	95.2	85.5
0.5	0.0003	83.8	54.5	39.2	20.8	14.0	7.7	6.5	5.3
	0.001	129.6	79.2	55.8	30.9	18.7	9.7	8.2	6.8
	0.010	233.7	156.2	108.6	65.6	32.7	20.1	16.3	13.4
	0.100	321.3	223.6	164.3	122.3	64.5	32.5	29.5	26.1
	1.000	403.1	311.9	237.0	169.7	95.1	54.0	51.7	41.2
	10.00	458.2	403.8	297.3	236.7	135.9	80.5	79.7	68.3
	100.0	513.2	436.0	349.1	274.3	184.2	116.9	92.0	83.1

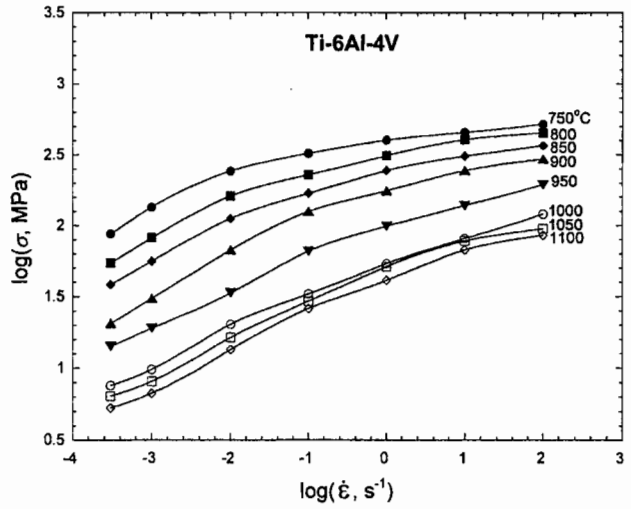

Fig. 3. Variation of flow stress of Ti–6Al–4V with strain rate at different temperatures.

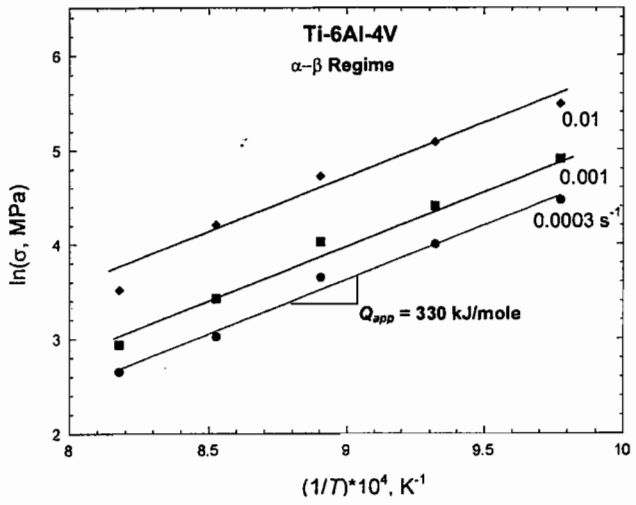

Fig. 4. Arrhenius plot showing the variation of flow stress with inverse of temperature in the α–β regime of Ti–6Al–4V at different strain rates.

950°C) and single phase β region (1000–1100°C). The flow stress values are markedly different in these two regions (Fig. 3).

In the α–β region, the value of stress exponent, n, is estimated to be about 3.4 in the limited strain rate range of 0.0003–0.01 s^{-1}. The Arrhenius plot for estimating the apparent activation energy for hot deformation in the two phase region is shown in Fig. 4. The plot shows that very good correlation exists at lower strain rates while at the strain rate of 0.01 s^{-1} the data at lower and higher temperatures have shown some deviation. The apparent activation energy estimated from this plot is $\sim$330 kJ mol^{-1}, which is in agreement with the values reported in the literature [3,9,10,16,17]. This value is much higher than that for self diffusion in α-Ti (150 kJ mol^{-1}) [22] ruling out the possibility of diffusion in α phase being the rate controlling process. It should be noted, however, that the β volume fraction and α grain size are not constant over the experimental range and Eq. (3) does not include the influence of these factors on deformation kinetics. Continuing the analysis on the basis of the kinetic rate equation, the temperature compensated strain rate parameter, Z, given by:

$$Z = \dot{\varepsilon} \exp(Q/RT) \quad (4)$$

is evaluated on the basis of the above apparent activation energy and plotted as a function of flow stress in Fig. 5. The plot exhibits a good fit for the data and confirms that the kinetic rate equation is obeyed in the limited temperature and strain rate range being considered.

The microstructures obtained on the specimens deformed under different temperature and strain rate conditions relevant to the above analysis are examined and typical microstructures obtained at a strain rate of 0.0003 s^{-1} and different temperatures, are shown in Fig. 6a–d. From these microstructures, it is seen that the α grain size as well as the β volume fraction has increased with increasing temperature. The α grain size variation is shown in Fig. 7 along with the variation of β vol.% (β approach curve) estimated by Sastry et al. [10]. From this plot, it may be noted that beyond 900°C, the β volume fraction increases rapidly from about 40 to 100% at the transus and causes a steep increase in the α grain size. The variation of the α grain size with the Zener–Hollomon parameter is plotted in Fig. 8. Such a correlation is useful in deciding the mechanism of hot deformation, since a linear fit between these two is considered to be an indication of DRX [18]. However, Fig. 8 exhibits a non-linear variation ruling out the occurrence of DRX. Nevertheless, the plot is useful in predicting the α grain size for various temperature-strain rate combinations.

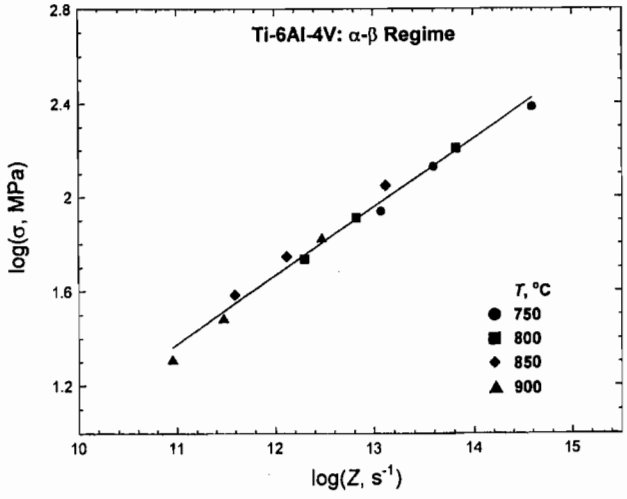

Fig. 5. Variation of flow stress with Zener–Hollomon parameter (Z) in the α–β regime of Ti–6Al–4V.

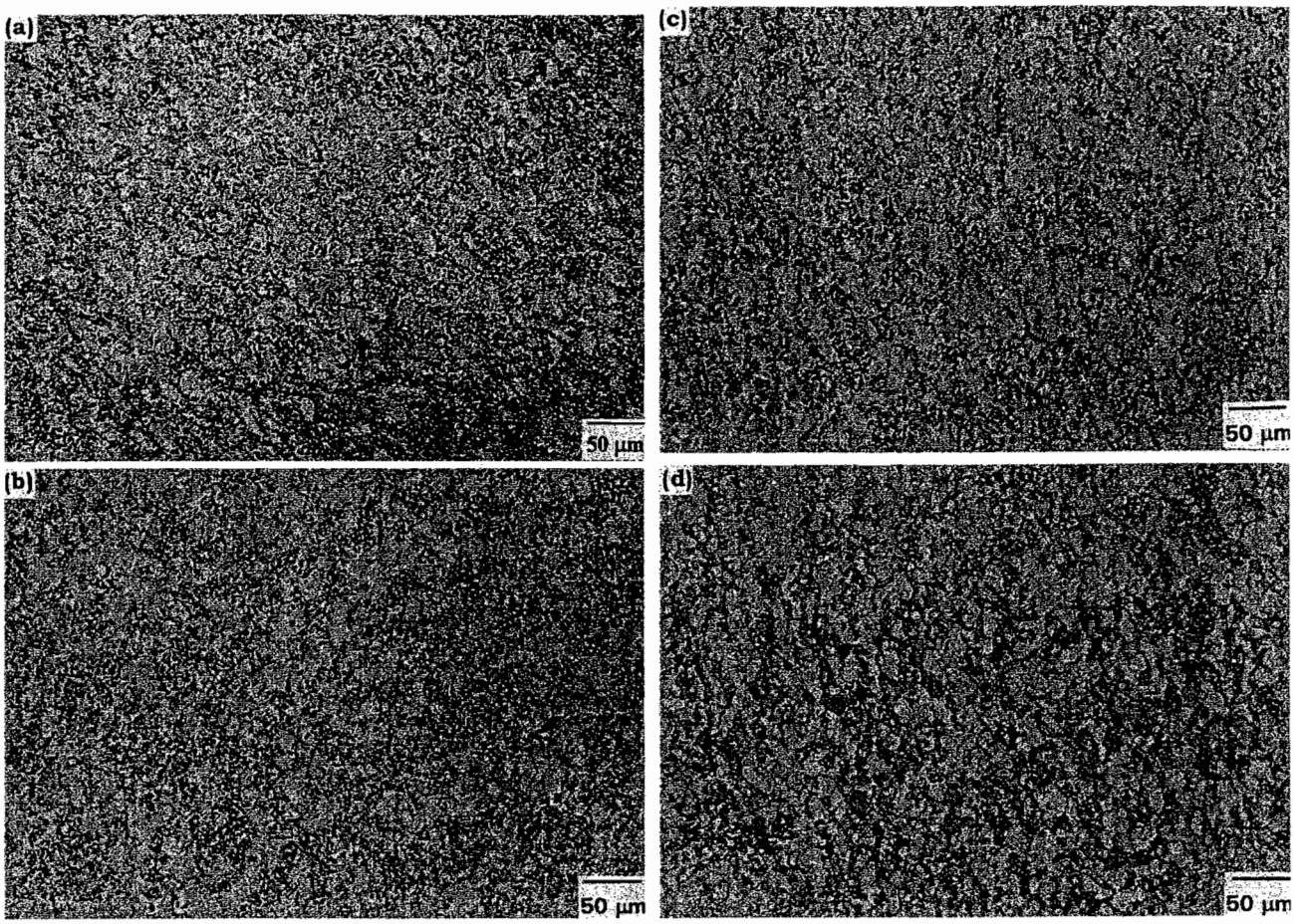

Fig. 6. Microstructures of Ti–6Al–4V specimens deformed in compression at a strain rate of 0.0003 s^{-1} and different temperatures: (a) 750°C; (b) 800°C; (c) 850°C; and (d) 900°C.

In the β region, the value of the stress exponent, n, is estimated to be ~ 3.6 and the Arrhenius plot is shown in Fig. 9. The data fit at lower strain rates (< 0.01 s^{-1}) is very good while deviation is found at the strain rate of 0.1 s^{-1}, particularly at the lower temperature (1000°C). The apparent activation energy estimated from this plot is ~ 210 kJ mol^{-1} which is close to that for self diffusion in β (153 kJ mol^{-1}) [23]. The value estimated by Sheppard and Norley [16] (170 kJ mol^{-1}) from hot torsion data is also in agreement with the above values. The prior β grain sizes in the specimens deformed under different temperatures in this region and at different strain rates below 0.1 s^{-1}, are measured and correlated with the Z parameter in Fig. 10. The data for the deformation temperatures of 1050 and 1100°C have correlated well with the Z parameter while those at 1000°C (close to transus) exhibited a shift towards finer grain sizes. Thus, the analysis suggests that at temperatures higher than 1050°C, the mechanism of hot deformation in β is likely to be DRX, while further analysis is required to understand the mechanism at the transus.

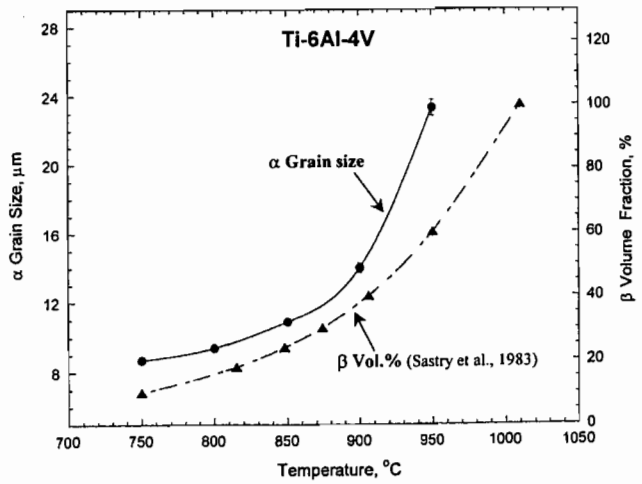

Fig. 7. Variation of α grain size with temperature of Ti–6Al–4V specimens deformed at a strain rate of 0.0003 s^{-1}. Also plotted is the variation of β volume fraction with temperature (β approach curve) [10].

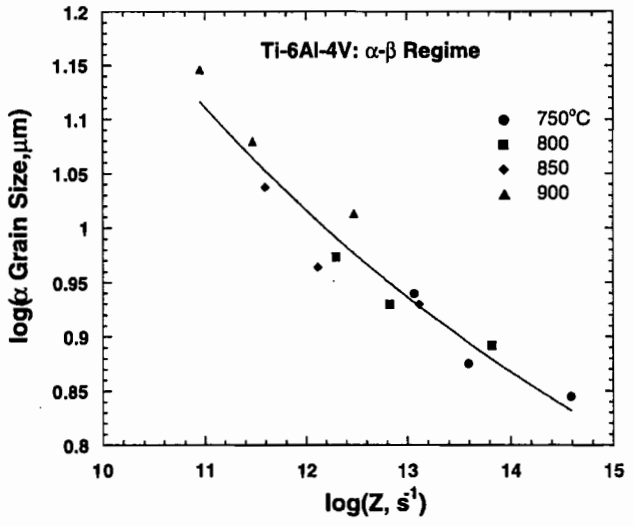

Fig. 8. Variation of α grain size with Zener–Hollomon parameter (Z) in the α–β regime of Ti–6Al–4V.

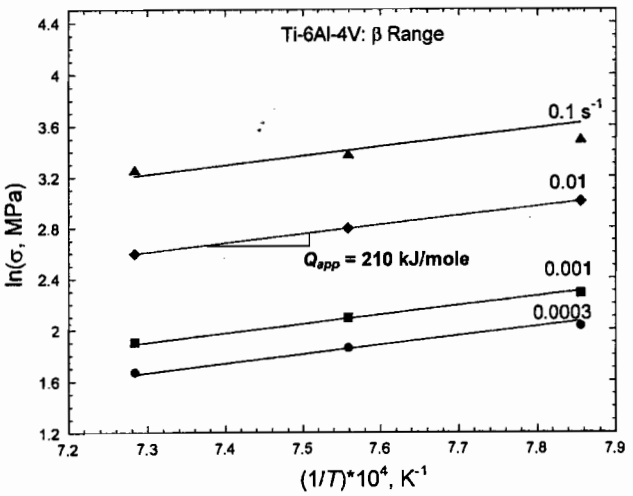

Fig. 9. Arrhenius plot showing the variation of flow stress with inverse temperature at different strain rates in the β range of Ti–6Al–4V.

3.3. Processing maps

The power dissipation map obtained at a strain of 0.5 is shown in Fig. 11. The maps obtained at lower strains exhibited similar features indicating that the processes involved in hot working had very short transients and are essentially of steady-state type. It may be noticed that the iso-efficiency contours in the map exhibit a distinct change in their curvature at about the transus (1010°C). This feature is commonly observed in all materials which show phase transformation including precipitate dissolution [21]. Although the transus is at 1010°C, it may be noted that the β volume fraction exceeds 50% above a temperature of ~960°C (Fig. 7) and hence the characteristics of β deformation may dominate.

The map exhibits two domains — one in the α–β temperature range and the other in the β range, both being in the lower strain rate regime. Other than these two domains, all contours with efficiency values lower than about 39% indicate a transient behavior where no stable microstructural mechanism occurs. The microstructural characteristics of the processes occurring in these domains are discussed below.

3.3.1. Domain in the α–β range

The domain occurs in the temperature range 750–950°C and at strain rates below about 0.002 s^{-1} with a peak efficiency of ~55% at about 825°C and 0.0003

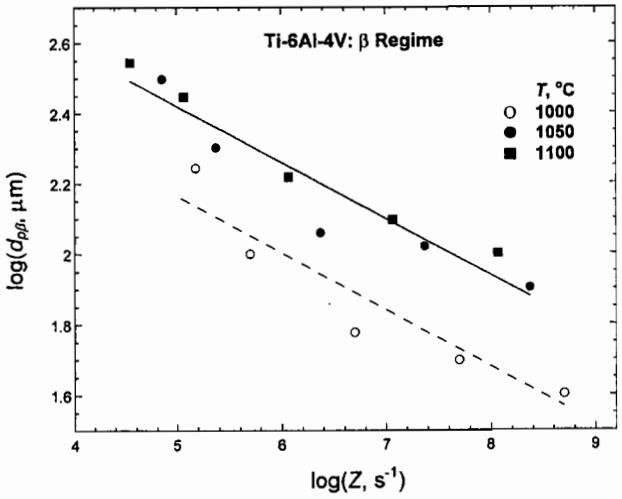

Fig. 10. Variation of prior β grain size ($d_{p\beta}$) with Zener–Hollomon parameter (Z) in the β range of Ti–6Al–4V.

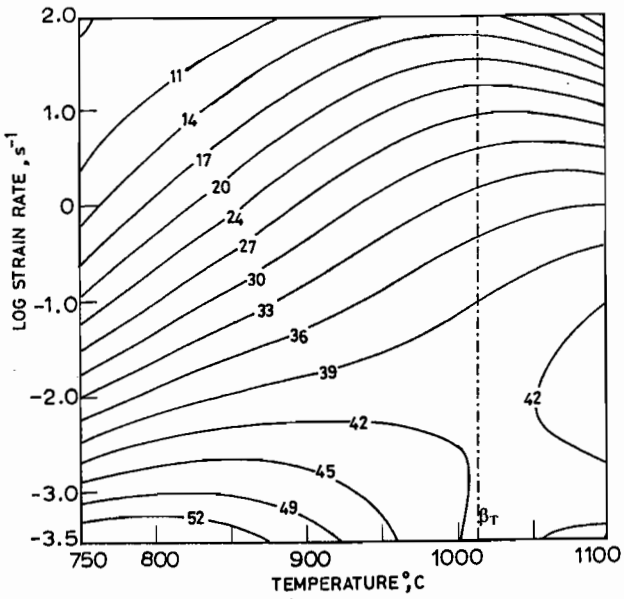

Fig. 11. Power dissipation efficiency map obtained on Ti–6Al–4V at a strain of 0.5. Contour numbers represent per cent efficiency of power dissipation.

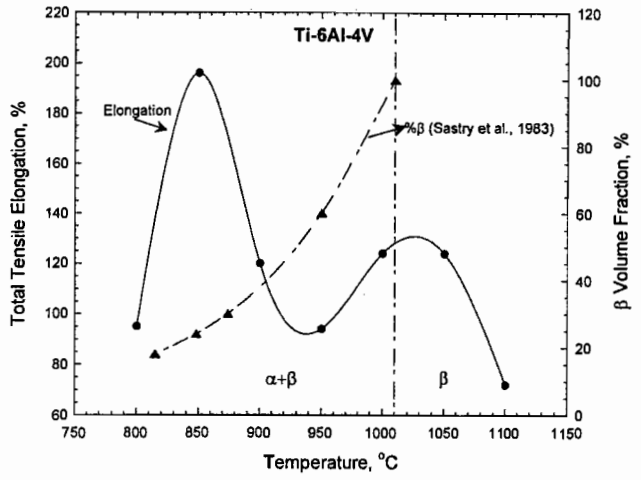

Fig. 12. Variation of tensile ductility at a nominal strain rate of 0.01 s^{-1} and β volume fraction [10] with temperature for Ti–6Al–4V.

s^{-1}. The domain appears to extend to lower temperatures and strain rates and may reach even higher peak efficiency values. A similar domain has been recorded by Seetharaman et al. [17] on commercial Ti–6–4 with an average α grain size of ~25 μm. Efficiency values as high as 55–60% indicate superplastic deformation process since the strain rate sensitivities associated with this efficiency range are about 0.4–0.5. On the other hand, the characteristic efficiency for DRX in α-Ti is only about 43% ($m \approx 0.27$) [21]. The occurrence of superplasticity is best confirmed by tensile ductility measurements. The variation of tensile ductility with temperature at a nominal strain rate of 0.01 s^{-1} (true strain rate will be much lower) is shown in Fig. 12. A high ductility value of about 200% has been recorded at 850°C. At lower strain rates (10^{-4} s^{-1}), ductilities as high as 800% have been recorded on this material [7]. Thus the domain represents the process of superplasticity. The steady state stress–strain curves in this regime (Fig. 2a) are in support of this mechanism.

On the basis of the above ductility variation features and the change in the volume fraction of β with temperature, the mechanism of superplasticity in this material may be deduced. Superplasticity involves sliding of grain boundaries with simultaneous relaxation of the stresses generated at the grain boundary triple junctions by processes involving diffusional flow or plastic deformation. At the temperature of peak efficiency in the domain (825°C), the volume fraction of β is about 20% and this low value of β content permits many α–α interfaces to slide during hot deformation of the two phase alloy. Whether such a sliding leads to superplasticity or wedge cracking is decided by the relaxation processes occurring at the triple junctions. It may be noted that the β phase is present essentially at the triple junctions and is in fact responsible for arresting the grain growth in this material, which is another important requirement for superplasticity. Thus, the deformation behavior of β phase at the triple junctions will be the controlling factor for achieving superplasticity. At high temperatures, β may exhibit several processes that would help to relax the stress concentration and these include dynamic recovery involving thermally activated cross-slip, or DRX, or diffusional creep. The apparent activation energy estimated in the domain (330 kJ mol^{-1}) is much higher than that for self diffusion in β (153 kJ mol^{-1}) ruling out the possibility for the occurrence of diffusional creep or DRX (since DRX in β of Ti–6–4 is controlled by the rate of diffusion as shown in the previous section). It may be therefore deduced that dynamic recovery of β by cross-slip is the rate controlling step for superplasticity in this alloy. In β titanium alloys, the apparent activation energy for deformation in a similar temperature range is estimated to be about 294 kJ mol^{-1} [24] and the mechanism has been identified to be dynamic recovery by cross-slip. These results are in support of the present conclusion regarding the relaxation mechanism chosen by the β phase at the triple junctions

Referring to the ductility variation with temperature (Fig. 12), a sharp drop in ductility occurs in the temperature range 850–950°C when the β volume fraction increases from about 20 to 60%. This observation is in good agreement with the results reported in the literature [25,26] and the near equal volume fraction rule [27] commonly cited for achieving highest ductility due to superplasticity does not seem to be valid. This ductility drop may be attributed to an increase in the α–β interfaces which do not slide easily in view of the mismatch in their individual deformation characteristics. Therefore, the volume fraction of β is very critical for superplasticity since a smaller amount (~20%) is essential for maintaining a stable fine grained structure while a higher volume fraction will increase the undesirable α–β boundaries.

The processing window for superplastic deformation as indicated in the map consists of a temperature range 750–900°C and strain rate range 0.0003–0.002 s^{-1}. It is in these ranges that the kinetic rate equation is obeyed very well, as is expected of any deterministic domain. In an industrial practice, highest possible strain rates and lowest possible flow stresses (highest possible temperatures) are preferred from productivity view point. Also, in the lower temperature side of the domain, the superplasticity process is known to result in grain boundary cavitation, particularly at very large strains [12] and a tensile state of stress. These aspects must be kept in mind while designing the processes involving superplasticity.

3.3.2. Domain in the β range

The map (Fig. 11) exhibits a domain in the β phase field in the temperature range 1050–1100°C and strain

rate range 0.001–0.1 s^{-1} with a peak efficiency of about 45% at 1100°C/0.01 s^{-1}. The domain does not appear to be fully developed and may expand beyond 1100°C. The kinetic considerations discussed before are in support of DRX process in this domain. The microstructure recorded on a specimen deformed at 1100°C/0.01 s^{-1} is shown in Fig. 13. Although cooling across the transus destroys the deformation features, some signatures of DRX like curved prior β boundaries are noticeable. The prior β grain size ($d_{p\beta}$) in this domain may be related to the Z parameter (Fig. 10) according to equation:

$$\log(d_{p\beta}) = 3.22 - 0.16\log(Z) \quad (5)$$

It is interesting to consider the behavior of the material near the transus. While the map indicated only a transient behavior, the ductility measurements (Fig. 12) revealed a peak with a high value of 125% suggesting the possibility of β superplasticity. It may be noted that

Fig. 13. Microstructure of Ti–6Al–4V specimen deformed in compression at 1100°C and 0.01 s^{-1}.

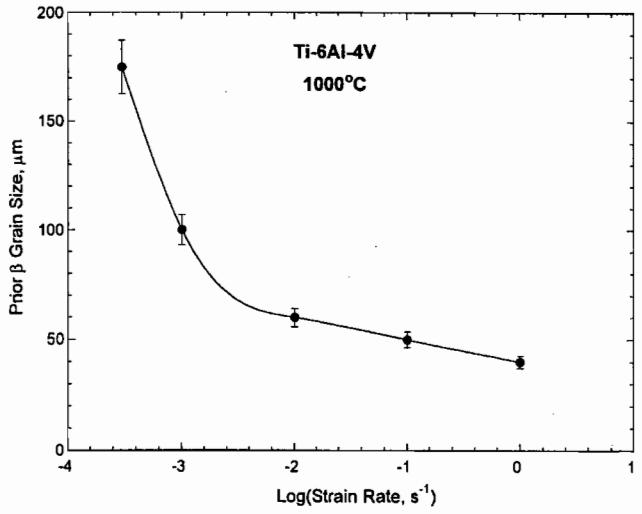

Fig. 14. Variation of prior β grain size with strain rate of Ti–6Al–4V specimens deformed at 1000°C.

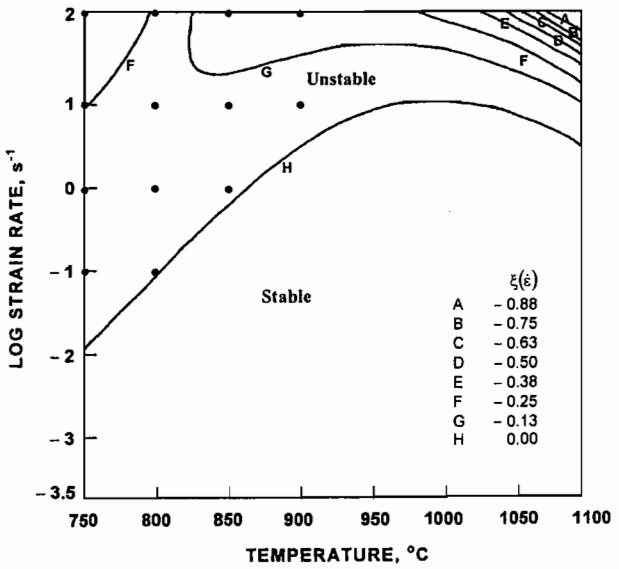

Fig. 15. Instability map obtained on Ti–6Al–4V at a strain of 0.5. Contour numbers represent the value of instability parameter given by Eq. (2). The deformation conditions under which deformed specimens exhibited flow instabilities are indicated by bullets.

the ductility increases with temperature beyond about 950°C and the volume fraction of β increases beyond ~70%, thus providing higher β–β boundary population for sliding. Further, the kinetic analysis has shown that the prior β grain size versus Z relation (Fig. 10) has moved towards finer grain sizes in comparison with that in the β DRX region. It is important to consider the variation of prior β grain size near the transus (1000°C) as a function of strain rate and this is shown in Fig. 14. While the prior β grain size is smaller and not significantly varying at strain rates higher than 0.01 s^{-1}, there is considerable grain growth at lower strain rates. Thus, the transient superplasticity of β may be specific to a strain rate of about 0.01 s^{-1} as is used in the tensile testing since superplasticity will be reduced at lower strain rates due to grain growth and at higher strain rates due to a lower rate of grain boundary sliding.

3.3.3. Flow instabilities

The instability map obtained for Ti–6–4 exhibiting contours of the instability parameter $\xi(\dot{\varepsilon})$ (Eq. (2)) at a strain of 0.5 is shown in Fig. 15. The criterion predicts a large regime of flow instability at strain rates higher than 1 s^{-1} in the entire test temperature range. These predictions are validated with microstructural observations in the α–β regime. The macro and micrographs recorded on a specimen deformed at 750°C/100 s^{-1} are shown in Fig. 16. These exhibit flow localization bands formed at an angle of about 45° to the compression axis. The macrographs of the specimens deformed at different conditions in the instability regime are shown in Fig. 17a–d. These indicate that the bands become

diffused with increasing temperature and decreasing strain rates. The formation of these bands may be attributed to the adiabatic conditions created during deformation and the low thermal conductivity of Ti–6–4. The microstructural features of flow instability described above fully validate the continuum criterion given by Eq. (2).

The instability features in the β regime could not be captured in the microstructures of deformed specimens because of the phase transformation that occurs during cooling. However, the stress–strain curves in this regime (Fig. 2b) exhibited oscillations which are also signatures of flow instabilities [21].

4. Conclusions

Hot deformation behavior of a commercial grade Ti–6–4 with an equiaxed α–β starting microstructure is characterized with the help of isothermal compression tests in the temperature range 750–1100°C and strain rate range 0.0003–100 s^{-1}. The data are analyzed with the help of available materials models and the following conclusions are drawn from this study:

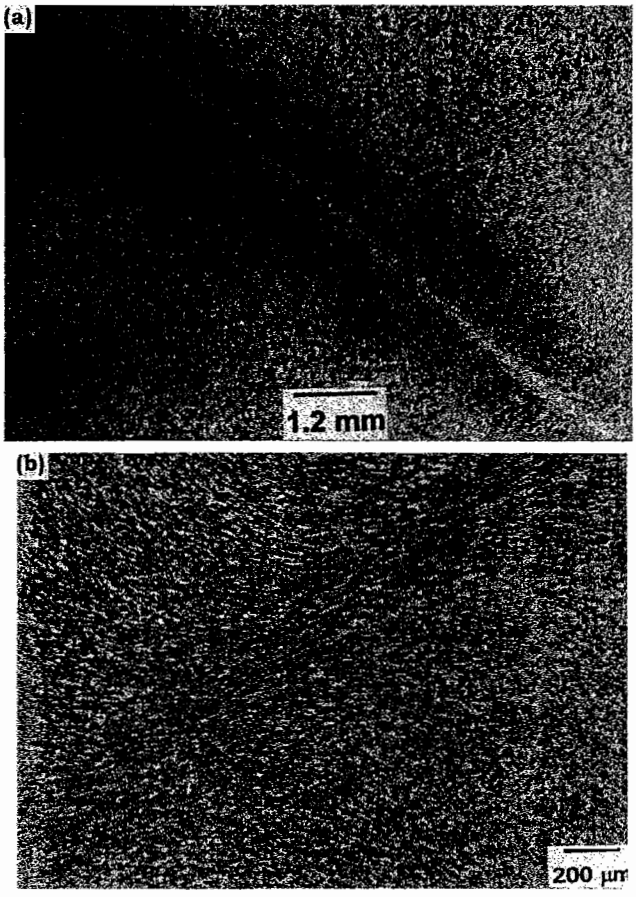

Fig. 16. (a) Macro and (b) microstructure of Ti–6Al–4V specimen deformed at 750°C and 100 s^{-1}. The compression axis is vertical.

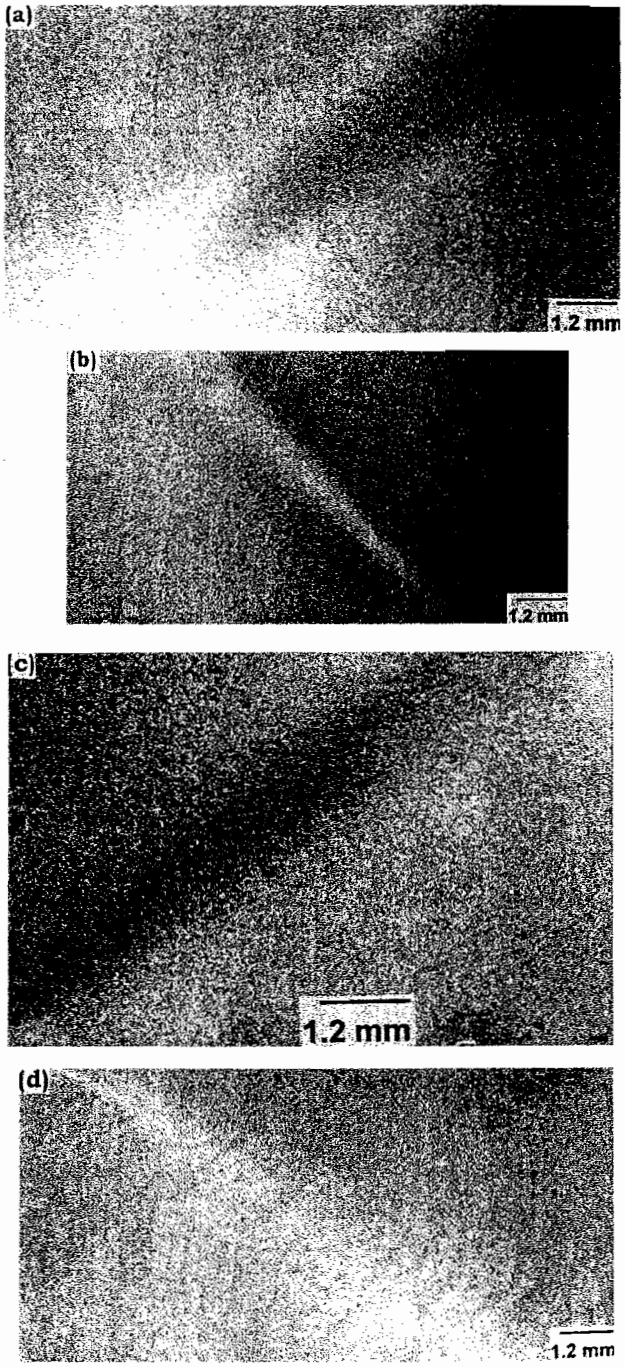

Fig. 17. Macrostructures of Ti–6Al–4V specimens deformed in the flow instability regime: (a) 750°C/1 s^{-1}; (b) 750°C/10 s^{-1}; (c) 800°C/100 s^{-1}; and (d) 850°C/100 s^{-1}. The compression axis is vertical.

(1) The material exhibits fine-grained superplasticity in the temperature range 750–950°C and strain rates slower than 0.002 s^{-1}. The apparent activation energy estimated for this process is ~330 kJ mol^{-1} which suggests that dynamic recovery of grain boundary β is the rate-controlling step.

(2) The β phase undergoes DRX at higher temperatures (> 1050 C) and the apparent activation energy for β-DRX (210 kJ mol^{-1}) is close to that for self-diffusion in β.

(3) At the transus, a high ductility is observed at a nominal strain rate of 0.01 s^{-1} and this is attributed to the occurrence of a transient superplasticity mechanism of fine-grained β phase.

(4) The material exhibits a wide regime of flow instabilities at strain rates higher than 0.1 s^{-1}. These are manifested as adiabatic shear bands in the α–β range and must be avoided for obtaining microstructural control.

Acknowledgements

The authors would like to thank Dr J.C. Malas of WPAFB for many stimulating discussions. One of the authors (YVRKP) is thankful to the National Research Council, USA, for awarding him an associateship and to the Director of the Indian Institute of Science, Bangalore, for granting him a sabbatical leave. The assistance rendered by S. Sasidhara and R. Ravi of Department of Metallurgy, Indian Institute of Science is gratefully acknowledged.

References

[1] Advanced Materials and Processes, ASM Intl. 154 (1999) 39–41.
[2] R.R. Boyer, G.E. Welsch, E.W. Collings (Eds.), Materials Properties Handbook: Titanium Alloys, ASM International, Materials Park, OH, 1994, pp. 488.
[3] C.C. Chen, J.E. Coyne, Metall. Trans. 7A (1976) 1931–1941.
[4] H.M. Flower, Mater. Sci. Technol. 6 (1990) 1082–1092.
[5] I. Weiss, F.H. Froes, D. Eylon, G.E. Welsch, Metall. Trans. 17A (1986) 1935–1947.
[6] I. Weiss, S.L. Semiatin, Mater. Sci. Eng. A263 (1999) 243–256.
[7] D. Lee, W.A. Backofen, Trans. AIME 239 (1967) 1034–1040.
[8] A. Arieli, A. Rosen, Metall. Trans. 8A (1977) 1591–1596.
[9] W.A. Bryant, J. Mater. Sci. 10 (1975) 1793–1797.
[10] S.M.L. Sastry, R.J. Lederich, T.L. Mackay, W.R. Kerr, J. Metals (1983) 48–53.
[11] M.T. Cope, D.R. Evetts, N. Ridley, J. Mater. Sci. 21 (1986) 4003–4008.
[12] M.T. Cope, N. Ridley, Mater. Sci. Technol. 2 (1986) 140–145.
[13] B. Bai, H.S. Yang, N. Chen, A.K. Mukherjee, Scripta Mater. 40 (1999) 1079–1088.
[14] J.S. Kim, J.H. Kim, Y.T. Lee, C.G. Park, C.S. Lee, Mater. Sci. Eng. A263 (1999) 272–280.
[15] N. Ridley, AGARD Lecture Series No. 168, Chapter 4, NATO, France, 1989.
[16] T. Sheppard, J. Norley, Mater. Sci. Technol. 4 (1988) 903–908.
[17] V. Seetharaman, L. Boothe, C.M. Lombard, in: Y.W. Kim, R.R. Boyer (Eds.), Microstructure/Property Relationships in Titanium Aluminides and Alloys, TMS, Warrendale, PA, 1991, pp. 605–622.
[18] J.J. Jonas, C.M. Sellars, W.J. McTegart, Metall. Rev. 14 (1969) 1–24.
[19] Y.V.R.K. Prasad, H.L. Gegel, S.M. Doraivelu, J.C. Malas, J.T. Morgan, K.A. Lark, D.R. Barker, Metall. Trans. 15A (1984) 1883–1892.
[20] Y.V.R.K. Prasad, T. Seshacharyulu, Intl. Mater. Rev. 43 (1998) 243–258.
[21] Y.V.R.K. Prasad, S. Sasidhara (Eds.), Hot Working Guide: A Compendium of Processing Maps, ASM International, Materials Park, OH, 1997.
[22] F. Dyment, C.M. Libanati, J. Mater. Sci. 3 (1968) 349–359.
[23] N.E.W. de Reca, C.M. Libanati, Acta Metall. 16 (1968) 1297–1305.
[24] D.G. Robertson, H.B. McShane, Mater. Sci. Technol. 14 (1998) 339–345.
[25] C.H. Hamilton, in: B. Baudelet, M. Suery (Eds.), Superplasticity, Centre National de la Recherche Scientifique, Paris, Grenoble, France, 1985, pp. 13–22.
[26] T.G. Nieh, J. Wadsworth, O.D. Sherby, Superplasticity in Metals and Ceramics, Cambridge University Press, Cambridge, 1997, p. 81.
[27] O.A. Kaibyshev, Superplasticity of Alloys, Intermetallics, and Ceramics, Springer-Verlag, Berlin, 1992, p. 198.

TITANIUM ALLOY PROCESSING

Improvements in processing Ti-6Al-4V can have a significant impact on manufacturing costs.

Y.V.R.K. Prasad, T. Seshacharyulu,* Steve C. Medeiros,* William G. Frazier, James T. Morgan, and James C. Malas, FASM*
Air Force Research Laboratory
Wright Patterson Air Force Base, Ohio

Among all titanium alloys, Ti-6Al-4V is the most widely used and accounts for more than 50% of all applications, including aerospace, automotive, energy, marine, chemical, prosthetics, and sports. In aerospace, it accounts for critical components ranging from bulkheads, wing spars, and skin (airframe), to compressor disks and blades (engine), and panels and gas bottles (plate and sheet components). For example, 36% of the weight of the U.S. Air Force F-22 Raptor fighter aircraft consists of Ti-6Al-4V. Therefore, any innovation in the design and optimization of manufacturing processes for Ti-6Al-4V components will help in achieving a large overall cost saving.

The key to innovation is in achieving a thorough understanding of its microstructural response through effective materials models. This article summarizes some of the recent developments in the area of titanium processing that have helped in the design and optimization of hot working processes for Ti-6Al-4V.

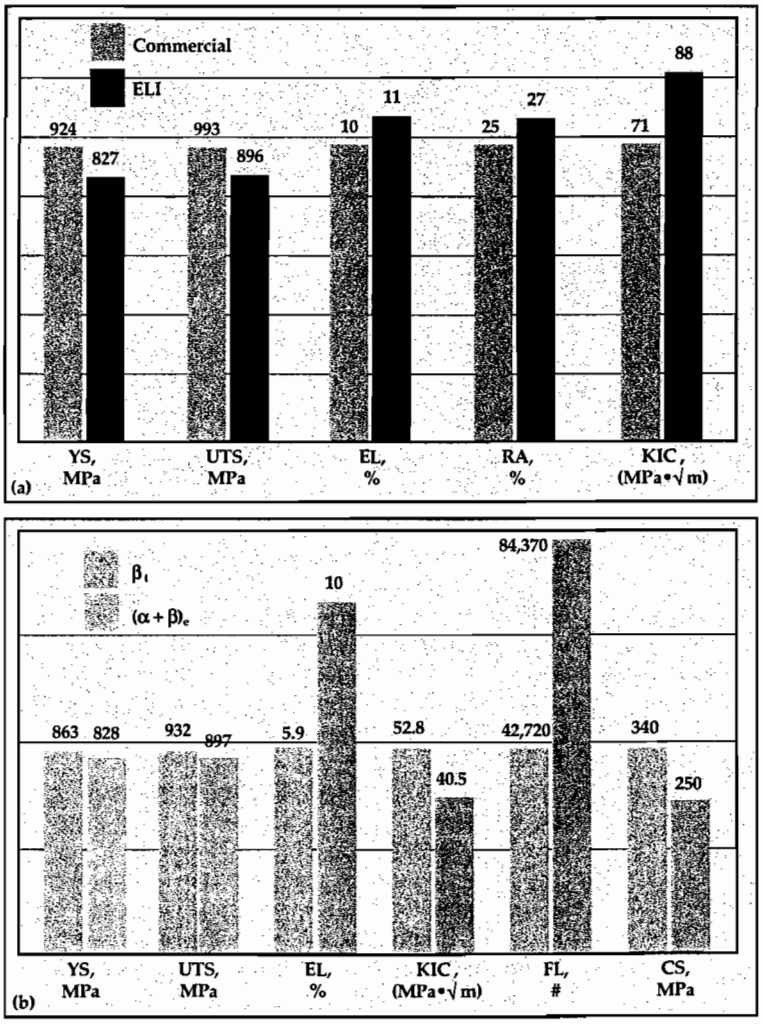

Fig. 1 — Comparison of room temperature mechanical properties of Ti-6Al-4V: (a) Commercial vs. ELI grade (b) transformed beta vs. equiaxed (α+β) starting microstructure. (YS, yield strength; UTS, ultimate tensile strength; EL, elongation; RA, reduction in area; K_{Ic}, fracture toughness; FL, fatigue life taken as the cycles to crack initiation; CS, creep strength.)

Titanium grades

Ti-6Al-4V material is marketed in two interstitial grades, the essential difference being the oxygen content. The commercial grade has an oxygen content in the range 0.16 to 0.20 wt.%, and the extra low interstitial (ELI) grade has 0.1 to 0.13 wt.%. In the ELI grade, the aluminum content is kept slightly lower than in the commercial grade. Room temperature mechanical properties for the two grades are compared in Fig. 1(a). The commercial grade has a higher strength and slightly lower ductility than the ELI grade, while the fracture toughness of ELI material is higher by about

*Member of ASM International

Microstuctures range from acicular to equi-axed.

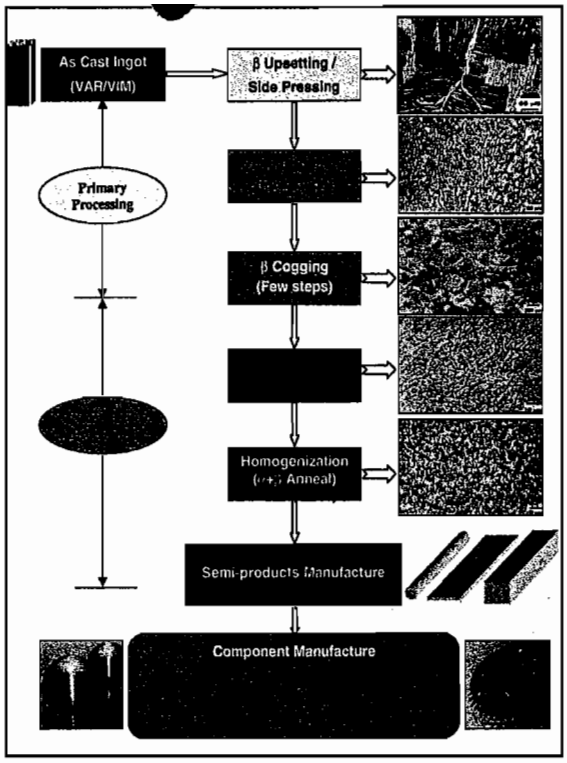

Fig. 2 — Thermomechanical processing steps and resulting microstructures in the manufacture of Ti-6Al-4V semi-products and components. (VAR: Vacuum Arc Remelting, VIM: Vacuum Induction Melting)

25%. Thus, the ELI grade is preferred for applications such as bulkheads in fighter aircraft, where damage tolerance is a critical requirement. For other applications, and where tensile strength is the design criterion, the commercial grade is generally the choice.

Ti-6Al-4V is a near-α alloy and has a two-phase (α+β) microstructure. The temperature at which (α+β) transforms to β (β transus) depends on the interstitial grade, because oxygen acts as an a stabilizer. The transus is important not only for mechanical working, but also for heat treatment of this alloy. The transus is about 1010 to 1020°C (1850 to 1870°F) for the commercial grade and about 970 to 980°C (1780 to 1800°F) for the ELI grade.

The alloy may be thermomechanically treated to develop microstructures ranging from acicular or lamellar (called transformed β) at one extreme, to equiaxed (α+β) at the other. The mechanical properties of these extremes are compared in Fig. 1(b). While the tensile strength is not significantly different for the two microstructures, the equiaxed (α+β) has twice the ductility and fatigue life. As a result, the equiaxed (α+β) microstructure is preferred for rotating components such as compressor disks, where resistance to low cycle fatigue is critical. However, the transformed β microstructure has better fracture toughness and higher-temperature creep strength.

Thermomechanical processing

The steps involved in the thermomechanical processing of Ti-6Al-4V alloy are shown schematically in Fig. 2.

- *The primary step of deforming the as-cast ingots* consists of mechanical working at temperatures above the β transus. It involves upset forging, side pressing, and cogging operations, which are all slow-speed processes. However, they help achieve chemical homogeneity, and they break the as-cast microstructure (transformed β).
- *Beta processing followed by faster cooling rates* including air cooling results in an acicular or Widmanstatten (lamellar) microstructure with a thin α layer at the prior β boundaries. It is preferred that the prior β grain size not exceed 100 to 200 μm and that the thickness of the α layer be less than about 5 μm. To reduce the prior β grain size, the general practice is to insert a few steps of cogging in the (α+β) phase field in the overall β processing schedule, and to lower the temperature of the final β processing step. However, recent studies have indicated that reducing the prior β grain size does not offer much benefit in hot working.
- *Secondary processing* involves several steps of cogging in the two-phase region, followed by a homogenization treatment such that the transformed β microstructure is fully converted to a very fine-grained equiaxed (α+β) through a process of "globularization." Thermomechanical processing routes for component manufacture consist of β forging and heat treatment or (α+β) forging, followed by a stress relief anneal.

Thus, transformed β and equiaxed (α+β) preform (or starting) microstructures are critical to processing because of their different responses to deformation and heat treatment. Therefore, control of microstructure is of the essence during industrial processing, because product properties and the acceptability of the semi-products depend upon producing defect-free material with a close control of grain size.

The evolution of the microstructure during hot working depends not only on the response of the material to the imposed processing parameters (temperature, strain rate, and strain), but also on the "history" of the material (chemistry and starting microstructure). This aspect is generally covered by studies of the constitutive behavior of the material and is explicitly analyzed by materials models.

Processing maps

One of the recent methods of materials modeling that directly addresses the issues of design and optimization in hot working is the approach of processing maps. Developed on the basis of flow stress data over wide ranges of temperature, strain rate, and strain, the processing map depicts domains of "safe" microstructural processes as well as deleterious regimes. The safe and preferred mechanisms are dynamic recrystallization, superplasticity, globularization, and dynamic recovery.

Regimes to be avoided are void formation, wedge or grain boundary cracking, adiabatic shear band formation, and flow localization. From the processing maps, it is possible not only to arrive at conditions for optimizing hot workability, but also to design the processing sequence based on the limiting conditions for the onset of defect-generating mechanisms or flow instabilities.

Commercial grade

The temperature-strain rate regimes representing the various microstructural processes in the hot deformation of commercial grade Ti-6Al-4V with *transformed β* (lamellar) starting microstructure are shown in Fig. 3, as revealed by its processing map. This map suggests that microstructural conversion through cogging is best done in the globularization domain, for which the optimum temperature is 960°C (1760°F) and the strain rate is 10^{-3}/s (hydraulic press). The highest strain rate limit for this mechanism is about 10^{-2}/s, because at faster strain rates, deleterious microstructures consisting of either adiabatic shear bands (at lower temperatures) or lamellae kinking (at higher temperatures) will result in the billet.

Likewise, the lower temperature limits are set by the occurrence of prior β boundary cracking, and higher temperature limits are set by the transus. Since the surface layers of the ingot are cooled during the cogging operation, adhering to the lower temperature limit is of particular importance in this case. Otherwise, strain induced porosity (SIP) will develop in the surface layers, manifested as wedge cracks at triple junctions of prior β boundaries. This type of SIP may be avoided by introducing suitable resoaking cycles during sequential cogging. However, cogging at temperatures higher than the optimum (960°C, 1760°F) results in a larger α grain size and a lower primary α content.

The microstructural response of Ti-6Al-4V to hot deformation changes considerably when the preform microstructure is equiaxed (α+β,) as seen from the map in Fig. 4. Unlike the transformed β preform, the map does not exhibit globularization, prior β boundary cracking, or lamellae kinking. Instead, these are replaced by a domain of superplasticity at lower strain rates and a wide regime of dynamic recovery at intermediate strain rates.

The regime of adiabatic shear banding is not significantly different. Superplastic forming of Ti-6Al-4V is a well established manufacturing process for making complex shapes and is often coupled with diffusion bonding in the case of sheet metal components. The optimum processing parameters for superplastic forming are a temperature of 825°C (1520°F), and strain rates less than 10^{-3} /s. In view of the slower strain rates, component manufacture is time consuming and also expensive, since it has to be done under isothermal conditions (i.e. the dies are at the same temperature as the workpiece). The elongation in the superplasticity domain is very sensitive to temperature, strain rate, and the grain size. In particular, the temperature range in which the elongation reaches a peak is very narrow and demands close control around the optimum.

The material is sensitive to temperature because of the critical requirement that the β volume fraction be about 25% for optimum superplasticity. This differs from conventional α+β alloys such as the Zn-Al system, in which a 50:50 ratio is considered ideal. Furthermore, although superplasticity enables abnormal elongations, paradoxically the process generates cavitation at large strains, and needs close control of the state of stress in the deformation zone to minimize damage.

Because of the slow speeds of forming, superplasticity is not commercially viable except for high-value, small-lot production, such as those for aero-

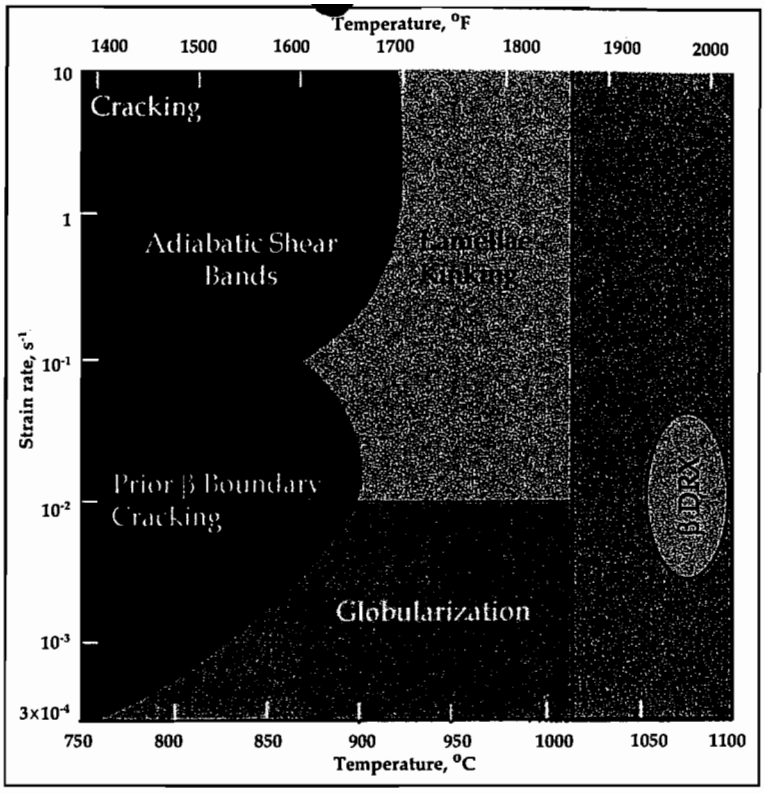

Fig. 3 — Processing map for hot working of commercial grade Ti-6Al-4V with transformed β starting microstructure illustrating microstructurally "safe" and damage mechanisms. Microstructures: Bottom left – prior β boundary cracking; bottom right – globularization; top left – adiabatic shear band cracking; top right – lamellae kinking.

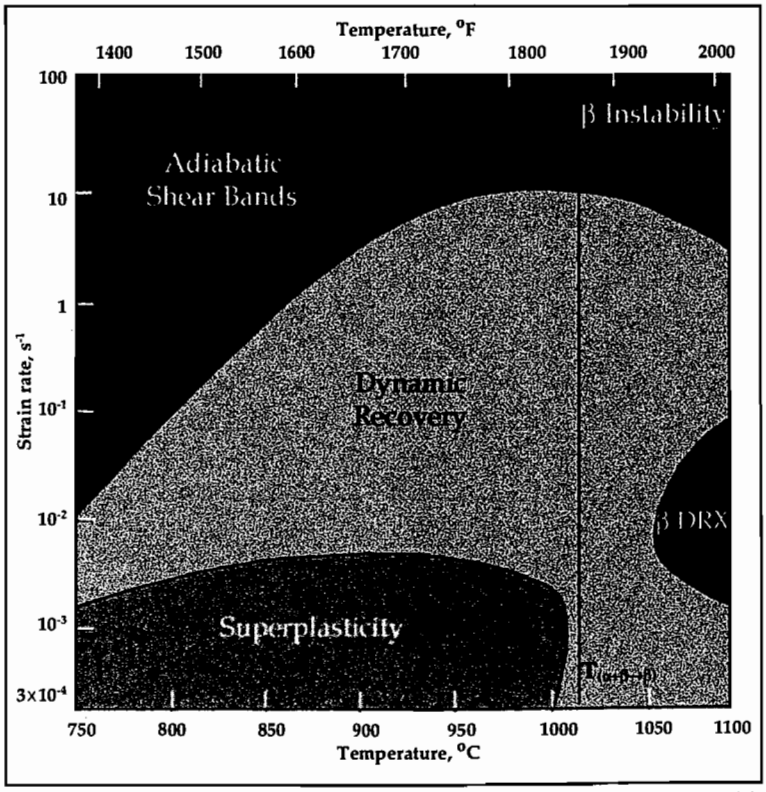

Fig. 4 — Processing map for hot working of commercial grade Ti-6Al-4V with equiaxed (α+β) starting microstructure.

The higher strain rate limit may be extended by raising the deformation temperature.

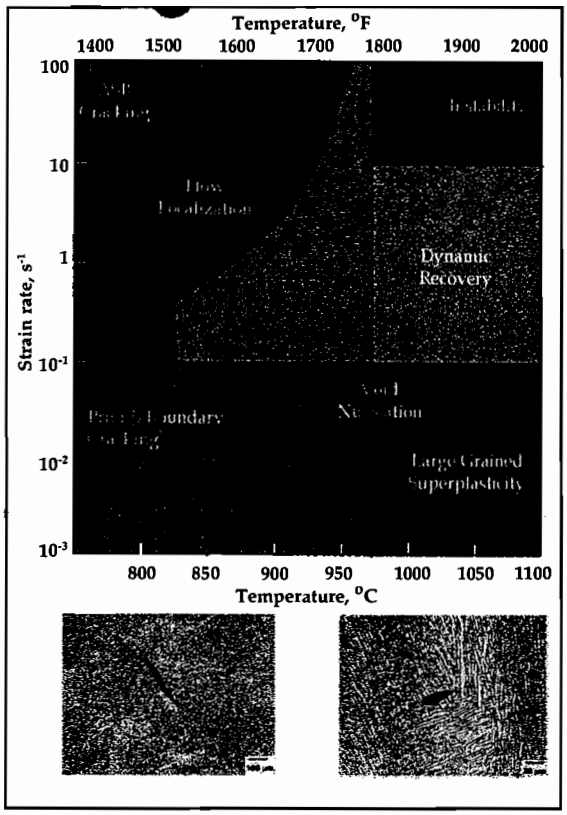

Fig. 5 — Design and optimization of cogging process for ELI grade Ti-6Al-4V. Processing map for transformed β starting microstructure, showing the preferred window of globularization (green) and its limits of prior β boundary cracking at lower temperatures. The microstructure on the left shows prior beta boundary cracking at lower temperatures. The microstructure on the right shows void nucleation and growth at higher temperatures.

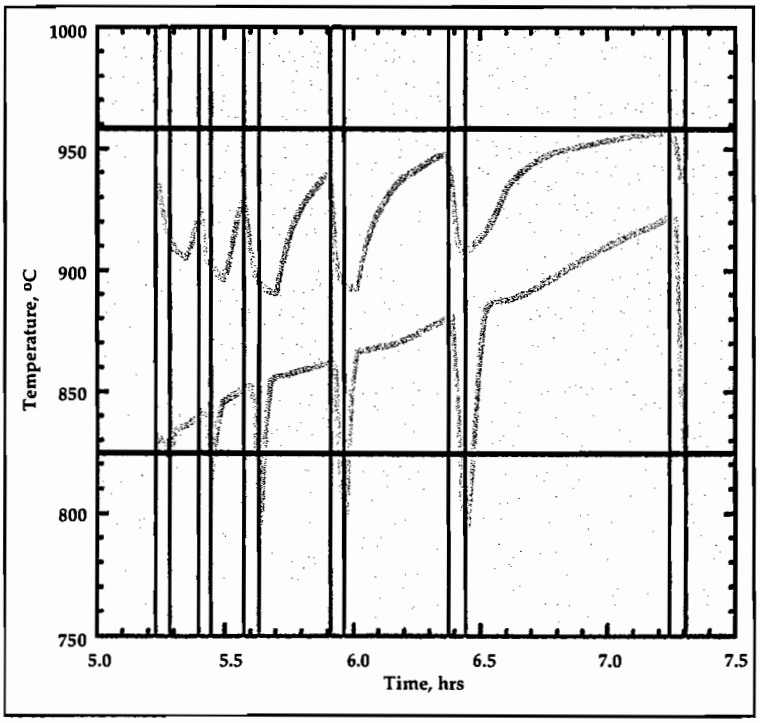

Fig. 6 — Optimization of the resoaking times during differential temperature cogging of ELI Ti-6Al-4V. The higher and lower temperature limits for avoiding prior β cracking and void nucleation are marked by red and blue lines respectively. The temperature profile giving maximum and minimum temperatures within the billet is given by the green curve, and the vertical bands represent the time spent by the ingot out of the furnace.

space components. Alternatively, Ti-6Al-4V components may be forged at higher speeds by friction screw or mechanical presses under non-isothermal conditions (hot-die forging); and flat products may be manufactured by hot rolling. These are in the regime of dynamic recovery (Fig. 4), and may be called "transient" processes. In such a regime, it is difficult to optimize hot workability. However, higher strain rates are preferred for increased productivity, and the limit is set by a value of strain rate that does not cause adiabatic shear band formation. As seen in Fig. 4, the higher strain rate limit may be extended further by increasing the deformation temperature up to about 950°C (1740°F). Following deformation processing in this regime, the material is mill annealed in the two-phase region to soften the material and relieve residual stresses.

Extra-low interstitial grade

Ironically, the ELI grade is more difficult to process. This is clear from the processing map shown in Fig. 5, which corresponds to the transformed β preform structure. The optimum hot working parameters for (α+β) cogging of this material are 925°C and 0.001 / s. The optimum temperature is lower than that for the commercial grade by about 35 to 40°C (63 to 72°F), which is nearly the difference in their transus. Unlike that for the commercial grade, the map exhibits additional regimes of void nucleation near the transus and large-grained superplasticity of β. The implication of the void nucleation process near the transus is that it puts an upper limit to the cogging temperature, the lower limit being the temperature for the onset of prior β boundary cracking.

Further, if the ELI grade is cogged under conditions similar to the commercial grade (at 960°C, 1760°F), void nucleation develops in the mid-plane region where the temperature is close to its transus. The void nuclei grow during the resoaking period under a state of residual tensile stress existing at the mid-plane of the cogged billet. The void population is multiplied during repeated cogging and resoaking steps, and will render the semi-product unacceptable for further processing. These voids are the second type of SIP essentially within the prior β grains, and are mostly located at the triple junctions of Widmanstatten colonies.

Therefore, the temperature limits set by the two-defect-generation processes require that the temperature at the surface of the ingot be higher to avoid prior β boundary cracking, and lower at the mid-plane to prevent void nucleation.

One of the ways to satisfy this requirement is to design temperature-differential cogging, in which the heating and resoaking cycles are controlled to maintain the differential until the process is completed. A typical cogging cycle with the above criterion is shown in Fig. 6, which optimizes the time of soaking and resoaking such that SIP is mitigated, while cutting the total processing time to an extent of about 40%.

Equiaxed (α+β) of the ELI grade has a hot deformation behavior similar to that of the commercial

Fig. 7 — Macrostructure of ELI Ti-6, 4V extruded at high speeds (140 inch/min) and an extrusion ratio of 15:1. Billet temperature is 1010°C (corrected temperature: 1060°C), and it exhibits flow localization bands manifesting instability in β. The extrusion direction is horizontal.

grade, except that the regimes move to lower temperatures in accordance with the lowering of the transus. Also, β processing is not normally a problem, because the material is soft and requires low press loads. Finer prior β grain size may be achieved by working at lower temperatures in the β range and/or higher strain rates. However, if processed rapidly at speeds corresponding to strain rates higher than 10/s (such as extrusion), the β phase exhibits adiabatic shear bands as manifestations of its flow instability, Fig. 7. This type is not encountered at conventional processing speeds.

Although the above information pertains to only two standard preform microstructures encountered in the processing of Ti-6Al-4V, the material has a high potential for a large variety of preform microstructures, some of which may be of direct benefit to the processing industry. Research is under way at the Materials and Manufacturing Directorate of WPAFB for inventing newer preform microstructures that would help in designing faster and more affordable processes for manufacturing superior quality products in Ti-6Al-4V. ■

For more information: Steve Madeiros, Materials and Manufacturing Directorate, Air Force Research Laboratory, Wright-Patterson Air Force Base, OH 45433; tel: 937/904-4324; e-mail: Steve.Medeiros@wpafb.af.mil.

Materials and Manufacturing Processes, Vol. 15, No. 4, 581–604, 2000

Microstructural Modeling and Process Control During Hot Working of Commercial Ti-6Al-4V: Response of Lamellar and Equiaxed Starting Microstructures

Y. V. R. K. Prasad, T. Seshacharyulu,
S. C. Medeiros, and W. G. Frazier
Materials Process Design Branch (AFRL/MLMR)
Materials and Manufacturing Directorate
Air Force Research Laboratory
Wright-Patterson Air Force Base, OH 45433-7746

Abstract

The microstructural changes that occur during hot deformation of Ti-6Al-4V alloy with β transformed (β_t) and equiaxed α+β ($(\alpha+\beta)_e$) starting microstructures have been modeled in the temperature range 750-1100°C and strain rate range 0.0003-10 s^{-1}. The stress-strain behavior, the kinetic parameters, and the processing maps have been compared for these two preforms with a view to evaluate the mechanisms of hot deformation and to establish correlations between the microstructural changes and the process parameters. The β_t preform exhibits continuous flow softening behavior below the transus (α-β range) and is harder than the $(\alpha+\beta)_e$ preform. In the β range, the stress-strain curves were of steady-state type except at the highest strain rate where oscillations have been observed. In the α-β range, the apparent activation energies for hot deformation are 455 and 330 kJ/mole for the β_t and $(\alpha+\beta)_e$ preforms respectively and the stress exponents are similar. In the β range, the apparent activation energy is in the range 172-210 kJ/mole which is close to that for self diffusion in β titanium. The grain size variation with temperature and strain rate could be correlated with the Zener-Hollomon (*Z*) parameter. Deformed at slow strain rates in the two phase range, the β_t preform undergoes a microstructural conversion by the process of globularization of lamellar colony structure. The optimum parameters for globularization are 960°C/0.0003 s^{-1}. The size of globules is not dependent on strain but on temperature and strain rate of deformation and could be correlated with *Z*. The $(\alpha+\beta)_e$ preform, on the other hand, deforms superplastically and the optimum processing parameters are 825°C/ 0.0003 s^{-1}. In this domain, the variation of α grain size with Z is linear on a log-log scale. The processing windows are similar in both the preforms except at the lower

temperature limit which is higher for the β_t preform by about 100°C than the $(\alpha+\beta)_e$ preform. The β phase undergoes dynamic recrystallization irrespective of the preform structure and the resulting grain size is dependent on the Z parameter. Both the preforms exhibit flow instabilities when deformed in the two phase range at higher strain rates and these are manifested as adiabatic shear bands causing flow localization.

1.0 Introduction

Manufacturing of Ti-6Al-4V (Ti-6-4) components involves two major deformation processing steps. These include cogging/extrusion of as-cast ingots with a β transformed lamellar microstructure (hereafter referred to as β_t preform) to "convert" it into an equiaxed α+β structure (hereafter referred to as $(\alpha+\beta)_e$ preform) and forging of equiaxed microstructure into component shapes. There is also an intermediate anneal which essentially ensures that the converted microstructure is homogeneous. The response of the material to each hot deformation step is different since the starting microstructures are different. In order to design a manufacturing process for controlled workability as well as microstructural evolution, it is necessary to know the constitutive behavior of the material with these two different starting microstructures so that "safe" processing windows can be established. Further, it would be valuable to quantitatively predict some of the microstructural features as a function of process parameters such that the microstructure can be incorporated into the process models. The aim of the present investigation is to develop microstructural models specific for two different preforms in a manner that is compatible with their use in conjunction with other process models like finite element methods and heat transfer models.

Considerable work has been done on the constitutive behavior of β_t preform of commercial Ti-6-4 during hot working (1-8), and the mechanism of importance was globularization of lamellar structure. While Semiatin et al.(4) attempted to relate the kinetics of globularization to the plastic strain in the specimen, Seshacharyulu et al. (8) established a correlation between the size of the globules with temperature and strain rate through the Zener-Hollomon (Z) parameter. Both these studies identified the conditions for the formation of wedge cracks during hot working of this material where Semiatin and coworkers (5,6) developed plasticity controlled cavity growth and coalescence models to correlate crack formation with strain. On the other hand, Seshacharyulu et al. (8) evaluated the processing limits for globularization by taking into consideration the onset of wedge cracking at lower temperatures and flow localization at higher strain rates, in addition to the prediction of optimum processing conditions. As regards the behavior of $(\alpha+\beta)_e$ preform, the occurrence of superplasticity in the α-β range has been established by a number of investigators (9-13). Considerable effort has also gone into the study of the

nature of cavitation and its control during superplastic forming (14-16). The emphasis in the majority of the above investigations has been deformation in the α-β phase field. However, it was recognized (17) that β deformation mechanisms are also of interest, not only for optimizing the workability in the β range but also for understanding the behavior of the alloy when the deformation temperature is close to the transus.

In this paper, the constitutive responses of the β_t and the $(\alpha+\beta)_e$ starting microstructures are evaluated and compared with a view to model the microstructural evolution during hot working. For this purpose, the stress-strain behavior, the kinetic parameters, the processing maps, the globule/grain size variations and the tensile ductility are considered in detail.

2.0 Experimental

Ti-6-4 having the following composition (wt.%) was used in this study: 6.28 Al, 3.97 V, 0.18 O, 0.052 Fe, 0.0062 N, 0.008 C, 0.0049 H, balance Ti. As-received 20 mm diameter bars in the mill annealed condition possessed an $(\alpha+\beta)_e$ microstructure. In order to obtain β_t starting microstructure these bars were β solution treated at 1050°C for 1 hour and air-cooled.

Isothermal, constant true strain rate compression tests were conducted using a servohydraulic testing machine over the temperature range 750-1100°C in 50°C intervals and at constant strain rates 3×10^{-4}, 10^{-3}, 10^{-2}, 10^{-1}, 10^{0}, and 10^{1} s^{-1}. Additional tests were conducted at 10^{2} s^{-1} on $(\alpha+\beta)_e$ preform. Specimens of 15 mm height and 10 mm diameter were used for testing in the α-β range while larger specimens of 22.5 mm height and 15 mm diameter were used for accurate flow stress measurements in the β range. All specimens were coated with a borosilicate glass paste for lubrication and environmental protection. They were soaked for 10 minutes at the test temperatures and deformed to half the height in each case to impose a true strain of about 0.6 and were air-cooled to room temperature after deformation. The resulting load-stroke data were evaluated to obtain true stress-true plastic strain curves using the standard method. Deformed specimens were sectioned parallel to the compression axis and the cut surface was prepared for metallographic examination. The specimens were etched with Kroll's reagent and polarized light micrographs were recorded.

Hot tensile tests were conducted in the temperature range 800-1100°C at a nominal strain rate of 0.01 s^{-1} (constant actuator speed of 0.25 mm s^{-1}). Cylindrical specimens of 25 mm gauge length and 4 mm gauge diameter were used for this purpose. The specimens were pulled to fracture and total elongation as a function of temperature was recorded.

3.0 Results and Discussion

3.1 Initial Microstructure

The starting microstructure of the β_t preform is shown in Figure 1a and it consists of large prior β grains of average size of ~200 μm separated by an α layer of 5 μm thick at the grain boundary.

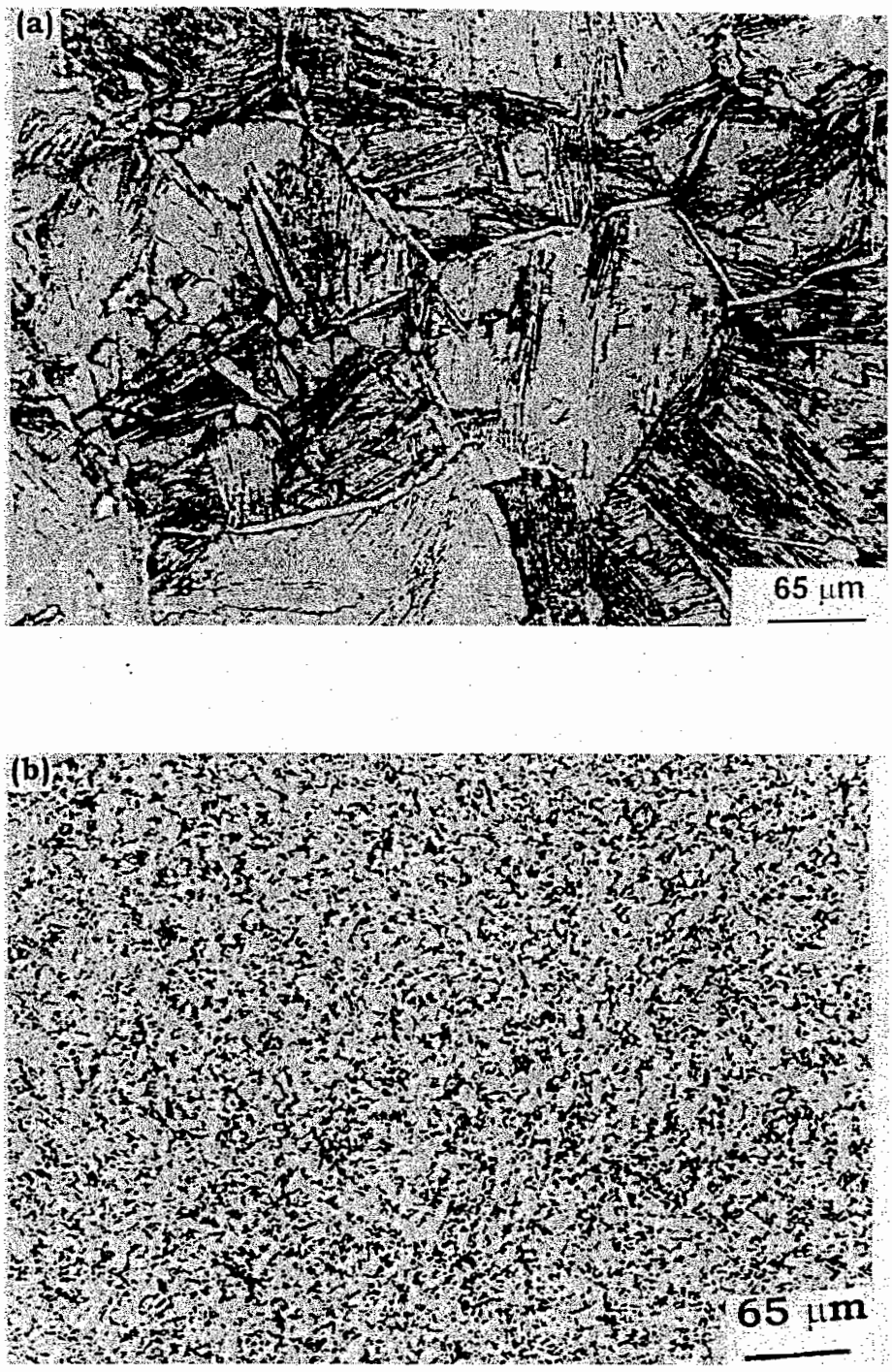

Figure 1: Starting microstructures of Ti-6Al-4V used in this study: (a) β_t preform and (b) $(\alpha+\beta)_e$ preform.

Widmanstätten colonies of lamellar ($\alpha+\beta$) with different orientations are present within these prior β grains. The $(\alpha+\beta)_e$ starting microstructure is shown in Figure1b and it has an average α grain size of about 8 μm and a β volume fraction of about 10%. The β phase is present mostly at the grain boundary triple junctions. The $(\alpha+\beta)\rightarrow\beta$ transformation temperature (β transus) for this material is about 1010°C.

3.2 Stress-Strain Behavior

The true stress-true plastic strain curves obtained in compression at 850°C on β_t preform and $(\alpha+\beta)_e$ preform are shown in Figure 2a, and these are representative of the deformation behavior in the α-β temperature range. All the curves for the β_t preform exhibit flow softening while in the case of $(\alpha+\beta)_e$ preform, only those obtained above a strain rate of above 0.1 s^{-1} show flow softening. At lower strain rates (<0.01 s^{-1}), the $(\alpha+\beta)_e$ preform deforms in a steady-state manner unlike the β_t preform which flow-softens to reach a steady state asymptotically close to that observed in the equiaxed structure at higher strains. At all strain rates, the flow stress for the β_t preform is higher than that for the $(\alpha+\beta)_e$ preform. In titanium alloys, flow softening type stress-strain curves indicate a process of globularization of the lamellar microstructure and in the absence of lamellar structure in the preform, flow localization is expected to occur in the material. Thus, the flow behaviors observed in the two preforms suggest that globularization occurs at slow strain rates in the β_t preform while at higher strain rates, both the preforms are likely to exhibit flow localization. It may be mentioned here that the flow localization process causes instability of plastic flow and is undesirable for processing.

The stress-strain curves obtained at 1100°C are shown in Figure 2b and these are representative of the β phase behavior. Figure 2b shows that the two preforms behave in an identical manner in the β range. This similarity can be attributed to the all β microstructure in both the preforms above the β transus. At lower strain rates (<0.1 s^{-1}), the curves are of steady-state type while at higher strain rates they exhibited low rates of work hardening associated sometimes with oscillations (e.g. at 10 s^{-1}). The steady-state curves indicate that softening is occurring sufficiently fast to balance work hardening and the oscillations suggest either dynamic recrystallization (DRX) or flow instability. The curves obtained at 1000°C are shown in Figure 2c which is similar to those in Figure 2b indicating that the deformation near the transus is governed essentially by the β behavior.

The above results show that the shapes of stress-strain curves are *necessary* indications of some microstructural mechanisms occurring during hot deformation, but they are not *sufficient* to predict them definitely. Further analysis of the temperature and strain rate dependency of flow stress is required for this purpose. A comparison of the flow behaviors of two preform structures reveals that sufficient differences exist that warrants detailed analysis.

3.3 Kinetic Analysis

The flow stress data as a function of temperature, strain rate, and strain for the

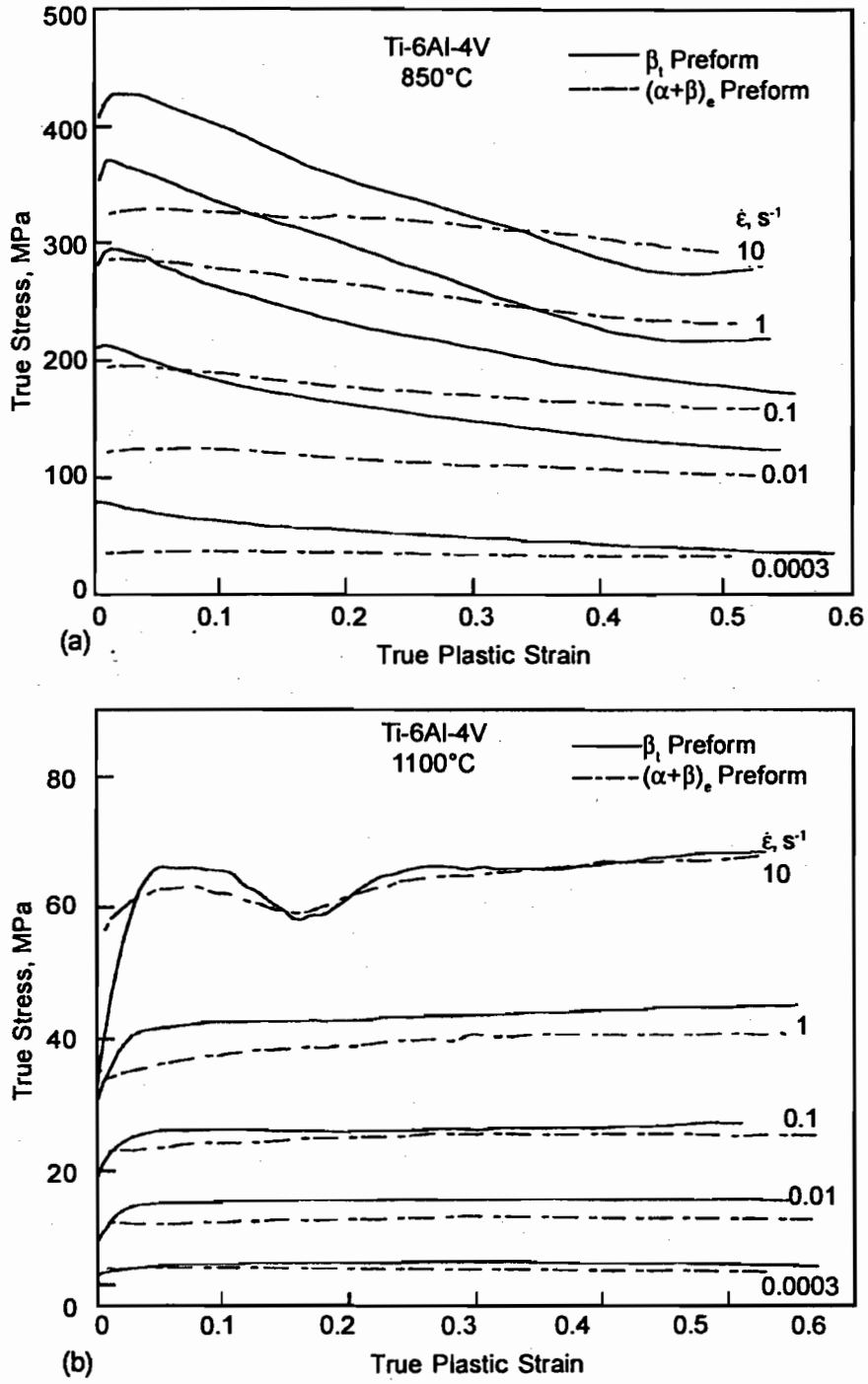

Figure 2: Compressive flow curves as a function of strain rate for Ti-6Al-4V in the (a) α-β range (850°C), (b) β range (1100°C), and (c) near transus (1000°C). [Please see (c) in next page].

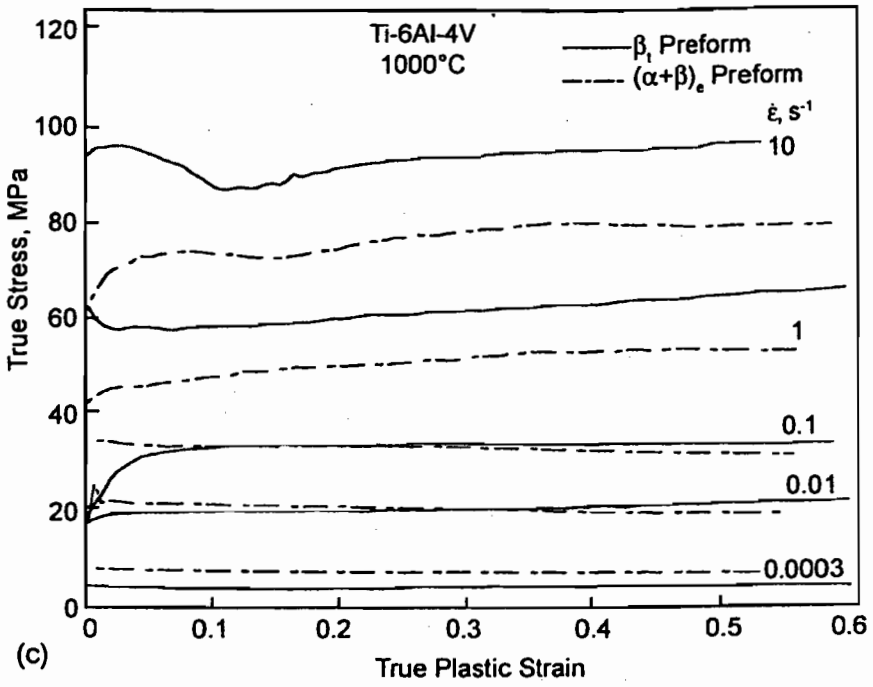

Figure 2: Continued.

two preforms are given elsewhere (8, 17). These data can be used for process design and control in two different ways:

(i) as constitutive equations in the finite element analysis of metalworking processes, and

(ii) to evaluate the mechanisms of hot deformation either conventionally by using kinetic analysis or more recently by developing processing maps as discussed subsequently.

In the kinetic analysis, the steady state flow stress (σ) is related to the temperature and the strain rate ($\dot{\varepsilon}$) of deformation by a rate equation (18):

$$\dot{\varepsilon} = A\sigma^n \exp(-Q/RT) \qquad (1)$$

where A: constant, n: stress exponent, Q: activation energy, R: gas constant, and T: the absolute temperature. It has been observed that when considered over a wide range of strain rate, the stress exponent, n, is strain rate dependent (17) and hence the applicability of eq.(1) is limited to a narrow range of strain rate. In view of this, strain rate ranges of 3×10^{-4}-10^{-2} s^{-1} and 3×10^{-4}-10^{-1} s^{-1} have been chosen for calculating the stress exponent values in the α-β and the β range respectively. The values of n are ~3.4 for the α-β range and ~3.6 for the β range which are not significantly different in the two preforms. Arrhenius plots showing the variation of flow stress with temperature are given in Figure 3 from which the apparent activation energy values have been estimated in the α-β and β ranges: 455 kJ/mole for the β_t preform and

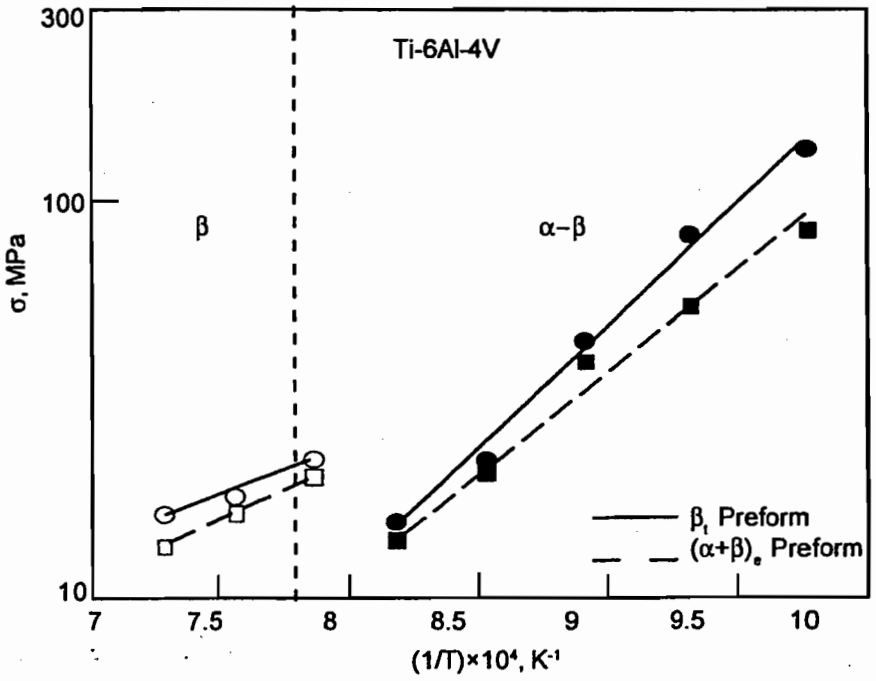

Figure 3: Arrhenius plots showing the variation of flow stress (σ) with inverse of temperature (T) in the α-β and β ranges of Ti-6Al-4V.

330 kJ/mole for the $(\alpha+\beta)_e$ preform. Neither of these are comparable to that for self diffusion in α titanium (150 kJ/mole) (19). In the β range, however the values are 172 kJ/mole for β_t preform and 210 kJ/mole for $(\alpha+\beta)_e$ preform which are close to that for self-diffusion in β titanium (153 kJ/mole) (20).

The combined temperature and strain rate effects in hot deformation are generally expressed in terms of a single parameter, Z (Zener-Hollomon) given by:

$$Z = \dot{\varepsilon} \exp(Q/RT) \qquad (2)$$

Variations of Z with σ on a log-log scale are shown in Figure 4 for the two preforms and the linear relation confirms the validity of the kinetic rate equation within the narrow strain rate range of 3×10^{-4}-10^{-2} s^{-1}. The lines are nearly parallel since the stress exponents representing their slopes are about the same. In kinetic analysis, Z parameter is of significance since the microstructural variations like grain size may be correlated with this parameter and on the basis of these variations, the mechanisms may be inferred and compared. The microstructures of specimens deformed under conditions covered by the kinetic rate equation have been examined in detail with a view to identify the changes that have occurred

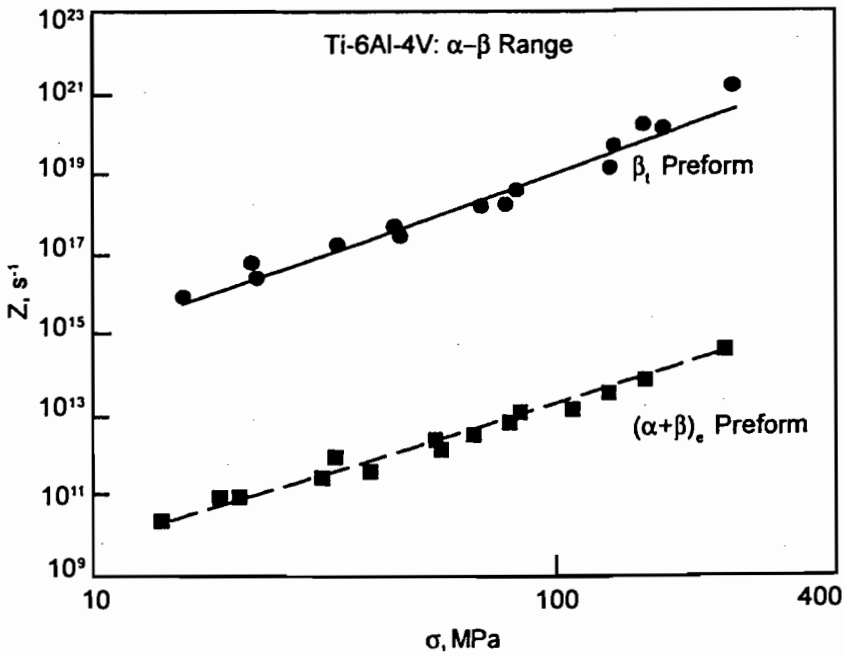

Figure 4: Variation of Zener-Hollomon (Z) parameter with flow stress (σ) in the α-β range of Ti-6Al-4V.

during hot deformation. Typical microstructures are shown in Figure 5a and b which correspond to β_t and $(\alpha+\beta)_e$ preforms respectively. These show that the lamellar structure of β_t preform is converted into globular structure (Figure 5a) while the general features of $(\alpha+\beta)_e$ structure remained unchanged even though α grain growth has occurred (Figure 5b). The mechanisms involved in the hot deformation of these two preforms have been discussed in detail elsewhere (8, 17) and these result in the globularization process in the β_t preform and superplastic deformation in the $(\alpha+\beta)_e$ preform. From the microstructural study, the size of the α globules in the β_t preform as well as the α grain size in the $(\alpha+\beta)_e$ preform have been measured as a function of temperature and strain rate and are plotted against the Z parameter on a log-log scale in Figure 6. A linear relation is found in both the preforms and may be expressed in the following equations,

$$g = 1396.4\, Z^{-0.139} \text{ for } \beta_t \text{ preform, and} \quad (3a)$$

$$d_\alpha = 92.26\, Z^{-0.079} \text{ for } (\alpha+\beta)_e \text{ preform} \quad (3b)$$

where g is the average α globule size and d_α is the average α grain size, both in microns. These equations would be useful

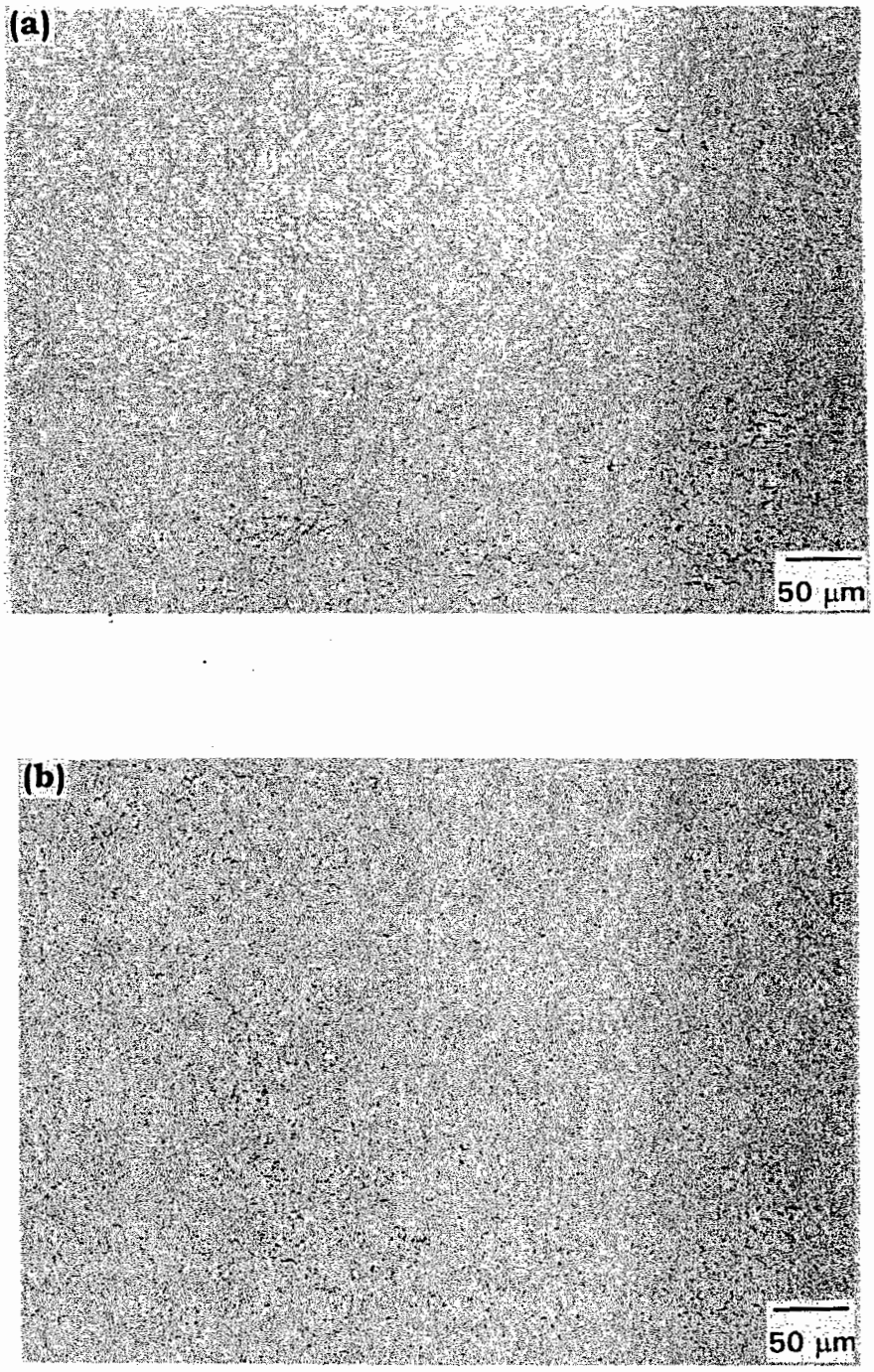

Figure 5: Microstructures of Ti-6Al-4V specimens deformed in the α-β range: (a) β_t preform (950°C/0.0003 s^{-1}), and (b) $(\alpha+\beta)_e$ preform (850°C/0.0003 s^{-1}).

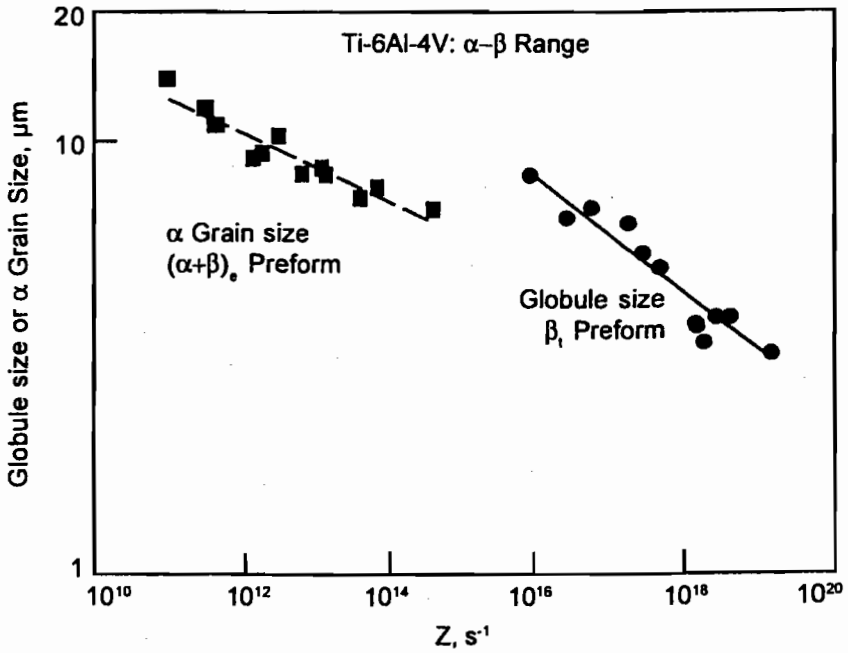

Figure 6: Variation of globule size (β_t preform) and α grain size ($(\alpha+\beta)_e$ preform) with Zener-Hollomon (Z) parameter in the α-β range of Ti-6Al-4V.

to predict the grain size distribution in a component where the local values of temperature and strain rate vary within the ranges in which the above equations apply. From Figure 6, it may be noted that the globule size is more sensitive to variations in Z than the α grain size and so a closer microstructural control in the component requires a more stringent process control.

In the β range, the variations of Z with σ are shown in Figure 7, which confirms that the kinetic rate equation (eq.1) is obeyed in both the preforms. The correlation of prior β grain size ($d_{p\beta}$) with Z is shown in Figure 8, which exhibits a non-linear relation common to both the preforms given by,

$$d_{p\beta} = 1954.3\ Z^{-0.172} \quad (4)$$

It is interesting to note that the initial β grain size did not have much influence on eq.(4) since the data for the coarser grained β_t preform as well as coarse grained $(\alpha+\beta)_e$ preform fall on the same line. This suggests that processing steps specially designed to refine the prior β grain size may not have significant effect on the hot working characteristics of the material, as was found in a low oxygen (ELI) grade Ti-6Al-4V (21).

The above discussion shows that the kinetic analysis is valid only over limited ranges of strain rate and temperature and within these ranges, a good correlation exists between the microstructural

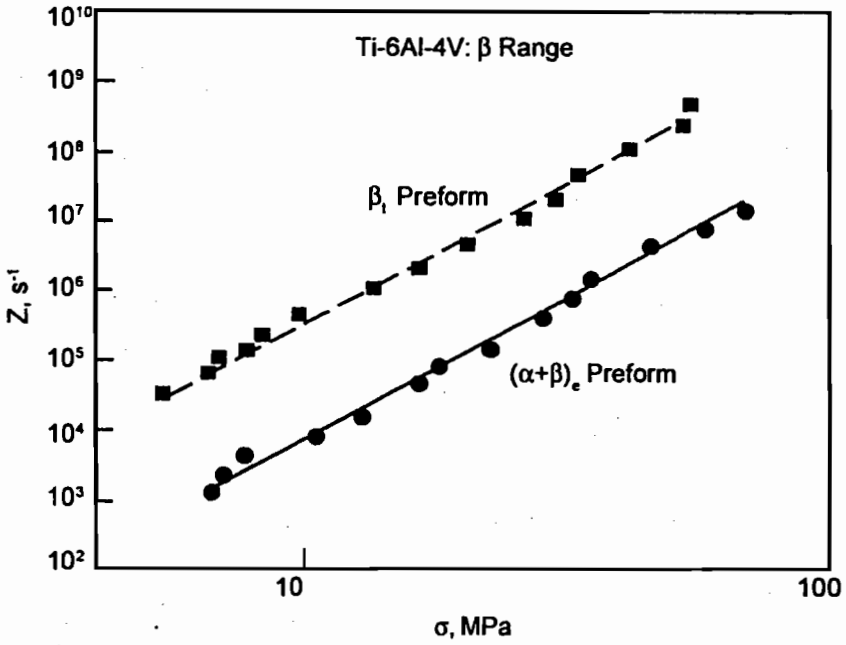

Figure 7: Variation of Zener-Hollomon (Z) parameter with flow stress (σ) in the β range of Ti-6Al-4V.

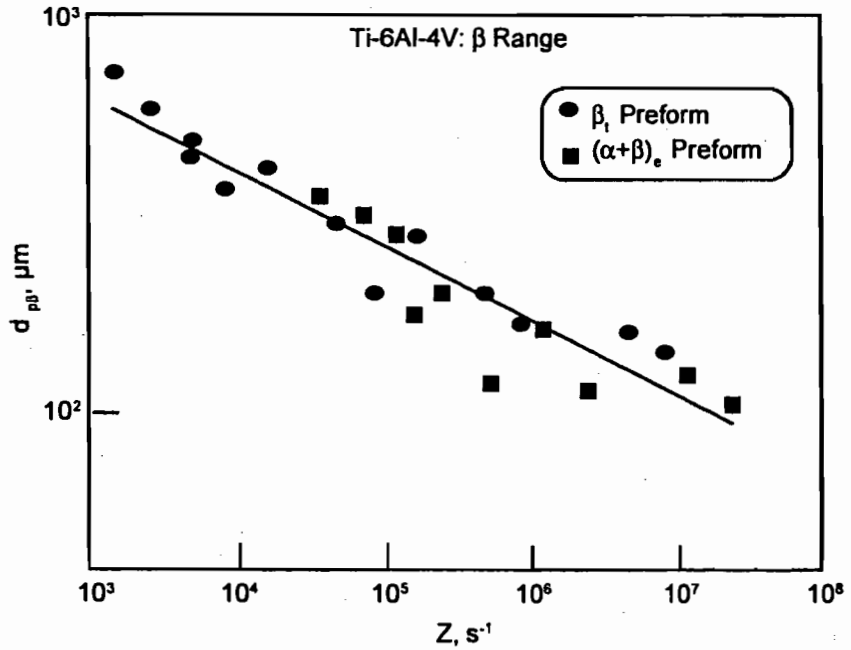

Figure 8: Variation of prior β grain size ($d_{p\beta}$) with Zener-Hollomon (Z) parameter in the β range of Ti-6Al-4V.

parameters and the process variables. However, the analysis does not lead to either optimization of process variables or establishment of processing limits for effective microstructural control.

3.4 Processing Maps

In recent years, processing maps have been used for analyzing the temperature, strain rate and strain dependence of flow stress and for establishing microstructurally "safe" processing windows. The principles and basis of this approach have been reviewed recently (22) and their application to the hot working of a wide variety of materials also has been compiled (23). In brief, the processing map consists of two parts - a power dissipation map which depicts the manner in which the workpiece dissipates power through microstructural changes and an instability map which delineates regimes of flow instabilities like localized microstructural change. The rate at which energy is dissipated through a change in the microstructure is expressed relative to a linear dissipator in terms of a dimensionless parameter called efficiency of power dissipation given by:

$$\eta = \frac{2m}{m+1} \qquad (5)$$

where m is the strain rate sensitivity of flow stress. The three-dimensional plot showing the variation of η with temperature and strain rate at a given strain comprises of the power dissipation map which is generally depicted as an isoefficiency contour map. An instability map is developed on the basis of a continuum instability criterion using the extremum principles of irreversible thermodynamics of large plastic flow (24), which is given by

$$\xi(\dot{\varepsilon}) = \frac{\partial \ln[m/(m+1)]}{\partial \ln \dot{\varepsilon}} + m \leq 0 \qquad (6)$$

where $\xi(\dot{\varepsilon})$ is a dimensionless instability parameter. Flow instabilities are predicted to occur when $\xi(\dot{\varepsilon})$ is negative. The power dissipation map exhibits domains with local efficiency maxima representing certain specific microstructural mechanisms while the instability map reveals regimes of flow instabilities. The instability map may be superimposed on the power dissipation map to obtain a processing map. Details of the steps involved in developing processing maps on the basis of the experimental flow stress data are described elsewhere (23), and these consist of evaluating the strain rate sensitivity from the $\log(\sigma)$ vs. $\log(\dot{\varepsilon})$ variations at different temperatures, calculation of η and $\xi(\dot{\varepsilon})$ parameters and plotting them as contour maps in the temperature-strain rate plane at different strains.

The power dissipation maps obtained on the β_t and $(\alpha+\beta)_e$ preforms are shown in Figures 9a and b, respectively. These correspond to a strain of 0.5 and the maps at lower strains are not significantly different. Referring to Figure 9a, the map exhibits two domains - one at lower strain rates with a peak efficiency of 58% at 960°C and 0.0003 s^{-1} and the other at higher strain rates with a peak efficiency of about 50% at 750°C and 10 s^{-1}. Based on extensive microstructural observations, these are interpreted (8) to represent globularization of the lamellar structure,

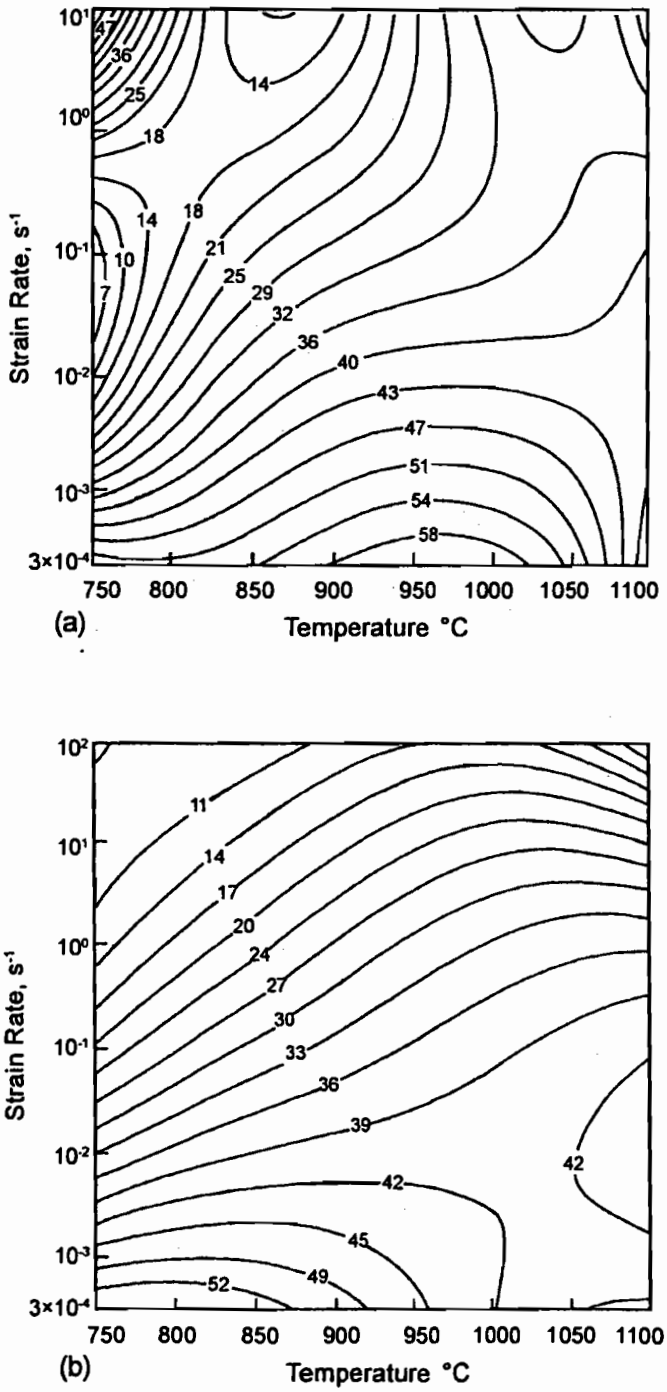

Figure 9: Power dissipation efficiency maps obtained for Ti-6Al-4V at a strain of 0.5: (a) β_t preform and (b) $(\alpha+\beta)_e$ preform. Contour numbers represent percent efficiency of power dissipation.

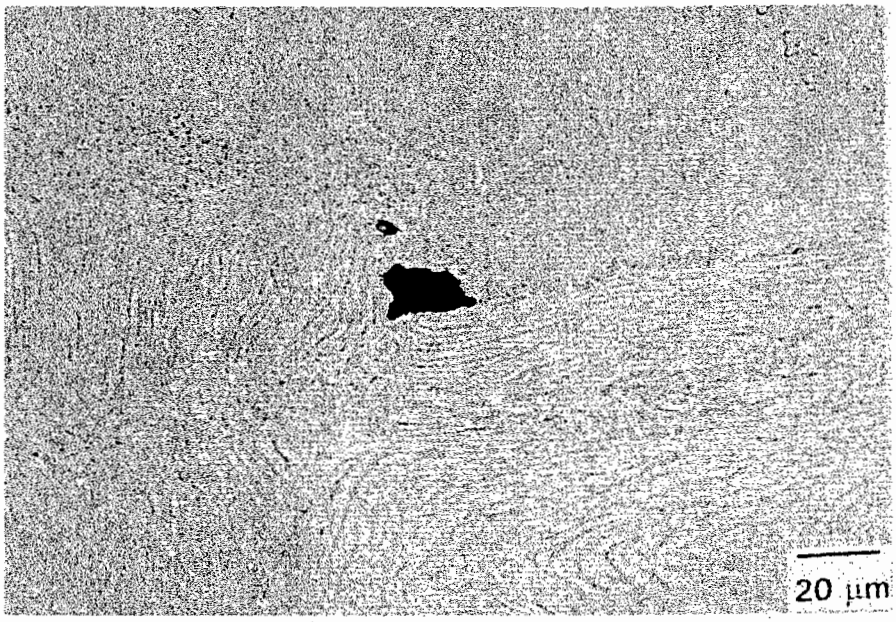

Figure 10: Microstructure obtained in a Ti-6Al-4V β_t preform specimen deformed at 750°C and 0.001 s^{-1}. The compression axis is vertical.

and cracking along adiabatic shear bands, respectively. It is interesting to note that the globularization domain has not changed significantly with strain in spite of the flow softening behavior. This indicates that the rate-controlling step for globularization is independent of strain, but the extent to which globularization is occurring is strain dependent. Since the colonies in the transformed β microstructure have different orientations, only those that are favorably oriented for shear (~45° with respect to the stress axis) will participate in globularization while the neighboring ones will reorient themselves. At large strains, all the colonies would have undergone globularization to complete the conversion process. Typical microstructure representing globularization has already been shown in Figure 5a which is recorded on a specimen deformed at 950°C/ 0.0003 s^{-1}.

At temperatures lower than about 850°C, the map indicates a change in the curvature of power dissipation efficiency contours. Microstructures of specimens deformed at temperatures less than 850°C and at lower strain rates have revealed that wedge cracking occurs at the prior β boundaries, a typical microstructure of which is shown in Figure 10. The mechanism of the formation of this type of wedge cracking has been discussed earlier (8) and it is caused due to the sliding of the prior β boundaries at the thin β layer between the grain boundary α layer and the Widmanstätten colony. The wedge

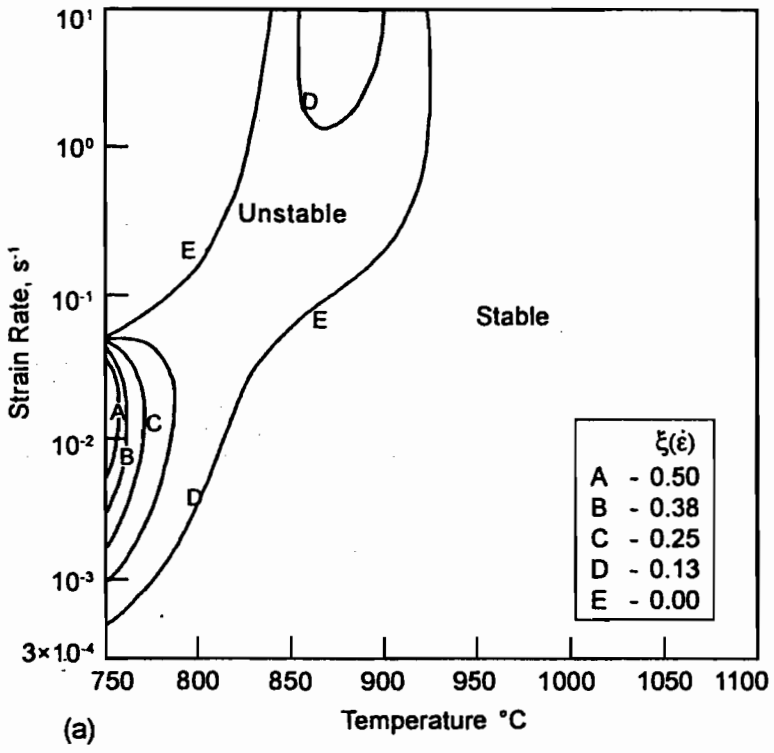

Figure 11: Instability maps obtained for Ti-6Al-4V at a strain of 0.5: (a) β_t preform and (b) $(\alpha+\beta)_e$ preform. Contour numbers represent the value of instability parameter $\xi(\dot{\varepsilon})$. [Please see (b) in next page].

cracking is mitigated when the stress concentration at the triple junctions is relaxed by the thermally activated DRX of the grain boundary α phase.

The high strain rate domain occurring in the map for the β_t preform (Figure 9a) represents a steep increase in the efficiency of power dissipation. Such steep hills in the power dissipation map are suggestive of a cracking process. To understand the origin of this type of cracking, the instability behavior of the material has been analyzed with the help of the continuum criterion given by eq.6. The corresponding instability map is shown in Figure 11a. As per eq.6, the material is expected to exhibit flow instabilities when $\xi(\dot{\varepsilon})$ is negative. In Figure 11a, such a condition is satisfied within the area bounded by the contours 'E'. Microstructures of the specimens deformed at conditions within this regime have exhibited flow localization due to adiabatic shearing (8). At higher strain rates, the adiabatic shear is so intense that the specimens have fractured along the shear plane. Along the adiabatic shear band, cracking has occurred and under these conditions the continuum criterion breaks down. A typical microstructure of a specimen deformed in such a cracking domain (800°C/10 s^{-1}) is shown in Figure 12a. The regimes of

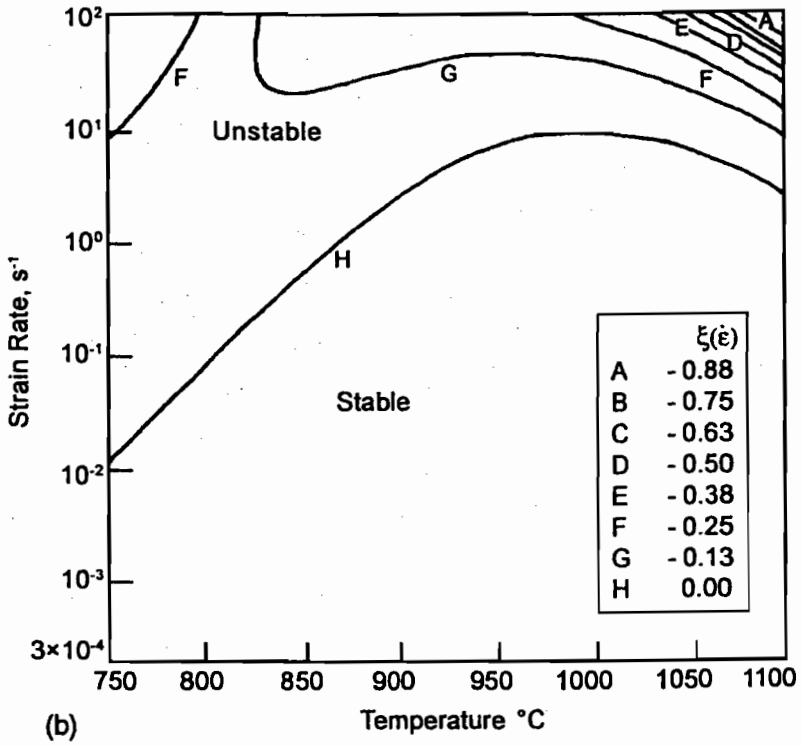

Figure 11: Continued.

Figure 12: (a) Microstructure obtained in Ti-6Al-4V β_t preform specimen deformed at 800°C and 10 s^{-1}, and (b) macrostructure of $(\alpha+\beta)_e$ preform specimen deformed at 750°C and 10 s^{-1}. The compression axis is vertical. [Please see (b) in next page].

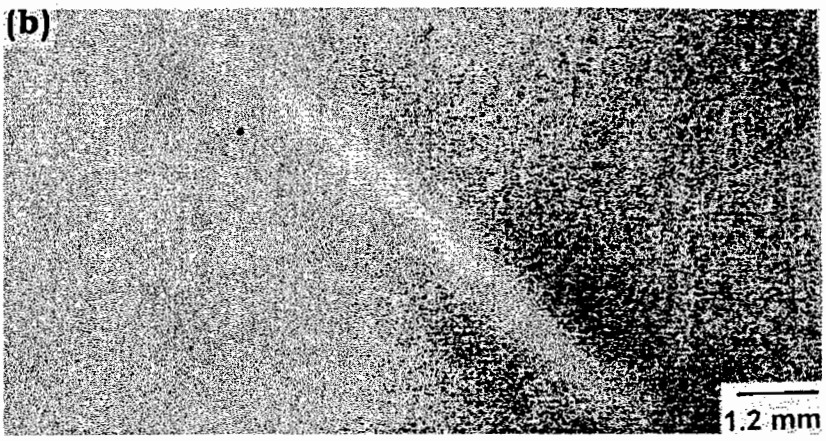

Figure 12: Continued.

instability and adiabatic shear cracking are undesirable and have to be avoided during processing of this material.

On the basis of the processing map, the optimum conditions for processing the β_t preform are 960°C and 0.0003 s^{-1}. The lowest allowable temperature is ~850°C and highest permissible strain rate is ~0.01 s^{-1} to avoid microstructural defects.

The power dissipation map for the $(\alpha+\beta)_e$ preform is shown in Figure 9b. The map exhibits two domains - one in the α-β range and the other in the β range. On the basis of ductility measurements, the lower temperature-lower strain rate domain has been interpreted to represent superplasticity which occurs by the sliding of α/α boundaries with a concurrent accommodation of stress concentration by the dynamic recovery of β phase at triple junctions (17). The kinetic rate equation is obeyed in this domain and the variations in the α grain size with temperature and strain rate correlate with the *Z* parameter, as discussed before. The map suggests that the optimum conditions for superplasticity are 825°C and 0.0003 s^{-1} and the processing window is 750 - 950°C and 0.0003 - 0.002 s^{-1}. Similar to the lower temperature limit set by wedge cracking at the prior β boundary triple junctions in the β_t preform, the superplasticity process has a lower temperature restriction due to the formation of cavities particularly at very large strains (14-16). This limit is dependent on the extent of strain, the state of stress, and the applied strain rate which are determined by the geometry of the workpiece and the process stress state.

The second domain occurs in the β range and at 1100°C/0.01 s^{-1}. As discussed before, this domain represents DRX of the β phase. Comparing this region with the corresponding one for the β_t preform, it may be noted that a clear domain has not formed in the map for the β_t preform and may develop at higher temperatures. According to these two

maps, the β deformation behavior is not significantly different and the optimum processing conditions are about 1100°C and 0.01 s^{-1}. The kinetic considerations discussed earlier are further supported by this conclusion.

The instability map for the $(\alpha+\beta)_e$ preform is shown in Figure 11b. Flow instability is predicted to occur within the contour represented by 'H'. Typical macrostructure of the flow localization that occurs in this material is shown in Figure 12b which corresponds to a specimen deformed at 750°C/10 s^{-1}. In comparison with the instability behavior of β_t preform (Figure 11a), it may be seen that the strain rate limit for the onset of instability is much higher and the intensity of adiabatic shear is considerably less in the $(\alpha+\beta)_e$ preform. However, this higher strain rate limit cannot be taken advantage of for processing the $(\alpha+\beta)_e$ preform since the superplasticity domain ends at a strain rate of 0.002 s^{-1}. High strain rate deformation in the β range also causes flow instability which is difficult to record microstructurally since the phase transformation occurs during cooling. However, the stress-strain curves (Figure 2b and 2c) show oscillations under these conditions.

It is interesting to compare the variation of tensile ductilities of the two preforms with temperature which are shown in Figure 13. In the β_t preform, the ductility increases with temperature right up to the transus and then decreases in the β range. On the other hand, the $(\alpha+\beta)_e$ preform exhibits two peaks in the ductility - one in the α-β range corresponding to superplasticity and the other close to the β transus. The plot suggests that the optimum temperature for superplasticity is 825°C agreeing with the results obtained from the processing map. The variation of β volume fraction with temperature (12) is also plotted in Figure 13 which rapidly increases beyond 850°C. The ductility peak observed at ~25 vol.% β is in good agreement with the results reported in the literature (25, 26) and the near equal volume fraction rule (27) commonly cited for achieving highest ductility due to superplasticity does not seem to be valid. The dip in ductility occurring at 950°C may be attributed to the increase in the β volume fraction to about 50%. This increases the population of α/β boundaries which are undesirable for superplastic deformation. The second peak represents transient deformation of the β phase at the transus and is associated with somewhat abnormal elongation (~120%). The grain size of β at the transus is considerably smaller (~50 μm) than that at higher temperatures well in the β phase field (~1-2 mm) and hence can exhibit transient superplasticity. It may be noted that the strain rate for obtaining this superplasticity is critical since the β grain size is strain rate dependent as shown in Figure 14. At strain rates lower than about 0.01 s^{-1}, rapid grain growth occurs while at strain rates higher than 0.1 s^{-1} grain boundary sliding is restricted due to insufficient time. Such a transient superplasticity is absent in the β_t preform obviously because of the very large prior β grain size.

A summary of the microstructural mechanisms as revealed by the processing maps for the two preforms of Ti-6-4 is given in Figure 15. The safe processing windows of globularization of β_t preform

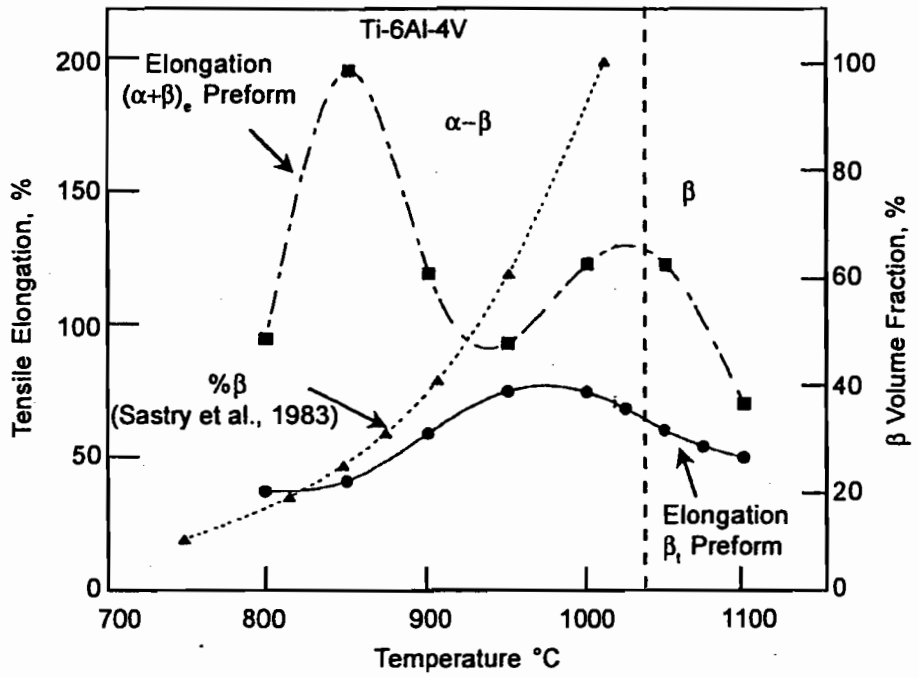

Figure 13: Variation of tensile elongation at a nominal strain rate of 0.01 s^{-1} and β volume fraction with temperature for Ti-6Al-4V (12).

and superplasticity of $(\alpha+\beta)_e$ preform occur at slow strain rates (hydraulic press) and would require isothermal processes with close temperature control in order to avoid microstructural defect formation. For microstructural control during globularization, the temperature and strain rate relationships given by eq.3a can be used while eq.3b can be used for arriving at the process controls to maintain a stable fine grained α structure during superplastic deformation. The grain size control during β deformation can be achieved through a very similar temperature and strain rate control in both preforms although considerable β grain refinement can be obtained in the $(\alpha+\beta)_e$ preform by deforming at temperatures around the transus.

4.0 Summary and Conclusions

The microstructural models for the β_t and $(\alpha+\beta)_e$ preforms of Ti-6-4 alloy during hot working have been developed for process optimization and microstructural control. With the help of hot compression data in the temperature range 750-1100°C and strain rate range 0.0003-10 s^{-1}, the stress-strain behavior, kinetic parameters and processing maps have been compared

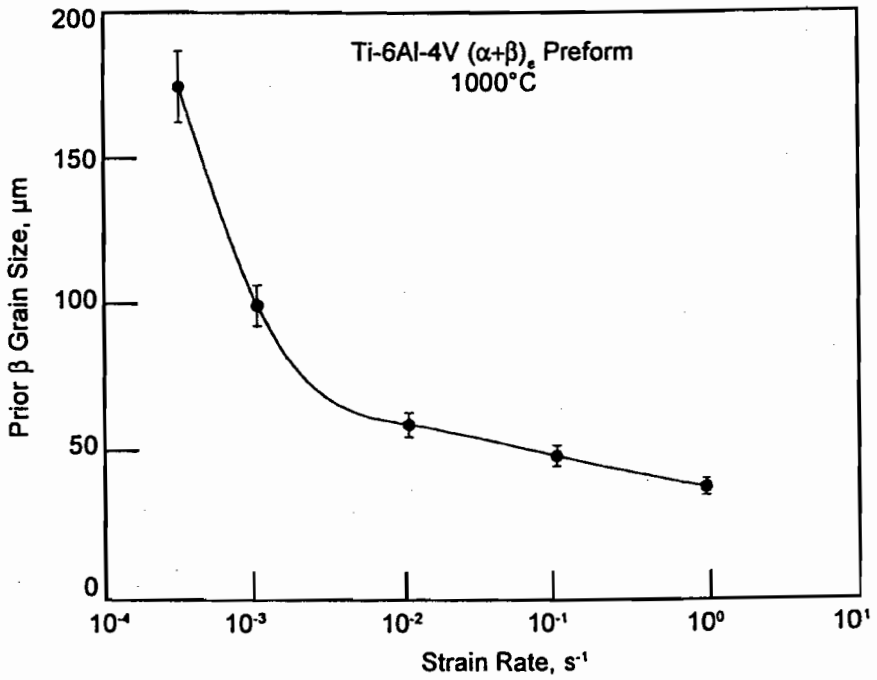

Figure 14: Variation of prior β grain size with strain rate of Ti-6Al-4V $(\alpha+\beta)_e$ preform specimens deformed at 1000°C.

for the two preforms and processing windows for cogging and component forging of Ti-6-4 have been identified such that microstructural defects are avoided and grain size control is achieved. The following conclusions have been drawn from this investigation.

1. The β_t preform exhibits continuous flow softening behavior below the β transus and is harder than the $(\alpha+\beta)_e$ preform. Above the transus, the stress-strain curves of both the preforms were of steady-state type except at the highest strain rate where oscillations have been observed.
2. The apparent activation energies for hot deformation are 455 and 330 kJ/mole for the β_t and $(\alpha+\beta)_e$ preforms respectively and the stress exponents are similar. In the β range, the behavior of the two preforms is similar and the apparent activation energy is in the range 172-210 kJ/mole which is very near that for self diffusion in β titanium (153 kJ/mole). The grain size variation with temperature and strain rate could be correlated with the Z parameter.
3. The β_t preform undergoes globularization of lamellar structure during deformation at slow strain rates in the two phase

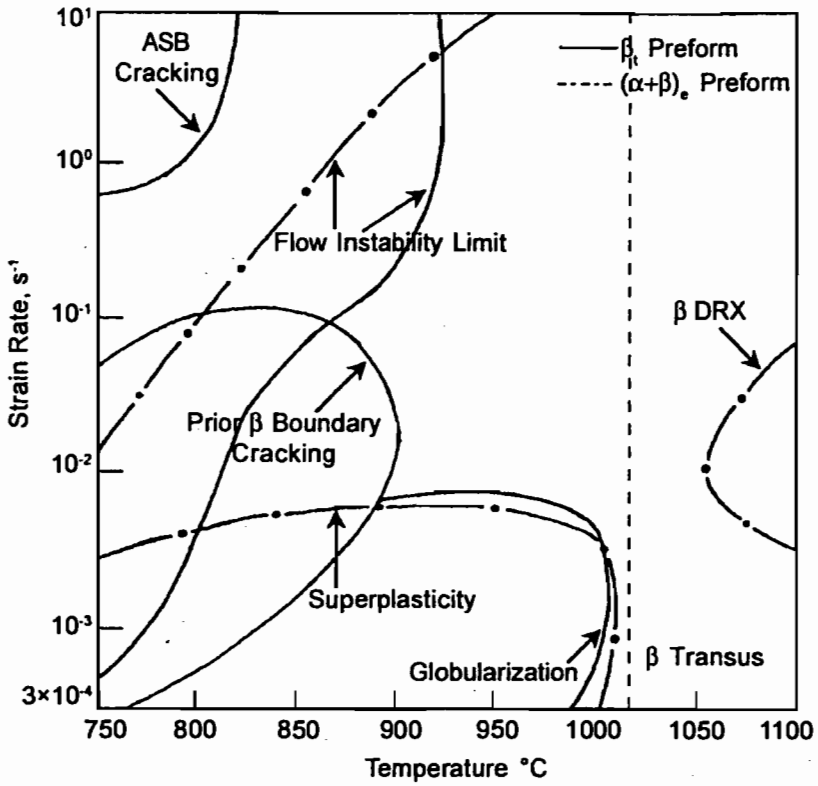

Figure 15: Microstructural mechanism maps of Ti-6Al-4V with β_t and $(\alpha+\beta)_e$ preform microstructures.

range and the optimum parameters for globularization are 960°C and 0.0003 s^{-1}. The globule size is not dependent on strain but on temperature and strain rate of deformation and hence could be correlated with the *Z* parameter. The $(\alpha+\beta)_e$ preform, on the other hand, deforms superplastically and the optimum processing parameters are 825°C/0.0003 s^{-1}. In this domain also, a good correlation exists between α grain size and *Z* parameter.

4. The processing windows in the α-β range are similar in both the preforms except the lower temperature limit which is higher for the β_t preform by about 100°C.
5. The β phase undergoes dynamic recrystallization irrespective of the preform structure and the resulting grain size is dependent on the *Z* parameter.
6. Both the preforms exhibit flow instabilities when deformed in the two phase range at higher strain rates and

these are manifested as adiabatic shear bands causing flow localization.

5.0 Acknowledgments

The authors would like to thank Dr. J.C. Malas for many stimulating discussions. One of the authors (YVRKP) is thankful to the National Research Council, USA, for awarding him an associateship and to the Director of the Indian Institute of Science, Bangalore, India for granting him a sabbatical leave. The assistance rendered by S. Sasidhara and R. Ravi of Department of Metallurgy, Indian Institute of Science, India is gratefully acknowledged.

6.0 References

1. Chen, C. C. and J. E. Coyne, Metallurgical Transactions, A, Vol.7A, pp.1931-1941, (1976).

2. Margolin, H. and P. Cohen, Titanium '80, Conference Proceedings of 4th International Conference on Titanium, H. Kimura and O. Izumi, eds., TMS, Warrendale, PA, pp.1555-1561, (1980).

3. Weiss, I., F. H. Froes, D. Eylon, and G. E. Welsch, Metallurgical Transactions A, Vol.17A, pp.1935-1947, (1986).

4. Semiatin, S. L., V. Seetharaman, and I. Weiss, Materials Science and Engineering, Vol.A263, pp.257-271, (1999).

5. Semiatin, S. L., V. Seetharaman, A. K. Ghosh, E. B. Shell, M. P. Simon, and P. Fagin, Materials Science and Engineering, Vol.A256, pp.92-110, (1998).

6. Semiatin, S. L., R. L. Goetz, E. B. Shell, V. Seetharaman, and A. K. Ghosh, Metallurgical and Materials Transactions, A, Vol.30A, pp.1411-1424, (1999).

7. Miller, R. M., T. R. Bieler, and S. L. Semiatin, Scripta Materialia, Vol.40, No.12, pp.1387-1393, (1999).

8. Seshacharyulu, T., S. C. Medeiros, J. C. Malas III, W. G. Frazier, and Y. V. R. K. Prasad, Manuscript submitted to Metallurgical Transactions, A.

9. Mahoney, M. W., in Materials Properties Handbook, Titanium Alloys, R. Boyer, G. Welsch, and E. W. Collings, eds., ASM International, Materials Park, OH, pp.1101-1109, (1994).

10. Lee, D. and W. A. Backofen, Transactions of AIME, Vol.239, pp.1034-1040, (1967).

11. Arieli, A. and A. Rosen, Metallurgical Transactions A, Vol.8A pp.1591-1596, (1977).

12. Sastry, S. M. L., R. J. Lederich, T. L. Mackay, and W. R. Kerr, Journal of Metals, Vol.35, No.1, pp.48-53, (1983).

13. Cope, M. T., D. R. Evetts, and N. Ridley, Journal of Materials Science, Vol.21, pp.4003-4008, (1986).

14. Cope, M. T., and N. Ridley, Materials Science and Technology, Vol.2, pp.140-145, (1986).

15. Ridley, N., AGARD Lecture Series No.168, Chap. 4, NATO, France, pp.4.1-4.14, (1989).

16. Ito, Y. and A. Hasegawa, Titanium '80, Conference Proceedings of 4th International Conference on Titanium, H. Kimura and O. Izumi, eds., TMS, Warrendale, PA, pp.983-992, (1980).

17. Seshacharyulu, T., S. C. Medeiros, W. G. Frazier, and Y. V. R. K. Prasad, Materials Science and Engineering, A, Vol.284, pp184-194, (2000).

18. Jonas, J. J., C. M. Sellars, and W. J. McG. Tegart, Metallurgical Review, Vol.14, pp.1-24, (1969).

19. Dyment, F. and C. M. Libanati, Journal of Materials Science, Vol.3, pp.349-359, (1968).

20. De Reca, N. E. W. and C. M. Libanati, Acta Metallurgica, Vol.16, pp.1297-1305, (1968).

21. Prasad, Y. V. R. K., T. Seshacharyulu, S. C. Medeiros, J. C. Malas III, and W. G. Frazier, Journal of Materials Engineering and Performance, (in print).

22. Prasad, Y. V. R. K. and T. Seshacharyulu, International Materials Review, Vol.43, pp.243-258, (1998).

23. Prasad, Y. V. R. K. and S. Sasidhara, eds., Hot Working Guide, A Compendium of Processing Maps, ASM International, Materials Park, OH, (1997).

24. Ziegler, H., Progress in Solid Mechanics, I. N. Sneddon and R. Hill, eds., Vol.4, North-Holland, Amsterdam, pp.93-193, (1963).

25. Hamilton, C. H., Superplasticity, B. Baudelet and M. Suery, eds., Centre National de la Recherche Scientifique, Paris, Grenoble, France, pp.14.1-14.16 (1985).

26. Nieh, T. G., J. Wadsworth, and O. D. Sherby, Superplasticity in Metals and Ceramics, Cambridge University Press, p.81, (1997).

27. Kaibyshev, O. A., Superplasticity of Alloys, Intermetallics, and Ceramics, Springer-Verlag, Berlin, p.198, (1992).

Hot deformation mechanisms in Ti–6Al–4V with transformed β starting microstructure: commercial *v.* extra low interstitial grade

Y. V. R. K. Prasad, T. Seshacharyulu, S. C. Medeiros, W. G. Frazier, and J. C. Malas III

The hot deformation behaviour of commercial and extra low interstitial (ELI) grades of Ti–6Al–4V (Ti-6-4) alloy with a transformed β starting microstructure has been studied in the temperature range 750–1100°C and strain rate range 0·001–10 s^{-1}. On the basis of the flow stress data as a function of temperature and strain rate, processing maps have been developed for these two grades and compared in order to bring out the differences, if any. While the stress–strain behaviour has not varied appreciably with the grade of Ti-6-4, significant differences have been observed in the processing maps as well as the tensile ductility variation with temperature. At lower strain rates in the $\alpha-\beta$ range ($<0{\cdot}01$ s^{-1}), both the grades exhibit globularisation of the lamellar structure, the optimum temperature being higher for the commercial grade than the ELI grade. The apparent activation energy for globularisation is higher in the commercial grade (455 kJ mol^{-1}) than that of the ELI grade (370 kJ mol^{-1}). At temperatures lower than about 900°C and strain rates less than about 0·1 s^{-1}, a regime of strain induced porosity (SIP) at the prior β grain boundaries has been observed and the SIP regime is narrower in the ELI grade than the commercial grade. Strain induced porosity cracks are nucleated as a result of the stress concentrations produced by the sliding of prior β grain boundaries which is promoted by the lower strain rates. The mechanism of hot deformation in the β range is sensitive to the grade of Ti-6-4. In the ELI grade, the β phase deforms by large grained superplasticity, but deformation close to the transus nucleates voids within the prior β grains resulting in a drop in the tensile ductility. On the other hand, the commercial grade exhibits dynamic recrystallisation of β phase. The apparent activation energy for β deformation is lower in the commercial grade (173 kJ mol^{-1}) than the ELI grade (287 kJ mol^{-1}), although both the values are comparable to that for self-diffusion in β. The flow instability regime, as predicted by the continuum instability criterion, is not significantly different in the two grades of Ti-6-4 even though the domain of cracking along the adiabatic shear bands is wider in the commercial grade than the ELI grade.

MST/4390

At the time the work was carried out the authors were in the Materials Process Design Branch (AFRL/MLMR), Materials and Manufacturing Directorate, Air Force Research Laboratory, Wright-Patterson Air Force Base, OH 45433–7746, USA. Dr Prasad is now Professor, Department of Metallurgy, Indian Institute of Science, Bangalore 560012, India and Dr Malas is now Branch Chief, Non-destructive Evaluation Group (AFRL/MLLP) at Wright-Patterson Air Force Base. *Manuscript received 22 June 1999; accepted 9 March 2000.*

Introduction

The most widely used titanium alloy for aerospace applications, Ti–6Al–4V (Ti-6-4), is commercially produced in two grades which are primarily distinguished by the interstitial impurity content. These are designated as extra low interstitial (ELI) and commercial grades. One of the most important interstitial impurities is the oxygen content, which is about 0·10–0·13 wt-% in the ELI grade and 0·16–0·20% in the commercial grade. The effects of oxygen on the room temperature tensile properties and plane strain fracture toughness have been established.[1,2] While the tensile strength increases with the oxygen content, the fracture toughness decreases by about 30–50%.[2] In view of this, the ELI grade is preferred for applications where defect tolerance is of primary concern. It is well known that oxygen is an α stabiliser and increases the β transus in Ti-6-4 from about 965–975°C in the ELI grade to about 995–1020°C in the commercial grade.[3]

The alloy Ti-6-4 can be thermomechanically processed to obtain a variety of microstructures depending on the temperature, amount of deformation, and rate of cooling. The two most common microstructures relevant to industrial processing practice are the transformed β (Widmanstätten) and the equiaxed ($\alpha+\beta$). In the bulk metalworking of cast ingots, the transformed β type microstructure is 'converted' into an equiaxed ($\alpha+\beta$) structure by mechanical working in the $\alpha-\beta$ temperature range using processes like cogging, forging, or extrusion. An $\alpha-\beta$ annealing step after the conversion process ensures homogeneous microstructure. While the mechanism of microstructural conversion involves globularisation of the lamellar structure, the occurrence of strain induced porosity (SIP) is often reported during the $\alpha-\beta$ deformation.[4,5] To seal SIP, expensive and time consuming batch type processes like hot isostatic pressing are required. A better approach would be to control the $\alpha-\beta$ processing conditions such that SIP is avoided, and this may be achieved by understanding the deformation mechanisms over a wide range of processing parameters. Recent investigations have revealed that the hot deformation behaviour of Ti-6-4 is sensitive to the alloy grade and the starting microstructure.[6,7] The aim of the present investigation is to examine the effect of grade of Ti-6-4 on the mechanisms of hot deformation including those that generate microstructural defects. In view of its industrial importance, a transformed β starting microstructure is chosen for the comparison.

In the present study, the approach of processing maps has been adopted to represent and analyse the constitutive behaviour of Ti-6-4 during hot deformation. The basis and principles of this approach have been described earlier,[8,9] and its application to the hot working of a wide range of materials has been compiled recently.[10] In brief, depicted

in a frame of temperature T and strain rate $\dot{\varepsilon}$, power dissipation maps represent the pattern in which power is dissipated by the material through microstructural changes. The rate of this change is given by the dimensionless parameter called the efficiency of power dissipation

$$\eta = \frac{2m}{m+1} \quad \ldots\ldots\ldots\ldots\ldots\ldots \quad (1)$$

where m is strain rate sensitivity of flow stress. Over this frame is superimposed a continuum instability criterion for identifying regimes of flow instabilities, developed on the basis of extremum principles of irreversible thermodynamics as applied to large plastic flow[11] and given by

$$\xi(\dot{\varepsilon}) = \frac{\partial \ln(m/m+1)}{\partial \ln \dot{\varepsilon}} + m \leqslant 0 \quad \ldots\ldots\ldots \quad (2)$$

where $\xi(\dot{\varepsilon})$ is a dimensionless instability parameter. The variation of $\xi(\dot{\varepsilon})$ with T and $\dot{\varepsilon}$ constitutes an instability map. These two maps together constitute a processing map which exhibits domains with local efficiency maxima representing certain specific microstructural mechanisms and regimes of flow instabilities.

Experimental

Specimens of Ti-6-4 having the following compositions (wt-%) were used in this study. Commercial grade: Ti-6·28Al-3·97V-0·052Fe-0·18O-0·0062N-0·008C-0·0049H; ELI grade: Ti-6·02Al-3·91V-0·08Fe-0·13O-0·008N. The chemical analyses as supplied by the manufacturer were confirmed by analysis of the specimens. The commercial grade material in the form of hot rolled and annealed bars was beta solution treated at 1050°C for 1 h followed by air cooling to obtain a transformed β starting microstructure. The ELI grade material was taken from a billet that was subjected to a few steps of β cogging followed by water quenching. The initial microstructures of these two grades are shown in Fig. 1*a* and *b* respectively. These are typical Widmanstätten structures consisting of lamellar α (transformed β) colonies in large prior β grains, a grain boundary α layer of 5 μm thick at the prior β grain boundaries, and a thin β layer in between the colony boundaries and grain boundary α. In the commercial grade, the prior β grain size was about 200 μm while in the ELI grade it was about 1000 μm. The commercial grade microstructure contains a small volume fraction of primary α particles although the other features of transformed β microstructure are similar to those in ELI grade.

Isothermal, constant true strain rate compression tests were conducted using a servohydraulic testing machine over the temperature range 750-1100°C in 50°C intervals and at constant true strain rates 0·001, 0·01, 0·1, 1, and 10 s^{-1}. Additional tests were conducted at 0·0003 s^{-1} on the commercial grade and at 100 s^{-1} on the ELI grade. Specimens of 15 mm height and 10 mm dia. were machined with the compression axis parallel rolling/forging direction for testing in the $\alpha-\beta$ range. Larger specimens of 22·5 mm height and 15 mm dia. were used for accurate flow stress measurements in the β range. All specimens were coated with a borosilicate glass paste for lubrication and environmental protection. They were held for 10 min at the test temperatures before testing and deformed to half the height in each case to impose a true strain of about 0·6 followed by air cooling to room temperature. The resulting load-stroke data were evaluated to obtain true stress-true plastic strain curves using the standard method. The flow stress data at different temperatures, strain rates and strains were used to compute the power dissipation efficiency parameter η, given by equation (1). Power dissipation maps were developed by plotting the variation of efficiency with temperature and strain rate. Regimes of flow instability were delineated using the continuum criterion given by equation (2).

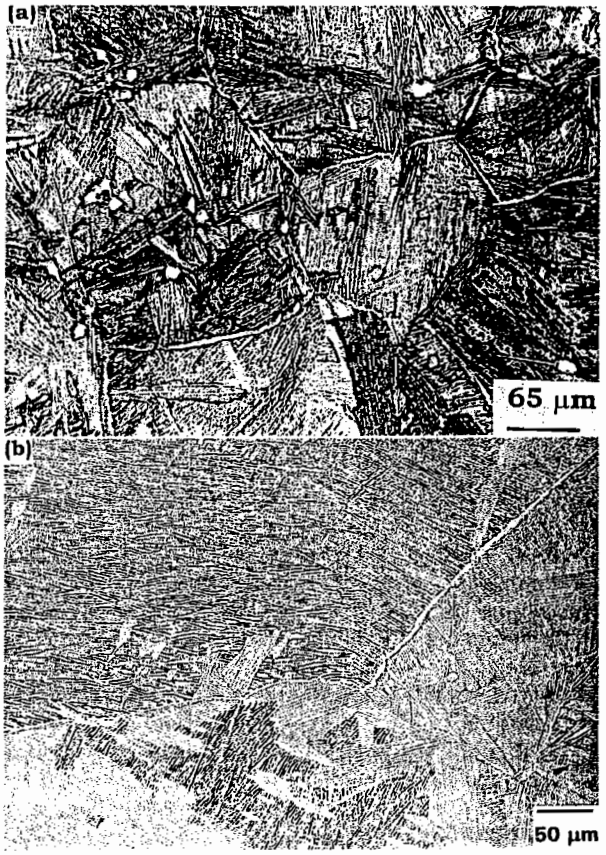

a commercial grade; *b* ELI grade

1 Starting microstructures of Ti-6-4

Hot tensile tests were conducted in the temperature range 800-1100°C at a nominal strain rate of 0·01 s^{-1} (constant actuator speed of 0·25 mm s^{-1}). Cylindrical specimens of 25 mm gauge length and 4 mm gauge dia. were used for this purpose. All specimens were coated with a glass lubricant for environmental protection. Specimens were pulled to fracture and total elongation as a function of temperature was recorded.

Results and discussion

STRESS-STRAIN BEHAVIOUR

At temperatures in the $\alpha-\beta$ range, both the grades exhibited continuous flow softening behaviour which is typical of transformed β starting microstructure. In the β range, the stress-strain curves are of steady state type at lower strain rates but broad oscillations were observed at a strain rate of 10 s^{-1}. For the purpose of comparison, the variation of flow stress with true plastic strain is shown in Fig. 2 in the $\alpha-\beta$ range and the β range. Fig. 2 shows that the flow behaviour of the two grades is essentially the same from the viewpoint of the shapes of flow curves. The lower flow stress values in the $\alpha-\beta$ range of the commercial grade may be attributed to the differences in the initial prior β grain size and other microstructural features like lamellae width and colony size. In Fig. 3, the variation of flow stress with temperature at strain rates of 0·001 and 0·1 s^{-1} for both the grades are shown and these again indicate no significant differences. Thus, a study of the stress-strain behaviour does not reveal any major differences between the two grades.

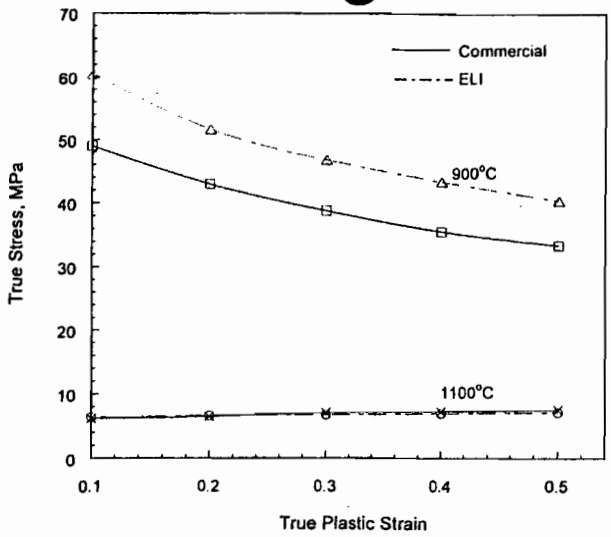

2 Flow curves of commercial and ELI grade Ti-6-4 at strain rate of 0·001 s^{-1} and different temperatures

POWER DISSIPATION MAPS

Power dissipation maps exhibiting contours of efficiency of power dissipation through microstructural changes in the temperature range 750–1100°C and strain rate range 0·0003–10 s^{-1} for the commercial grade, and 0·001–100 s^{-1} for the ELI grade, are shown in Figs. 4 and 5 respectively. These maps correspond to a true plastic strain of 0·5. Maps at lower strains are not significantly different from these suggesting that the transients are fast and the fundamental mechanisms responsible for the occurrence of the domains (basins of attraction) are not dependent on the strain in the range of study. A comparison of Figs. 4 and 5 reveals the following differences between the two grades.

Beta transus

The β transus is about 1010°C for the commercial grade and is about 975°C for the ELI grade used in this study. The volume fraction of β increases with temperature in the $\alpha-\beta$ range according to the β approach curve shown in Fig. 6 and reaches full β at the β transus. The β approach curves

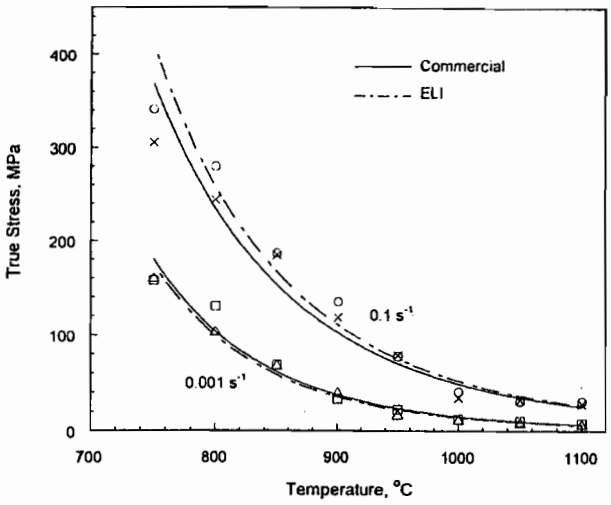

3 Variation of flow stress with temperature at different strain rates in commercial and ELI grades of Ti-6-4

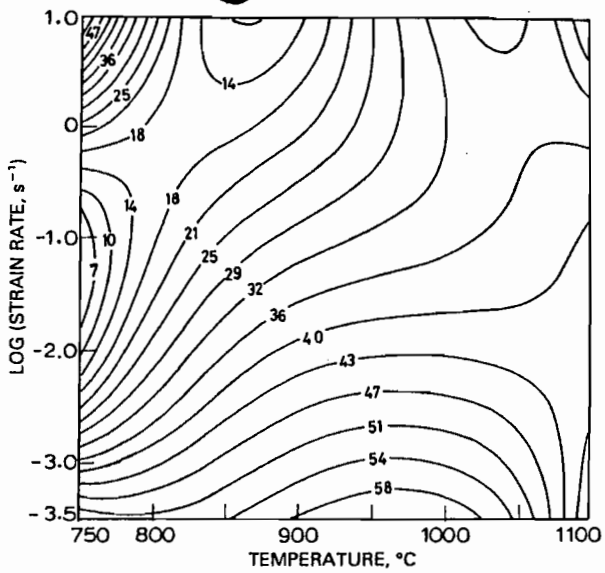

4 Power dissipation map obtained on commercial grade Ti-6-4 at a strain of 0·5: contour numbers represent percentage efficiency of power dissipation

for the commercial grade and the ELI grade Ti-6-4 as reported by Sastry *et al.*[12] and Cope *et al.*[13] are shown in Fig. 6. Since the efficiency of power dissipation represents the relative rate of entropy production,[8,9] the phase transformation is expected to manifest itself in the form of inflexions in the efficiency contours. The map for the commercial grade Ti-6-4 (Fig. 4) indicates that this is indeed the case. At strain rates lower than about 0·01 s^{-1} the inflexions result in closing of the domain with increasing temperature, while at higher strain rates the contours exhibit an opposite curvature. However, in the map for the ELI grade (Fig. 5), this is not clearly exhibited at the transus which may be interpreted to be a result of merging of domains representing microstructural processes with similar power dissipation characteristics across the transus. This difference is of great importance as discussed further in the following sections.

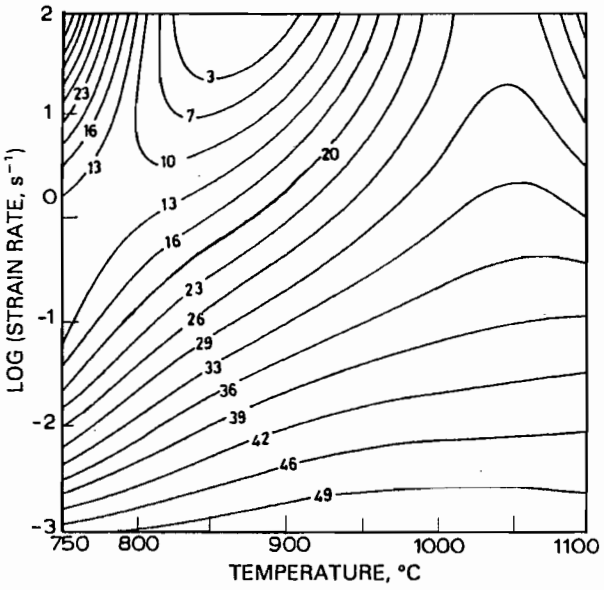

5 Power dissipation map obtained on ELI grade Ti-6-4 at a strain of 0·5: contour numbers represent percentage efficiency of power dissipation

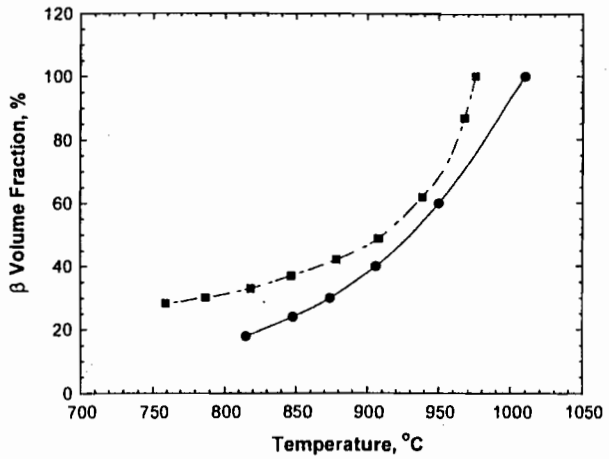

—— commercial, Sastry *et al.*[12]; —·— ELI, Cope *et al.*[13]

6 Beta approach curves for commercial and ELI grades of Ti-6-4

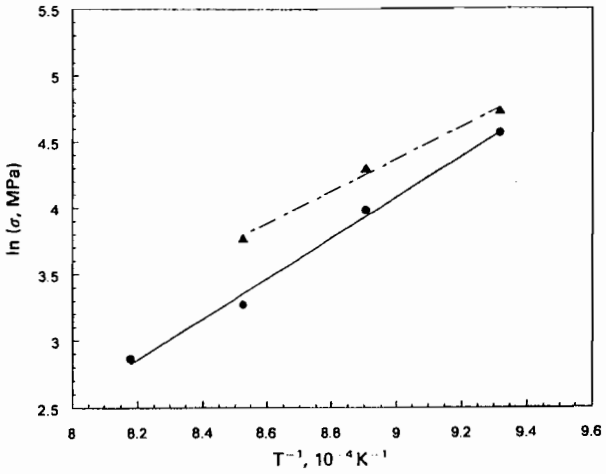

—— commercial —·— ELI

8 Arrhenius plots showing the variation of flow stress with inverse temperature in globularisation domain for commercial and ELI grade Ti-6-4

Globularisation domain

The power dissipation maps of both the grades (Figs. 4 and 5) exhibit two domains with local maxima of efficiency of power dissipation. A domain occurs at higher strain rates ($>1\ s^{-1}$) and lower temperatures ($<800°C$) while the other domain occurs at lower strain rates ($<0{\cdot}01\ s^{-1}$) and over a wider temperature range. These are individually characterised in detail and validated with microstructural observations.[6,7] The higher strain rate domain represents cracking along the maximum shear stress planes which are oriented at ~45° with respect to the compression axis. As this cracking is related to the occurrence of adiabatic shear bands, its interpretation is discussed later along with the instability interpretation.

The lower strain rate domain represents the process of globularisation of the lamellar microstructure involving the sequence of shearing of lamellae, simultaneous recovery by cross-slip to nucleate interfaces, and formation of globules by migration of boundaries involving diffusional processes to lower the interfacial energy. The rate controlling step during the microstructural conversion has been found to be the cross-slip of screw dislocations.[14] The temperature for the local efficiency maximum in this domain is about 960°C for the commercial grade (Fig. 4), which corresponds to about 65 vol.-% β according to the β approach curve (Fig. 6). However in the case of ELI grade (Fig. 5), this temperature is not so clearly revealed because of the merging of domains across the transus. From the β approach curve for the ELI grade (Fig. 6), a similar β volume fraction occurs at about 925°C where the efficiency has the highest value of about 51% (Fig. 5). At a strain rate of $0{\cdot}001\ s^{-1}$, the efficiency values at the above characteristic temperatures for globularisation are similar (~51%) in both grades. The variation of tensile ductility with temperature for the two grades of Ti-6-4 is shown in Fig. 7. It may be noted here that the ductility values reported are not likely to be influenced by the prior β grain size since the hot deformation mechanisms in the transformed β starting microstructure occur within the interiors of the β grains. Hence the number of β grains in the cross-section of the tensile specimen may not be a critical factor in deciding the hot ductility. Figure 7 exhibits peaks at about ~960°C for the commercial grade and at ~920°C for the ELI grade. Thus, the occurrence of globularisation at these characteristic temperatures gives optimum hot workability.

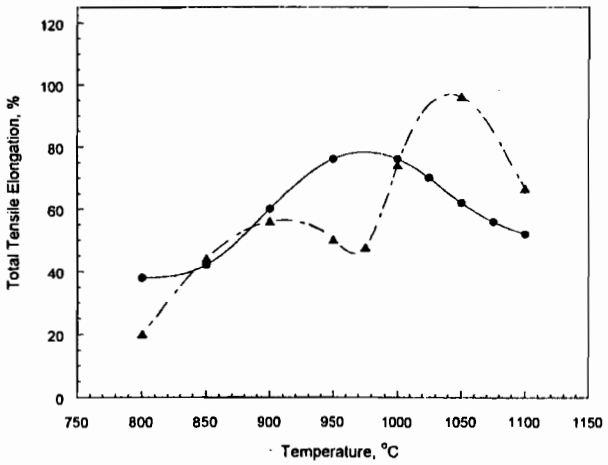

—— commercial; —·— ELI

7 Variation of tensile ductility with temperature for commercial and ELI grade Ti-6-4 at nominal strain rate of $0{\cdot}01\ s^{-1}$

The above discussion indicates that while the general characteristics of the globularisation domain are not significantly affected by the Ti-6-4 grade, the optimum temperature is higher in the commercial grade than the ELI grade. This can be rationalised in terms of the rate controlling step of the mechanism, namely cross-slip.[14] Arrhenius plots showing the variation of flow stress with inverse of temperature at a true strain of 0·5 are given in Fig. 8, which shows that the kinetic rate equation relating the flow stress σ to strain rate $\dot{\varepsilon}$ and absolute temperature T given by

$$\dot{\varepsilon} = A\sigma^n \exp(-Q/RT) \quad . \quad . \quad . \quad . \quad . \quad . \quad . \quad . \quad . \quad . \quad (3)$$

is obeyed in the globularisation domain. In the above equation Q is the activation energy for hot deformation, n the stress exponent and R the gas constant. An apparent activation energy of 455 kJ mol^{-1} for the commercial grade and 370 kJ mol^{-1} for the ELI grade are estimated. Since oxygen strengthens the α phase, higher activation energy is required for the globularisation process. It may be concluded that the strengthening of α phase by oxygen in the commercial grade is responsible for increasing the optimum globularisation temperature. However, the globularisation microstructures as given in Fig. 9*a* and *b* for the two grades of Ti-6-4 at the optimum temperature and strain rate conditions are similar.

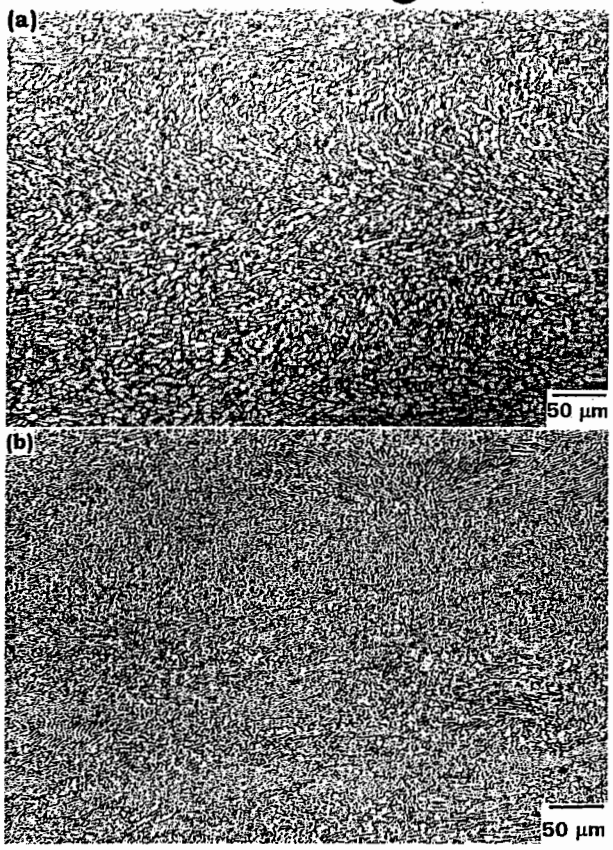

a commercial grade (950°C/0·0003 s^{-1}); *b* ELI grade (900°C/0·001 s^{-1})

9 Microstructures obtained in Ti-6-4 specimens deformed in globularisation domain

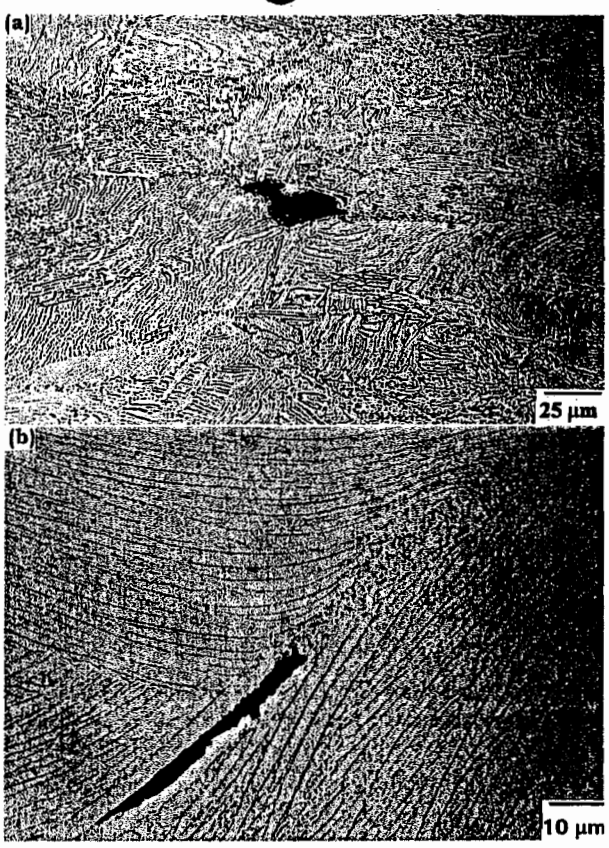

a commercial grade; *b* ELI grade

10 Microstructures of Ti-6-4 specimens deformed at 800°C/0·01 s^{-1} exhibiting cracking at the prior β boundaries: compression axis is vertical

Prior beta boundary cracking

At lower temperatures (<900°C) and lower strain rates (<0·1 s^{-1}), microstructural observations (Fig. 10) showed that cracks occur at the prior β boundaries during deformation and this type of damage is referred to as strain induced porosity (SIP),[4,5] the mechanism of which is discussed in earlier publications.[6,7] Under a resolved shear stress, the prior β boundaries at about 45° orientation with respect to the compression axis slide along the thin soft β layer in between the Widmanstätten colonies and grain boundary α layer and produce stress concentrations at the boundaries and triple junctions. As a result of specific crystallographic orientation relationships the colonies are harder than the grain boundary α layer, and hence the stress concentrations can be relieved only by the softening of grain boundary α at rates at least as fast as the build up of boundary stress. Otherwise shear cracks at the boundaries and/or wedge cracks at the triple junctions are expected. One such softening mechanism is the dynamic recrystallisation (DRX) of grain boundary α. It has been noticed that the limiting conditions for the cracking process depend upon the alloy grade, although in general the temperature for their mitigation is lower at lower strain rates. For avoiding SIP, forging of the commercial grade Ti-6-4 will have to be stopped for resoaking when the temperature of the forging stock is at least 70°C higher than that of the ELI grade. This difference becomes increasingly small at lower strain rates since the DRX of the grain boundary α is more pronounced. The DRX characteristics of the α phase are influenced by the oxygen content since it is an α stabiliser and partitions preferentially to α sites. Another significant difference in the microstructures in this regime (Fig. 10*a* and *b*) is in the morphology of SIP cracks. In case of the commercial grade with fine prior β grains, the cracks are of 'wedge' type and occur mostly at the prior β boundary triple junctions, while they are of 'shear' type in the coarser ELI grade material. However, it may be noted that the morphology of SIP depends not only on the prior β grain size but also on the state of stress existing during deformation. While lower temperatures are known to induce SIP, lower strain rates are normally thought to be beneficial during $\alpha-\beta$ processing. The present study reveals that SIP occurs even at low strain rates which actually promote sliding of the prior β boundaries initiating the damage.

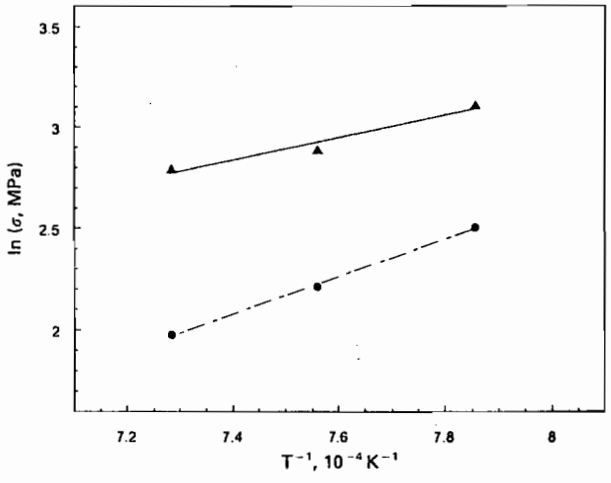

—— commercial; —·— ELI

11 Arrhenius plots showing the variation of flow stress with inverse temperature in the beta region of commercial and ELI grade Ti-6-4

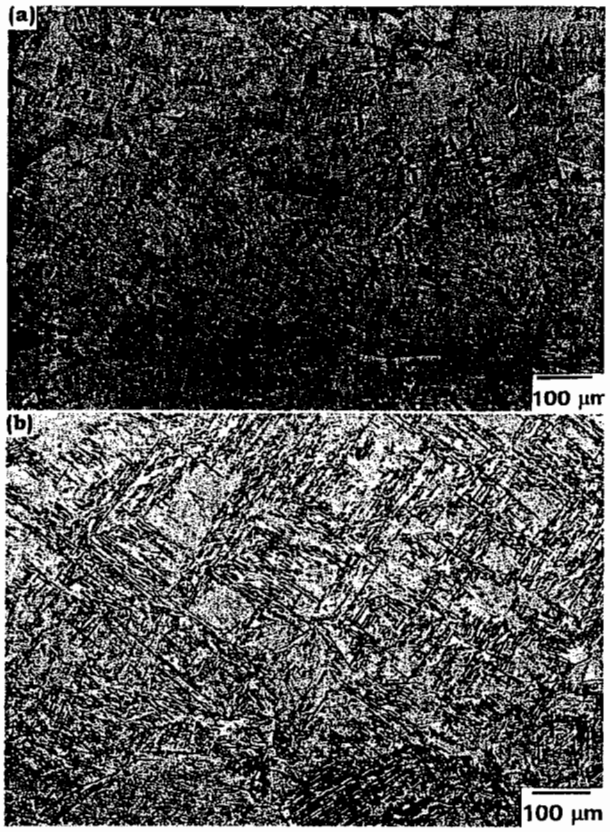

a commercial grade (1100°C/0·01 s^{-1}); *b* ELI grade (1050°C/0·001 s^{-1})

12 Microstructures of specimens deformed in the β region

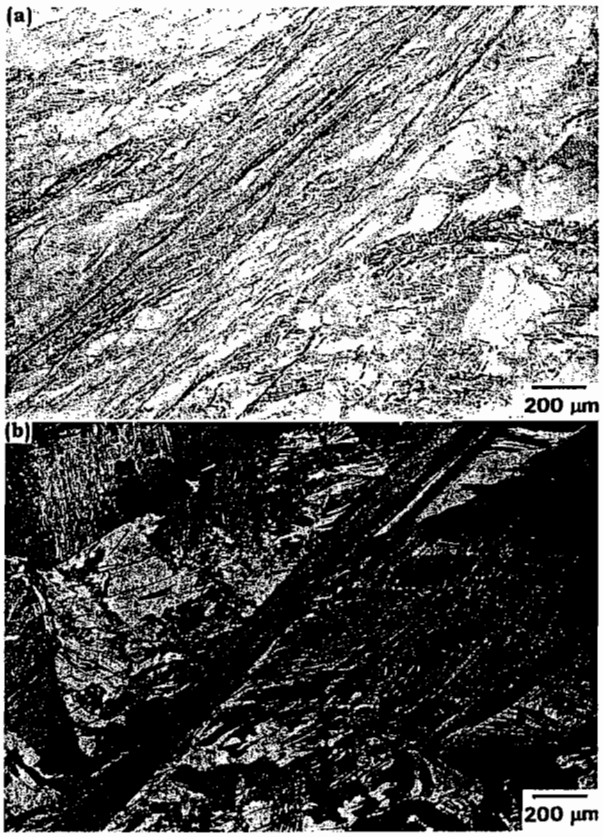

a commercial grade (800°C/10 s^{-1}); *b* ELI grade (750°C/100 s^{-1})

14 Microstructures of Ti-6-4 deformed specimens exhibiting cracking along the adiabatic shear bands: compression axis is vertical

Beta deformation mechanisms

Since the maps do not exhibit clear cut domains in the β region of deformation, the microstructural observations and the tensile ductility measurements (Fig. 7) help in revealing the differences in the behaviours of the commercial grade and ELI grade Ti-6-4. While the ductility continuously drops beyond the transus in the commercial grade, the ELI grade exhibited high ductility with a peak value of about 100% at 1050°C (Fig. 7). At the transus (~975°C), however, the ELI grade showed a minimum in ductility unlike the smooth variation at the transus (~1010°C) in the commercial grade. Since β deformation dominates at the transus, the above results suggest that the mechanisms are different in the two grades and that the mechanism operating in the ELI grade may nucleate defects at lower temperatures towards transus.

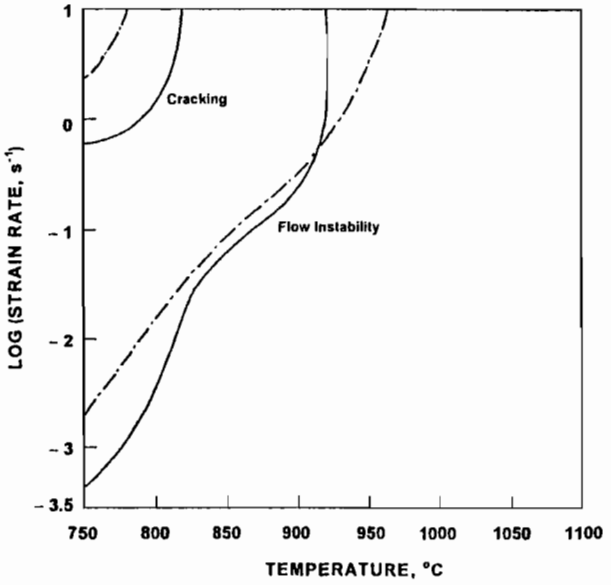

—— commercial; —·— ELI

13 Instability regime and cracking domain boundaries in commercial and ELI grade Ti-6-4

Kinetic analysis of the limited flow stress data available in the β range is conducted and the Arrhenius plots relating the flow stress with the inverse of temperature are shown in Fig. 11. The apparent activation energy is estimated to be about 172 kJ mol^{-1} for the commercial grade and 287 kJ mol^{-1} for the ELI grade. These are comparable with the activation energy reported[15] for self-diffusion in β-Ti (153 kJ mol^{-1}) although an abnormal diffusion behaviour has been reported.[16] Studies on the effect of oxygen on self-diffusion in β-Ti are not available in the literature, but theoretical considerations indicate that interstitial elements like oxygen cause an anomalous increase in the diffusion coefficient due to the formation of vacancy–interstitial pairs.[17] Thus, the anomalous behaviour is dependent on the concentration of oxygen, most likely in an exponential fashion.

In view of the high elongations (~100%) and moderate strain rate sensitivity (~0·33) in the β range of the ELI grade, the mechanism of deformation is interpreted[6] as large grained superplasticity (LGSP) which is generally referred to as 'class I superplasticity in coarse grained materials'.[18] A number of materials like β brasses, β titanium alloys and aluminides are found to exhibit LGSP. In transformed β microstructures, as the volume fraction of β increases with

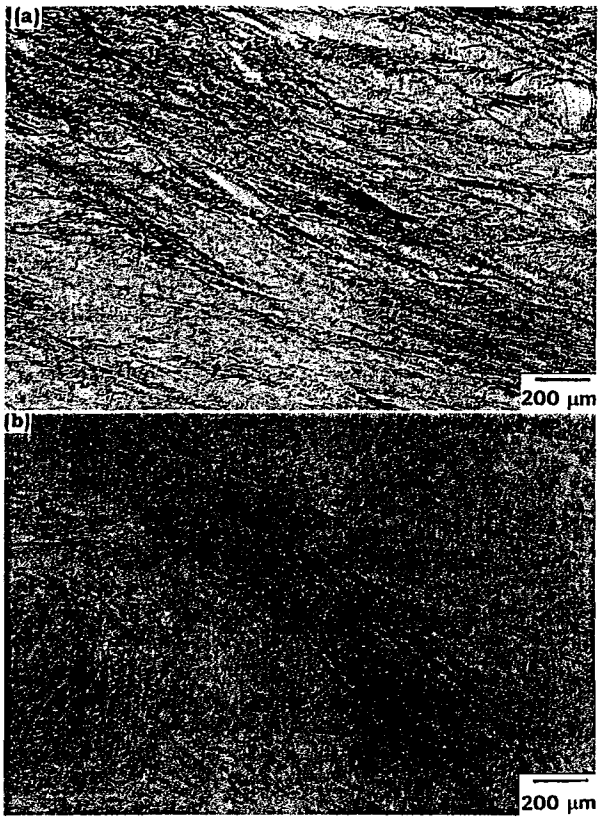

a commercial grade (900°C/10 s^{-1}); *b* ELI grade (850°C/100 s^{-1})

15 Microstructures of Ti-6-4 deformed specimens exhibiting flow localisation: compression axis is vertical

temperature the Widmanstätten colony structure dissolves leaving behind the colony boundaries. These colony boundaries within large β grains are stable during deformation and slide under shear stress when their orientation is near 45° with respect to the compression axis. This sliding process contributes significantly to the total strain if the stress at their triple junctions is accommodated by diffusional flow which is possible at higher temperatures (e.g. 1050°C). Conversely, at lower temperatures (e.g. near the transus at ~975°C) the diffusional flow is too slow to relax the stress concentration at triple junctions, and therefore voids can be nucleated within the prior β grains. Under favourable conditions like high temperatures and tensile residual stresses, for example as in cogging and resoaking cycles, the nuclei may grow into voids and cause porosity. In the commercial Ti-6-4, however, such void nucleation will not occur since the transus is higher, the diffusion rates are enhanced by oxygen–vacancy pairing, and the prior colony boundary structure itself may become unstable which is essential for LGSP. The microstructure of a commercial Ti-6-4 specimen deformed at 1100°C/0·01 s^{-1} is shown in Fig. 12*a* which reveals refinement of the prior β grain size and curved boundaries unlike in the ELI grade (Fig. 12*b*), suggesting DRX of β phase.

FLOW INSTABILITIES

The regimes of flow instabilities as predicted by the continuum criterion given by equation (2) and boundaries of the cracking domain are shown in Fig. 13 for the two grades of Ti-6-4. These results are validated in detail using microstructural observations on specimens deformed under several combinations of temperature and strain rate in these regimes.[6,7] The instabilities in the $\alpha-\beta$ range manifest as adiabatic shear bands which are very intense at temperatures less than 800°C and strain rates higher than 1 s^{-1} leading to cracking along the bands (Fig. 14*a* and *b*). The cracking regime is wider in the commercial grade than in the ELI grade as a result of the hardening of the α phase by oxygen. In the rest of the instability regime, localised flow has been observed (Fig. 15*a* and *b*) and the limiting conditions are not sensitive to the alloy grade. This is as expected since the flow behaviour and physical properties (e.g. density, specific heat, and thermal conductivity) are not significantly dependent on the alloy grade.

Conclusions

The hot deformation characteristics of commercial and ELI grades of Ti-6-4 with a transformed β starting microstructure were studied using processing maps developed in the temperature range 750–1100°C and strain rate range 0·001–10 s^{-1}. The following conclusions have been drawn from this investigation on the differences in the hot working behaviour of the two grades of Ti-6-4.

1. The stress–strain behaviour is not significantly affected by the grade of the alloy: flow softening occurs in the $\alpha-\beta$ range and the β phase exhibits steady state flow.
2. Globularisation of the lamellar structure occurs at lower strain rates in the $\alpha-\beta$ range, the optimum temperature and apparent activation energy being higher for the commercial grade than the ELI grade.
3. At low temperatures and slower strain rates, a regime of strain induced porosity at the prior β boundaries occurs in both the grades and the regime is wider for the commercial grade than the ELI grade. The limiting temperature for the mitigation of this damage process is lower for slower strain rates in both grades.
4. The mechanism of hot deformation in the β range is sensitive to the Ti-6-4 grade. In the ELI grade, the β deforms by large grained superplasticity at higher temperatures with a possible void nucleation when deformed close to the transus. Conversely, commercial Ti-6-4 exhibits dynamic recrystallisation of the β phase.
5. The flow instability regime is not significantly influenced by the grade of the alloy, even though the domain of cracking within the adiabatic shear bands is wider in the commercial grade than the ELI grade.

Acknowledgements

One of the authors (YVRKP) is thankful to the National Research Council, USA, for awarding him an associateship and to the Director of the Indian Institute of Science, Bangalore, for granting him a sabbatical leave. The assistance rendered by S. Sasidhara and R. Ravi of Department of Metallurgy, Indian Institute of Science is gratefully acknowledged.

References

1. R. BOYER, G. WELSCH, and E. W. COLLINGS (eds.): 'Materials properties handbook: titanium alloys', 448; 1994, Materials Park, OH, ASM International.
2. R. W. HERTZBERG: 'Deformation and fracture mechanics of engineering materials', 3rd edn., 366; 1987, New York, Wiley.
3. R. BOYER, G. WELSCH, and E. W. COLLINGS (eds.): 'Materials properties handbook: titanium alloys', 516; 1994, Materials Park, OH, ASM International.
4. S. L. SEMIATIN, V. SEETHARAMAN, and I. WEISS: *Mater. Sci. Eng. A*, 1998, **A243**, 1–24.

5. S. R. SEAGLE, K. O. YU, and S. GIANGIORDANO: *Mater. Sci. Eng. A*, 1999, **A263**, 237–242.
6. T. SESHACHARYULU, S. C. MEDEIROS, J. T. MORGAN, J. C. MALAS, W. G. FRAZIER, and Y. V. R. K. PRASAD: *Mater. Sci. Eng. A*, 2000, **A279**, 289–299.
7. T. SESHACHARYULU, S. C. MEDEIROS, J. C. MALAS, W. G. FRAZIER, and Y. V. R. K. PRASAD: Unpublished work, Wright-Patterson Air Force Base, OH, USA.
8. Y. V. R. K. PRASAD: *Indian J. Technol.*, 1990, **28**, 435–451.
9. Y. V. R. K. PRASAD and T. SESHACHARYULU: *Int. Mater. Rev.*, 1998, **43**, 243–258.
10. Y. V. R. K. PRASAD and S. SASIDHARA (eds.): 'Hot working guide: a compendium of processing maps'; 1997, Materials Park, OH, ASM International.
11. H. ZIEGLER: in 'Progress in Solid Mechanics', (ed. I. N. Sneddon and R. Hill), Vol. 4, 93–193; 1963, Amsterdam, North-Holland.
12. S. M. L. SASTRY, R. J. LEDERICH, T. L. MACKAY, and W. R. KERR: *JOM*, 1983, **35**, (1), 48–53.
13. M. T. COPE, D. R. EVETTS, and N. RIDLEY: *J. Mater. Sci.*, 1986, **21**, 4003–4008.
14. T. SESHACHARYULU, S. C. MEDEIROS, J. T. MORGAN, J. C. MALAS, W. G. FRAZIER, and Y. V. R. K. PRASAD: *Scr. Mater.*, 1999, **41**, 283–288.
15. N. E. W. DE RECA and C. M. LIBANATI: *Acta Metall.*, 1968, **16**, 1297–1305.
16. A. D. LE CLAIRE: in 'Diffusion in body-centered cubic metals', (ed. J. A. Wheeler and F. R. Winslow), 3–25; 1965, Metals Park, OH, ASM.
17. G. V. KIDSON: in 'Diffusion in body-centered cubic metals', (ed. J. A. Wheeler and F. R. Winslow), 329–347; 1965, Metals Park, OH, ASM.
18. T. G. NIEH, J. WADSWORTH, and O. D. SHERBY: 'Superplasticity in metals and ceramics', 219–223; 1997, Cambridge, Cambridge University Press.

Seshacharyulu, T., Steve C. Medeiros, William G. Frazier, and Prasad, Y. V. R. K.
Materials Process Design Brach (AFRL/MLMR) Materials and Manufacturing Directorate, Air Force Research Laboratory
Wright-Patterson Air Force Base, OH, USA

Mechanisms of Hot Working in Extra-Low Interstitial Grade Ti-6Al-4V with Equiaxed ($\alpha + \beta$) Microstructure

The hot deformation mechanisms in an extra-low interstitial (ELI) grade Ti-6Al-4V with equiaxed ($\alpha + \beta$) starting microstructure are evaluated in the temperature range 750 to 1100 °C and strain rate range 0.001 to 100 s^{-1}. Several available materials modeling techniques, viz. stress-strain behavior, kinetic analysis, processing maps are considered for this purpose. The stress-strain curves exhibited three different generic shapes and no conclusions on mechanisms could be drawn on the basis of these shapes. The kinetic rate equation is found to be obeyed in the limited temperature and strain rate ranges. The processing map exhibited two domains – one in the temperature range 750 to 975 °C ($\alpha + \beta$ region) representing the process of fine-grained superplasticity and the other in the β phase field (> 975 °C) representing its dynamic recrystallization. The apparent activation energy in the $\alpha-\beta$ range (~ 295 kJ/mol) is much higher than that for self-diffusion in α-titanium (150 kJ/mol) and is indicative of dynamic recovery of β phase at the triple junctions as the rate-controlling step during superplasticity. In the β range, the apparent activation energy (151 kJ/mol) is very close to that for self-diffusion in β-titanium (153 kJ/mol). The material exhibited flow instabilities at higher strain rates (> 1 s^{-1}) and the manifestation of these instabilities in the $\alpha-\beta$ range is in the form of adiabatic shear bands.

1 Introduction

Ti-6Al-4V (Ti-6-4) is a most widely used titanium alloy for structural applications in view of its high specific strength. The mechanical properties of this alloy are very sensitive to oxygen content [1] and it is available in two grades. While commercial grade Ti-6-4 contains 0.16 to 0.18 wt.% oxygen, extra-low interstitial (ELI) grade contains 0.1 to 0.13 wt.% oxygen. The ELI grade possesses 30 % more fracture toughness than the commercial grade and is preferred in aerospace components where fracture toughness is a critical requirement [2]. Bulk metalworking of this alloy involves a few initial hot working steps in the β range followed by air-cooling which results in a lamellar (β transformed) microstructure. The lamellar structure is broken down by extensive mechanical working in the $\alpha-\beta$ range to obtain fine $\alpha + \beta$ equiaxed (referred to hereafter as $(\alpha + \beta)_e$) structure. The mill-annealed products are in this microstructural condition and are further worked in the $\alpha-\beta$ range to manufacture components of desired shapes. An understanding of the response of this $(\alpha + \beta)_e$ microstructure during forging will be beneficial for optimizing process design during component manufacture. In this paper, the hot deformation mechanisms in ELI grade Ti-6-4 with $(\alpha + \beta)_e$ starting microstructure are evaluated with a view to optimize the hot workability and control the microstructure during processing in both $\alpha-\beta$ and β phase fields. A wide strain rate range that encompasses the speeds of most commonly used machines is considered in this investigation. Also, several available materials modeling techniques like the flow curves, kinetic analysis, and processing maps are utilized for this purpose.

Studies on the hot deformation mechanisms in ELI grade Ti-6-4 are scanty in the literature. Early creep studies by Grant et al. [3] on the ELI grade with $(\alpha + \beta)_e$ structure identified that grain size is an important variable in determining its hot ductility. It is established that the material exhibits fine-grained superplasticity in the $\alpha-\beta$ range [4 to 8]. Wu and Lowrie [4] established the constitutive equations between temperature, strain rate and stress in the superplastic forming range. Arieli and Rosen [5], and Paton and Hamilton [6] have studied several aspects of superplastic deformation at very low strain rates and correlated the behavior with several microstructural parameters like grain size and α/β volume ratio. Cope and coworkers [7, 8] have identified optimum temperature and strain rate for obtaining highest superplastic elongation and observed that this process is associated with cavitation at large strains.

2 Experimental

ELI grade Ti-6-4 having the following composition (in wt.%) was used in this study: 6.02Al, 3.78V, 0.10O, 0.08Fe, 0.0074N, 0.007C, 0.0082H, and balance Ti. The β transus for this material is about 975 °C. As received bar stock of 20 mm diameter in the mill-annealed (hot rolled and annealed) condition was used for testing.

Compression specimens of 15 mm height and 10 mm diameter were machined keeping the compression axis parallel to the rolling direction. Larger specimens of 22.5 mm height and 15 mm diameter were used in the β range to obtain an accurate measurement of flow stress. Concentric

grooves of 0.5 mm depth were made on the top and bottom faces of the specimens to trap lubricant and assist in reducing the friction. A 1 mm 45° chamfer was provided on the specimen edges to avoid fold-over of the material during the initial stages of compression. A small hole of 0.8 mm diameter and 5 mm depth was drilled at mid height of the specimen for inserting a thermocouple which is used to monitor the actual temperature of the specimen as well as to measure any adiabatic temperature rise during testing. Isothermal hot compression tests were conducted using a computer-controlled servohydraulic testing machine. A resistance heating split furnace with silicon carbide heating elements was used to surround the platens and specimen. A borosilicate glass paste was coated on specimens for lubrication and environmental protection.

The test matrix consisted of temperature range 750 to 1100 °C at an interval of 50 °C and strain rate range 0.001 to 100 s^{-1} at an order magnitude interval. The specimens were deformed to half the height in each case to impose a true strain of about 0.7 and were air-cooled from the test temperature. The deformed specimens were sectioned parallel to the compression axis and cut surfaces were prepared for microstructural examination using standard techniques. The load-stroke data obtained were processed to obtain true stress-true plastic strain using the standard method. True plastic strain was obtained by subtracting the elastic strain components of material as well as test machine from the total true strain. The flow stress data obtained at different temperatures, strain rates and strains were corrected for adiabatic temperature rise (significant at higher strain rates) by linear interpolation between log σ and $1/T$ where σ is the flow stress and T is the absolute temperature. This data were used for further analysis using the approaches of kinetic analysis and processing maps.

3 Results and Discussion

3.1 Starting Microstructure

The starting microstructure of the ELI Ti-6-4 used in this study is shown in Fig. 1, which is typical of mill-annealed condition. It consisted of slightly elongated primary α grains in the rolling direction with an average grain diameter of approximately 7 μm and a small amount of intergranular β.

3.2 Stress-Strain Behavior

The shapes of stress-strain curves indicate some features that may help in identifying the hot deformation mechanism, although not in a conclusive fashion. Flow curves exhibited by ELI grade Ti-6-4 with $(\alpha + \beta)_e$ perform microstructure at 800 °C and 1100 °C and different strain rates are shown in Figs 2a and b which are representative of the behavior in the α−β and β ranges respectively. These curves exhibited three generic shapes.

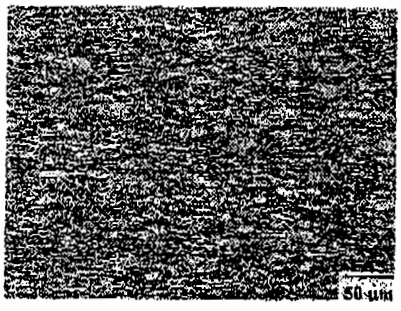

Fig. 1. Starting microstructure of Ti-6Al-4V used in this study.

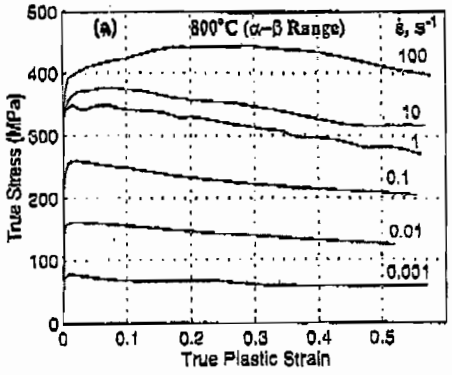

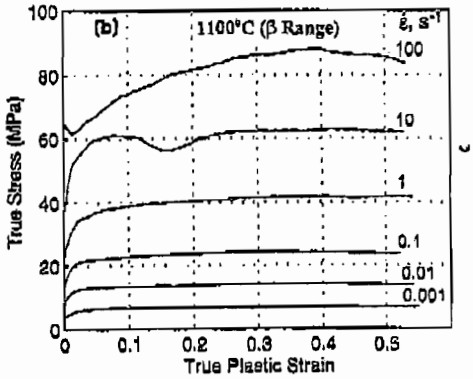

Figs 2a and b. True stress-true plastic strain curves obtained on Ti-6Al-4V at (a) 800 °C and (b) 1100 °C and at different strain rates.

(i) At strain rates slower than 0.1 s^{-1} and all temperatures, the curves were of steady-state type. Such curves indicate that the mechanisms of softening are occurring at sufficiently fast rates to balance the rate of work hardening and are suggestive of mechanisms like dynamic recovery, dynamic recrystallization (DRX) in high stacking fault energy (SFE) materials like aluminum, or superplasticity. In view of the possibility of several mechanisms leading to the same shape of stress-strain curves, further analysis of flow stress data in terms of its variation with temperature and strain rate is required to determine the exact mechanism.

(ii) At higher strain rates (> 0.1 s^{-1}) in the α−β range (Fig. 2a), the curves exhibited continuous flow softening behavior. This type of flow behavior is commonly observed during globularization of lamellar structures or flow localization during deformation. Since the starting structure in the present case is an equiaxed one, the possibility of globularization can be ruled out. However, detailed microstructural examination is required to confirm the type of flow instability.

(iii) At higher strain rates (> 1 s^{-1}) in the β range, oscillatory flow curves were observed (Fig. 2b). Oscillations in the stress-strain curves are indications of either DRX

Table 1. Flow stress values (corrected for adiabatic temperature rise) of ELI Ti-6Al-4V at different temperatures, strain rates and strains.

Strain	Strain rate, s^{-1}	Temperature, °C							
		750	800	850	900	950	1000	1050	1100
0.1	0.001	108.4	67.6	42.9	22.2	17.2	7.8	6.8	6.5
	0.01	219.2	155.7	112.3	65.1	27.9	14.6	12.5	12.2
	0.1	380.5	275.8	195.7	117.7	57.9	27.8	25.2	23.6
	1.0	445.7	376.5	293.6	193.4	87.7	45.4	43.5	38.9
	10.0	431.7	395.4	328.5	247.3	138.2	80.4	70.4	62.3
	100.0	517.5	454.3	382.2	288.4	182.3	111.8	86.2	77.1
0.2	0.001	98.8	66.7	42.7	22.5	16.9	8.2	6.9	6.7
	0.01	207.2	146.4	103.5	62.1	26.9	15.2	14.0	13.6
	0.1	367.9	260.0	189.1	113.8	55.3	29.6	26.2	23.5
	1.0	434.8	364.7	283.4	188.2	88.6	48.3	45.4	40.4
	10.0	450.5	390.3	316.8	239.0	132.0	79.4	69.1	60.3
	100.0	533.1	472.2	397.7	300.7	195.4	119.1	92.6	84.6
0.3	0.001	95.9	60.9	41.7	22.1	16.7	8.5	7.1	6.7
	0.01	196.9	139.3	101.5	61.1	26.2	15.5	14.4	14.0
	0.1	351.6	247.4	180.5	109.9	54.0	30.4	27.3	24.1
	1.0	428.8	350.6	271.2	183.4	87.4	49.4	46.8	41.3
	10.0	454.9	382.6	309.9	237.1	136.5	82.0	72.0	63.9
	100.0	535.7	474.8	397.6	299.6	197.8	126.2	101.3	90.3
0.4	0.001	94.3	57.6	44.7	23.1	16.5	8.8	7.4	6.7
	0.01	189.6	131.5	97.5	60.5	25.4	15.7	14.2	14.0
	0.1	342.3	240.0	176.4	106.8	52.4	31.4	27.6	24.0
	1.0	411.1	333.1	256.7	174.7	84.8	51.0	47.3	41.7
	10.0	452.6	371.0	293.0	227.4	135.7	84.6	74.1	64.6
	100.0	522.4	463.5	386.9	291.3	194.5	125.3	101.5	91.5
0.5	0.001	87.9	57.5	44.5	24.0	16.2	9.0	7.7	6.8
	0.01	182.7	125.2	93.4	59.2	25.2	15.7	14.5	13.7
	0.1	333.1	234.7	175.8	104.5	50.9	31.3	27.6	23.7
	1.0	393.9	317.9	245.7	168.0	83.5	51.5	47.2	41.8
	10.0	447.8	361.9	283.0	218.6	131.4	84.4	73.7	63.9
	100.0	497.9	441.2	367.5	275.6	183.6	119.5	98.1	89.2

in low SFE materials like copper, or unstable deformation (for example flow localization), or cracking. Again, further analysis is required to decide as to which one of these mechanisms has resulted in these stress-strain features.

3.3 Kinetic Analysis

The flow stress data (corrected for adiabatic temperature rise) as a function of temperature, strain rate and strain are given in Table 1. Conventionally, hot deformation is modeled by relating the steady-state flow stress (σ) to the applied strain rate ($\dot{\varepsilon}$) and temperature (T in Kelvin) using an Arrhenius type rate equation given by [9]

$$\dot{\varepsilon} = A\sigma^n \exp(-Q/RT) \quad (1)$$

where n is the stress exponent, Q is the activation energy, R is the gas constant, and A is proportionality constant. In order to identify the hot deformation mechanism(s), the kinetic parameters n and Q are to be evaluated. The variation of flow stress with strain rate at different temperatures is shown in Fig. 3 on a log-log scale. From Fig. 3, it is evident that logσ-log $\dot{\varepsilon}$ variations are non-linear when considered over the entire range of strain rate employed in this study, and therefore, the kinetic rate equation is not valid. However, in a limited strain rate range of 0.001 to 0.1 s^{-1}, a linear fit with good correlation factor could be obtained at all temperatures. It may be noted that the β transus in this material is about 975 °C and the kinetic parameters are evaluated separately in the α–β region (750 to 975 °C) and in the (region (975 to 1100 °C).

In the α–β range, a stress exponent (n) of 3.2 is estimated in the strain rate range 0.001 to 0.1 s^{-1}. This value is higher compared to the reported n value (~2) in the literature at lower strain rates. [4, 5]. The Arrhenius plot showing the variation of flow stress with the inverse of temperature is shown in Fig. 4 from which an apparent activation energy, $Qapp$, of 295 kJ/mol has been estimated in the two-phase region. This value is in agreement with the values reported in the literature [4, 5] and is higher than that for self-diffusion in α-titanium (150 kJ/mol) [10] which rules out the possibility of diffusion being the rate controlling step. It should be noted, however, that the β volume fraction and α grain size are not constant over the experimental range and Eq. (1) does not include the influence of these factors on the deformation kinetics.

Continuing the kinetic analysis further, the temperature compensated strain rate parameter (Zener-Hollomon) Z given by

$$Z = \dot{\varepsilon} \exp(Q/RT) \quad (2)$$

is evaluated on the basis of the above apparent activation energy and its variation with flow stress is plotted in Fig. 5. The plot exhibits a good linear fit and confirms that the kinetic rate equation is obeyed in the limited strain rate range.

The microstructures of the specimens deformed in the above temperature-strain rate combinations are examined and typical microstructures at a strain rate of 0.001 s^{-1} and different temperatures are shown in Fig. 6. These microstructures reveal that the α grain size as well as β volume fraction increases with increase in temperature. The variation of α grain size with temperature at two strain rates is shown in Fig. 7 along with the variation of β volume fraction (so-called β approach curve) reported by Cope and Ridley [8]. From this plot, it may be noted that above 900 °C the β volume fraction increases rapidly from about 45 % to 100 % at the transus (~975 °C) and this causes a steep increase in the α grain size. Further, tensile elongation as high as 1000 % was reported by Cope and Ridley [8] in this range which supports the occurrence of superplastic deformation in this range.

In the β range, the value of n is about 3.8 and the Arrhenius plot in this range is also shown in Fig. 4. The apparent activation energy estimated from this plot is about 151 kJ/mol which is very close to that for self-diffusion in β-titanium (153 kJ/mol) [11].

3.4 Processing Maps

In recent years, the approach of processing maps has been found to be a valuable guide in modeling the hot deformation and understanding the microstructural evolution. The principles and basis of this approach have been discussed in a recent review [12] and its application to a wide range of materials has been compiled [13]. In brief, the processing map consists of a superposition of a power dissipation efficiency map and an instability map developed in a frame of temperature and strain rate. The power dissipation map represents the manner in which the input power is dissipated by the material in the form of microstructural changes. The

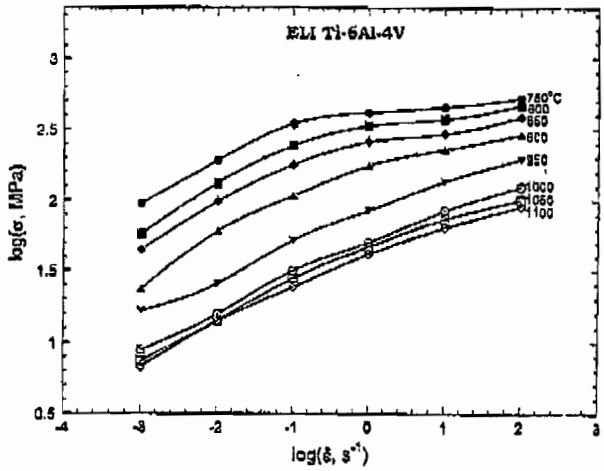

Fig. 3. Variation of flow stress of Ti-6Al-4V with strain rate at different temperatures.

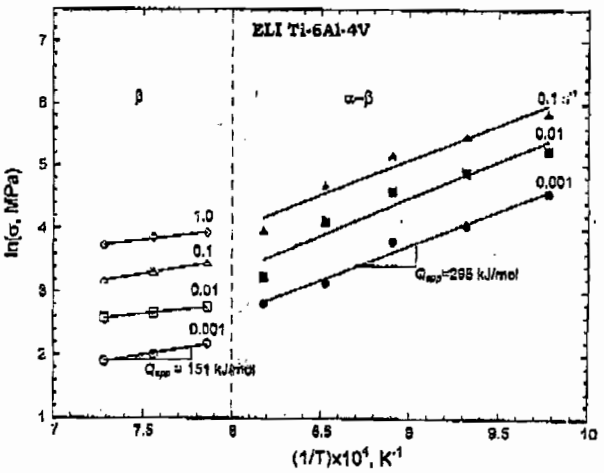

Fig. 4. Arrhenius plot showing the variation of flow stress of Ti-6Al-4V with inverse of temperature at different strain rates in the α–β and β temperature ranges.

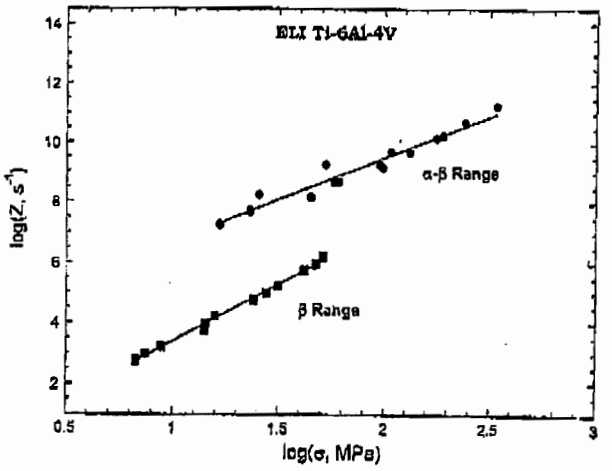

Fig. 5. Variation of flow stress of Ti-6Al-4V with Zener-Hollomon parameter (Z) in the α–β and β phase temperature ranges.

rate of this change is given by a dimensionless parameter, called the efficiency of power dissipation:

$$\eta = \frac{2m}{m+1} \tag{3}$$

where m is the strain rate sensitivity of flow stress. Over this frame is superimposed a continuum instability criterion developed on the basis of extremum principles of irreversible thermodynamics as applied to large plastic flow [14], and given by

$$\xi(\dot{\varepsilon}) = \frac{\partial \ln(m/m+1)}{\partial \ln \dot{\varepsilon}} + m \leq 0 \tag{4}$$

where $\xi(\dot{\varepsilon})$ is another dimensionless parameter. Flow instabilities are predicted to occur when $\xi(\dot{\varepsilon}$ becomes negative. The processing maps exhibit domains in which specific microstructural mechanisms operate as well as regimes where flow instabilities like adiabatic shear bands or flow localization occur.

Processing map obtained on ELI Ti-6-4 with $(\alpha+\beta)_c$ perform structure at a strain of 0.4 is shown in Fig. 8. Maps obtained at other strains also exhibited similar features. The contour numbers in Fig. 8 represent percent efficiency of power dissipation and the shaded region corresponds to flow instability with negative $\xi(\dot{\varepsilon})$ values. The map exhibits two domains – one in the α–β temperature range and the other in the β range, both occurring at slower strain rates; and a large regime of flow instability at strain rates higher than about 1 s^{-1}. The efficiency contours at higher strain rates exhibit a distinct change in their curvature at about the transus (~975 °C) and this feature is commonly observed in several materials which exhibit phase transformation including precipitate dissolution [13].

A. Domain in the α–β Range

The domain in the α–β phase field occurs in the temperature range 750 to 975 °C and at strain rates below about 0.01 s^{-1} with a peak power dissipation efficiency of 61 % at 800 °C/0.001 s^{-1}. Efficiency values as high as 60 % indicate the process of superplastic deformation since the associated strain rate sensitivities (m) are more than 0.4. Large tensile elongations (~1000 %) reported by several researchers [3 to 8] in this range and the strain independent stress-strain behavior (Fig. 2a) further corroborate this interpretation.

Superplasticity mechanism generally involves sliding of grain boundaries with simultaneous relaxation of the stresses generated at the grain boundary triple junctions by processes involving either diffusion flow or plastic deformation. At the temperature of peak efficiency (800 °C), the β volume fraction is about 30 % which permits many α/α interfaces to slide during hot deformation. Whether such sliding leads to superplasticity or wedge cracking is decided by the relaxation processes occurring at the triple junctions. It may be noted that the β phase is essentially present at the triple junctions and is in fact responsible for arresting the α grain growth in this material, which is another important requirement for superplasticity. Thus the deformation behavior of β phase at the triple junctions controls the superplastic deformation process. At elevated temperatures, β phase may exhibit diffusional creep, or dy-

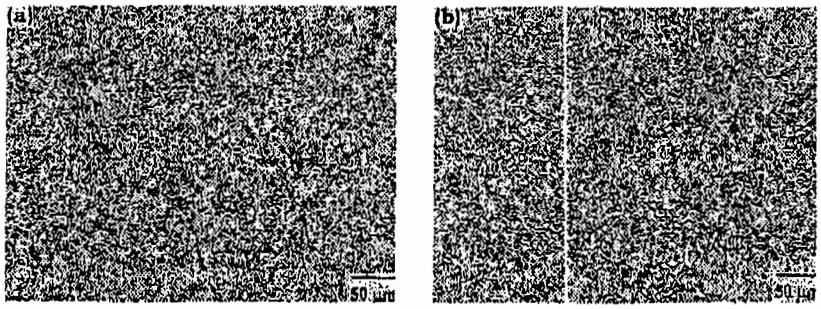

Figs 6a and b. Microstructures obtained on Ti-6Al-4V specimens deformed at 0.001 s^{-1} and (a) 750 °C and (b) 850 °C.

namic recovery involving thermally activated cross-slip. The apparent activation energy estimated in this region (295 kJ/mol) is much higher than that for self-diffusion in β (153 kJ/mol) which rules out the possibility of occurrence of diffusional creep. Hence it may be deduced that dynamic recovery of β phase by cross-slip is the rate-controlling step for the superplasticity in this material.

The higher temperature limit for optimum superplastic properties in this material may be determined as 800 °C beyond which the β volume fraction increases rapidly with temperature creating large number of α/β interfaces which do not slide easily in view of the mismatch in their individual deformation characteristics. From microstructural defect view point, the lower temperature limit is set by the occurrence of cavitation at large strains [8] and the higher strain rate limit ($\sim 0.1\ s^{-1}$) is set by the onset of flow instabilities which is discussed in the later section. Further, in view of slower strain rates involved in the superplastic forming, the process needs to be carried out isothermally.

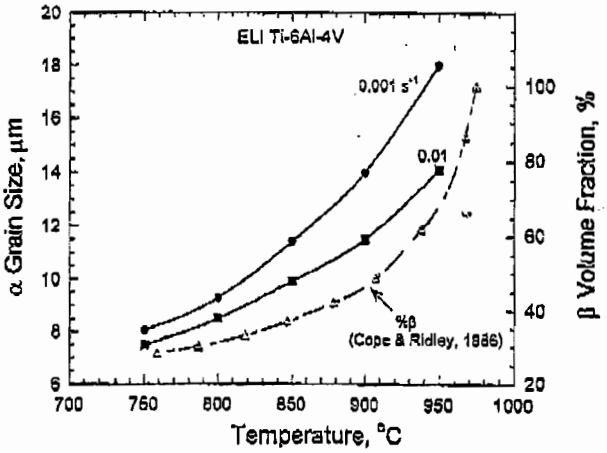

Fig. 7. Variation of α grain size with temperature for Ti-6Al-4V specimens deformed at 0.001 and 0.01 s^{-1}. Also plotted is the variation of β volume fraction with temperature (β approach curve).

B. Domain in the β Range

The domain in the β phase field has a peak efficiency of 43 % at 1100 °C/0.001 s^{-1} and appears to be not fully developed in the testing temperature range considered in this study. The stress-strain curves (Fig. 2b) exhibited steady-state behavior at slower strain rates in the β range and the tensile ductility recorded at 1100 °C and a nominal strain rate of 0.001 s^{-1} is about 60 %. Based on the domain characteristics, stress-strain behavior and ductility, this domain is interpreted to represent the process of DRX of β phase. The kinetic analysis conducted in this range (discussed in the previous section) suggests that this process is controlled by diffusion in β phase. The microstructural features exhibited by the specimens deformed in this range could not be captured due to the phase transformation occurring while cooling to room temperature. During industrial β processing of this material, lower temperatures and faster strain rates ($< 1\ s^{-1}$) may be adopted for avoiding β grain growth.

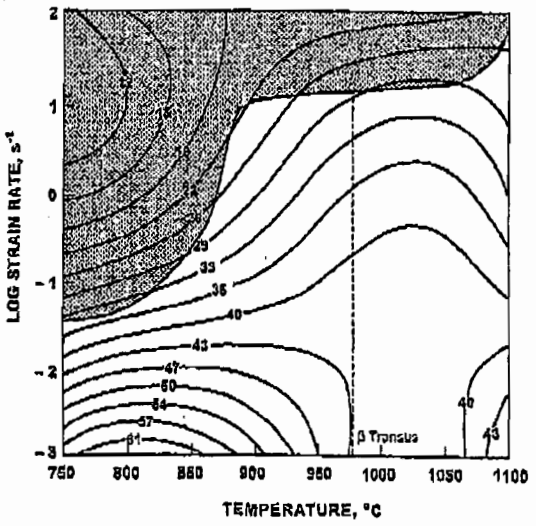

Fig. 8. Processing map obtained on Ti-6Al-4V at a strain of 0.4. Contour numbers represent percent efficiency of power dissipation. Shaded region corresponds to flow instability predicted by the continuum criterion given in Eq. (4).

C. Flow Instabilities

The continuum instability criterion given by Eq. (4) predicts a large regime of flow instability when this material is deformed at strain rates higher than about 1 s^{-1} and is shown as shaded region in Fig. 8. The flow softening and oscillating stress-strain curves in this regime (Fig. 2) support this prediction. The macrographs recorded on specimens deformed under different conditions of this regime in the α–β range are shown in Fig. 9. These exhibit flow localization bands formed at an angle of about 45° to the compression axis. The bands become diffused with increasing temperature and decreasing strain rate. The formation of these bands may be attributed to the adiabatic conditions

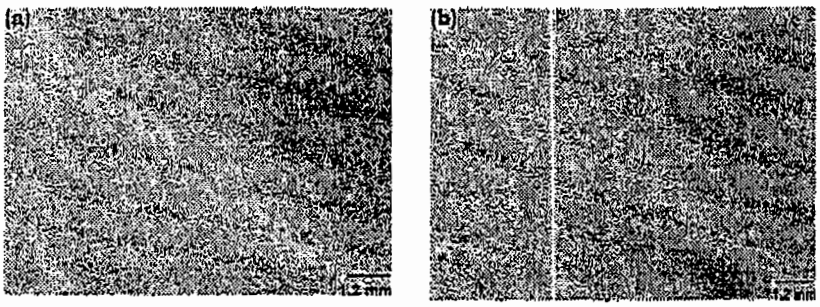

Figs 9a and b. Macrostructures obtained on Ti-6Al-4V specimens deformed in the flow instability regime: (a) 750 °C/100 s^{-1} and (b) 800 °C/100 s^{-1}. The compression axis is vertical.

created during deformation and the low thermal conductivity of Ti-6-4.

The instability manifestations in the β regime could not be captured in the microstructures of deformed specimens as cooling across the transus destroys the features. However, the stress-strain curves in this regime (Fig. 2b) exhibited oscillations which are also signatures of unstable flow.

4 Conclusions

Hot deformation behavior of an ELI grade Ti-6Al-4V with equiaxed α + β starting microstructure is characterized with the help of isothermal hot compression tests in the ranges 750 to 1100 °C and 0.001 to 100 s^{-1}. On the basis of the analysis of the flow stress using available materials models, the following conclusions are drawn.

(i) The material exhibits fine-grained superplasticity in the temperature range 750 to 950 °C and strain rates slower than 0.01 s^{-1}. The apparent activation energy estimated for this process is about 295 kJ/mol which suggests that dynamic recovery of β phase at the triple junctions by cross-slip is the rate-controlling step.

(ii) The β phase undergoes DRX at higher temperatures (> 1050 °C) and the apparent activation energy for β-DRX is very close to that for self-diffusion in β.

(iii) The material exhibits a wide regime of flow instabilities at strain rates faster than 1 s^{-1} and these are manifested as adiabatic shear bands in the α−β range.

The authors would like to thank Dr. J.C. Malas of WPAFB for many stimulating discussions. One of the authors (YVRKP) is thankful to the National Research Council, USA, for awarding him an associateship and to the Director of the Indian Institute of Science, Bangalore, for granting him a sabbatical leave. The assistance rendered by S. Sasidhara and R. Ravi of Department of Metallurgy, Indian Institute of Science is gratefully acknowledged.

Literature

1. *In: Boyer, R.; Welsch, G.; Collings, E. W.* (eds), Materials Properties Handbook: Titanium Alloys, ASM International, Materials Park, OH (1994) 596.
2. *Hertzberg, R. W.:* Deformation and Fracture Mechanics of Engineering Materials, 3rd Edition, John Wiley and Sons, New York (1987) 366.
3. *Grant, N. J.; Ioup, W.; Kane, R. H.:* in: R. I. Jaffe, N. E. Promisel, (eds), Proc. The Science, Technology and Application of Titanium, Pergamon Press, London (1990) 607–613.
4. *Wu, K. C.; Lowrie, R. E.:* Metall. Engn. Qtrly. (1972) 25–29.
5. *Arieli, A.; Rosen, A.:* Metall. Trans. A *8A* (1977) 1591.
6. *Paton, N. E.; Hamilton, C. H.:* Metall. Trans. A *10A* (1979) 241–250.
7. *Cope, M. T.; Evetts, D. R.; Ridley, N.:* J. Mater. Sci. *21* (1986) 4003.
8. *Cope, M. T.; Ridley, N.:* Mater. Sci. Technol. *2* (1986) 140.
9. *Jonas, J. J.; Sellars, C. M.; Tegart, W. J. McG.:* Metall. Rev. *14* (1969) 1.
10. *Dyment, F.; Libanati, C. M.:* J. Mater. Sci. *3* (1968) 349.
11. *de Reca, N.E.W.; Libanati, C.M.:* Acta metall. *16* (1968) 1297.
12. *Prasad, Y. V. R. K.; Seshacharyulu, T.:* Intern. Mater. Rev. *43* (1998) 243.
13. *in: Y. V. R. K. Prasad; S. Sasidhara* (eds), Hot Working Guide: A Compendium of Processing Maps, ASM International, Materials Park, OH (1997).
14. *Ziegler, H:* in: Sneddon, I.N.; Hill, R. (eds) Progress in Solid Mechanics, Vol. 4, North-Holland, Amsterdam (1963) 93–193.

(Received February 11, 2000)

Correspondence Address

Materials Process Design Branch (AFRL/MLMR)
Materials and Manufacturing Directorate
Air Force Research Laboratory
Wright-Patterson Air Force Base
OH 45433-7746, USA

ELSEVIER

Journal of Materials Processing Technology 4779 (2000) 1–8

Journal of Materials Processing Technology

www.elsevier.com/locate/jmatprotec

Influence of oxygen content on the forging response of equiaxed ($\alpha + \beta$) preform of Ti–6Al–4V: commercial vs. ELI grade

Y.V.R.K. Prasad, T. Seshacharyulu, S.C. Medeiros, W.G. Frazier*

Materials Process Design Branch, Air Force Research Laboratory (AFRL/MLMR) Wright-Patterson Air Force Base, OH 45433-7746, USA

Received 12 September 2000

Abstract

The hot deformation characteristics of equiaxed ($\alpha + \beta$) preform of Ti–6Al–4V have been evaluated in two oxygen grades viz., commercial grade and extra-low interstitial (ELI) grade. Constant strain rate hot compression tests were conducted on cylindrical specimens in the temperature range 750–1100°C and strain rate range 10^{-3}–100 s^{-1} up to a true strain of about 0.5. The shapes of stress–strain curves in the $\alpha-\beta$ region and β-region, the kinetic parameters, and the processing maps obtained on the two grades have been compared with a view to evaluate the effect of oxygen on the processing of Ti–6Al–4V with equiaxed ($\alpha + \beta$) preform. The shapes of the stress–strain curves are similar in the two oxygen grades although the flow stress of the commercial grade is slightly higher than that of the ELI grade. While the values of the stress exponent are similar in both grades, the apparent activation energy for hot deformation of commercial grade is higher than that of the ELI grade in both $\alpha-\beta$ and β ranges. The processing maps revealed that superplasticity occurs in the $\alpha-\beta$ range while dynamic recrystallization (DRX) occurs in the β range. In the commercial grade, the superplasticity domain is spread over a wider temperature range and occurs at lower strain rates than that in the ELI grade. On the other hand, the ductility peak in the ELI grade is narrow and may require closer temperature control during processing. The DRX of β occurs at 1100°C in both grades but at a higher strain rate in the commercial grade than in the ELI grade. Unlike the commercial grade, deformation of the ELI grade close to the β transus has to be avoided since a possibility of void nucleation or wedge crack formation exists at slow strain rates. Both grades exhibit flow instabilities manifested as adiabatic shear bands and flow localization when deformed at strain rates higher than about 1 s^{-1}.

Keywords: Ti–6Al–4V; Equiaxed preform; Hot working; Microstructural control; Oxygen effect; Processing maps

1. Introduction

Ti–6Al–4V (Ti–6–4) is one of the important titanium alloys used for aerospace, power generation, chemical, and biomedical applications. The mechanical properties of this alloy are very sensitive to the oxygen content and the microstructure [1]. For industrial applications, Ti–6–4 is available in two different grades: commercial (or regular) grade with 0.16–0.20 wt.% oxygen and extra-low interstitial (ELI) grade with 0.10–0.13 wt.% oxygen. Oxygen is an α stabilizer and shifts the $(\alpha + \beta) \rightarrow \beta$ transformation temperature (β transus) to higher temperatures. Ti–6–4 may be heat treated to obtain different microstructures ranging from transformed β (acicular or Widmanstätten) to equiaxed ($\alpha + \beta$) structures. The transformed β microstructure provides better fracture toughness and creep rupture properties while the equiaxed ($\alpha + \beta$) microstructure has superior low cycle fatigue properties. The commercially available semi-products have a fine grained equiaxed ($\alpha + \beta$) microstructure and components like compressor disks and gas bottles for aerospace applications are forged in the two phase region with this preform (or starting) microstructure [2]. For this purpose, superplastic forming is commonly used and the processing parameters for superplasticity are sensitive to the grain size and volume fractions of the phases in the two-phase structure [3]. Since the transus and the volume fractions of the phases at a given temperature are dependent on the oxygen grade, it is important to know the influence of oxygen content on the hot deformation characteristics of the material. The aim of the present investigation is to evaluate the influence of oxygen on the forging response of the Ti–6–4 with equiaxed ($\alpha + \beta$) preform in terms of its effect on the microstructural mechanisms including damage processes. Such a study would help in achieving workability optimization and process control during forging of Ti–6–4 components.

*Corresponding author. Tel.: +1-937-904-4325; fax: +1-937-656-7995.
E-mail address: william.frazier@afrl.af.mil (W.G. Frazier).

0924-0136/00/$ – see front matter
PII: S0924-0136(00)00832-3

2. Approach

In comparing the microstructural responses of commercial and ELI grades of Ti–6–4, the results on the stress–strain behavior, kinetic analysis, and processing maps have been considered along with their impact on industrial processing. Details of analyzing hot deformation mechanisms using these approaches have been discussed in a recent review [4]. In particular, the approach of processing maps has been found [5] to be beneficial in arriving at optimum processing parameters and in avoiding microstructural defects including flow instabilities.

The conventional approach [6] of analyzing the hot deformation behavior has been the kinetic analysis. It is shown that the steady state flow stress (σ) is related to the strain rate ($\dot{\varepsilon}$) and temperature (T) through a Arrhenius type rate equation given by the following:

$$\dot{\varepsilon} = A\sigma^n \exp\left[\frac{-Q}{RT}\right] \tag{1}$$

where A is a constant, n the stress exponent, Q the activation energy and R the gas constant. On the basis of the stress exponent and activation energy values, the rate-controlling atomistic mechanisms are identified. In recent years, the approach of processing maps has been applied for characterizing and optimizing the hot deformation behavior of materials. The principles and basis for this approach have been discussed elsewhere [4] and its application to a wide range of materials has been described in a recent compilation [5]. Briefly, this approach considers the workpiece as a dissipator of power which is converted into thermal (temperature rise) and microstructural forms. The factor that partitions the input power ($\sigma\dot{\varepsilon}$) into these two forms is the strain rate sensitivity (m) of flow stress. By comparing the dissipation characteristics of the workpiece, which is a nonlinear dissipator, with that of an ideal linear dissipator, a dimensionless parameter called efficiency of power dissipation has been defined as [4]:

$$\eta = \frac{2m}{m+1} \tag{2}$$

The variation of η with temperature and strain rate at a constant strain constitutes a power dissipation map. This map depicts the manner in which power is dissipated through microstructural changes that occur dynamically during deformation and hence reveals domains in which a specific mechanism may become an attractor for minimizing the energy of the dissipated state. By utilizing the principle of maximum rate of entropy production [7], a continuum criterion for the occurrence of flow instabilities is derived as the following:

$$\xi(\dot{\varepsilon}) = \frac{\partial \ln[m/(m+1)]}{\partial \ln \dot{\varepsilon}} + m \leq 0 \tag{3}$$

where $\xi(\dot{\varepsilon})$ is a dimensionless instability parameter. The variation of $\xi(\dot{\varepsilon})$ with temperature and strain rate constitutes an instability map in which the negative $\xi(\dot{\varepsilon})$ regimes represent flow instabilities. A superposition of the power dissipation map and the instability map constitutes a processing map which may be used for characterizing different domains where different microstructural mechanisms occur as well as regimes of flow instabilities, if any.

3. Experimental

The chemical compositions (wt.%) of the commercial and ELI grade Ti–6–4 used in this investigation are given in Table 1. The initial microstructures of these two grades, shown in Fig. 1(a) and (b), respectively, exhibited fine-grained equiaxed α with a small amount of intergranular β. The average grain diameters were estimated to be about 8 and 10 μm, respectively. The β transus is approximately 1010°C for the commercial grade and 975°C for the ELI grade.

Cylindrical specimens of 10 mm diameter and 15 mm height were machined from the as-received bar stocks of 20 mm diameter by keeping the compression axis parallel to the rolling direction. Constant true strain rate compression tests were conducted in the temperature range 750–1100°C at intervals of 50°C and at true strain rates of 10^{-3}, 10^{-2}, 10^{-1}, 1, 10, and 100 s^{-1}. In the case of commercial grade additional tests were conducted at a slower strain rate of 3×10^{-4} s^{-1}. Details of the testing procedure are described elsewhere [5]. All the specimens were deformed to a true strain of about 0.5 and air-cooled to the room temperature. The load–stroke data obtained from the experiments were converted into true-stress–true-plastic strain curves using the standard equations. For the analysis of the hot deformation behavior, the input data consisted of flow stress values (corrected for adiabatic temperature rise, if any) as a function of temperature, strain rate and strain.

The deformed specimens were sectioned parallel to the compression axis and prepared for metallographic examination using standard polishing and etching techniques. Hot tensile tests were also conducted on commercial grade at 950, 1000, 1050 and 1100°C and at a nominal strain rate of 10^{-2} s^{-1} using cylindrical specimens of 4 mm gauge diameter and 25 mm length.

Table 1
Chemical compositions of the two Ti–6Al–4V grades used in the study

Ti–6–4 grade	Al	V	O	Fe	C	N	H
Commercial	6.28	3.97	0.18	0.052	0.008	0.0062	0.0049
ELI	6.02	3.91	0.13	0.08	0.01	0.03	0.012

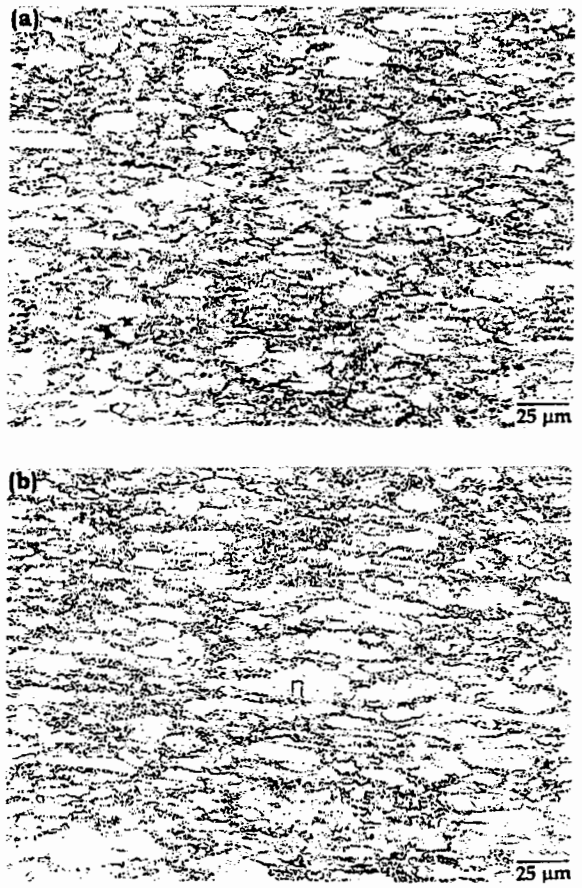

Fig. 1. Starting microstructures of equiaxed (α + β) preform Ti-6Al-4V used in the study: (a) commercial grade; (b) ELI grade.

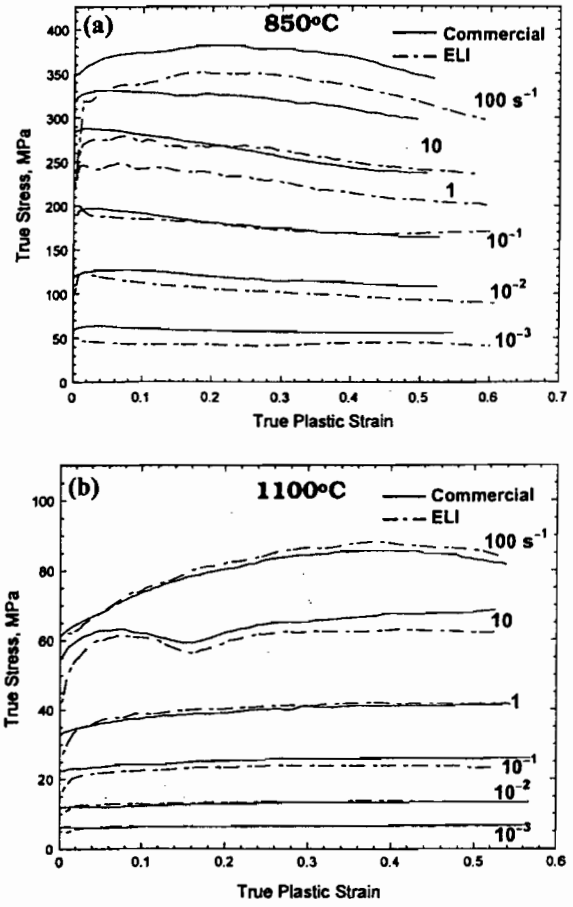

Fig. 2. True-stress–true-plastic strain curves of commercial and ELI grades of Ti-6Al-4V with equiaxed (α + β) preform microstructure at different strain rates: (a) 850°C (α–β range); (b) 1100°C (β range).

4. Results and discussion

4.1. Stress–strain behavior

It may be reiterated at the outset that below the transus, the deformation of Ti-6-4 consists of that of a two phase (α + β) microstructure while above the transus, the deformation involves that of a single phase (β). Typical true-stress–true-plastic strain curves obtained on the commercial grade and ELI grade Ti-6-4 at 850°C (two phase region) and at different strain rates are shown in Fig. 2(a). The curves show that the commercial grade is harder than the ELI grade and the difference is higher at higher (>1 s^{-1}) strain rates. This behavior is as expected from the strengthening effect of oxygen and the non-linear strain rate sensitivity. In both the grades, the shapes of the stress–strain curves at strain rates lower than 10^{-1} s^{-1} are flat indicating steady-state behavior while flow softening is observed at higher strain rates.

The stress–strain curves obtained at 1100°C (β range) on the two oxygen grades of Ti-6-4 are compared in Fig. 2(b). The flow stress values of these two grades are nearly the same indicating that the strengthening of β by oxygen is not as significant as that of α–β. At strain rates lower than about 1 s^{-1}, the flow behavior is of steady state type while at higher strain rates broad oscillations or flow softening have occurred.

From the shapes of stress–strain curves, nothing conclusive can be said regarding the mechanisms of deformation since different mechanisms can exhibit similar features. For example, steady state flow curves may indicate superplasticity, wedge cracking, or dynamic recrystallization (in high stacking fault energy metals). Likewise, flow softening may indicate globularization of lamellar structure or unstable flow. In view of this difficulty, further analysis of the flow stress considering its variation with temperature, strain rate and strain needs to be conducted to evaluate the mechanisms of hot deformation.

4.2. Kinetic analysis

A plot of flow stress vs. strain rate over the entire testing range at different temperatures is shown in Fig. 3(a). The

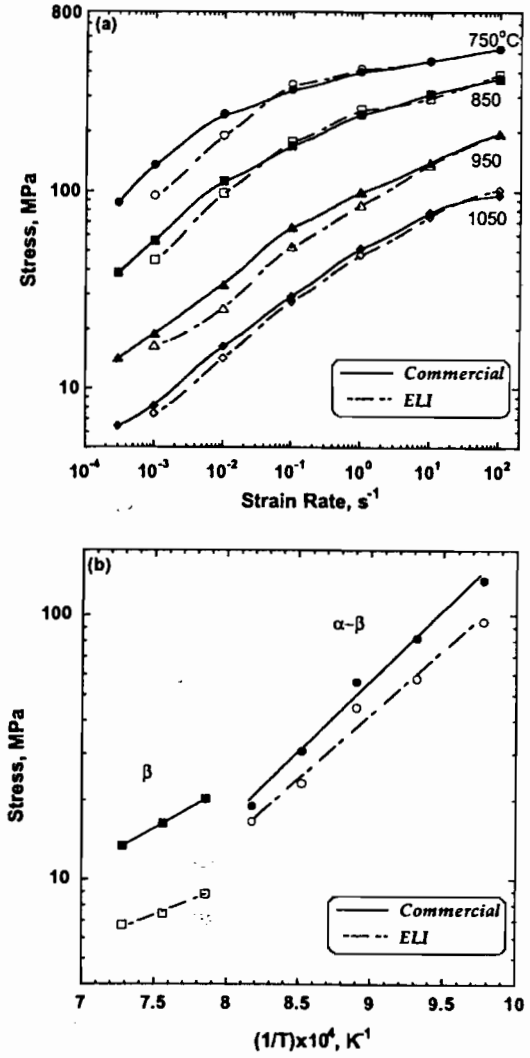

Fig. 3. Plot of: (a) stress vs. strain rate; (b) stress vs. inverse of temperature for two grades of Ti–6Al–4V.

variation indicates a non-linear behavior particularly in the two phase region. However, over a limited temperature range (750–950°C) and strain rate range (3×10^{-4}–10^{-1} s^{-1}), validity of the kinetic rate equation (Eq. (1)) has been established and the values of the stress exponent (n) are estimated. The Arrhenius plot showing the variation of flow stress with inverse of temperature is shown in Fig. 3(b) using which the values of apparent activation energy for hot deformation (Q_{app}) are estimated. The values of n and Q_{app} are given in Table 2 for the two grades of Ti–6–4. These values indicate that while n is not significantly different in the two grades, Q_{app} is higher in the commercial grade than that of the ELI grade. Although the higher Q_{app} value in commercial grade may be attributed to the strengthening effect caused by oxygen, neither of the values are comparable to that for the self-diffusion in α-titanium

Table 2
Kinetic parameters evaluated on the two Ti–6Al–4V grades

Ti–6–4 grade	α–βZ region		β region	
	n	Q_{app} (kJ/mol)	n	Q_{app} (kJ/mol)
Commercial	3.4	330	3.6	210
ELI	3.2	240	3.8	151

(150 kJ/mol) [8] and hence does not convey any physical meaning. In this region, large elongations (>200%) have been reported in the literature [3,9,10], which are suggestive of superplastic deformation.

A plot of the variation of flow stress with the temperature compensated strain rate parameter (Zener–Hollomon), Z is given by the following equation:

$$Z = \dot{\varepsilon} \exp\left[\frac{Q}{RT}\right] \quad (4)$$

This is shown in Fig. 4 which again confirms the validity of the kinetic rate equation for both the grades of Ti–6–4 in the limited temperature and strain rate ranges. It may be noted that a small change in the slope of the fit reflects the difference in the value of the stress exponent (Table 2).

The kinetic analysis was also done in the β range of testing and the corresponding values of n and Q_{app} are included in Table 2 for both the grades. As is the case in the α–β range, the value of n is similar in the β range for both grades while Q_{app} in commercial grade is higher than that of the ELI grade. However, it may be noted that the Q_{app} in both grades is close to that of the self diffusion in β-titanium (150 kJ/mol) [11], which indicates that the process is controlled by dislocation climb. A plot of the variation of flow stress with Z in the β range is also shown in Fig. 4 which confirms the validity of kinetic rate equation over limited

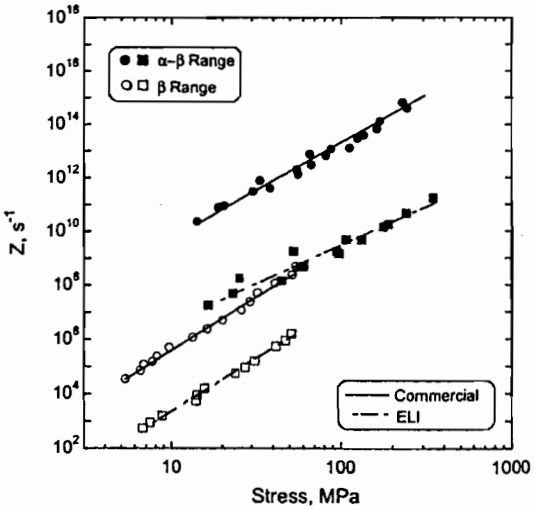

Fig. 4. Variation of flow stress with Zener–Hollomon parameter (Z) in the α–β and β ranges of two grades of Ti–6Al–4V.

ranges of temperature and strain rate. The kinetic analysis in the β range indicates that the influence of oxygen on the β deformation characteristics is insignificant.

4.3. Processing maps

The processing maps obtained at a strain of 0.4 are shown in Fig. 5(a) and (b) corresponding to the commercial grade and the ELI grade Ti–6–4, respectively. The contour numbers represent efficiency of power dissipation expressed in percent. The maps at other strains are not significantly different from the maps shown in Fig. 5. It may be noted

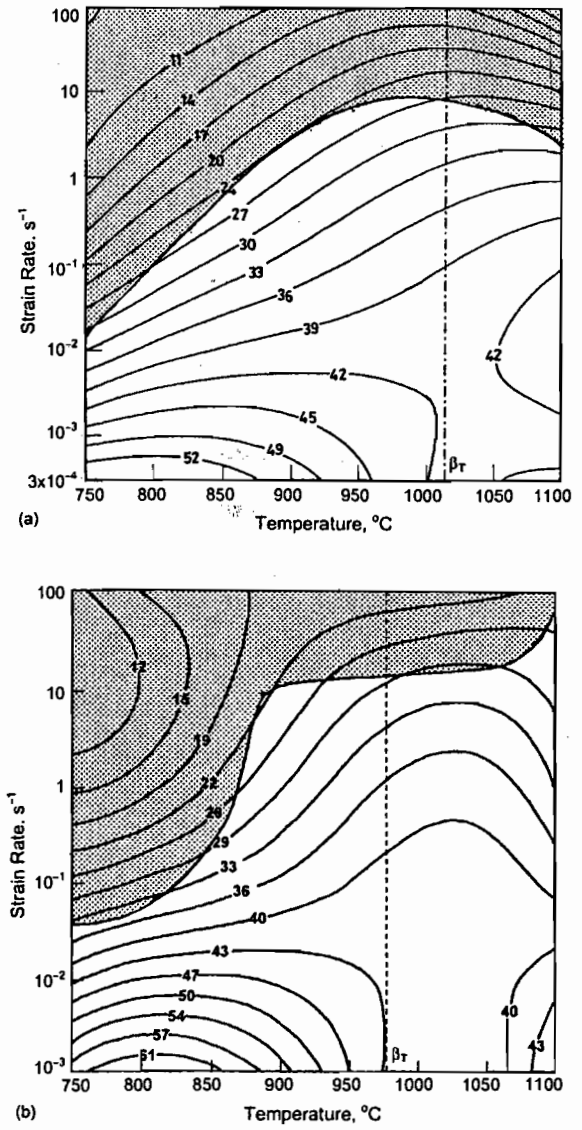

Fig. 5. Processing maps obtained on Ti–6Al–4V at a strain of 0.4: (a) commercial grade; (b) ELI grade. Contour numbers represent the percent efficiency of power dissipation. Shaded region represents flow instability.

that the contours in both maps exhibit a change in the curvature at the transus which is 1010°C for the commercial grade (Fig. 5(a)) and 975°C for the ELI grade (Fig. 5(b)). Such inflexions have been recorded in the maps for all materials which exhibit phase transformations including pure metals [5]. The maps exhibit two domains: one in the α–β region and the other in the β region. All the contours with efficiency values less than about 40% do not attract toward any domain and may therefore be considered to represent a transient behavior.

Referring to the map for the commercial grade (Fig. 5(a)), the domain in the α–β range has a peak efficiency of about 55% occurring at about 825°C and $3 \times 10^{-4}\,s^{-1}$. This domain is spread over a temperature range of 750–1000°C and a strain rate range of 3×10^{-4}–$3 \times 10^{-3}\,s^{-1}$. Since the spread in the temperature scale at the observed peak efficiency is wide, it is expected that the domain is likely to extend to lower strain rates where the efficiency values may be higher. Ito and Hasegawa [9] measured the tensile ductility in a similar temperature range at a strain rate of $7 \times 10^{-4}\,s^{-1}$ and showed that a peak ductility close to 400% occurs at about 875°C. Their data are reproduced in Fig. 6 and a comparison of these measurements with that of the efficiency variation in the domain clearly establishes that the domain represents superplastic deformation.

The map for the ELI grade (Fig. 5(b)) also reveals a similar domain in the α–β range but with a higher efficiency (64%) occurring at slightly higher strain rate ($10^{-3}\,s^{-1}$). The optimum parameters for superplasticity in this grade are about 800°C and $10^{-3}\,s^{-1}$ and the spread of temperature at the observed peak efficiency is small compared to commercial grade. The ductility data for the ELI grade as reported by Cope and Ridley [10] at a nominal strain rate of $10^{-3}\,s^{-1}$ are reproduced in Fig. 6. A peak ductility of more than 1000% has been recorded at optimum conditions in the domain which confirms the occurrence of superplastic deformation.

A comparison of the two maps clearly shows that superplasticity occurs in the two phase range and that with increasing oxygen content, the superplasticity domain moves to lower strain rates. Also, the ductility peak as well as the efficiency peak are broader in the commercial grade than the ELI grade. This effect may be rationalized in terms of the so-called β approach curves (also shown in Fig. 6) for the two grades [10,12]. These curves show how the β volume fraction increases with increasing temperature in the α–β range up to the transus. It may be noted in Fig. 6 that beyond 50%, the β volume fraction increases more gradually in the commercial grade than in the ELI grade, which may be attributed to the stabilizing effect of oxygen on α phase. Superplastic deformation relies on the sliding of α–α interfaces in the two phase structure and increase in the β volume fraction generates more of α–β and α–β interfaces which are undesirable. The rate of generation of these undesirable interfaces decides the rate at which the ductility drops with temperature. Such a result has an important implication in the industrial processing of these two grades. Superplastic

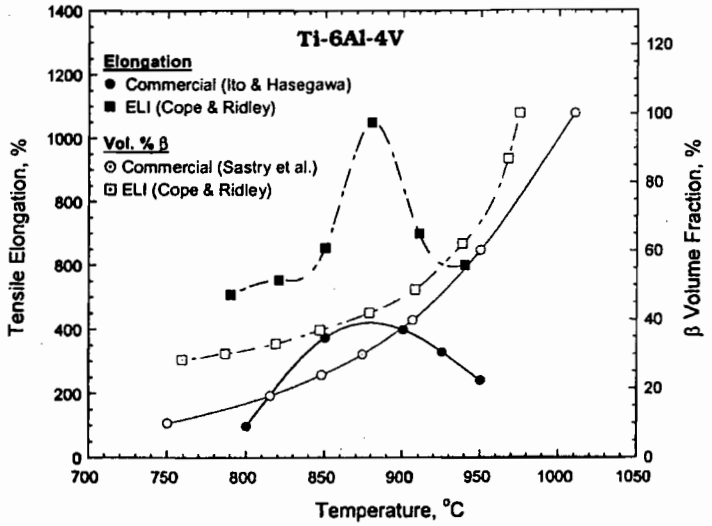

Fig. 6. Variation of tensile elongation and β volume fraction with temperature in the α–β range of commercial and ELI grade Ti-6Al-4V.

forming of ELI grade requires much closer temperature controls than the commercial grade, although it can be done at faster speeds.

The domain that occurs in the β range of the processing map for the commercial grade has a peak efficiency of 42% which occurs at 1100°C and $10^{-2}\,s^{-1}$ and has been interpreted to represent dynamic recrystallization (DRX) process [13]. Deformation in this domain has the following characteristics: (i) steady-state stress–strain curves (Fig. 2(b)), (ii) higher efficiency of power dissipation, (iii) grain refinement at lower temperatures in the domain, (iv) apparent activation energy is close to that for self-diffusion. These features are similar to that occurring in a high stacking fault energy material like aluminum [4] and hence DRX of β-phase is controlled by rate of grain boundary migration.

In the processing map for the ELI grade (Fig. 5(b)), the β DRX domain has occurred at a lower strain rate with a peak efficiency of about 43% at 1100°C and $10^{-3}\,s^{-1}$. Thus, in comparison, β-DRX domain occurs at higher strain rates in commercial grade than the ELI grade. It has been shown that the diffusion rate in β, which has a body centered cubic structure, is enhanced by the presence of interstitials like oxygen since they form pairs with vacancies and stabilize a higher vacancy concentration [14]. The enhanced diffusion rate increases the grain boundary migration rate which controls the DRX process in β. Such an effect will enhance the kinetics of the process and increases the strain rate at which it can occur. The implication of this result on industrial β processing is that the commercial grade may be processed faster than the ELI grade.

The deformation of equiaxed (α + β) Ti–6–4 close to the transus is sensitive to the oxygen content as revealed by the hot ductility variations shown in Fig. 7. The data for the ELI grade are taken from the work of Wu and Lowrie [15]. The data were obtained at a nominal strain rate of $10^{-2}\,s^{-1}$ for the commercial grade and at $2 \times 10^{-3}\,s^{-1}$ for the ELI grade. It may be noted that the commercial grade alloy exhibits abnormal elongation of more than 130% at the transus (1010°C) while the ELI grade shows a ductility dip (~50%) at its transus (975°C). The implication of such a result is that processing ELI grade close to the transus will cause microstructural damage like void nucleation or wedge crack formation while no such problem exists in the commercial grade. In terms of the deformation mechanisms at the transus, the β deformation occurs by sliding of β–β boundaries and causes a stress concentration at their triple junctions. Whether a void or wedge crack is produced at the triple junction depends on the process of stress accommoda-

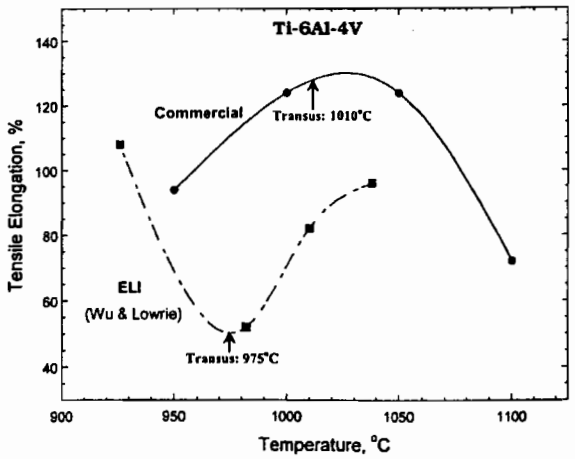

Fig. 7. Variation of tensile elongation with temperature in the β range of commercial and ELI grade Ti-6Al-4V.

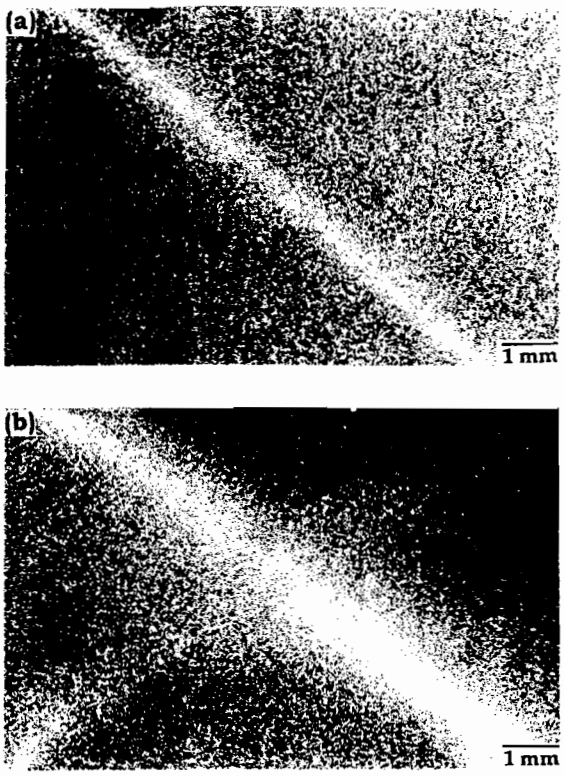

Fig. 8. Macrostructures of Ti–6Al–4V specimens deformed at 750°C and 100 s^{-1}: (a) commercial grade; (b) ELI grade. The compression axis is vertical.

tion which generally occurs by diffusional flow. Since the interstitials (oxygen) enhance the rate of diffusion in β Ti–6–4, the defect nucleation is mitigated in the commercial grade. The higher transus in the commercial grade also helps in enhancing the rate of diffusion in β at the transus.

Results of the application of the instability criterion given by Eq. (3) to delineate regimes of flow instability in the two grades of Ti–6–4 are shown in the processing maps (Fig. 5(a) and (b)) as shaded regions. Within these regimes, the $\xi(\dot{\varepsilon})$ parameter is negative and flow instabilities are predicted to occur. The microstructural manifestation of such instabilities is the flow localization due to adiabatic shear band formation. Typical macrostructures of specimens deformed at 750°C and 100 s^{-1} are shown in Fig. 8(a) and (b) for the commercial and ELI grade respectively, which exhibit adiabatic shear bands formed at an angle of approximately 45° to the compression axis and confirm the predictions of the instability criterion. As expected, the influence of oxygen on the conditions for the occurrence of flow instabilities is not significant. It may be noted that the lowest strain rate limit for their occurrence is the highest processing limit for forging these materials without producing microstructural defects.

5. Conclusions

On the basis of the characterization of deformation behavior of commercial grade and ELI grade Ti–6Al–4V with equiaxed (α + β) preform in the temperature range 750–1100°C and strain rate range 10^{-3}–100 s^{-1} using kinetic analysis and processing maps, the following conclusions are drawn on the influence of oxygen content:

1. The superplasticity domain in the commercial grade is spread over a wider temperature range and occurs at a lower strain rate than that of the ELI grade. On the other hand, the ductility peak in the ELI grade is narrow and may require closer temperature control during processing.
2. The deformation mechanism in the β range is by dynamic recrystallization which occurs at 1100°C and at a higher strain rate (10^{-2} s^{-1}) in commercial grade than in ELI grade (10^{-3} s^{-1}).
3. Unlike the commercial grade, deformation of the ELI grade at its transus has to be avoided since void nucleation or wedge crack formation may occur at slower strain rates.
4. Both grades exhibit flow instabilities manifested as adiabatic shear bands when deformed at strain rates higher than about 1 s^{-1} in the α–β range.

Acknowledgements

The authors would like to acknowledge Dr. J.C. Malas for many stimulating discussions. One of the authors (YVRKP) is thankful to the National Research Council, USA, for awarding him an associateship and to the Director of the Indian Institute of Science, Bangalore, for granting him a sabbatical leave. The assistance rendered by S. Sasidhara and R. Ravi of Department of Metallurgy, Indian Institute of Science is gratefully acknowledged.

References

[1] R. Boyer, G. Welsch, E.W. Collings (Eds.), Materials Properties Handbook: Titanium Alloys, ASM International, Materials Park, OH, 1994, pp. 483–491.
[2] Advanced Materials and Processes, ASM International, No. 3, 1999, pp. 39–41.
[3] M.W. Mahoney, in: R. Boyer, G. Welsch, E.W. Collings (Eds.), Materials Properties Handbook: Titanium Alloys, ASM International, Materials Park, OH, 1994, pp. 1101–1109.
[4] Y.V.R.K. Prasad, T. Seshacharyulu, Int. Mater. Rev. 43 (1998) 243–258.
[5] Y.V.R.K. Prasad, S. Sasidhara (Eds.), Hot Working Guide: A Compendium of Processing Maps, ASM International, Materials Park, OH, 1997.
[6] J.J. Jonas, C.M. Sellars, W.J.McG. Tegart, Metall. Rev. 14 (1969) 1–24.
[7] H. Ziegler, in: I.N. Sneddon, R. Hill (Eds.), Progress in Solid Mechanics, Vol. 4, Wiley, New York, 1963, p. 93.

[8] F. Dyment, C.M. Libanati, J. Mater. Sci. 3 (1968) 349–359.
[9] Y. Ito, A. Hasegawa, in: H. Kimura, O. Izumi (Eds.), Titanium: Science and Technology, TMS, Warrendale, PA, 1980, pp. 983–992.
[10] M.T. Cope, N. Ridley, Mater. Sci. Technol. 2 (1986) 140–145.
[11] N.E.W. de Reca, C.M. Libanati, Acta Metall. 16 (1968) 1297–1305.
[12] S.M.L. Sastry, R.J. Lederich, T.L. Mackay, W.R. Kerr, J. Met. (1983) 48–53.
[13] T. Seshacharyulu, S.C. Medeiros, W.G. Frazier, Y.V.R.K. Prasad, Mater. Sci. Eng. A284 (2000) 184–194.
[14] G.V. Kidson, in: J.A. Wheeler, F.R. Winslow (Eds.), Diffusion in body centered cubic metals, 1965, pp. 329–347.
[15] K.C. Wu, R.E. Lowrie, Met. Eng. Qtrly. (1972) 25–29.

January Vol·35

August Vol·12